PNE-1102

PNE-1102

Plowshare civil, industrial and scientific uses for nuclear explosives

UNITED STATES ARMY CORPS OF ENGINEERS

FORT PECK RESERVOIR
MONTANA

PROJECT
PRE-GONDOLA I

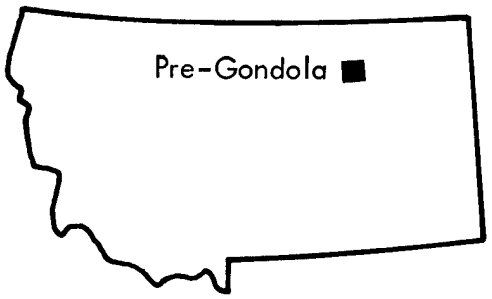

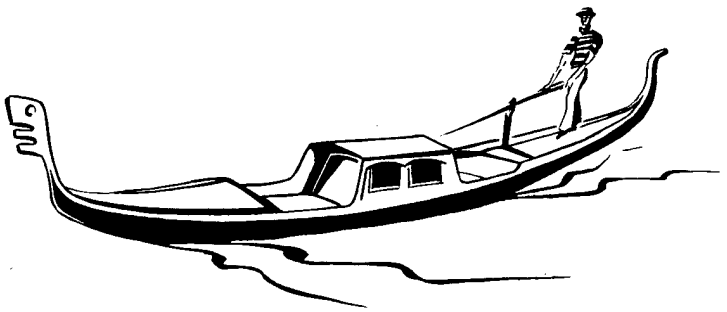

DISTRIBUTION STATEMENT A
Approved for Public Release
Distribution Unlimited

TECHNICAL DIRECTOR'S SUMMARY REPORT

LT. COLONEL MAURICE K. KURTZ, JR.
U. S. Army Engineer Nuclear Cratering Group
Livermore, California

U. S. Army Engineer Nuclear Cratering Group
Livermore, California

ISSUED: May 1968

PNE-1102
Final Report

PROJECT PRE-GONDOLA I

TECHNICAL DIRECTOR'S SUMMARY REPORT

Lt. Colonel Maurice K. Kurtz, Jr.
Captain W. G. Christopher
W. C. Day
P. R. Fisher
Captain R. W. Harlan
Lieutenant B. B. Redpath

U. S. Army Engineer
Nuclear Cratering Group
Livermore, California

J. C. Chandler

Fort Peck Area Engineer
U. S. Army Engineer District, Omaha
Fort Peck, Montana

12 January 1968

Preface

This is the Technical Director's final summary report on Project Pre-Gondola I, a series of high explosive cratering detonations to calibrate a new test site and to provide design input for subsequent row-charge cratering experiments. Preliminary results were reported in NCG/TM 66-20, "A Report of the Scope and Preliminary Results of Project Pre-Gondola I," December 1966.

The Technical Director and program leaders wish to acknowledge the participation of persons in the many agencies who helped make this experiment a success. We are particularly grateful for the assistance and cooperation of the technical support groups, specifically, the Lawrence Radiation Laboratory high explosive support group, personnel from the Air Resources Field Research Office (ARFRO), ESSA, and the photographic team from Edgerton, Germeshausen and Grier, Las Vegas. Mr. D. C. Beckman, Fort Peck Area Engineer, and his staff deserve special thanks for their ability to remain flexible and to provide needed assistance during the conduct of the experiment. The efforts of the District Engineer, U. S. Army Engineer District, Omaha and his Test Manager, C. O. Brunken, were commendable.

In addition to those who provided technical advice and assistance, many persons of the Lawrence Radiation Laboratory and the Corps of Engineers Waterways Experiment Station also participated in the Technical Programs. Their efforts and assistance are appreciated. Finally, the efforts of all those persons of the U. S. Army Engineer Nuclear Cratering Group who participated in fielding this experiment are gratefully acknowledged.

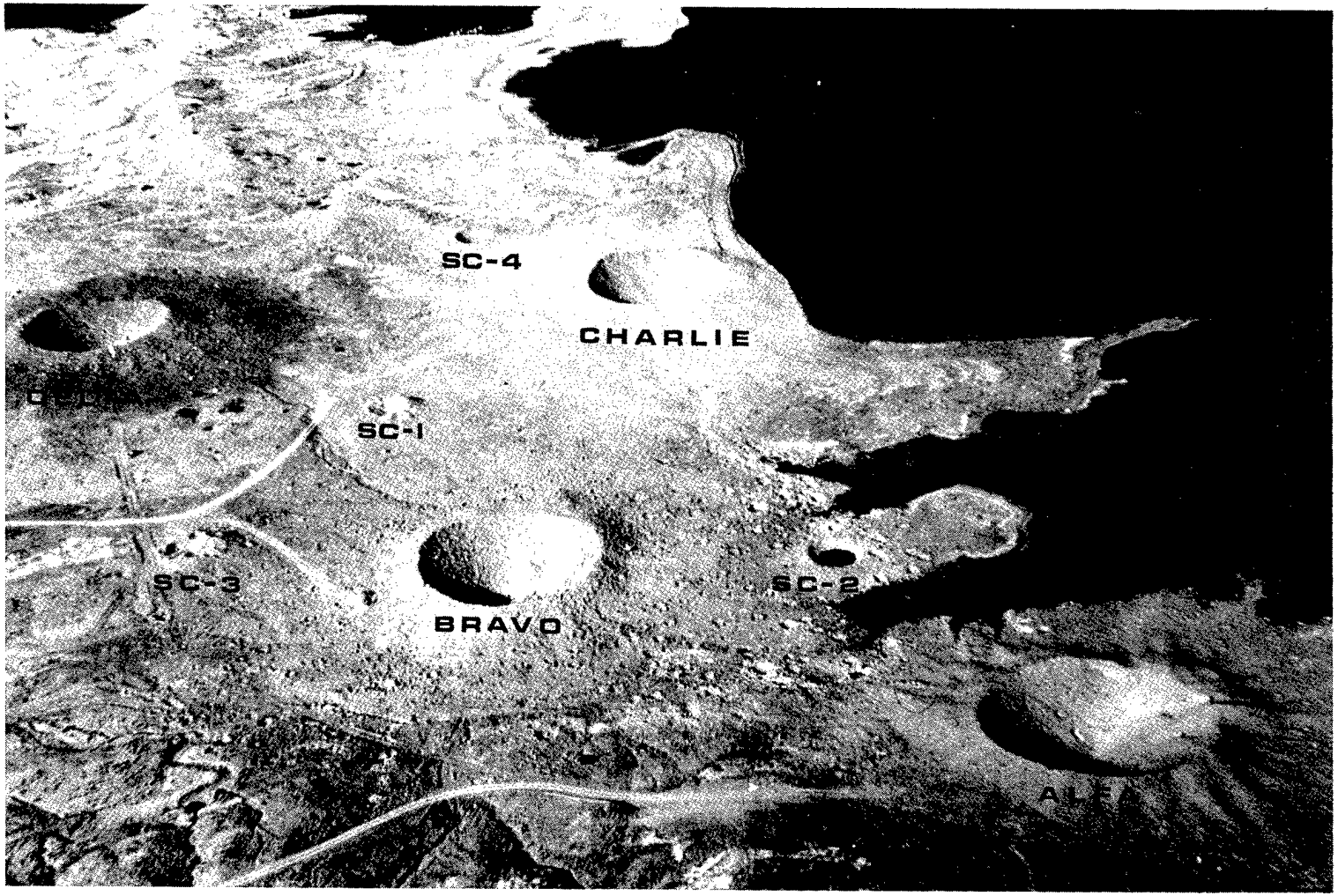

Frontispiece. Pre-Gondola Craters (4 November 1966).

Abstract

This report presents the concepts, technical programs, objectives, and summarized results of Project Pre-Gondola I, a series of four 20-ton high explosive cratering experiments conducted during October-November 1966, near Fort Peck, Montana. The experiments established the cratering characteristics of the weak, wet, clay-shale (Bearpaw) preparatory to row-charge cratering experiments. The results were used in the design of the 140-ton Pre-Gondola II row-charge cratering experiment detonated on 28 June 1967.

The site medium, project layout, construction, field operations, and explosive charge design and emplacement are described.

Cratering calibration of the site was accomplished with four single 20-ton nitromethane detonations at depths of burst from 42.49 to 56.87 ft. Apparent crater radii varied from 80.4 to 65.1 ft and apparent depths from 32.6 to 25.2 ft. The craters produced were both deeper and wider than craters produced in alluvium and basalt and had flatter slopes. Optimum depth of burst for maximum crater dimensions was established as $130\ \mathrm{ft/kt}^{1/3.4}$ for Bearpaw shale.

Surface motion velocities observed were higher than for any medium previously cratered. Peak surface ground zero velocities were significantly higher than those for high explosive craters in alluvium and nuclear craters in basalt, and were slightly higher than those observed for a high explosive crater in rhyolite (Pre-Schooner II).

A summary of preliminary results of engineering properties investigations is presented. Displacement studies indicate a movement of material in the region of the true crater boundary toward shot point.

Seismic data were obtained for both intermediate range ground motions and the response of the Fort Peck Dam, gate structure, and spillway. Predictions are made on the basis of these data for higher yield row-charge detonations. A depth of burst dependence for intermediate range ground motions was noted.

The clouds observed from the four detonations were unique. They were very diffuse, there were no main clouds, and steam was visible in the base surge clouds. Lidar tracking of the clouds was successful and indicated a capability to provide information as a function of time on the position, motion, growth, and internal structure of cratering explosion clouds.

The accumulated effects of the detonations were not injurious to fish in adjacent waters.

Final results of these studies not completed will be reported in the individual technical program reports listed in Appendix A.

CRATER NOMENCLATURE

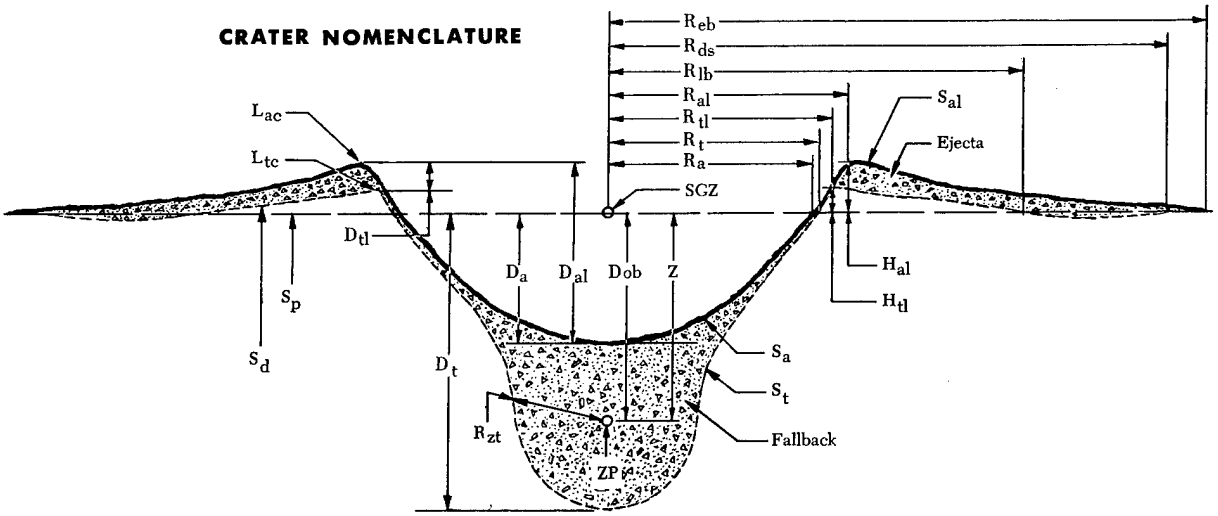

D_a . . . Maximum depth of apparent crater below preshot ground surface measured normal to the preshot ground surface.*

D_{al} . . . Depth of apparent crater below average apparent crater lip crest elevation.

Dob . . Normal depth of burst (measured normal to preshot ground surface).

Dt . . . Maximum depth of true crater below preshot ground surface.

D_{tl} . . . Depth of true crater lip crest below apparent crater lip crest.

Ejecta . Material above and or beyond the true crater and includes: (1) foldback; (2) breccia—ballastic trajectory; (3) dust—aerosol transport; etc.

Fallback. Material fallen inside the true crater and includes: (1) slide blocks; (2) breccia and stratified fallback —ballastic trajectory; (3) dust—aerosol transport; (4) talus; etc.

H_{al} . . . Apparent crater lip crest height above preshot ground surface.

H_{tl} . . . True crater lip crest height above preshot ground surface.

L_{ac} . . . Apparent crater lip crest.

L_{tc} . . . True crater lip crest.

R_a . . . Radius of apparent crater measured on the preshot ground surface.

Note: The radius measurements pertain only to single charge craters and represent average dimensions. If crater shape deviates substantially from circular, the direction of measurement must be specified. An average radius value can also be determined by dividing the plan area by π and taking the square root.

R_{al} . . . Radius of apparent lip crest to center.

R_{ds} . . . Outer radius of displaced surface.

R_{eb} . . . Radius of outer boundary of continuous ejecta.

R_{lb} . . . Outer radius of true lip boundary.

R_t . . . Radius of true crater measured on the preshot ground surface.

R_{tl} . . . Radius of true lip crest to center.

R_{zt} . . . Distance between the zero point and the true crater surface measured in any specified direction. When measured in a direction below the zero point is equivalent to lower cavity radius.

S_a . . . Apparent crater surface, e.g. rock-air or rubble-air interface.

S_{al} . . . Apparent lip surface.

SGZ . . Surface ground zero.

S_d . . . Displaced ground surface.

S_p . . . Preshot ground surface.

S_t . . . . True crater surface, e.g. rock-air or rock rubble interface.

V_a . . . Volume of apparent crater below preshot ground surface.

V_{al} . . . Volume of apparent crater below apparent lip crest.

V_t . . . Volume of true crater below preshot ground surface.

V_{tl} . . . Volume of true crater below true crater lip crest.

Z . . . . Vertical depth of burst (equivalent to Dob when crater is formed on a horizontal surface).

ZP . . . Zero Point—effective center of explosion energy.

*All distances, unless specified otherwise, are measured parallel or perpendicular to preshot ground surface.

Contents

TABLES

Table

FIGURES

Figure

Figure

Figure

Introduction

Project Pre-Gondola is a phased series of chemical high explosive (HE) cratering experiments consisting of the following phases: (1) Seismic Site Calibration Series (SSC) of four 1000-lb detonations in June 1966; (2) four Pre-Gondola I 20-ton cratering calibration detonations in October-November 1966; (3) Pre-Gondola II five-charge, 140-ton, row-cratering experiment in June 1967; and (4) Pre-Gondola III, a planned future row-charge cratering experiment.

The purpose of this report is to present in summary form the results of Pre-Gondola I and to illustrate the manner in which the results of the SSC and Pre-Gondola I were used in the design of Pre-Gondola II.

DESCRIPTION AND PURPOSE

Project Pre-Gondola I was a series of chemical explosive single-charge cratering experiments in weak, wet clay-shale conducted by the U. S. Army Engineer Nuclear Cratering Group (NCG) as a part of the joint Atomic Energy Commission-Corps of Engineers nuclear excavation research program. The purpose of Pre-Gondola I was to calibrate the project site with respect to its cratering characteristics and to provide a basis for design of the proposed 140-ton Pre-Gondola II and the Pre-Gondola III row-charge cratering detonations in the same medium.

The Pre-Gondola I detonations were executed in Valley County, near the edge of the Fort Peck Reservoir approximately 18 mi south of Glasgow, Montana, on the following schedule:

Event	Date	Time (MST)	Longitude	Latitude
Bravo	25 October 1966	1000:00.760	W 106°38'24.894"	N 47°55'46.154"
Charlie	28 October 1966	1200:00.654	W 106°38'29.974"	N 47°55'53.294"
Alfa	1 November 1966	1000:00.275	W 106°38'15.325"	N 47°55'46.570"
Delta	4 November 1966	1000:00.032	W 106°38'38.134"	N 47°55'48.077"

The four 20-ton (nominal) spherical charges of liquid explosive nitromethane (CH_3NO_2) resulted in the following craters:

Event	Tons	Depth of burst (ft)	Depth of burst (m)	Apparent crater radius (ft)	Apparent crater radius (m)	Apparent crater depth (ft)	Apparent crater depth (m)
Charlie	19.62	42.49	12.95	80.4	24.50	32.6	9.94
Bravo	19.36	46.25	14.10	78.5	23.93	29.5	8.99
Alfa	20.35	52.71	16.07	76.1	23.19	32.1	9.78
Delta	20.24	56.87	17.34	65.1	19.84	25.2	7.68

To confirm site suitability, to assist in seismic site calibration, and to provide preliminary information for the design of the Pre-Gondola I experiment, NCG had earlier conducted the following Pre-Gondola Seismic Site Calibration Series at the Pre-Gondola I site:

Event	Date	Time (MST)	Longitude	Latitude
SC-1	20 June 1966	0845	W 106°38'30.573"	N 47°55'48.383"
SC-4	21 June 1966	0811	W 106°38'35.059"	N 47°55'53.380"
SC-2	22 June 1966	0805	W 106°38'20.792"	N 47°55'48.181"
SC-3	23 June 1966	0837	W 106°38'29.495"	N 47°55'44.579"

The four 1000-lb spherical charges of nitromethane resulted in the following craters:

Event	Tons	Depth of burst (ft)	Depth of burst (m)	Apparent crater radius (ft)	Apparent crater radius (m)	Apparent crater depth (ft)	Apparent crater depth (m)
SC-4	0.5	12.2	3.72	24.5	7.48	13.0	3.96
SC-2	0.5	15.8	4.81	27.3	8.32	12.5	3.81
SC-1	0.5	19.1	5.82	7.1*	2.16	2.8*	0.85
SC-3	0.5	23.3	7.10	14.6*	4.45	3.4*	1.04

*Anomalous and very asymmetrical; may have produced a mound on level terrain.

Figure 1, an index map of the Fort Peck Reservoir area, shows the location of the Pre-Gondola project site.

SCOPE OF REPORT

This summary report describes the overall results of a series of cratering detonations used to calibrate a particular site in preparation for the conduct of a row-charge and connecting row-charge cratering experiment. Introductory chapters include a description of the objectives, technical programs, site characteristics, and the explosive charge. The following chapters contain summaries of the technical programs and overall results achieved. This report is supplemented by detailed technical reports listed in Appendix A. References are listed at the end of the report. Nomenclature is described on page vi.

BACKGROUND

General Objectives of Joint Research Program

The Pre-Gondola chemical explosive cratering experiments are a part of the joint Atomic Energy Commission-Corps of Engineers Nuclear Excavation Research Program. The purpose of the joint research program, being conducted pursuant to Presidential Directive, is to determine

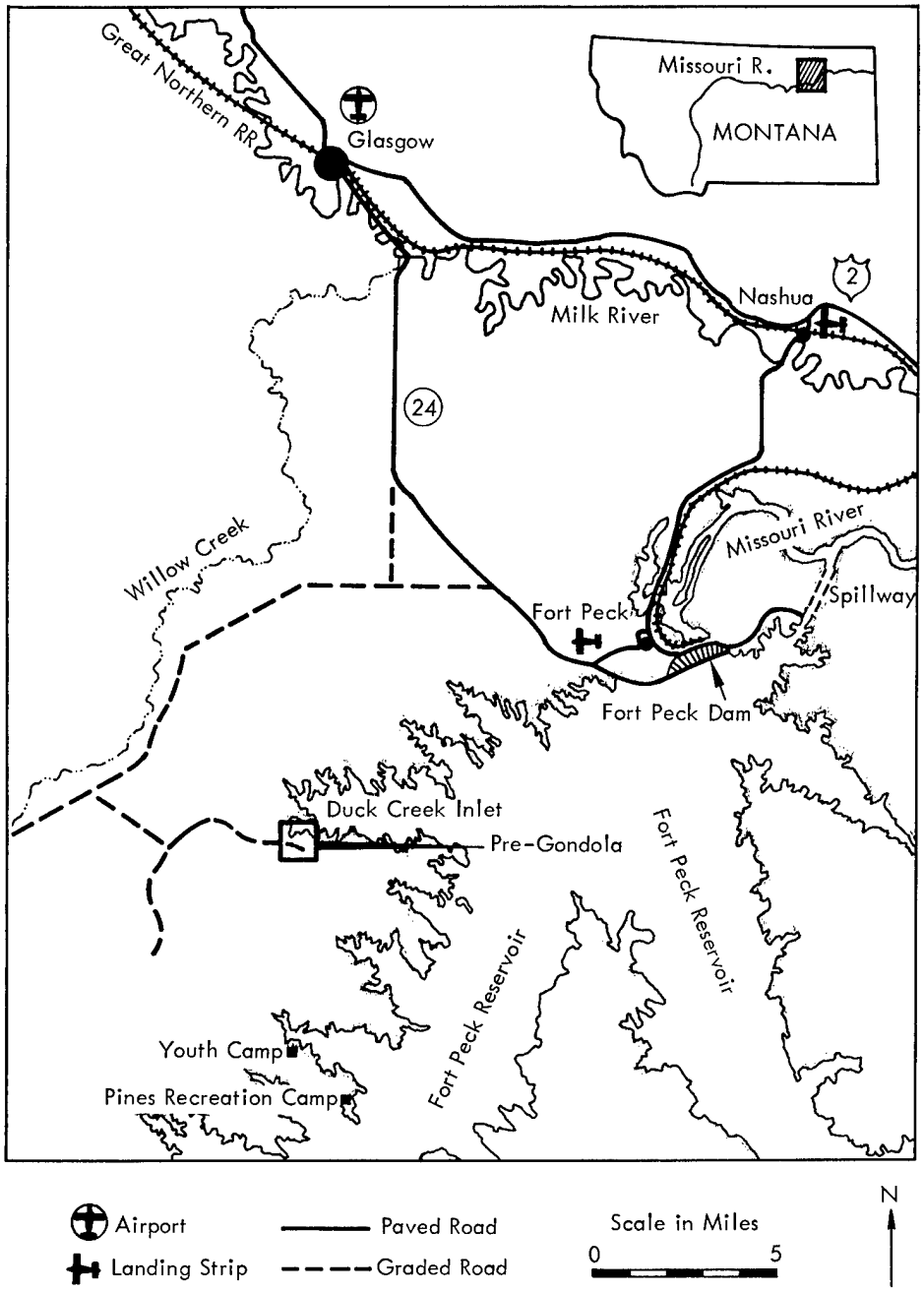

Fig. 1. Site location.

the feasibility, costs and other factors involved in the use of nuclear explosives for construction.

Under the agreement for the joint research program, the AEC is primarily responsible for nuclear device development, execution of nuclear cratering experiments, and the development of basic scaling relations. The Corps of Engineers is primarily responsible for the execution of a corollary chemical HE cratering program and the development of the requisite data on engineering and construction problems.

The objectives of the Corps' program, conducted by the NCG, include the determination

of the engineering properties of explosively produced craters and the identification and solution of the engineering problems associated with construction of useful public works projects using nuclear explosives as a construction tool. This program also includes the conduct of small scale HE experiments, such as Pre-Gondola, which involve detonation of single and row charges under various terrain and geological conditions.

Need for Additional Cratering Experience

Small-scale cratering experiments serve many purposes in the development of nuclear excavation technology to include developing information on cratering in those media which will be encountered in actual construction projects. Delays in the execution of the nuclear experimental program necessitated the acceleration of the HE program to develop needed data with priority to row-charge cratering experiments in a weak, wet clay-shale medium.

Previous single- and row-charge cratering experience had been restricted mainly to dry, hard rock and desert alluvium in essentially level terrain. There had been no cratering experience involving significantly large yields in weak, saturated media. The only cratering experience in a wet shale was based on the results of detonating 8- to 100-lb cylindrical charges of TNT.[1]

Purpose and Concept of Site Calibration

Because of the lack of meaningful cratering experience in wet clay shale for use in design of a planned row-charge excavation experiment, it was first necessary to obtain the cratering characteristics of the project site with a series of small-scale single-charge experiments. Project Pre-Gondola I at Fort Peck, Montana, was the cratering calibration series used for design of the 140-ton Pre-Gondola II row-charge cratering experiment (28 June 1967).

The general concept of site calibration reported in this and associated reports (Appendix A) is as follows:

1. Develop the Project concept.[2]
2. Conduct site selection investigations (PNE-1101).
3. Document the engineering properties of the site medium (PNE-1103, PNE-1111).
4. Conduct seismic site calibration experiments as required to confirm site safety (PNE-1100).
5. Conduct cratering calibration experiments to obtain design data (PNE-1102, PNE-1107).
6. Develop measurement techniques, calibrate instruments, and document side effects (PNE-1103, PNE-1111).
7. Evaluate data collection effort and recommend design criteria for subsequent detonations (PNE-1103, PNE-1107).
8. Predict side effects for subsequent detonations (PNE-1100, PNE-1105, PNE-1110) and establish additional safety programs as required.

TECHNICAL PROGRAMS AND OBJECTIVES

This section associates the Pre-Gondola I technical objectives with the technical programs that were conducted to accomplish the objectives. These technical programs involved the Lawrence Radiation Laboratory (LRL), the Corps

of Engineers Nuclear Cratering Group (NCG), the Waterways Experiment Station (WES), and the Air Force Weapons Laboratory (AFWL). The application of the information obtained is also indicated.

Crater Studies

This technical program, of first importance during Pre-Gondola I Cratering Calibration Series, included the following subprograms: (1) crater measurements and ejecta studies (NCG), and (2) ground surface motion studies (NCG/LRL). In addition, LRL performed code calculations of the Bravo crater dimensions. The common objectives of this combined program were:

1. To extend single-charge explosive cratering experience to a weak wet, clay-shale medium.
2. To calibrate the Pre-Gondola project site with respect to its cratering characteristics and to provide input to the design of the planned Pre-Gondola I and II row-charge cratering detonations at the same site.
3. To provide experimental data for use in theoretical studies of crater formation and for the design of future single- and row-charge cratering detonations in similar media.

The procedures used in this technical program (as described in the sections entitled Crater Measurements and Ejecta Studies and Surface Motion Studies) are similar to those previously reported for other HE cratering experiments.

The cratering information obtained has been or will be used to design the Pre-Gondola II and III row-charge detonations, to support engineering properties studies (such as permanent subsurface displacement), and to support engineering studies of nuclear excavation project feasibility in similar media.

Engineering Properties Investigations

This program included (1) preshot and postshot investigations to determine the effect of the explosion on the medium (NCG), (2) studies of displacement of slopes (NCG), (3) geophysical measurements (LRL), (4) close-in measurements with velocity, stress, and pore pressure gages on Bravo (WES), (5) close-in displacement measurements on Bravo (AFWL), (6) and ejecta-subsurface displacement studies (NCG). In addition, WES measured stress levels in and adjacent to the remaining explosive emplacement cavities during each detonation.

The detailed results of this technical program are presented in Ref. 3. A summary of results is contained in this report.

The principal objective of these investigations was to determine the engineering properties of explosively produced craters in a weak wet clay-shale.

Secondary objectives included (1) development of information on construction operations in and around explosively produced craters, (2) development of techniques for measuring pore water pressures and residual stresses, (3) development of various exploration techniques to assess the effect of a cratering detonation on the surrounding medium, (4) documentation of the subsurface deformation resulting from a single-charge detonation in a nearly homogeneous saturated clay-shale, (5) documentation of the residual displacement of craters and an active landslide

subjected to the ground motions induced by adjacent 20-ton cratering detonations, and (6) documentation of the transient stress levels in existing charge cavities due to ground shock effects from adjacent detonations.

These results were used to predict behavior of the Pre-Gondola II row crater and will become the subject of continuing studies to develop the capability to predict the properties of the various crater zones on the basis of preshot explorations.

Seismic Studies

This program, which will continue throughout the Pre-Gondola series, includes intermediate-range ground motion measurements sponsored by LRL and structures instrumentation by WES and Montana State University at the same locations occupied during the 1000-lb Seismic Site Calibration Series. The results of this program form the basis for a prediction scheme used to estimate the seismic effects from future row-charge detonations. Results of the seismic studies are presented in Ref. 4. A summary of results is included in this report.

The objectives during Pre-Gondola I were (1) to evaluate the effect of varying the depth of burst (DOB) on the amount of seismic energy coupled into the ground, (2) to evaluate yield scaling assumptions, (3) to investigate the propagation characteristics of the region surrounding the Fort Peck area, (4) to investigate the transmission of seismic energy through the Fort Peck Reservoir, (5) to determine the presence of any directional asymmetry of propagation, (6) to document the response of certain major structures in the vicinity of Fort Peck, (7) to provide measurements for use in a separate LRL-sponsored analytical study of the response of earth embankments to seismic loading, and (8) to develop a reliable basis for prediction of ground motions from higher yield detonations.

The results of these studies will be available for use in safety and feasibility studies of proposed nuclear excavation projects in similar media.

Cloud Development Studies

This program, common to all cratering experiments conducted under the joint research program, included measurement of cloud dimensions (NCG), laser-radar (lidar) tracking by Stanford Research Institute (SRI) under LRL sponsorship, and cloud sampling (NCG/LRL). The objectives were to evaluate cloud development for cratering detonations in a saturated medium and to demonstrate the use of the laser-radar in tracking visible and subvisible clouds from cratering detonations.

The results of these studies were used to develop improved cloud models for cratering detonations in saturated media and in the design of experimental programs for Pre-Gondola II. The resulting cloud parameters will be used to develop improved fallout prediction methods for nuclear cratering detonations in wet media and will be available for use in engineering studies of the feasibility of nuclear excavation in similar media.

TECHNICAL DIRECTORS ORGANIZATION

Figure 2 shows the organization for conduct of the Pre-Gondola I experiment and associated data collection efforts.

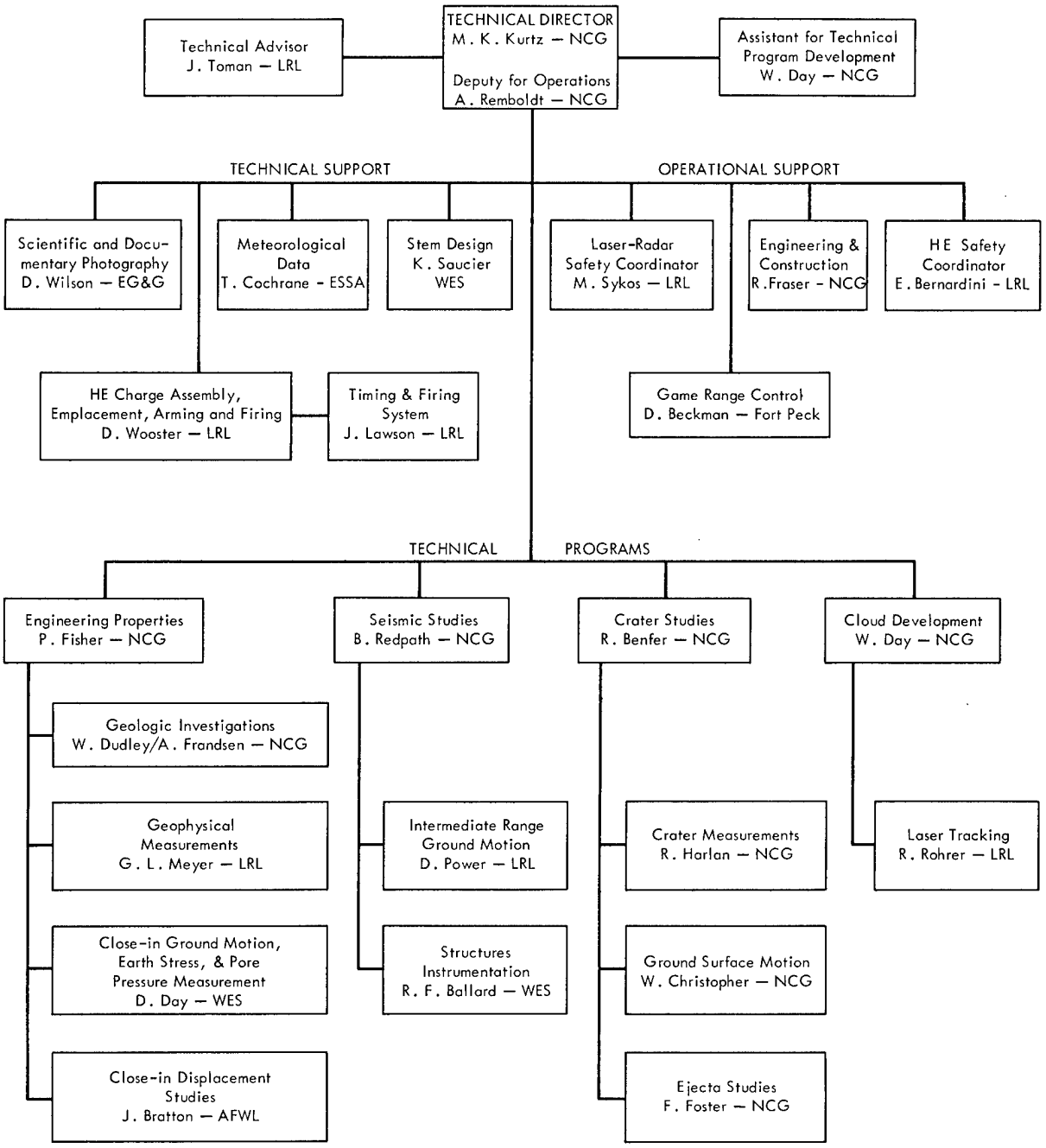

Fig. 2. Technical Director's Organization for Pre-Gondola I Cratering Calibration Series.

Description of Pre- Gondola I Experiment

This chapter describes the site, charge, and emplacement, and the detonations.

DESCRIPTION OF SITE

Location and Land Use[5]

The Pre-Gondola site is situated on the south fork of Duck Creek, adjacent to the Fort Peck Reservoir in Section 11, T25N, Valley County, Montana (Fig. 1). There are no inhabited dwellings within 4 mi of the site. The nearest population center is the town of Fort Peck, located 10 mi to the northeast. It has a population of about 650 people, mostly government employees engaged in the operation and maintenance of nearby Fort Peck Dam. The nearest structures are the huge earth-fill embankment of the Fort Peck Dam and the powerhouse located about 11 mi northeast of the site.

The primary reason for selecting a site at the edge of a reservoir was to take advantage of the expected high water table. Because most of the shale at the site has been below reservoir level for many years, it was expected to be in a saturated or near-saturated condition.

The entire Fort Peck site area is within the taking line of the reservoir and is therefore federal land under the control of the U. S. Army Corps of Engineers. The surrounding land is part of the Charles M. Russell National Wildlife Refuge. The sparse vegetation supports only limited grazing. Future plans include industrial and recreational use of the Duck Creek area with access to the Fort Peck Reservoir.

Site Selection Investigation[5]

The Fort Peck site was selected as a result of comprehensive investigations to locate a site within the continental United States which met specified geologic, terrain, operational, and safety criteria.[2] This was accomplished in three phases: (1) an initial phase of office studies during January 1966 (2) field reconnaissance during February and March 1966 of promising sites identified by the office studies and (3) subsurface explorations and laboratory testing of core samples from the most promising site and from one of two alternate sites during April, May, and June 1966. Reference 5 describes the procedures followed, summarizes the results of intermediate stages of the investigation, and provides the basic geologic and engineering characteristics at Fort Peck site.

Site Area and Geology[5]

1. Physiography

The Fort Peck site is located in the Bearpaw shale, a highly compacted, uncemented clay-shale of Cretaceous age. Where the Bearpaw shale outcrops, it forms either badlands or a terrain of small hills with moderately steep to gentle slopes. It supports only sparse vegetation. Drainage courses entering the Missouri trench from the north have eroded relatively short, steepsided gullies forming the so-called "Missouri Breaks."

The full difference in elevation between the Missouri floodplain and the ridges along the main reservoir is not apparent since the valley is inundated to a depth of nearly 250 ft by the reservoir. Along the Duck Creek inlet, however, the land adjacent to the reservoir is primarily gently rolling terrain situated slightly above reservoir level, as shown in Fig. 3. There are a few narrow ridges with moderately steep sides, providing a variety of topographic conditions for cratering experiments.

2. Stratigraphy

The Bearpaw shale of late Cretaceous age forms the bedrock at the Pre-Gondola I site and outcrops over most of the area. It is underlain at a depth of approximately 900 ft by the Judith River formation, a mid-Upper Cretaceous sandstone. The uppermost few hundred feet of the Bearpaw shale and the overlying Fox Hills sandstone, which caps the higher ridges along the reservoir south of the Pre-Gondola site, have been removed by erosion. An additional but unknown thickness of Tertiary and younger sediments, once overlying the area, has also been eroded. Thin scattered remnants of glacial deposits indicate that Pleistocene glaciers have advanced over the site.

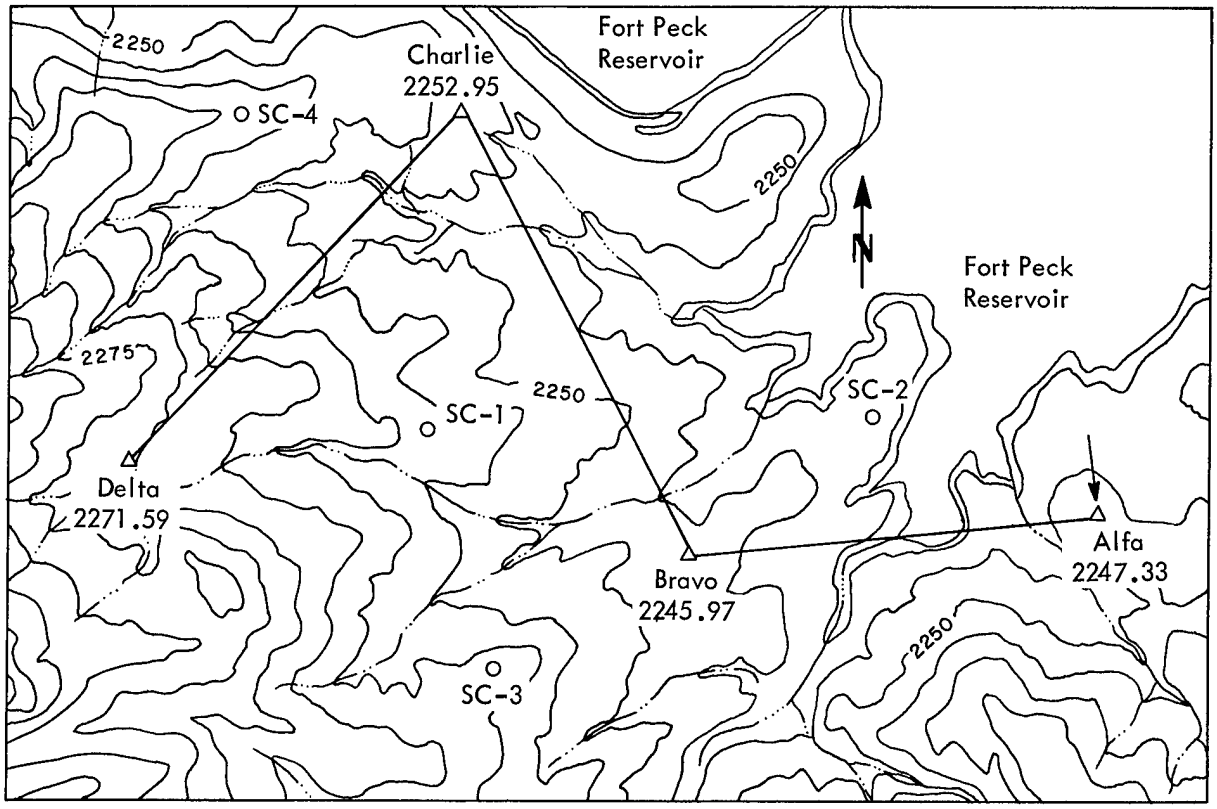

Fig. 3. Topographic map showing location of geologic profile and relative ground zero locations.

The shale at the Pre-Gondola I site is uniform, dark gray, highly compacted, and uncemented. It contains infrequent calcareous and iron-manganese concretions up to 1 ft thick, and waxy, light gray to tan bentonite layers. Several joint sets with inconsistent orientation occur at spacings of 1/2 to 3 ft, and numerous hairline cracks are visible between the major joints.

The base of the weathered zone occurs at a depth of 10 to 20 ft (Figs. 3 and 4). The visible effects of weathering include increased fracture frequency, opening of joints, and oxidation and mineral filling along joints and fractures. Within a few feet of the surface the shale is highly fragmented. Alternate wetting and drying at the surface causes further breakdown of the shale particles to form a fat clay.

Subdivisions within the Shale

Below the weathered zone, the Bearpaw shale is essentially homogeneous, except for thin but persistent bentonite layers and occasional disk-shaped calcareous concretions which range up to about 1 ft in diameter. The bentonite layers may be used to distinguish two distinct zones as shown in the stratigraphic section (Fig. 4). The upper member is, for the most part, devoid of bentonite layers except for a pair of bentonite layers whose thicknesses range up to 4 in. and which always occur about 30 ft above the base of the member. Underlying this

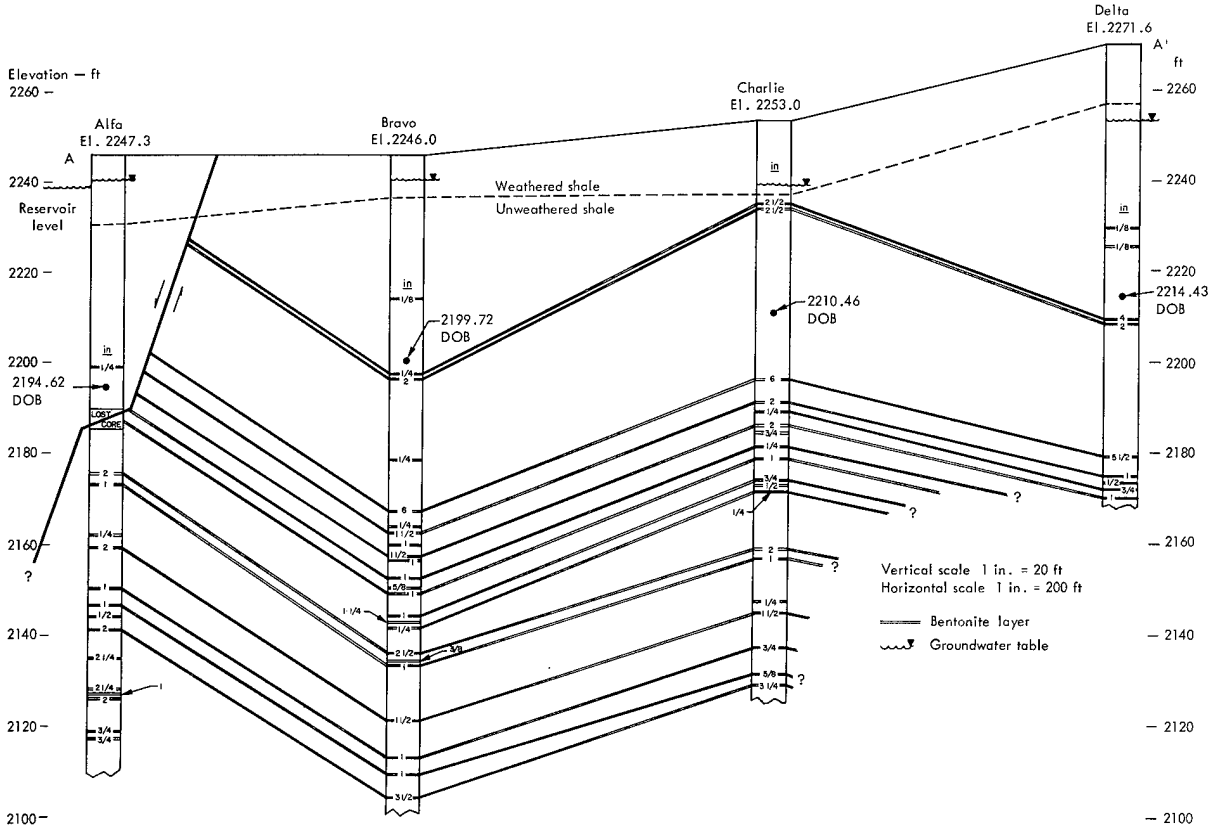

Fig. 4. Geologic cross section drawn through Alfa, Bravo, Charlie, and Delta Surface Ground Zero (Ref. 6).

upper member, the stratigraphic section contains numerous thin bentonite layers. The top of the lower member is distinctively marked by a 6-in. bentonite layer.

Structure

The regional dip of the Cretaceous rocks in the Fort Peck area is southeastward at about 25 ft per mi, but slumping of the Bearpaw shale produces local variations. Dips measured in cores from the Pre-Gondola I site generally range from 2 to 7 deg. At the Alfa site steeper dips are associated with an apparent slump block, which is bounded by a shear zone encountered at a depth of 58 ft in the ground-zero boring.

Ground Water

The shale is essentially impervious. Static water levels in observation wells open in the weathered shale show that the water table at the Alfa and Bravo sites is about 6 ft beneath the ground surface, while at Charlie and Delta it is about 15 ft. A Casagrande piezometer with the sand tip in unweathered shale at the Charlie site stabilized at a depth of 75 ft. This indicates that movement of water occurs primarily along fractures and that independent ground-water systems may exist within different fracture systems in the shale. Appreciable movement of water occurs only through fault or fracture zones. In the lowlands adjacent to the reservoir, the more previous overburden and weathered shale extend to depths well below the reservoir level and the water table is adjusted to the pool. The elevation of the water level in the reservoir during the conduct of Pre-Gondola I averaged 2238.5 ft.

Local Variation in Geology[6]

There were variations in the detailed geology between the specific sites for charge emplacement. These variations were noted because it was believed that they might assist in interpreting the measurements obtained in the several technical programs.

At the Bravo site, the shale was covered by a mantle of 5 to 6 ft of glacial till and alluvium, and at the Delta site the shale was covered by an insignificant amount of overburden. Weathering effects were observed to depths of about 5 ft at the Alfa and Bravo sites, while at the Charlie and Delta sites the effects of weathering extended to depths of about 14 ft.

A shear plane cut the boring at the Alfa surface ground zero (SGZ) at a depth of about 58 ft (Fig. 4). About 60 ft of the stratigraphic section was lost due to poor core recovery in this zone.

Preshot Engineering Properties of Site Medium

Figure 5 shows the range of the following physical properties of the Bearpaw shale at the Pre-Gondola site:[5]

Strength

The laboratory unconfined compressive strength of the intact shale is high; however, the mass strength of the in situ material is reduced by the bentonite seams and an extensive system of jointing and slumping. Figure 5 shows the general increase in strength with depth. The range of strengths probably reflects differences in fracturing rather than in the strength of the intact shale. Undrained triaxial compression tests on

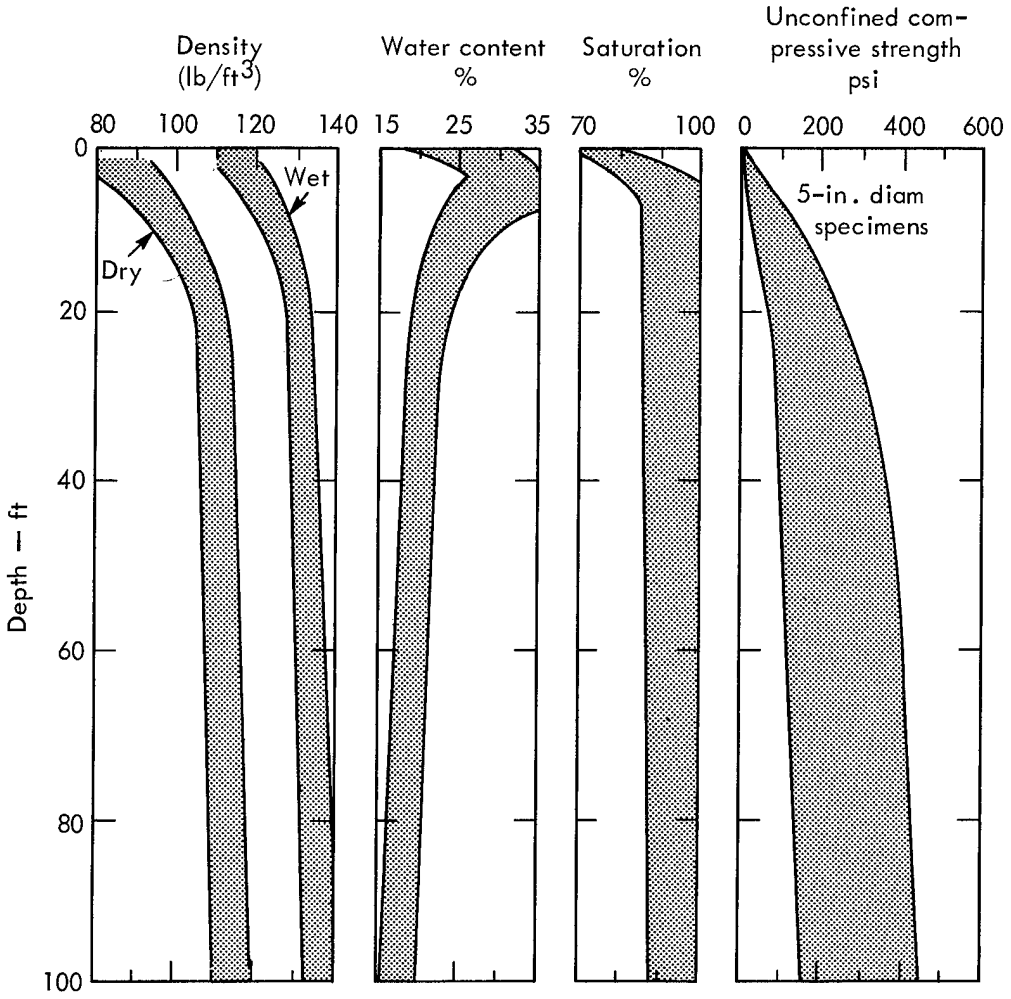

Fig. 5. Range of physical properties of Bearpaw shale at Pre-Gondola Site.

small-diameter, intact samples from the Bravo and Charlie SGZ boring confirm that the strength does increase with depth.

Moisture

Water contents range from as much as 30% near the surface to a rather consistent 16 to 18% at depth. Although most of the samples recovered were 100% saturated, a few were as low as 75%. The porosity ranges from 25 to 52%, and averages about 32%.

Density

The unweathered shale at the Fort Peck site has an average in situ wet density of 134 lb/ft^3 and a dry density of approximately 112 lb/ft^3. Samples recovered from the weathered zone are less dense and quite variable, with wet bulk densities of 110 to 125 lb/ft^3 and dry densities of 90 to 105 lb/ft^3.

Classification

When the shale is remolded, it classifies as a fat clay (CH), with a plastic limit of about 26% and a liquid limit ranging from 60 to 200%.

Seismic Velocity

The average seismic velocity for unweathered Bearpaw shale at the Pre-

Gondola site (to a depth of approximately 100 ft) is 6800 ft/sec.

Preshot Geophysical Measurements[7]

LRL performed a series of preshot geophysical measurements at the Pre-Gondola I site in the summer of 1966. These measurements, made in situ, were designed to fulfill two requirements: (1) to provide numerical values of properties of the medium which could be used in existing computer codes for predicting crater size, and (2) to aid in the interpretation and correlation of site geology.[5]

Four holes at the Pre-Gondola site were utilized for measurements: (1) I-19 at Delta, a satellite hole, (2) I-6 at Charlie, a satellite hole, (3) I-10 at Bravo, a satellite hole, and (4) I-9, the SGZ or emplacement hole at Bravo. These holes ranged in depth from 24.4 to 48.8 m, with a nominal diameter of 19 cm (7.5 in.).

The following logs were run in each hole: electric (except Delta I-19), density, gamma ray-neutron, caliper, continuous velocity (CVL), three-dimensional velocity (3-D), and seismic uphole-downhole. A detailed discussion of these measurements is contained in Ref. 7.

All measurements except gamma ray-neutron and electric logging appear to have yielded useful quantitative data. Average densities ranged from 2.11 to 2.42 g/cm^3, and average velocities fluctuated between 1732 and 2014 m/sec below the weathered zone. Laboratory density measurements performed by the U. S. Army Missouri River Division Laboratory compared favorably with those made by LRL.

GENERAL PROJECT LAYOUT AND SUPPORTING AGENCIES

Figure 6 shows the general layout of the project Pre-Gondola I experiment. The frontispiece shows the overall appearance of the site at the completion of the series to include the relative location of the earlier seismic site calibration series of June 1966.

Figure 6 shows the layout of support facilities. Support was provided as follows:

1. LRL provided HE charge assembly, emplacement, and arming and firing support. The timing and firing signals originated from the Control Point van (Fig. 7). Signals were transmitted to other technical program agencies, such as WES from this control point. LRL also provided HE and laser-radar safety coordinators.

2. Edgerton, Germeshausen and Grier (EG&G) provided scientific and documentary photography for all events (Figs. 8 and 9).

3. The Environmental Sciences Services Administration (ESSA-ARFRO) provided meteorological data throughout the series (Fig. 10).

4. The Corps of Engineers, Omaha District provided engineering design, construction, safety, operational, and logistical support to program participants (Fig. 11). The Missouri River Division, Corps of Engineers, provided overall supervision and services from the Division Laboratory. The Fort Peck Area Engineer was designated as the Contracting Officers Representative. The major construction work was accomplished under two lump sum contracts, one for subsurface and

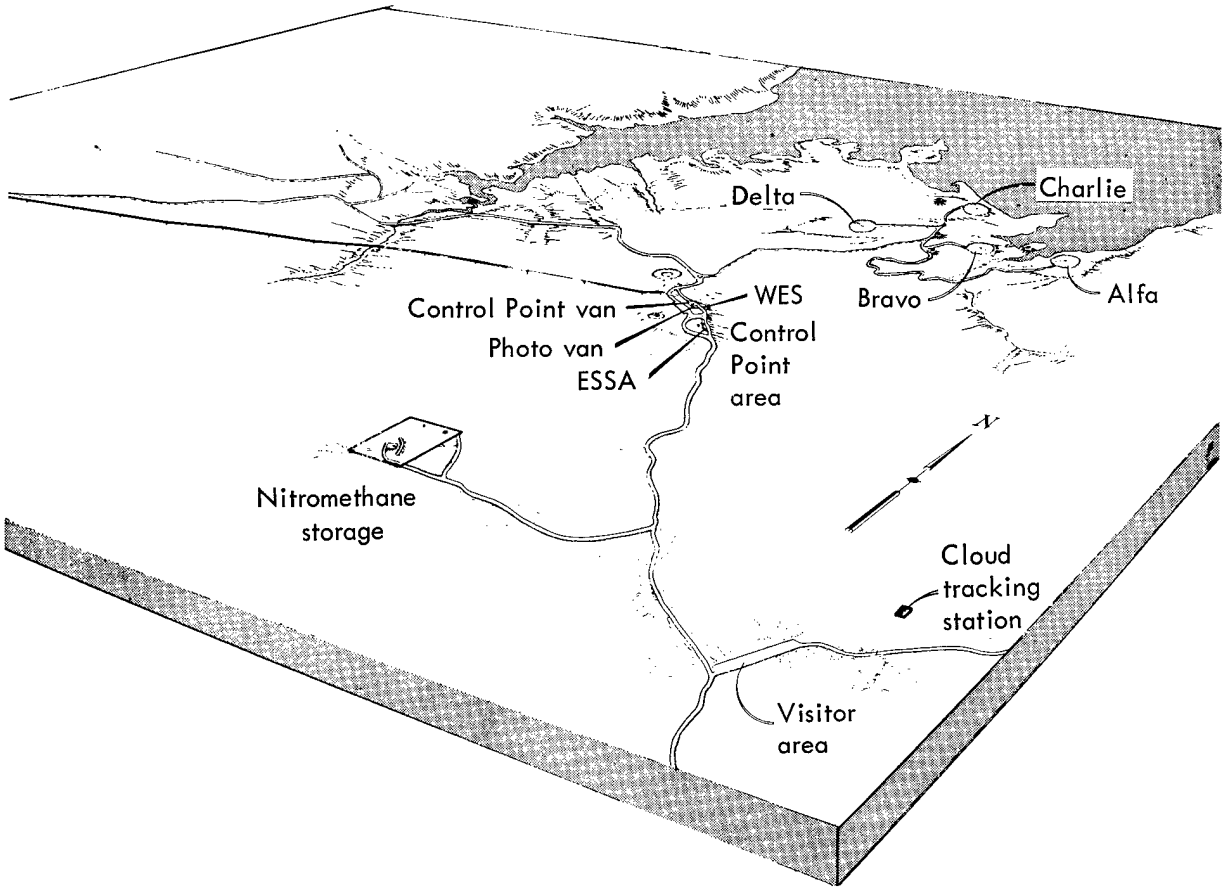

Fig. 6. General site layout.

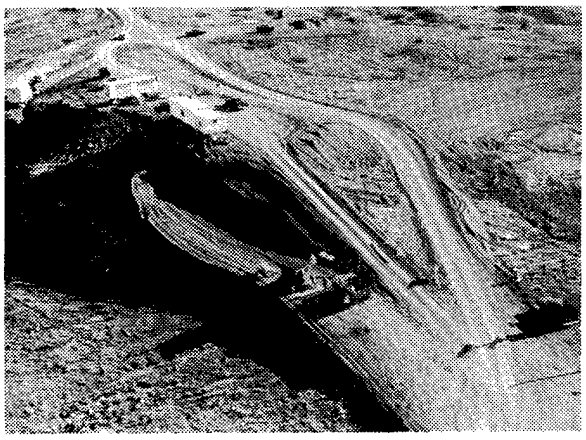

Fig. 7. Control point (L to R: WES, EG&G, and CP trailers).

Fig. 8. Support helicopter for aerial documentary photography by EG&G.

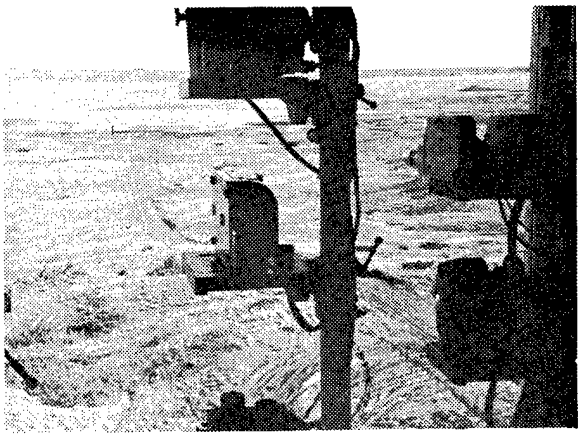

Fig. 9. View of Bravo GZ from EG&G photo van.

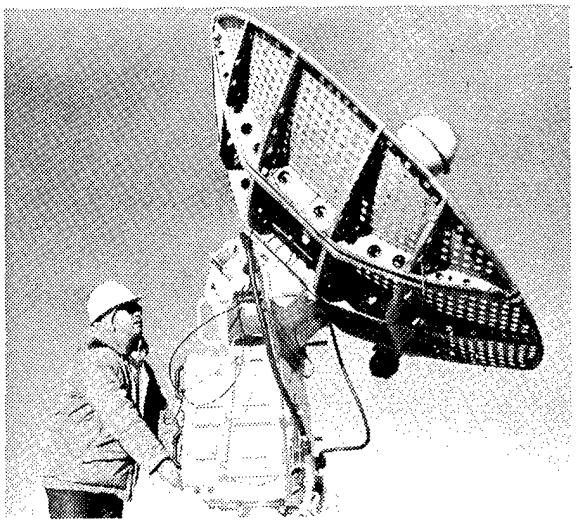

Fig. 10. Meteorological support.

Fig. 11. Bravo site under construction showing instrumentation cable trenches.

Fig. 12. Bravo Ground Zero area prior to arming by LRL.

one for surface facilities. Operational support was furnished by the surface contractor and hired labor. Logistics support was furnished by the Area Engineer.

5. The Fort Peck Area Engineer and representatives of the Montana State Fish and Game Department controlled access to the Charles M. Russell Game Range near the project site in the interest of public safety. They also conducted biological monitoring to determine the effects of the explosions on the fish in the reservoir (Fig. 12).

6. The WES Concrete Division developed access hole stem designs for Project Pre-Gondola I.

Figure 11 also shows the instrumentation cable trenches for AFWL and WES instrumentation for the Bravo Event. The instrumentation program evolved from earlier measurements taken during the SC-2 Event (Site Calibration) shown in the background.

Figure 12 shows the completed construction at the Bravo site. Surface motion targets were located at right angles to the line of sight of the EG&G cameras. Floating targets in the distance were used in cloud development studies. The captive fish were also stationed along the same line. A yellow dye marked the preshot ground surface in the vicinity of the expected crater; this aided postshot identification.

DESCRIPTION OF CHARGE AND EMPLACEMENT

General

Each chemical explosive charge for Pre-Gondola I consisted of approximately 40,000 lb (20 tons) of liquid explosive nitromethane, contained in a mined spherical cavity approximately 10 ft in diameter and center-detonated with a booster charge. Figure 13 shows the charge design. The centers of the cavities were located at the design DOBs (Fig. 14). The relationship to the geology and water table may be determined by comparing Figs. 4 and 14.

Cavity Construction

To construct the cavity, an access hole 38 in. in diameter was first drilled 8 ft 6 in. deeper than the center of the cavity. Figure 15 shows the auger attachment used for access hole drilling.

A spherical cavity, roughly 11 ft in diameter, was then excavated using standard mining methods with pneumatic and hand tools. Blasting was not required. During construction, a sump 3 ft deep was maintained at the bottom of the access hole for collection and control of ground water and to facilitate mucking operations. Rock anchors and shale pins were installed radially on a concentric ring pattern to insure personnel safety, cavity integrity, and support of the shotcrete wire fabric reinforcing. The cavity was brought into spherical tolerance, 10 ft 3-1/4 in. ± 1-1/4 in. in diameter, with pneumatically applied mortar (shotcrete) and made liquid tight with an elastomer seal coat reinforced with glass fabric. After completion, the cavities were filled with water which remained in the charge cavity during detonation of adjacent charges. Shortly before loading nitromethane, the water was removed by lowering a submersible pump down the vent line.

Booster Charge and Down-Hole Hardware Emplacement

The down-hole loading assembly (consisting of mounting ring, aluminum fill, and vent lines) was installed in the access hole above the cavity. The mounting ring was suspended from steel channels set in the access hole keyway by three 3/4-in. coil-proof chains and grouted in place. The booster charge, 6 lb of composition C-4 explosive in an aluminum canister detonated by two SE-1 high-energy detonators, was lowered down the vent line by hand and suspended at the cavity center after the emplacement of the nitromethane charge. Fill and vent lines were sand-stemmed.

Acess Hole Stemming

The access hole stemming material was designed to react to the explosion in the same manner as the surrounding *in situ* material. Stemming material consisted of colored concrete, the properties

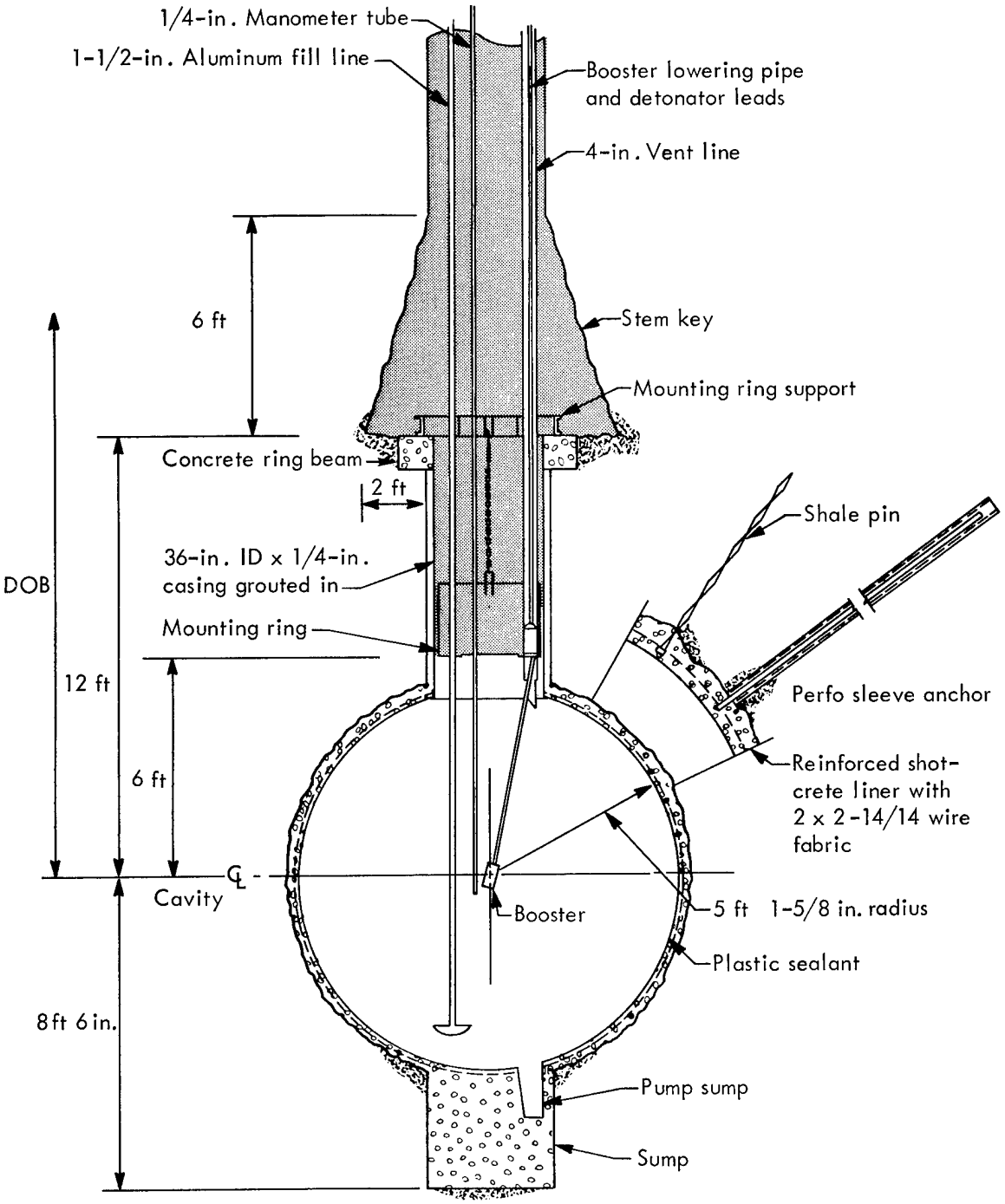

Fig. 13. Cross section of chemical explosive charge.

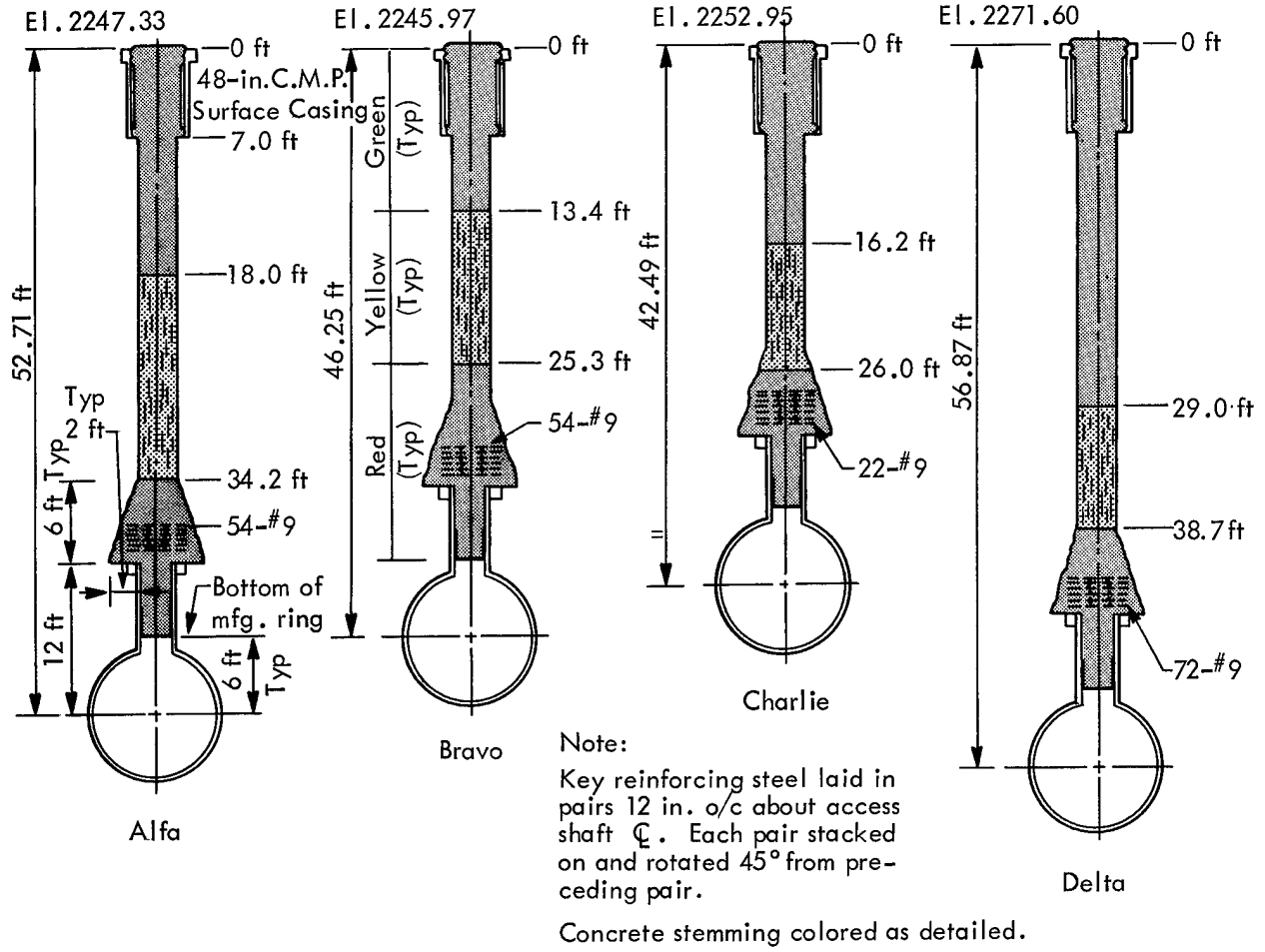

Fig. 14. Access hole stemming designs.

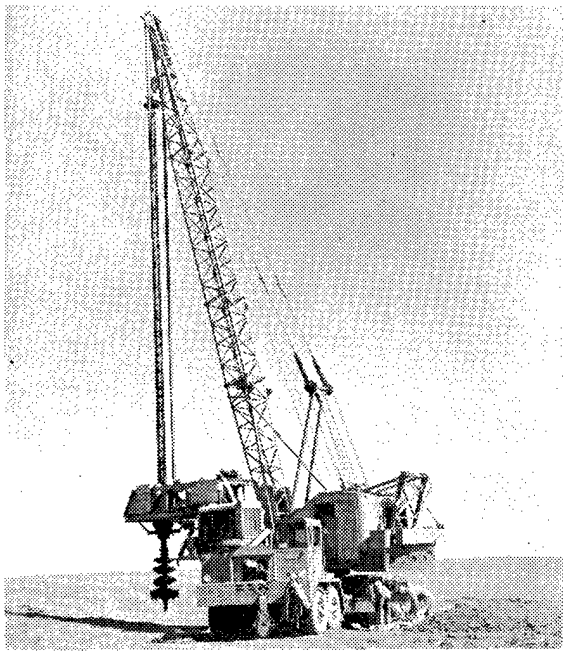

Fig. 15. Earth auger attached for drilling access hole.

of which matched as closely as possible the strength characteristics (compression, tension, shear) of the clay-shale. The concrete was color-layered to assist in the postshot identification and evaluation of the stemming effectiveness. The stemming configuration was designed to provide a total shear resistance equal to the total unconfined dynamic shear resistance of the in situ rock mass by bond (concrete to clay-shale) and reinforced shear keys.

Final stem designs, as developed by the WES Concrete Division, are shown in Fig. 14. The concrete design mixture used for stemming had a cement factor of 4.5 bags/yd^3, a water-cement ratio of 1.42 by weight, and slump of 3 in. ± 1/2 in.

The mixture proportions for one cubic yard were:

Material	Saturated surface dry weight (lb)
Cement Type III	423
Fine aggregate	2111
Lightweight aggregate (vermiculite)	161
Water	600
Concrete coloring	22.5
Aluminum powder	13.5 g

The results of tests on stemming concrete samples are as follows:

Site	Age, days (at detonation)	Average compressive strength (psi)
Alfa	13	445
Bravo	12	430
Charlie	15	360
Delta	21	520

Nitromethane Emplacement

The explosive, nitromethane, was transported to the project site in factory-sealed 55-gal drums. On the day preceding the scheduled detonation, the nitromethane was transferred from the drums to the cavity by gravity flow through plastic hoses connected to an aluminum manifold, thence to the 1-1/2-in. fill line extending down through the access hole stemming into the cavity. The loading operation is illustrated in Fig. 16.

Cavity Performance

Each cavity was instrumented during the detonation of adjacent prior events. A water shock gage was placed in the water in the cavity and a stress gage was placed in the ground outside the cavity. Details and results are reported under Engineering Properties Investigations. Under the loadings experienced, all cavities retained their integrity.

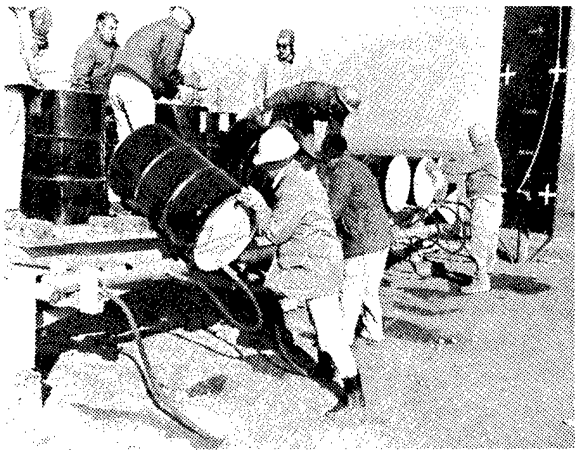

Fig. 16. Nitromethane transfer.

DESCRIPTION OF DETONATIONS

All events were planned for detonation in the forenoon on the scheduled date to insure adequate lighting for photography and to take advantage of minimal expected winds (surface winds generally increase around noon).

Pertinent information concerning the detonations is contained in the Introduction. Figures 17 through 21 depict the overall appearance characteristic of the detonations. Several observers noted the marked difference in mound growth and cloud formation as compared to previous cratering experience in hard dry rock and desert alluvium. Lack of massive venting of hot gases and very rapid dissipation of dust and steam in the clouds are

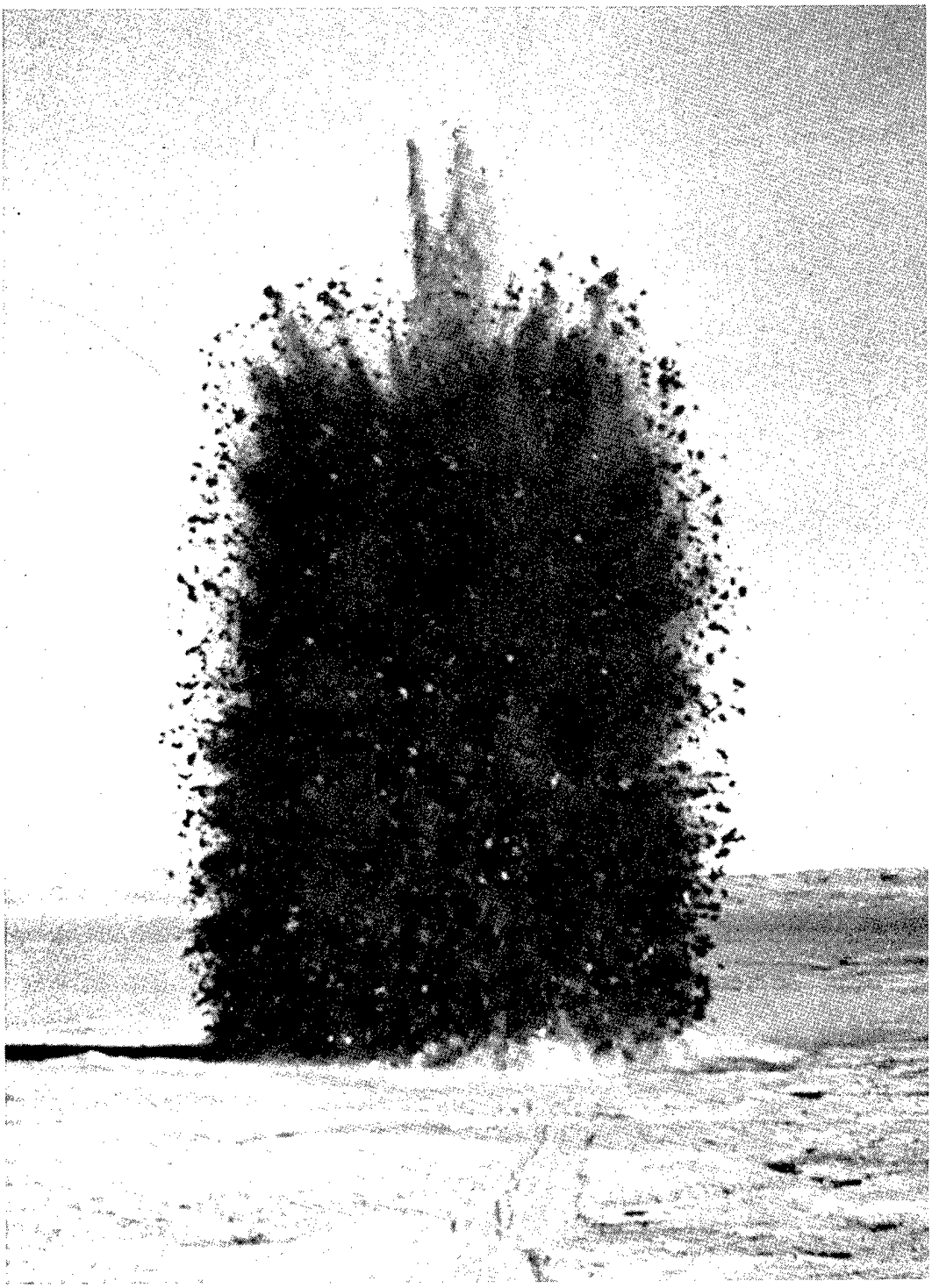

Fig. 17. Maximum mound development, Bravo.

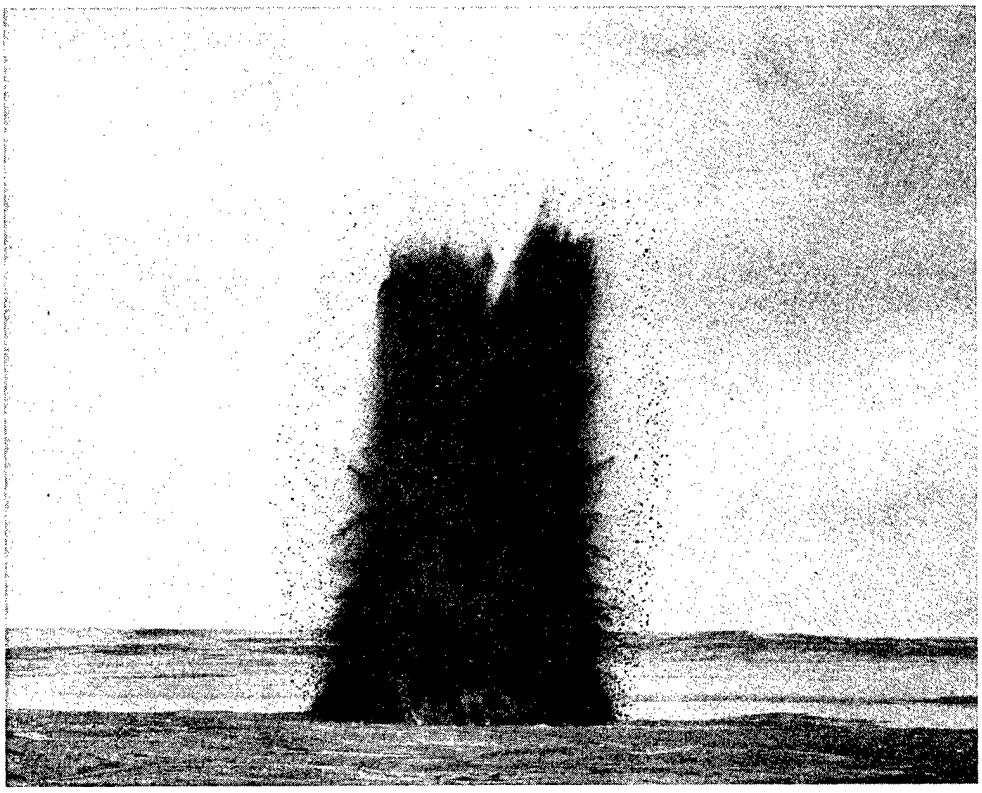

Fig. 18. Maximum mound development, Charlie.

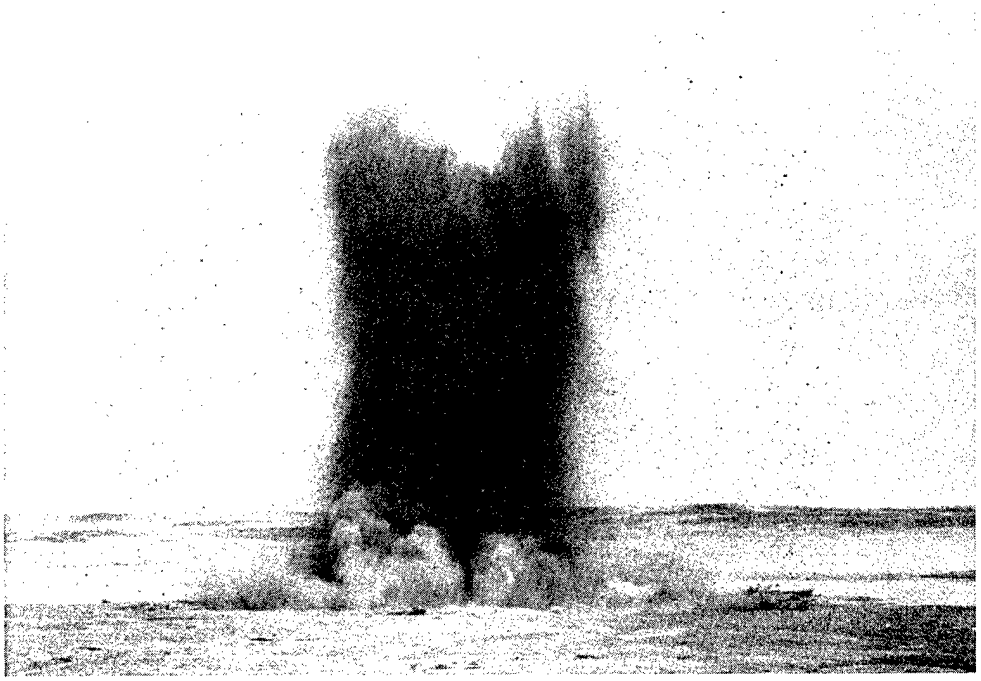

Fig. 19. Collapsing mound, Charlie.

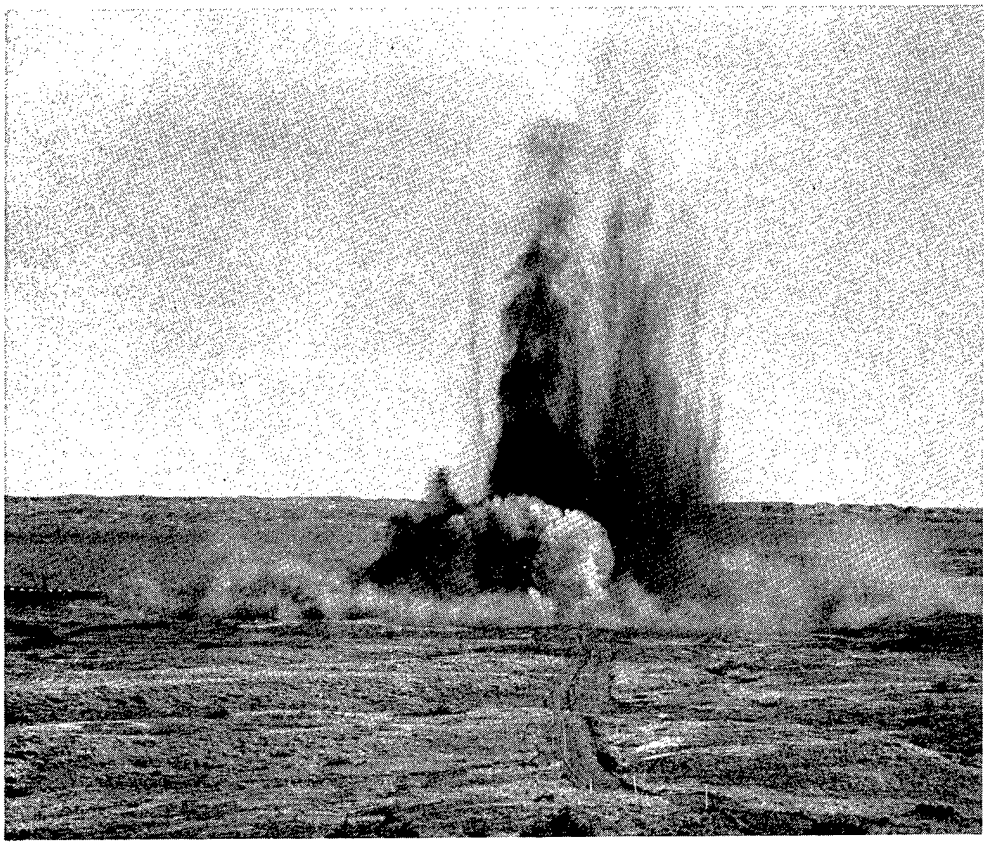

Fig. 20. Base surge development, Bravo (note steam cloud beginning to emerge at center and diffuse sand and vermiculite stemming material in main cloud).

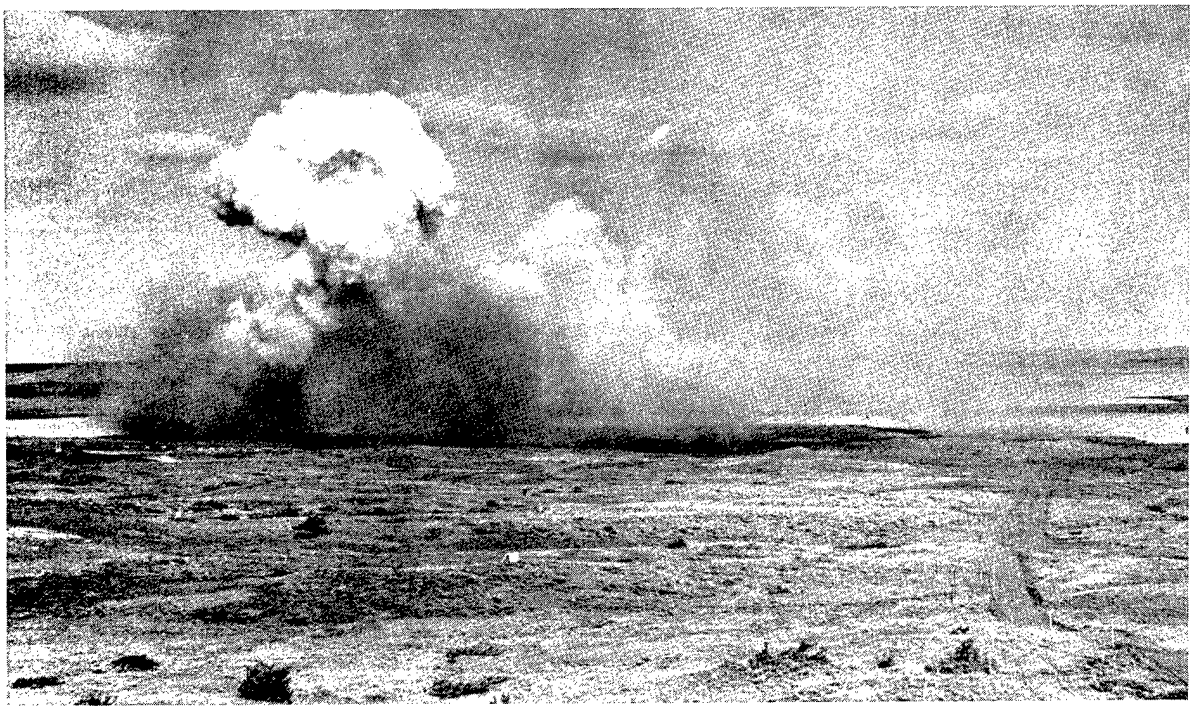

Fig. 21. Steam cloud from Charlie after base surge has diffused.

Table I. Energy equivalent yields.[a]

Event	Charge weight (tons)	Energy equivalent yield (kt)
Alfa	20.35	0.02239
Bravo	19.36	0.02130
Charlie	19.62	0.02158
Delta	20.24	0.02226

[a]Based on assumption that an energy equivalent yield of 1 ton releases 10^9 cal and that NM releases 1.227 cal/g of charge weight. A working value of 1 ton = 0.0011 kt is used for convenience.

characteristic of cratering detonations in wet clay shale at Fort Peck.

For purposes of data analysis, the energy equivalent yield was calculated from the weighed amount transferred to the cavity. There were no losses of nitromethane recorded by the manometer liquid level gage. Accuracy of gage readings was verified by bailing. Table I lists the energy equivalent yields.

Crater Measurements and Ejecta Studies

This section summarizes crater measurements and ejecta studies which have been reported separately.[6] Results of the related ground surface motion studies are presented in the next section. These crater studies technical subprograms had the following common objectives:

1. To extend single-charge explosive cratering experience to a weak, wet, clay-shale medium.

2. To calibrate the Pre-Gondola project site with respect to its cratering characteristics and to provide design input to the design of the planned Pre-Gondola II and III row-charge cratering detonations at the same site.

3. To provide experimental data for use in theoretical studies of crater formation and for the design of future single- and row-charge cratering detonations in similar media.

INTRODUCTION

Objectives

Crater Measurements

The technical objectives of the crater measurement program were: (1) to determine the size and shape of the apparent craters and crater lips produced by detonations at varying depths of burial; (2) to determine the maximum range of missiles resulting from each of the detonations; and (3) to analyze and to present the data in a manner readily useable in the design of future cratering events.

Ejecta Studies

The technical objectives of the ejecta study program were: (1) to determine the origin, residual displacement, and deposition of material ejected from the crater, and (2) to present the data in a manner readily useable in the design of future cratering events.

Background

After the Pre-Gondola project site was determined[5] the Pre-Gondola I SGZ locations were selected on the basis of suitable topography and suitable, though minimal, distances between the SGZ locations. The 1000-lb Seismic Site Calibration Events were then located to provide both a seismic source near each of the Pre-Gondola I sites and preliminary cratering data (see Frontispiece).

A wide range of DOBs was employed for the 1000-lb shots so that the cratering characteristics of Bearpaw shale could be approximated. The resulting preliminary cratering curves were utilized to select the depths of charge emplacement for the 40,000-lb Pre-Gondola I detonations.

Relationship of Subprograms

In past cratering experiments, crater measurements and studies of ejecta and surface motion have been separately reported with few deliberate attempts at correlation. In Pre-Gondola I, these studies coupled with a portion of the engineering properties technical program constituted an integrated effort to gain a better understanding of cratering phenomenology.

The shape and velocity of the mound rising over SGZ are indicators of the response of the medium to the detonation

and can be used to study crater formation. The ejecta data, along with surface motion observations, can be used to develop the medium response at various depths and to arrive at an estimate of subsurface motion. Crater measurements data define the preshot and postshot topography which represent boundary conditions in the interpretation of the mechanics of crater formation.

EXPERIMENTAL PROCEDURES

Surface Ground Zero Layout

Figure 22 shows the orientation and layout of the experimental programs. The SGZs were all visible from the command post and camera stations. The surface motion target array was perpendicular to the line of sight to the CP camera station. One ejecta pellet array was located along a surface motion target array for each shot. In addition, pellets were located along one of the Bravo instrumentation lines to correlate with the engineering properties technical program. After each detonation, pins were also installed on the crater slopes to measure displacements from subsequent dynamic loads and longer term effects.

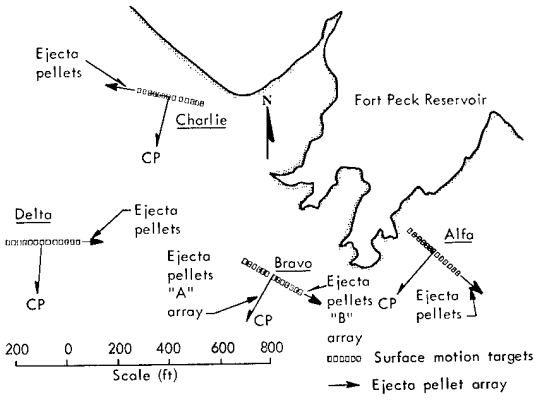

Fig. 22. Location of ejecta pellet arrays and surface motion targets.

Mapping and Photography

Aerial Stereophotogrammetric Mapping

Preshot and postshot topographic maps for each event were prepared from aerial photographs by Continental Engineers of Denver, Colorado. A 6-in. focal length camera and a 9- × 9-in. format were used. Flight altitude was 1200 ft above the ground resulting in a negative scale of 1 in. equals 200 ft. An area 800 ft square was mapped for each event. Additional preshot and postshot mapping photography was taken to document the site (Fig. 23).*

Isopach-Type Maps

The apparent crater dimensions were determined by comparing the preshot and postshot topographic surfaces of each crater area. In order to illustrate the changes in the ground surface caused by the detonation, a map very similar to an isopach map was used. The isopach-type maps were prepared by: (1) superimposing the preshot and postshot topographic maps (2) plotting the value of the positive or negative difference between the preshot and postshot contour lines at their points of intersection and (3) contouring the plotted points.[6] The resulting map consists of contours of the interval between the preshot and postshot ground surfaces. The zero contour lines follow the trace of the intersection of the preshot and postshot ground surfaces. The inner zero contour line delineates the outline of the apparent crater, and the outer zero contour line delineates the outer boundary

Fig. 23. Pre-Gondola I preshot aerial photography.

of continuous ejecta. Negative contour lines show the configuration of the apparent crater. Positive contour lines show the configuration of the apparent crater lip. This map may be used to determine directly all apparent crater measurements of interest.

Determination of Apparent Crater Dimensions and Maximum Missile Range[6]

(On page vi is a list of the nomenclature used for crater measurements.)

Average Apparent Crater Radii, R_a

The area inside the inner zero contour line on the isopach-type map was measured with a planimeter, and the average apparent crater radius, R_a, was calculated as the radius of a circle having the same area.

Apparent Crater Depth, D_a

Because all of the Pre-Gondola I sites were essentially level, the depths of the apparent craters, D_a, were measured as the difference in elevation between the deepest point in each crater and the elevation of the preshot ground surface vertically above that point. The apparent depths of each crater may be read directly from the isopach-type map.

Average Apparent Lip Radii, R_{al}

The trace of a line drawn along the crest of the apparent lip on either the postshot topographic map or the isopach-type map corresponds to the outline of the lip crest radius. The average lip crest radius, R_{al}, was determined in the same manner as the average apparent crater radii.

Average Apparent Lip Height, H_{al}

The average apparent lip height, H_{al}, was determined by: (1) plotting from the isopach-type map a profile of the relief along the apparent lip crest (2) using a planimeter to determine the area between the lip crest profile and the zero level on the profile, and (3) dividing the measured area by the length of the lip crest profile.

Average Radius of Outer Boundary of Continuous Ejecta, R_{eb}

The area inside the outer zero contour line on the isopach-type map was measured with a planimeter, and the average radius of the outer boundary of continuous ejecta, R_{eb}, was calculated as the radius of a circle having the same area.

Apparent Crater Volume, V_a

The apparent crater volume, V_a, was determined by (1) measuring with a planimeter the area inside each negative contour line on the isopach-type map, and (2) calculating, by use of an average end-area method applied to horizontal sections taken at 1-ft intervals (the contour interval of the large scale isopach-type map), the total volume of the apparent crater.

Apparent Lip Volume, V_{al}

The apparent lip volume, V_{al}, was determined in a manner similar to that of the apparent crater volume. The average end-area method was applied to the areas of the positive contour lines on the isopach-type map.

Maximum Range of Missiles

The maximum range of missiles was determined by (1) locating and marking

the most distant missiles found around the perimeter of each crater, (2) photographing the marked missiles found around the perimeter of each crater, and (3) measuring on aerial photographs the most distant missile marked.

Ejecta Pellets[6]

Emplacement

Prior to the event, individually coded pellets were placed in an array of five vertical holes which extended from a point near the SGZ to a point slightly beyond the predicted apparent crater radius. At the Bravo site two arrays of emplacement holes were constructed (Fig. 22).

Characteristics

The ejecta pellets consisted of cylinders (3 in. in diameter by 12 in. in length) of colored concrete grout which contained colored glass fragments. A separate color of concrete grout was used for each emplacement hole in any one array. Within each hole the position of each pellet was coded by the color or the combination of colors of its glass fragments. The elevation of the top of each pellet was recorded to the nearest one-tenth of a foot after which concrete grout was used to fill the space between the ejecta pellets and the walls of the emplacement holes.

Postshot Location and Data Reduction

After each detonation, the location, approximate size, and individual code of each pellet which could be found was determined and recorded. The distance and bearing from existing reference points to the postshot position of each pellet was provided by a field survey team. These field data were converted to the actual postshot locations and distances relative to the SGZ of the particular event and the location plotted with respect to the crater.

SCALING AND PREDICTIONS

Prediction Procedure

The predicted crater dimensions were based on data from the four 1000-lb Seismic Site Calibration shots,[6] scaling experience in hard rock and alluvium, and limited small-charge cratering data in other clay-shale formations.[1] The maximum missile range predictions were based on previous experience in hard rock and alluvial media and the observed ranges of the 1000-lb shots. It was believed that $W^{1/3.4}$ scaling should apply to crater dimensions and would also provide a conservative prediction of maximum missile range for operational safety. For convenience, all data are normalized to 1-kt energy equivalent yield.

Energy Equivalent Scaling Factor

The basis of the scaling calculations assumes the energy equivalent yield of 1 kt (2,000,000 lb) to be the same as the release of 10^9 kcal of energy. Thus, an energy equivalent yield of 1 g is:

$$1\ \text{g} = \frac{10^9\ \text{kcal of energy}}{(2{,}000{,}000\ \text{lb})\ (453.5924\ \text{g/lb})}$$

$$= 1.1023\ \text{kcal}$$

The experimental heat of detonation of nitromethane is 1.227 ± 5 kcal per g.[8] Therefore, the actual weights of nitromethane were converted to energy equivalent yields by multiplying the actual

weight of nitromethane by the ratio:

$\frac{1.227 \text{ kcal}}{1.1023 \text{ kcal}} = 1.113 \approx 1.1$ (1 ton = 0.0011 kt)

where the ratio value of 1.113 was rounded to a working value of 1.1.

Table II gives the actual weights, energy equivalent yields, and scaling factors for each of the Pre-Gondola I events.

Table II. Charge yields and scaling factors.

Event	Actual charge weight (tons)	Energy equivalent yield (kt)	Scaling factor, $kt^{1/3.4}$
Charlie	19.62	0.021582	0.3238
Bravo	19.36	0.021296	0.3225
Alfa	20.35	0.022385	0.3273
Delta	20.24	0.022264	0.3267

Predicted Crater Parameters

Table III gives the preshot predictions based on the stated prediction procedure and assuming all charges would be loaded with 20 tons of nitromethane (NM).

Table III. Predicted crater dimensions for Pre-Gondola I.[9]

	Depth of burst		Apparent crater radius		Apparent crater depth		Maximum range of missiles	
Event	1 kt	20 tons	1 kt	20 tons	1 kt	20 tons	1 kt	20 tons
Charlie	130	42.4	240	78.3	115	37.5	4200	1370
Bravo	142	46.3	240	78.3	113	36.8	3550	1160
Alfa	160	52.2	237	77.3	105	34.2	2750	900
Delta	174	56.7	227	74.0	93	30.3	2250	730

Notes: 1. Scaling factor $= \left[\frac{20 \times 1.1}{1000}\right]^{1/3.4} = 0.3261$.

2. All dimensions in feet.

LRL CODE CALCULATIONS

Terhune and Cherry calculated the dimensions of the Bravo crater using the Tensor code.[10,11] The calculated ejecta boundary and throwout distributions are shown in Fig. 24. The superimposed average apparent crater dimensions reflect differences between the volume defined by the calculated ejecta boundary and the bulked volume of throwout and fallback.[11] In addition, there is an increase in volume due to uplift in the rupture zone.

Experimental data used in the calculation were obtained from in situ geophysical

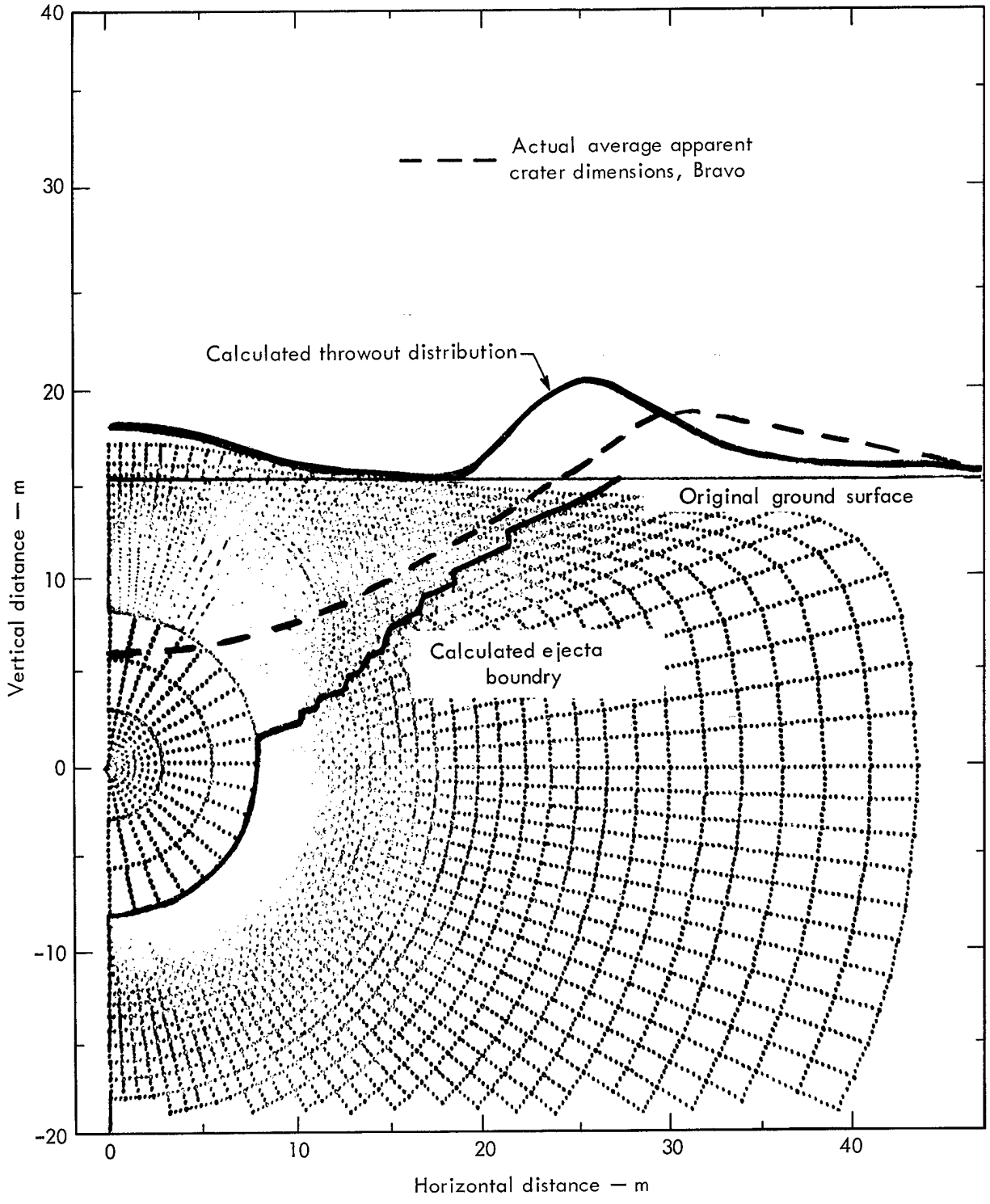

Fig. 24. Tensor calculations vs actual apparent crater dimensions, Pre-Gondola I Bravo (after Terhune and Cherry, Ref. 10).

logging measurements[7] and laboratory measurements of the strength properties of the shale. Compressional velocity as a function of depth was measured in situ. Mohr envelopes were obtained from triaxial tests. Figure 25 shows the results from Stephens' special hydrostatic compressibility tests (to 40 kbar) on a shale sample.[12] The medium density as determined from Birdwell density logs averaged 2.18 g/cm^3. The density used in the calculation 2.193 g/cm^3 was from a sample at shot depth.

The elastic constants used in the Tensor code calculation are listed in Table IV.

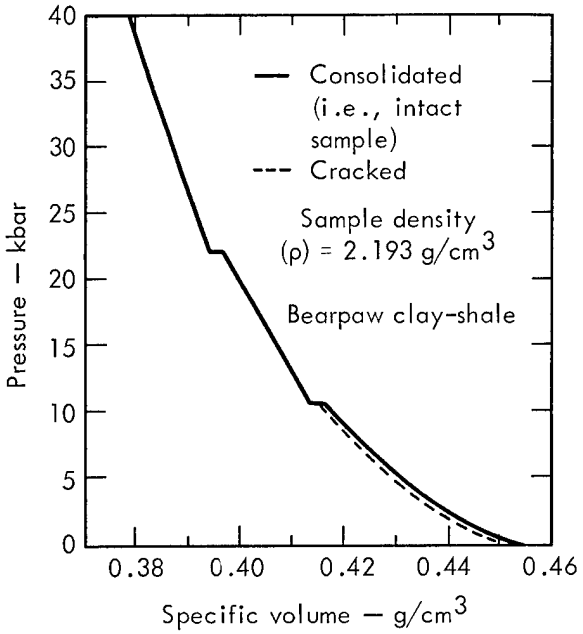

Fig. 25. Pressure-volume hydrostatic compression curve (Refs. 10, 12).

RESULTS

The apparent crater measurements, maximum missile range, and ejecta pellet recovery for the four detonations are tabulated in Table V in DOB order.

These results show that, except for the depth of the Bravo crater, the progressively shallower DOB produced craters with progressively greater dimensions. It is interesting to note that, although the difference of the average lip radius of the largest crater (Charlie) and the smallest crater (Delta) is only 6.3 ft, the difference between the average apparent crater radii of the same two craters is 15.3 ft. The small difference in the average lip radii causes the craters to appear to be about the same size (Fig. 26). However, the actual apparent crater volume of the largest crater is more than twice that of the smallest crater.

Detailed results of ejecta pellet recovery are contained in Ref. 6. Preshot and postshot locations of the pellets are shown in drawings in the following sections.

In addition to average data reported in Table V, it is noted that one sizeable ray of fallback was deposited in each crater, usually extending to the limit of continuous ejecta.

Charlie Event

The preshot ground surface for Charlie (Fig. 27) had a downhill slope of 2-1/2 deg

Table IV. Elastic constants for Tensor calculations.[10]

Constants		Consolidated[a]	Cracked
Bulk Modulus	K (kbar)	31.42	79.02
Poisson's Ratio	σ	0.1487	0.1487
Density	ρ_o (g/cm^3)	2.193	2.193

[a]Stephens' nomenclature for an intact sample.

Table V. Crater measurements.[6]

Dimension[a]	Units	Event			
		Charlie	Bravo	Alfa	Delta
Charge weight, W	(tons)	19.62	19.36	20.35	20.24
Energy equivalent scaling factor	($kt^{1/3.4}$)	0.3238	0.3225	0.3273	0.3267
Depth of Burst, DOB	(ft)	42.49	46.25	52.71	56.87
Scaled dob	($ft/kt^{1/3.4}$)	131.2	143.4	161.1	174.0
Average radius, R_a	(ft)	80.4	78.5	76.1	65.1
Scaled r_a	($ft/kt^{1/3.4}$)	248.0	243.4	232.5	199.3
Maximum radius	(ft)	84.0	80.9	80.8	70.5
Minimum radius	(ft)	74.3	75.0	60.0	52.0
Depth, D_a	(ft)	32.6	29.5	32.1	25.2
Scaled d_a	($ft/kt^{1/3.4}$)	100.7	91.5	98.1	77.1
Average lip crest radius, R_{al}	(ft)	101.8	102.1	100.4	94.5
Scaled r_{al}	($ft/kt^{1/3.4}$)	314.4	316.6	306.8	287.4
Maximum radius	(ft)	106.9	107.9	107.6	99.7
Minimum radius	(ft)	95.9	96.9	92.4	89.0
Average lip height, H_{al}	(ft)	14.5	13.7	13.9	13.0
Scaled h_{al}	($ft/kt^{1/3.4}$)	44.8	42.5	42.5	39.8
Maximum height	(ft)	17.2	16.1	18.4	20.0
Minimum height	(ft)	12.4	10.8	9.9	6.2
Average radius of lip Boundary, R_{eb}	(ft)	294	265	227	221
Scaled r_{eb}	(ft)	908	822	694	676
Apparent crater volume, V_a	(ft^3)	277,550	241,260	235,300	133,880
Scaled v_a	($ft^3/kt^{1/3.4}$)	857,150	748,090	718,906	409,800
Apparent lip volume, V_l	(ft^3)	694,452	533,620	483,057	427,033
Scaled v_l	($ft^3/kt^{1/3.4}$)	2,144,694	1,654,635	1,475,884	1,307,110
Maximum missile range, R_{me}	(ft)	800	905	545	453
Scaled r_{me}	($ft/kt^{1/3.8}$)[b]	2,200	2,500	1,490	1,240
Ejecta pellet recovery	(%)	28.3	10.6[c] 16.8[d]	14.9	31.2
Maximum ejecta pellet range	(ft)	327	325[c] 404[d]	277	294
Scaled	($ft/kt^{1/3.4}$)	1,010	1,008[c] 1,253[d]	846	900

[a]Scaled dimensions are indicated by lower case letters.

[b]Revised.

[c]Referred to as "A" array in text.

[d]Referred to as "B" array in text.

Fig. 26. Pre-Gondola site after completion of seismic and cratering calibration.

towards the southeast. The postshot topographic map (Fig. 28) shows the size and shape of the apparent crater and lip and also a ray of material extending in a direction of S70°E from the bottom of the crater. This ray lies almost directly downhill and is about 5 ft thick in the crater and somewhat smaller and broader outside the crater. Much of the material in this and similar rays was identified as the colored stemming material. There were many fine sand and vermiculite particles with very few pieces larger than 1 in. in diameter.

The Charlie crater was the most symmetrical of the four craters, although its deep point was displaced about 10.5 ft in a northeast direction from SGZ and the relatively flat bottom of the crater was rectangular in shape. Figure 29 shows orthogonal profiles drawn through the apparent crater and lip, and Fig. 30 is an isopach map of the interval between the preshot and postshot ground surfaces.

The block-size of the ejecta produced by the Charlie crater was generally less than 1.5 ft in diameter, except within the crater and along the lip crest where many blocks 2.0 ft or more in diameter were found. In general, the block size was comparable to that produced by the Alfa and Delta detonations, but was considerably less than that produced by the Bravo

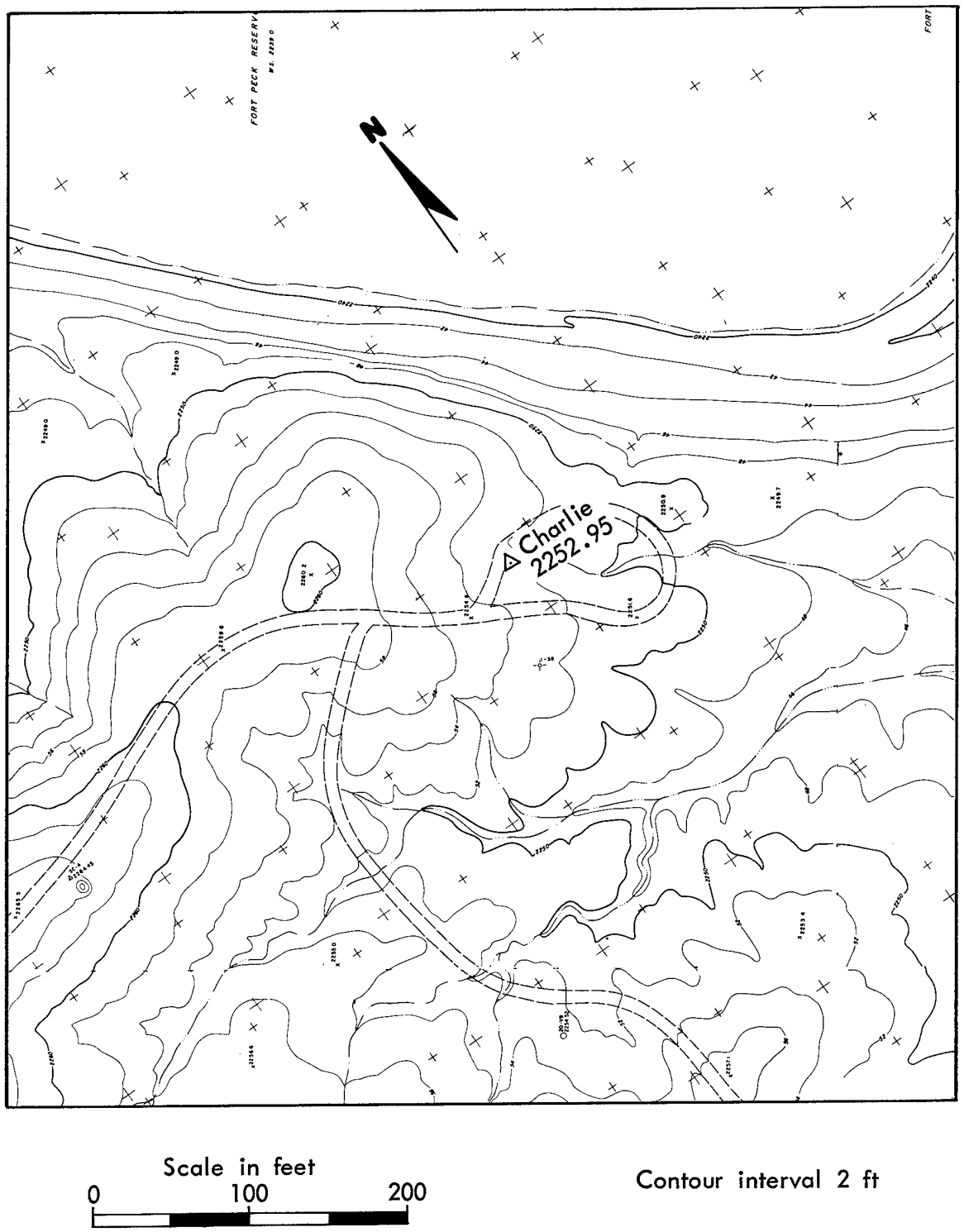

Fig. 27. Preshot topographic map for Pre-Gondola I Charlie.

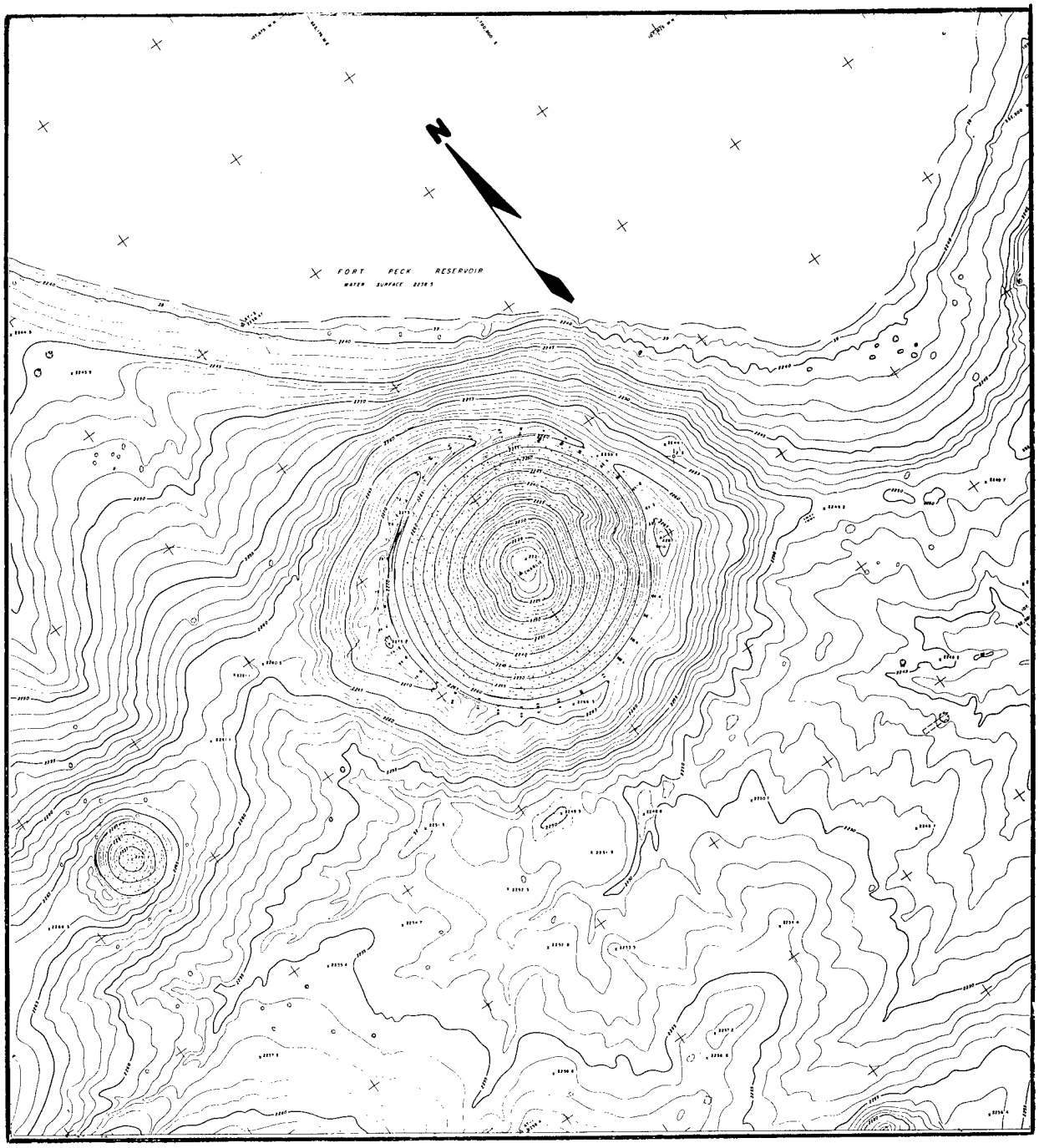

Fig. 28. Postshot topographic map for Pre-Gondola I Charlie.

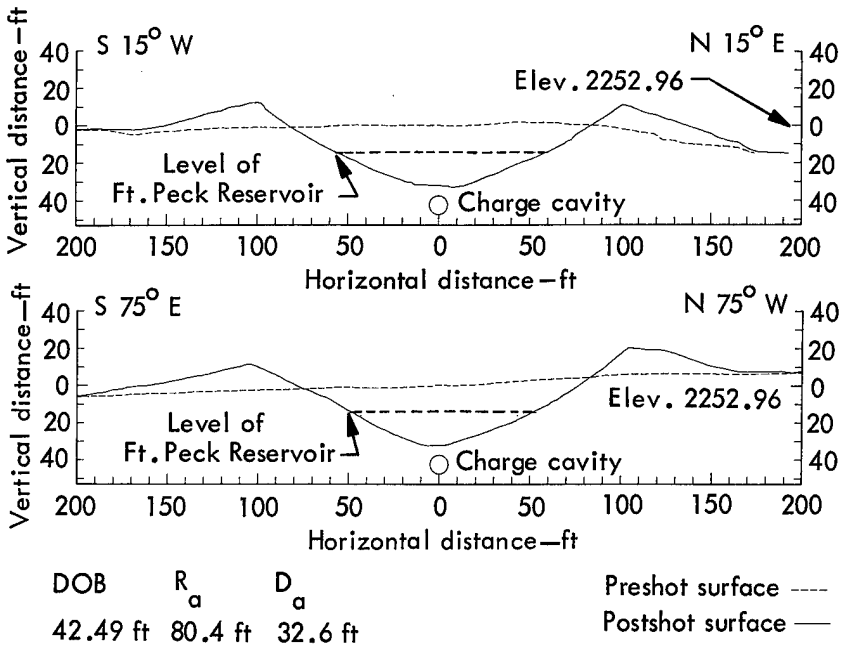

Fig. 29. Charlie crater profiles.

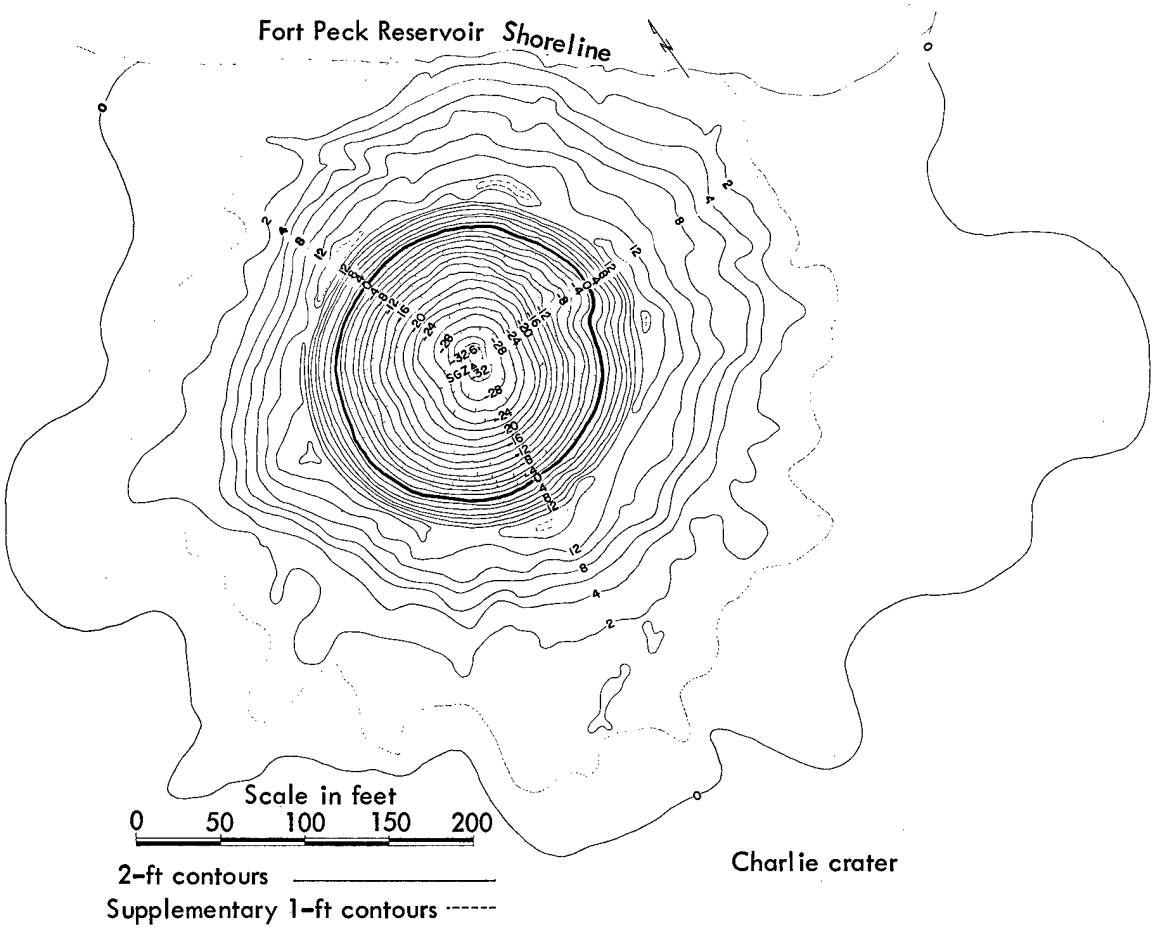

Fig. 30. Contour map of interval between preshot and postshot ground surface, Charlie crater.

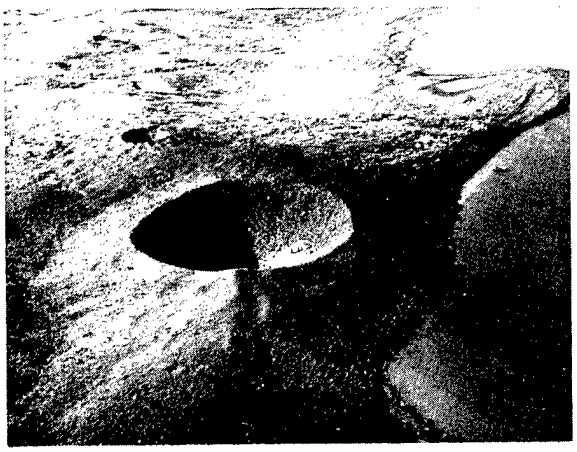

Fig. 31. Charlie crater, 28 October 1966.

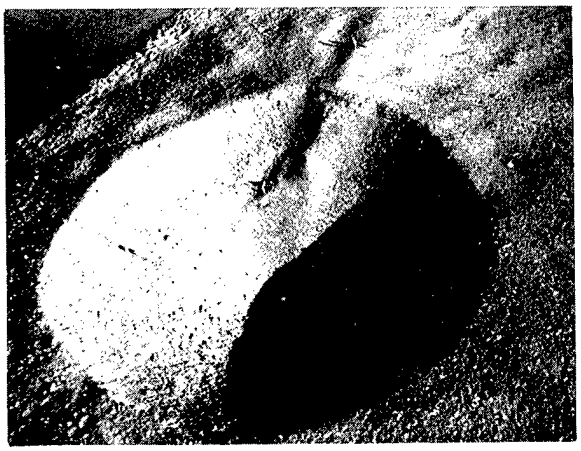

Fig. 32. Charlie crater measurements.

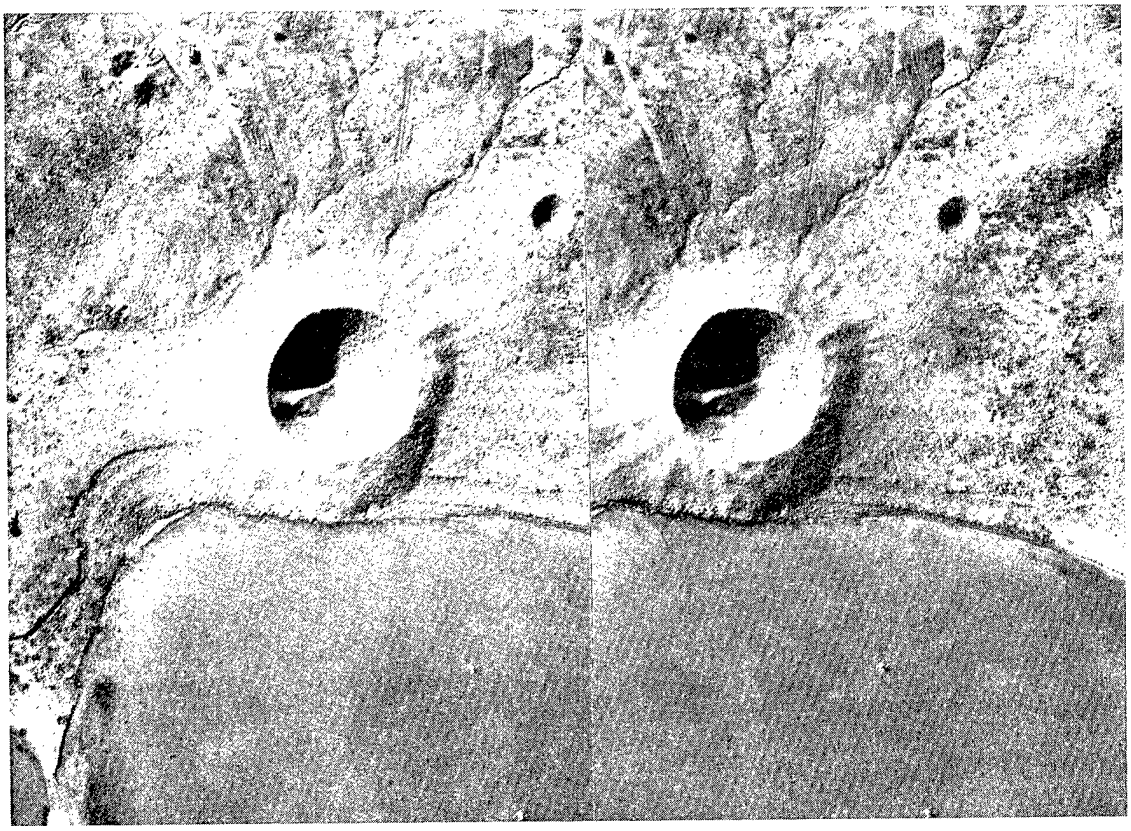

Fig. 33. Stereo-pair, Charlie crater.

Event. Figures 31 and 32 are photographs of the crater at the time crater measurements were taken. Both figures show the relative block-size produced by the detonation. Note the men in Fig. 32. A number of impact craters can be seen along the shoreline (Fig. 31).

Figure 33 is a stereo photograph which can be used to study the ray and ejecta pattern in more detail.

Harlan[6] noted details of cracks unique to this crater that were not found in the other craters. Two cracks developed in the inside upper (northwest) slope of the

Charlie apparent lip. The longest crack was more than 100 ft in length and its position ranged between 3 and 9 ft below the south-southeast segment of the lip crest. The other crack, which occurred on the west side of the crater, was less than 40 ft long and was located between 10 and 14 ft below the lip crest. The longest crack was first observed about 10 min after the detonation at which time its width was about 1 in. It gradually widened during the next 1/2 hr after which its growth stopped. No further growth of the crack was observed during the following week. The final average width of the crack was about 2 in. and the vertical displacement was about 3 in.

Plans were made in the field to monitor during the remaining detonations and before, during, and after the Pre-Gondola II row-charge cratering experiment the slopes and lips of all 20-ton craters which connected to the Charlie crater. Slope pins were installed in the Charlie crater and surveyed during the crater measurements. Results of measurements obtained after the Charlie crater was subjected to subsequent dynamic loadings from other detonations are reported under Engineering Properties Investigations.

Twenty-eight percent of 106 ejecta pellets installed at the Charlie site were recovered. This recovery percentage was second only to the Delta Event. The average recovery percentage was 20.4%. Figures 34 and 35 show the locations of the postshot positions of the ejecta pellets found after the Charlie Event.

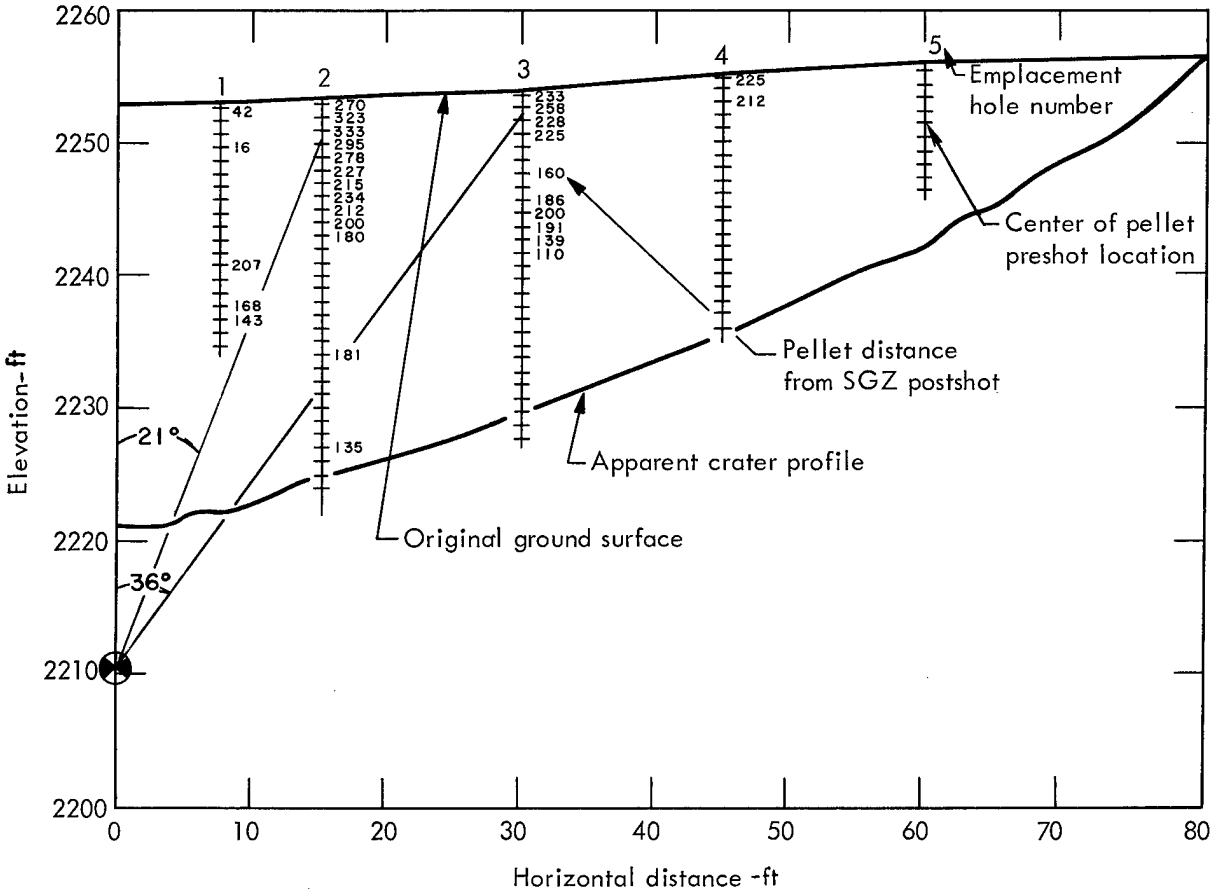

Fig. 34. Preshot and postshot location of Charlie ejecta pellets.

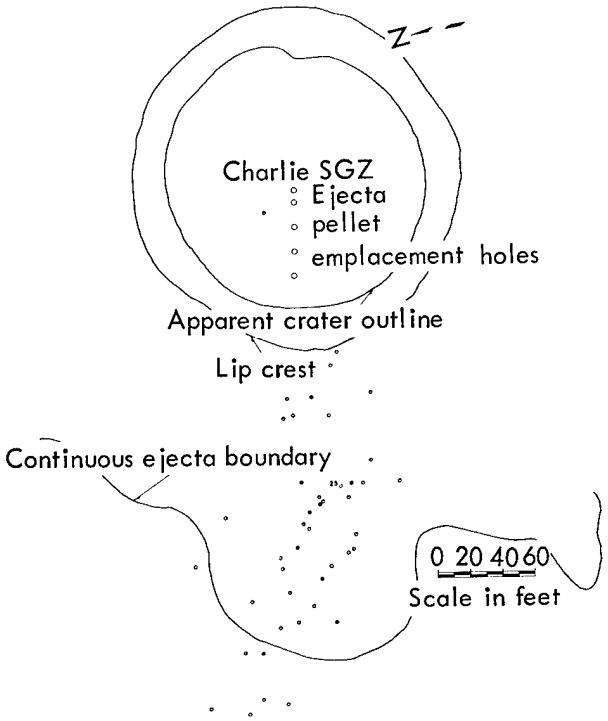

Fig. 35. Postshot locations of Charlie ejecta pellets.

Bravo Event

The preshot ground surface for Bravo (Fig. 36) had a slope of only 1 deg towards the north. The postshot topographic map (Fig. 37) shows the apparent crater and lip. The small ray or mound of stemming material extends in a northerly direction from the bottom of the crater but did not extend outside the crater as noticeably as the rays of the other three detonations. It may be identified also on the N30°E profile (Fig. 38) as an irregularity.

The shape of the Bravo crater was nearly symmetrical, except for a mound or shoulder on the north slope of the crater and a 9-ft displacement of the deepest point of the crater in a southeast direction from the SGZ. The volume of the Bravo apparent crater was second only to that of the Charlie crater. Figure 38 shows preshot and postshot orthogonal profiles drawn through the crater, and Fig. 39 is a contour map of the interval between the preshot and postshot ground surfaces. Figure 40, an oblique photograph of the Bravo crater, shows the mound in the crater, and Fig. 41 shows vividly the occurrence of large impact craters around the crater. Figure 42 shows the relatively large block-size of the fragments that make up the apparent lip and fallback material. The very large ejecta blocks, shown in Fig. 18 at the time of maximum mound development, produced impact craters in the softer shale at the edge of the reservoir. Figure 43 shows the numerous impacts sustained by the water-filled SC-2 crater which was well within the range of the large blocks.

Harlan[6] made a visual comparison of the apparent lips of each of the craters and noted that the maximum and average block-size produced by the Bravo Event was significantly greater than the block-size produced by the other events. Even more apparent was the greater number and size of impact craters produced by the Bravo Event. He reported blocks as large as 4 ft in diameter and several impact craters up to 15 ft in diameter.

Other than abundance and size, the impact craters of the Bravo site varied from those at the other sites in that many of the largest ones occurred at relatively great distances from the Bravo SGZ; i. e., well beyond the limit of continuous ejecta material. In addition, the missiles that produced the distant impact craters consisted of both weathered and unweathered shale fragments, although a visual inspection indicated that the most distant large

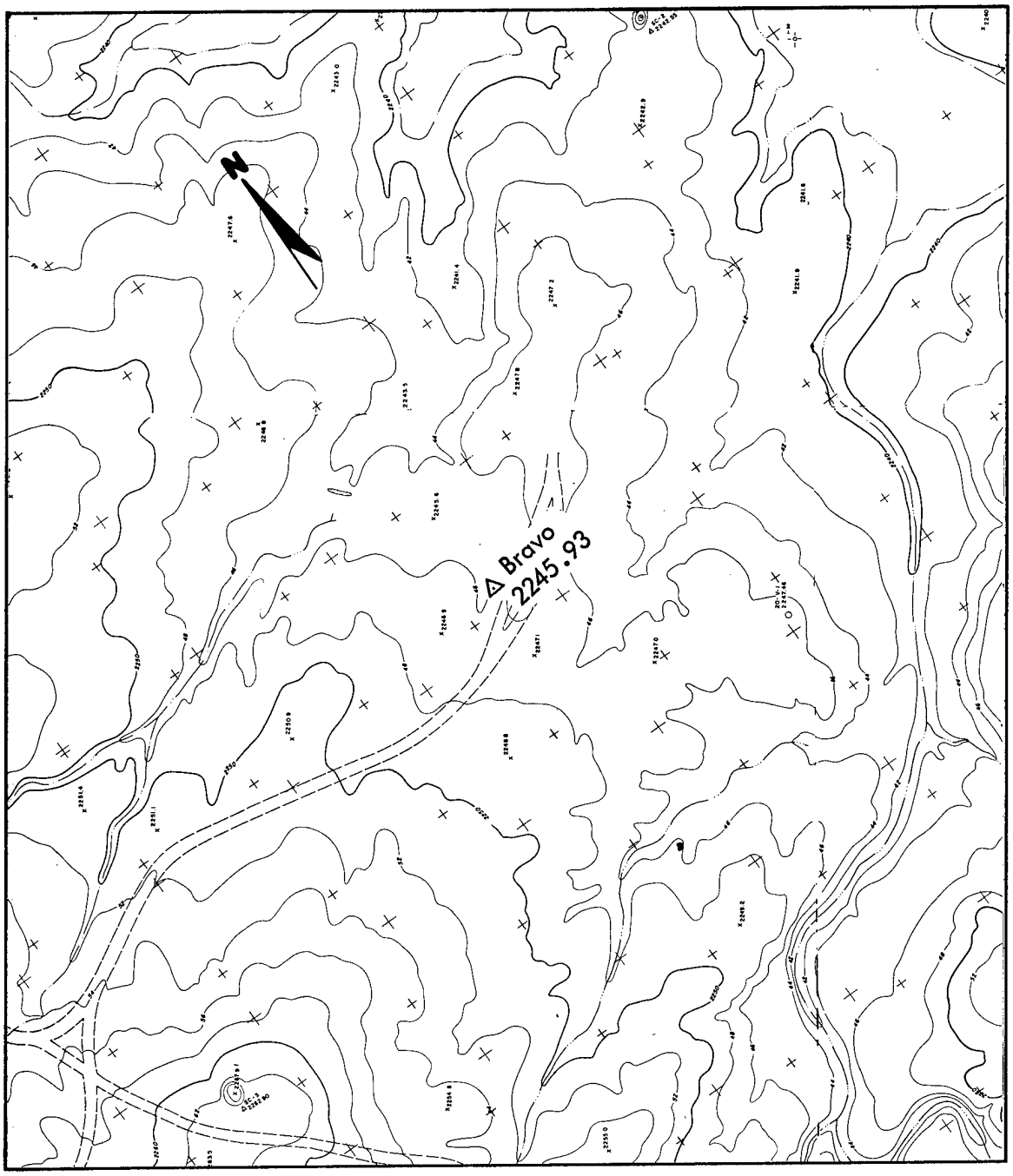

Fig. 36. Preshot topographic map for Pre-Gondola I Bravo.

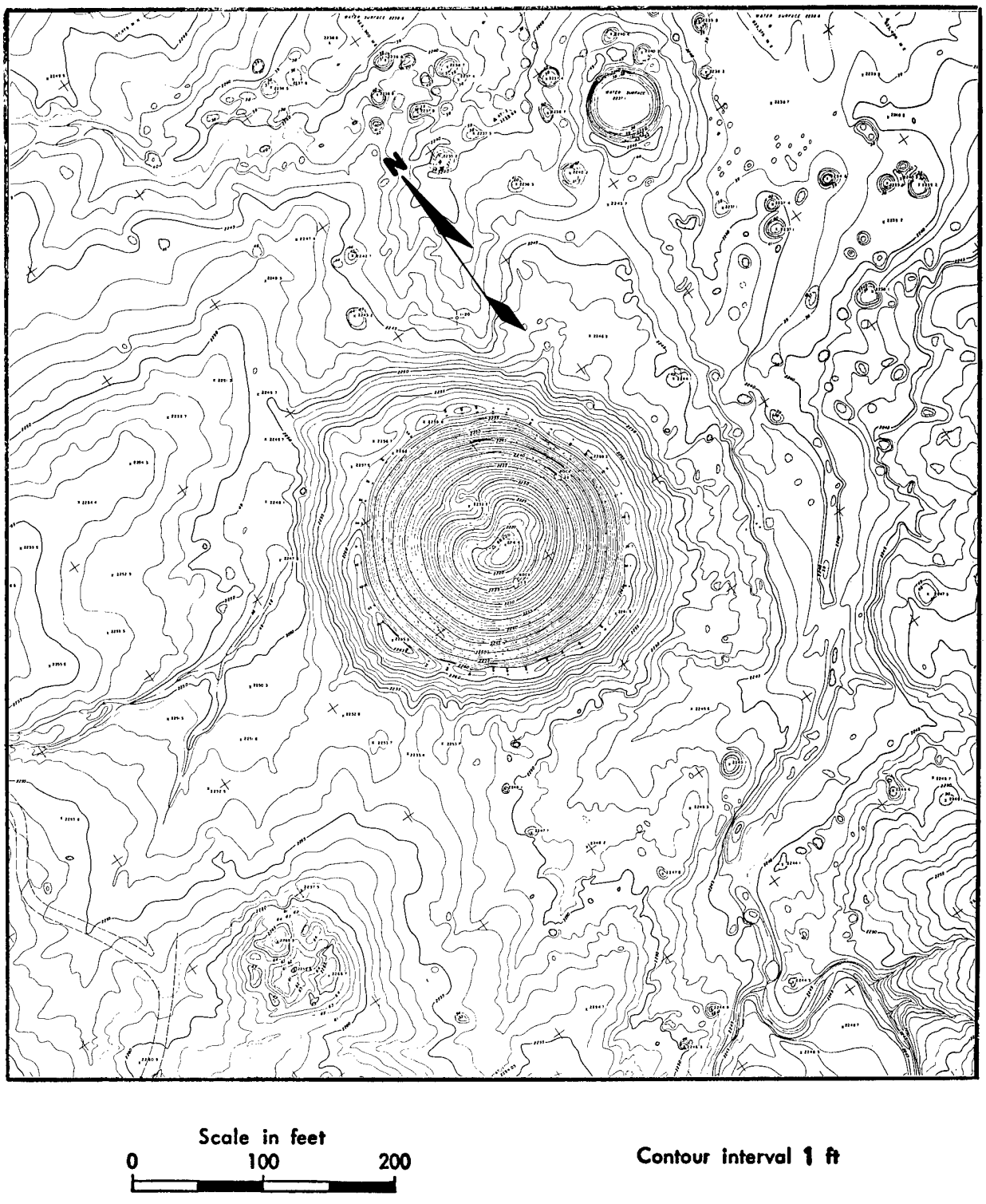

Fig. 37. Postshot topographic map for Pre-Gondola I Bravo.

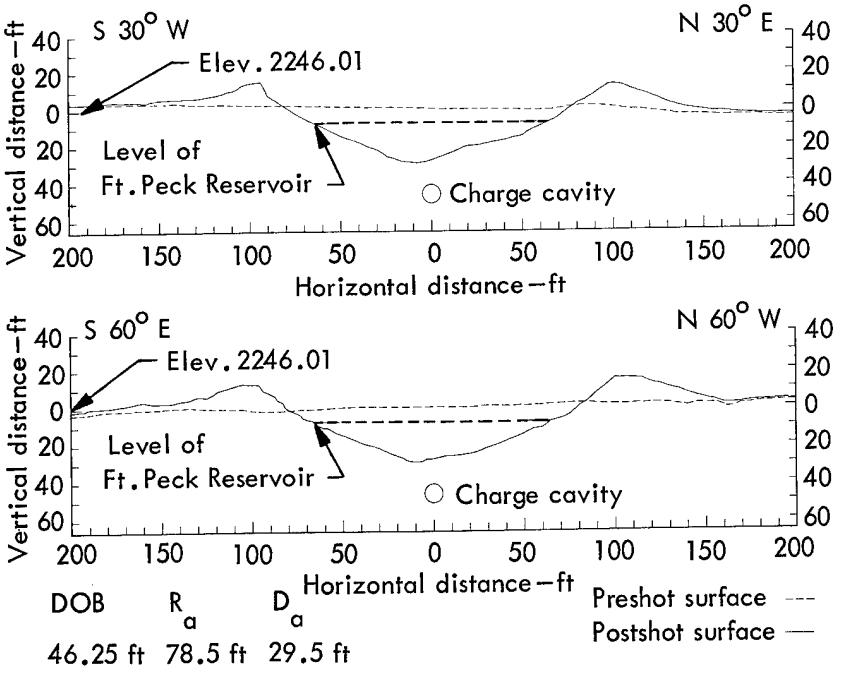

Fig. 38. Bravo crater profiles.

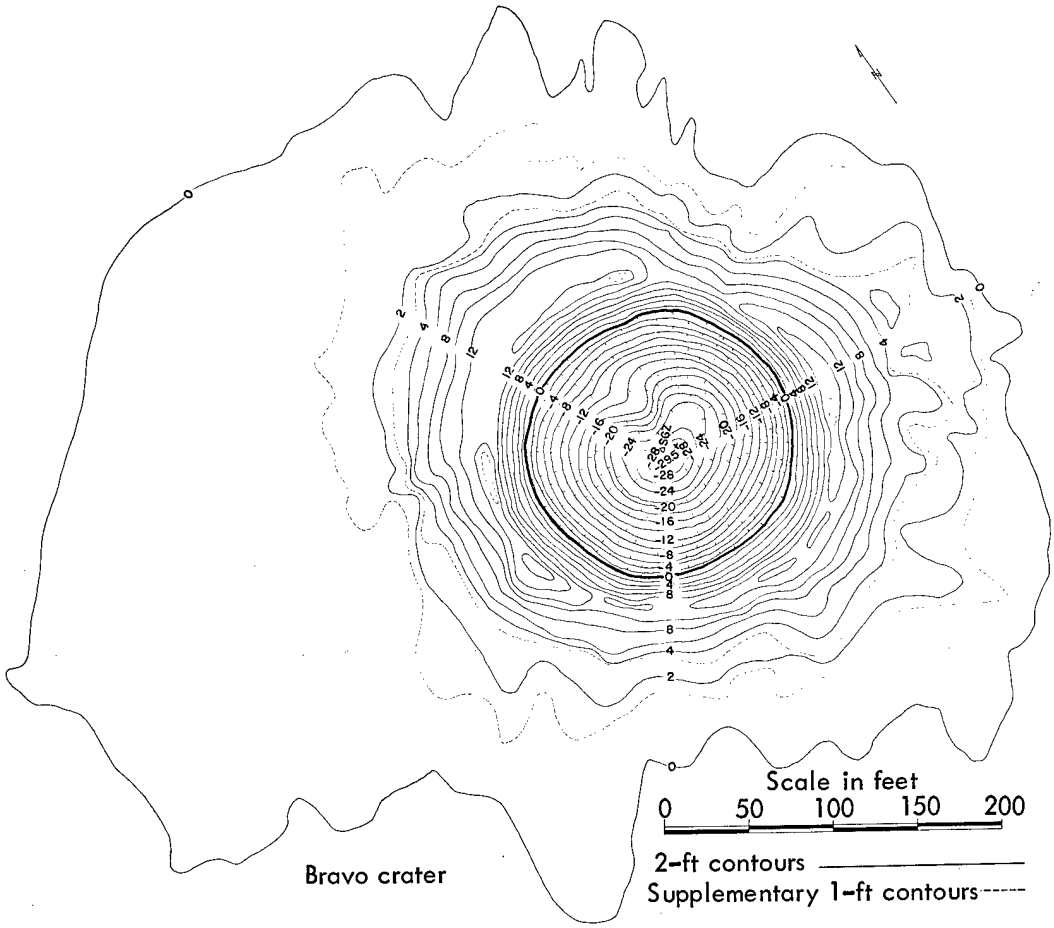

Fig. 39. Contour map of interval between preshot and postshot ground surface, Bravo crater.

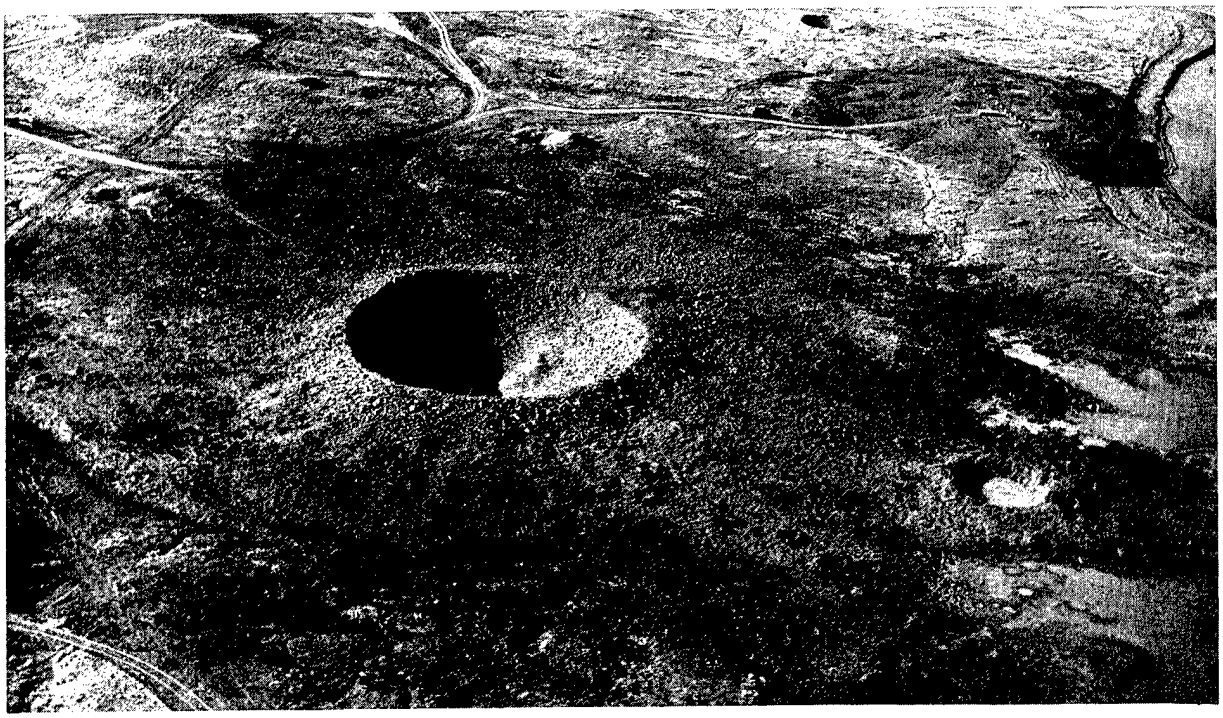

Fig. 40. Bravo crater, 25 October 1966.

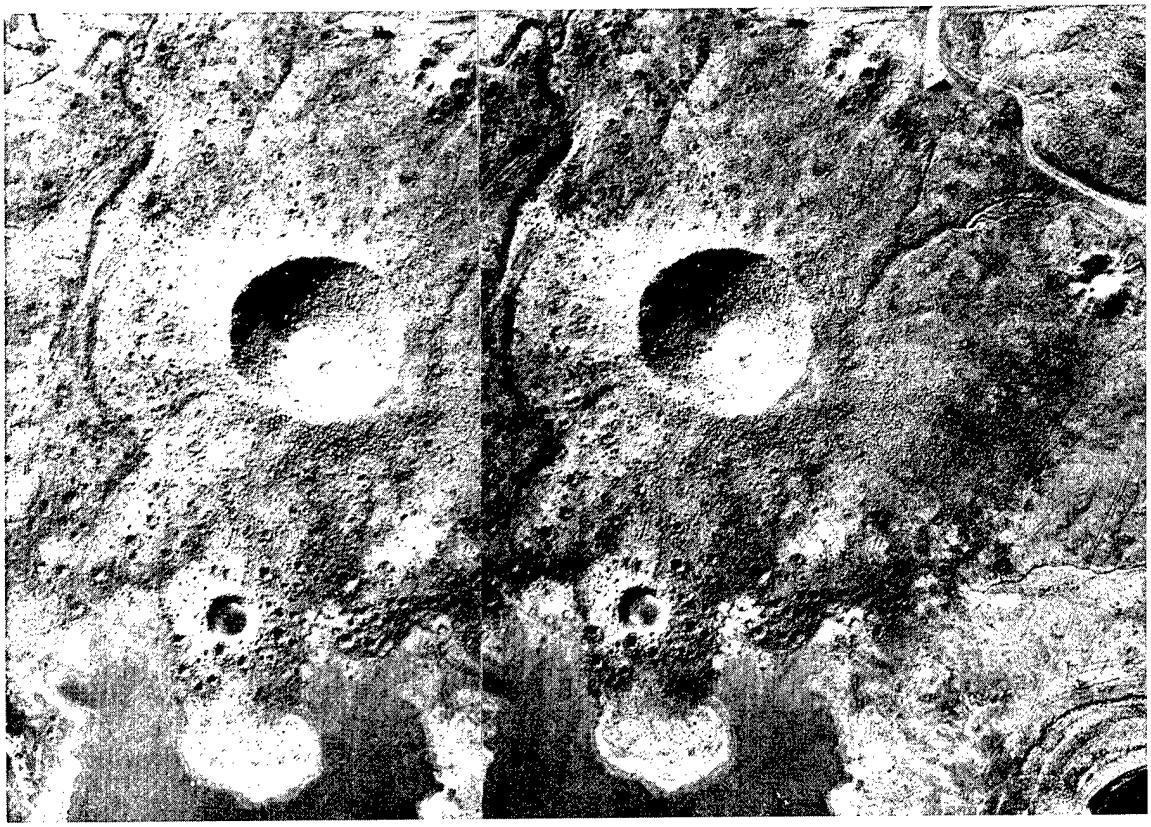

Fig. 41. Stereo-pair, Bravo crater.

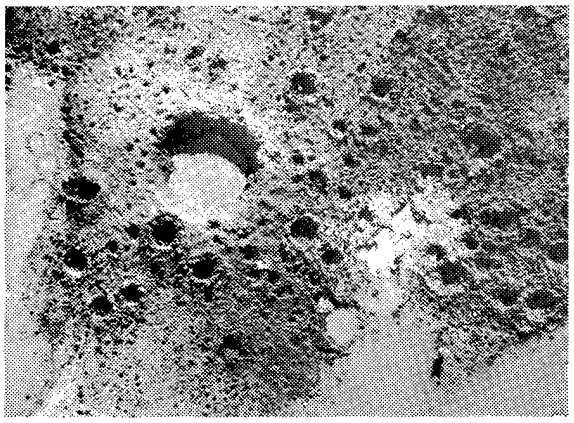

Fig. 42. Fallback material in Bravo crater.

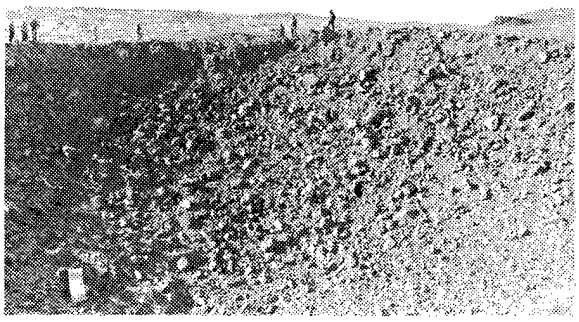

Fig. 43. Bravo ejecta impact craters in vicinity of 1000-lb SC-2 crater.

craters were predominantly produced by missiles of weathered shale which unlike missiles of unweathered shale tended to lose their identity upon impact.

Even though the DOB of the Bravo Event was intermediate between the shallowest DOB (Charlie Event) and the two greatest DOB (Alfa and Delta Events), the maximum missile range of the Bravo Event was significantly greater than that recorded for the Charlie Event and was twice that of the Delta Event. The most distant missiles located around the crater consisted of 1/2- to 1-lb fragments of shale which in every case appeared to be highly weathered and can be assumed to have come from relatively near the surface of the ground.

Two arrays of ejecta pellets were employed at the Bravo site. Although additional pellets were recovered during postshot investigations, immediately after the shot the recovery was only 11% of 156 pellets from the "A" array and 17% of 107 pellets from the "B" array. Both of these recovery percentages were below the average percentage of 20.4%. Figures 44 through 47 show the locations of the postshot positions of the recovered ejecta pellets from the "A" and "B" arrays, respectively.

Alfa Event

The preshot ground surface for Alfa (Fig. 48) had a downhill slope of 3 deg towards the northeast. The postshot topographic map (Fig. 49) shows the size and shape of the apparent crater and lip and the distinct ray of stemming material extending in a direction of N40°E from the bottom of the crater. This ray is clearly shown in the N42°E profile, especially on the lip, in Fig. 50. Ejecta along this ray carried much farther than ejecta in any other direction.

The shape of the Alfa crater was approximately symmetrical, except for a small mound or shoulder on the northeast slope of the crater and a 5.5-ft displacement of the deepest point of the crater in a south-southwest direction from SGZ. Figure 50 shows orthogonal profiles of the preshot and postshot ground surfaces. Figure 51 is a contour map of the interval between the preshot and postshot ground surfaces.

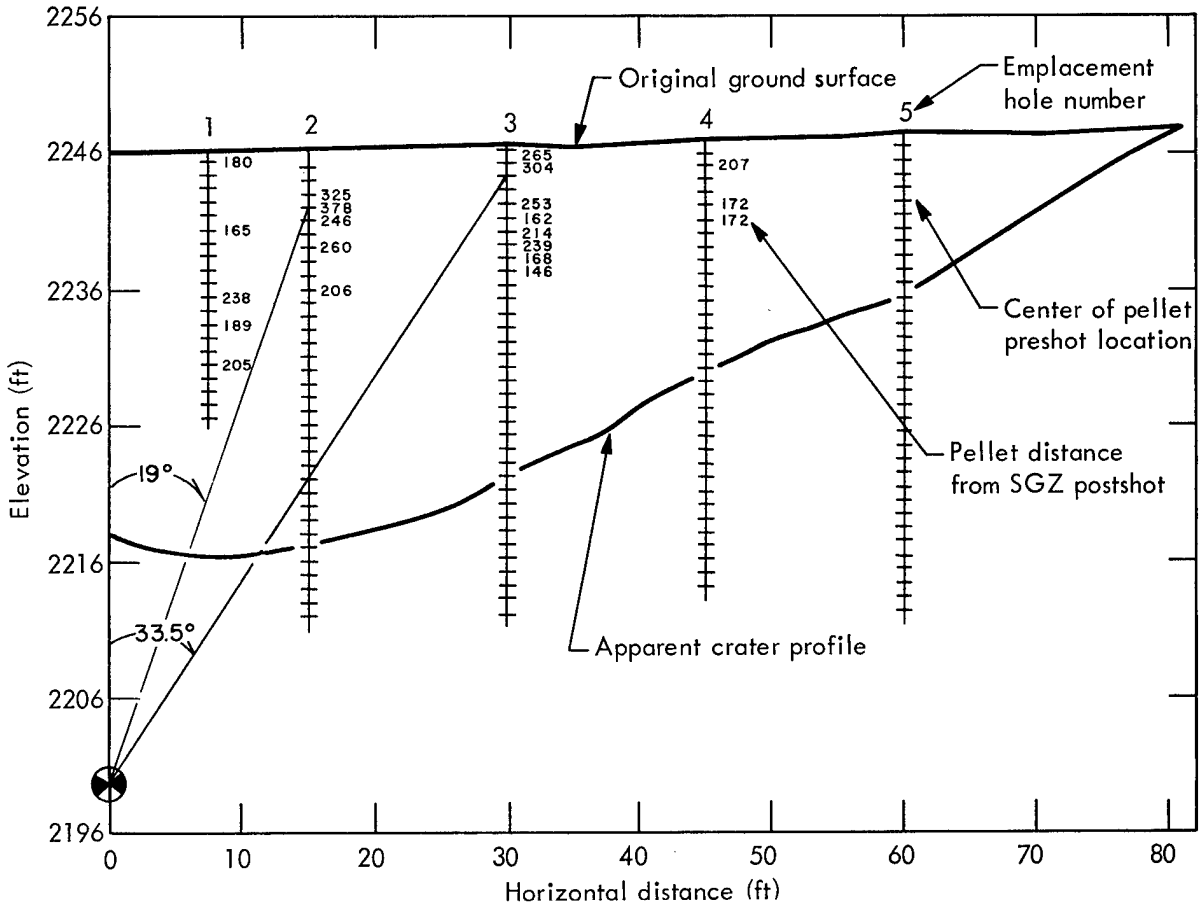

Fig. 44. Preshot and postshot locations of Bravo ejecta pellets, "A" array.

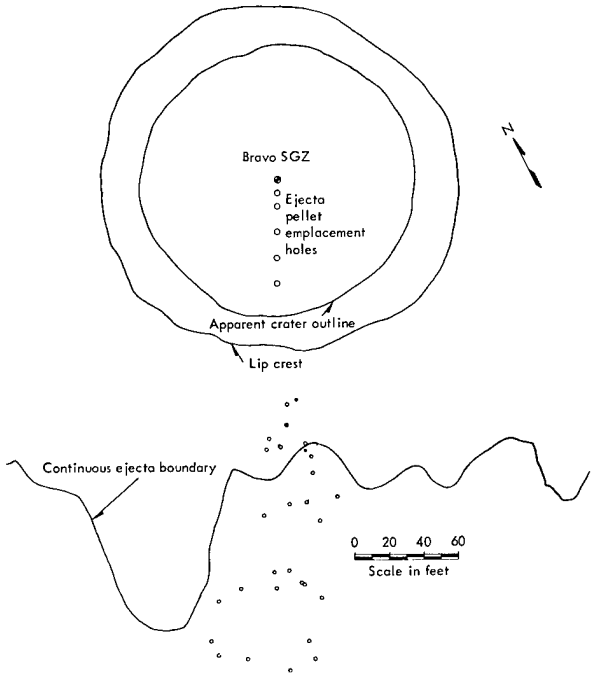

Fig. 45. Postshot locations of Bravo ejecta pellets, "A" array.

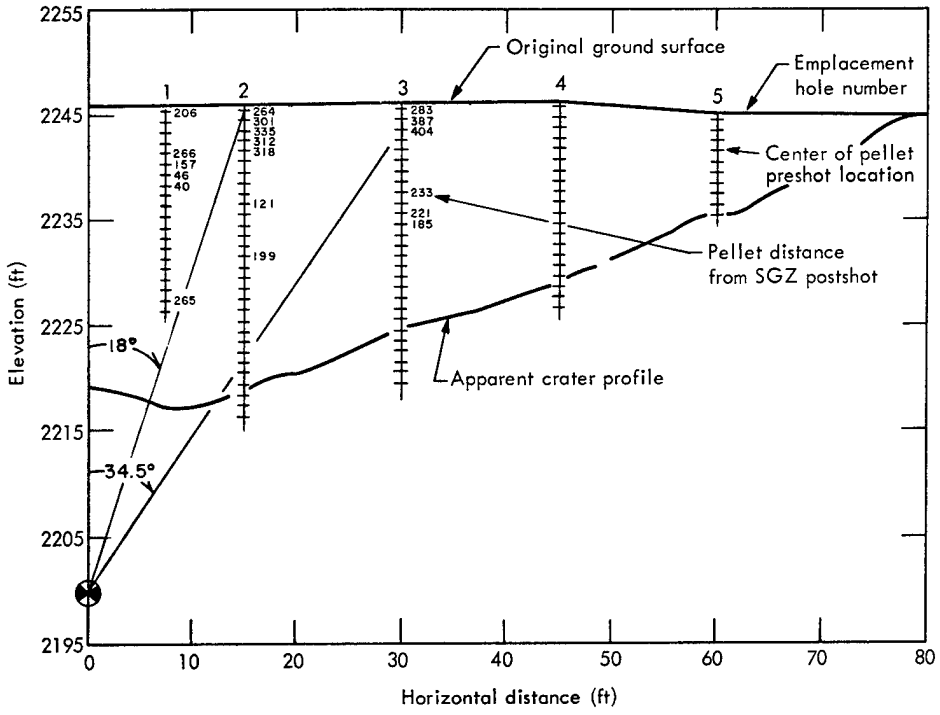

Fig. 46. Preshot and postshot locations of Bravo ejecta pellets, "B" array.

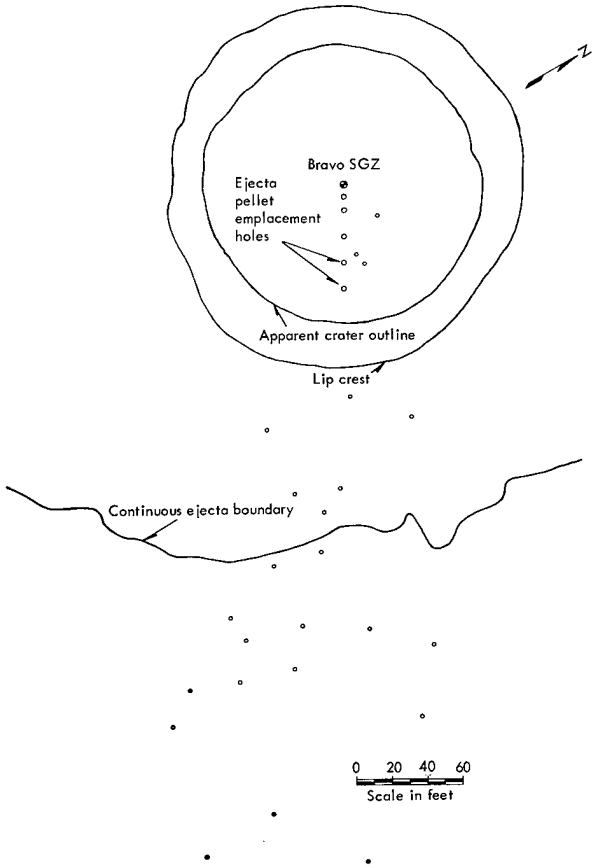

Fig. 47. Postshot locations of Bravo ejecta pellets, "B" array.

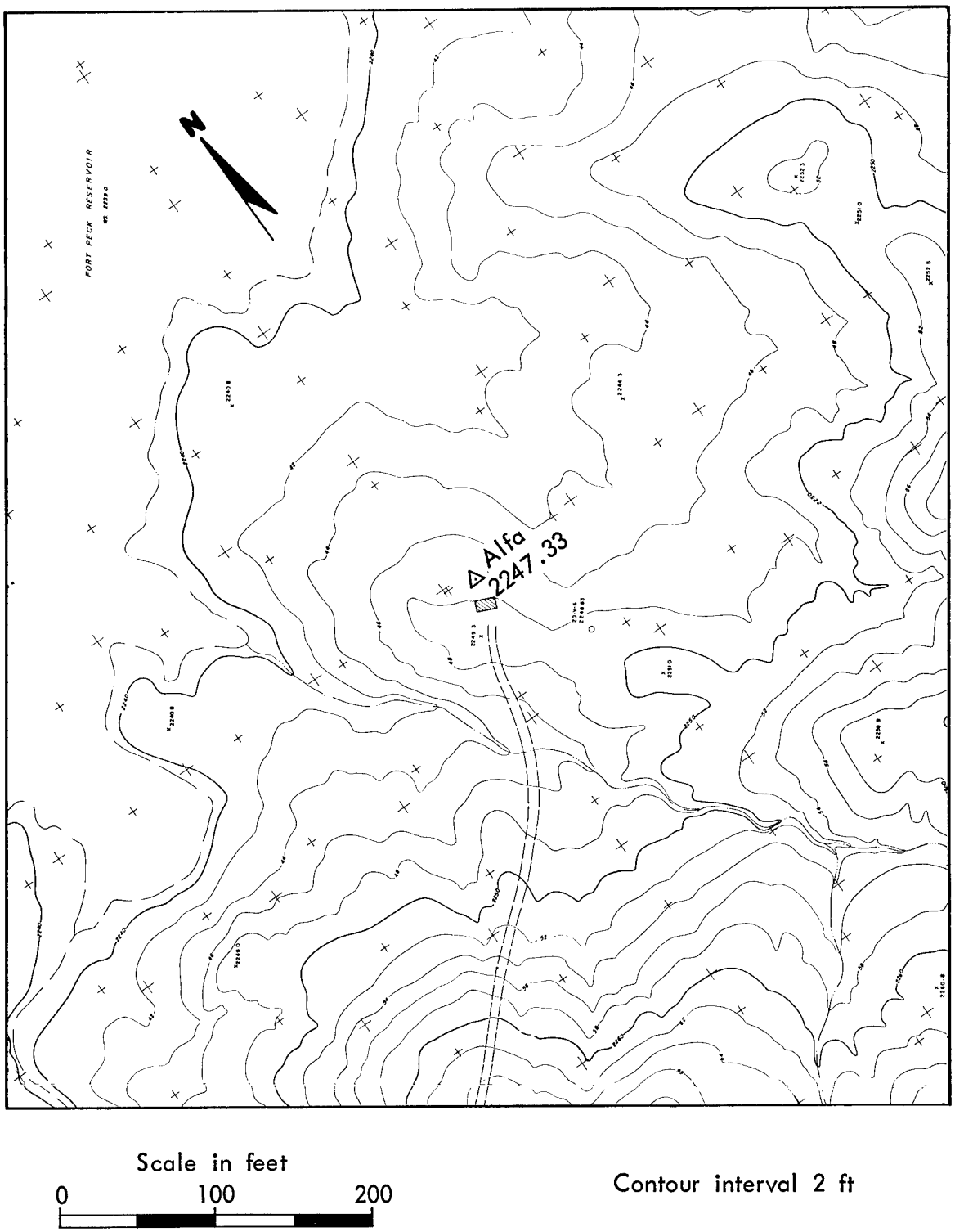

Fig. 48. Preshot topographic map for Pre-Gondola I Alfa.

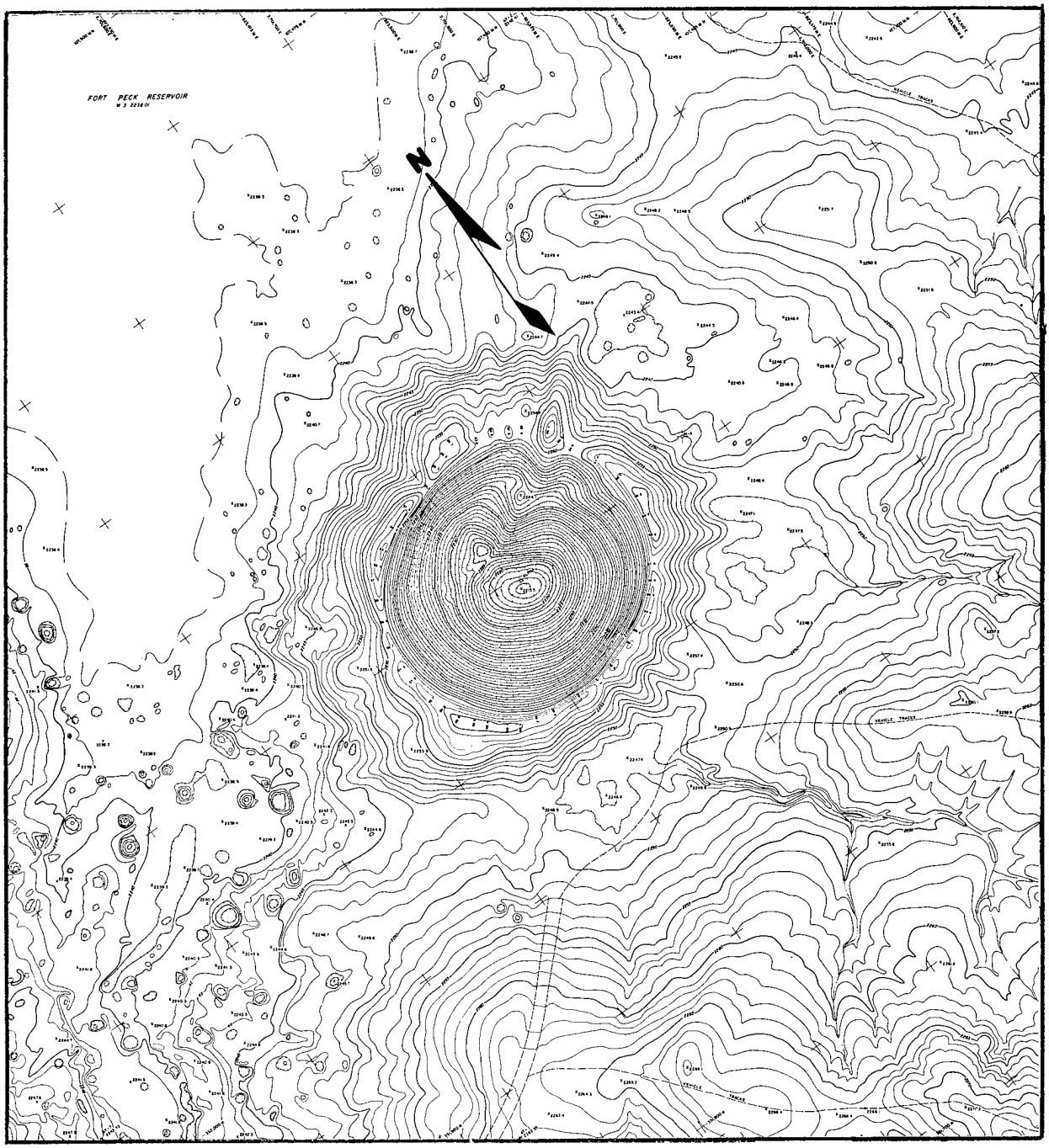

Fig. 49. Postshot topographic map for Pre-Gondola I Alfa.

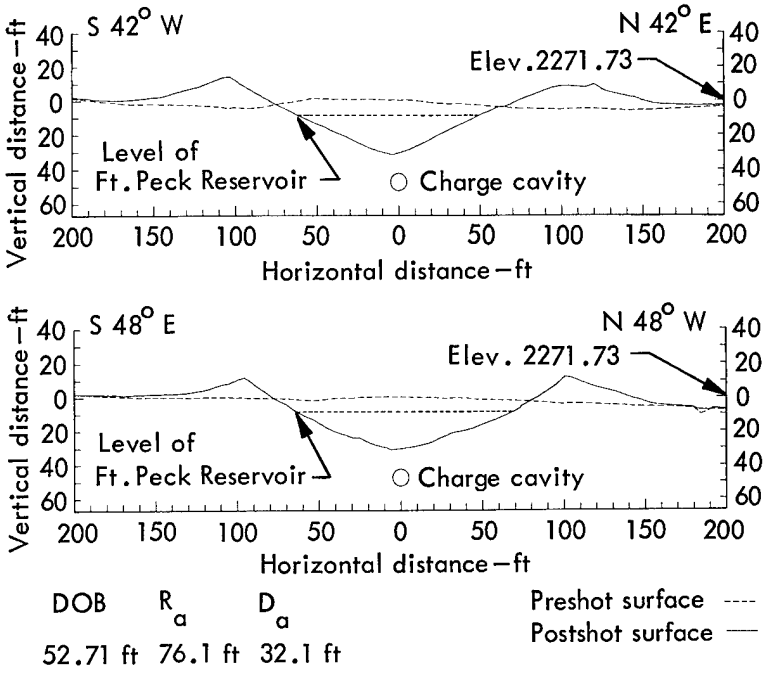

Fig. 50. Alfa crater profiles.

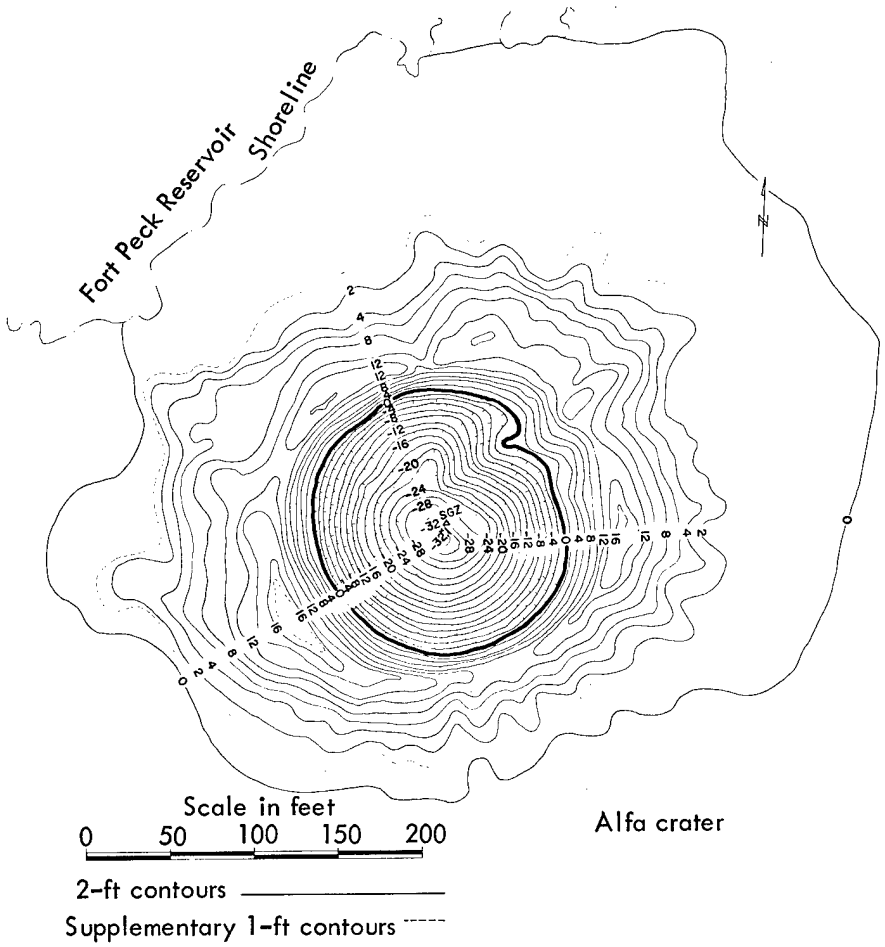

Fig. 51. Contour map of interval between preshot and postshot ground surface, Alfa crater.

Figure 52 is an oblique photograph of the Alfa crater. The mound within the crater is on the near crater slope. The impact craters in the foreground were produced by ejecta from the Alfa crater but those in the background were, for the most part, formed by ejecta from the Bravo crater. Ejecta rays are quite evident in the apparent crater lip (Fig. 53).

Although occasional blocks 2 to 3 ft in diameter (Fig. 54) were found within the crater and along the inner or higher regions of the lip, the predominant block-size is less than 1 ft in diameter. Figure 55 shows the largest impact crater from Alfa, but the smaller ones shown in Fig. 56 were more representative.

Only 15% of 107 ejecta pellets installed at the Alfa site were recovered. Figures 57 and 58 show the locations of the postshot positions of the recovered pellets.

Delta Event

The preshot ground surface for Delta (Fig. 59) had a definite downhill slope of 4 deg towards the east and northeast. Leading away from SGZ in these directions, there were two dry stream gullies. The postshot topographic map (Fig. 60) shows the ray of stemming material extending in a direction N55°E from the bottom of the crater. It was about the size of the Alfa ray and extended well beyond the apparent crater to the edge of continuous ejecta.

The volume of the Delta apparent crater was the least of the four craters and its shape was somewhat elongated. Figure 61 shows two orthogonal topographic profiles of the preshot and postshot ground surface drawn through the SGZ. Figure 62, a contour map of the interval between the preshot and postshot ground surfaces,

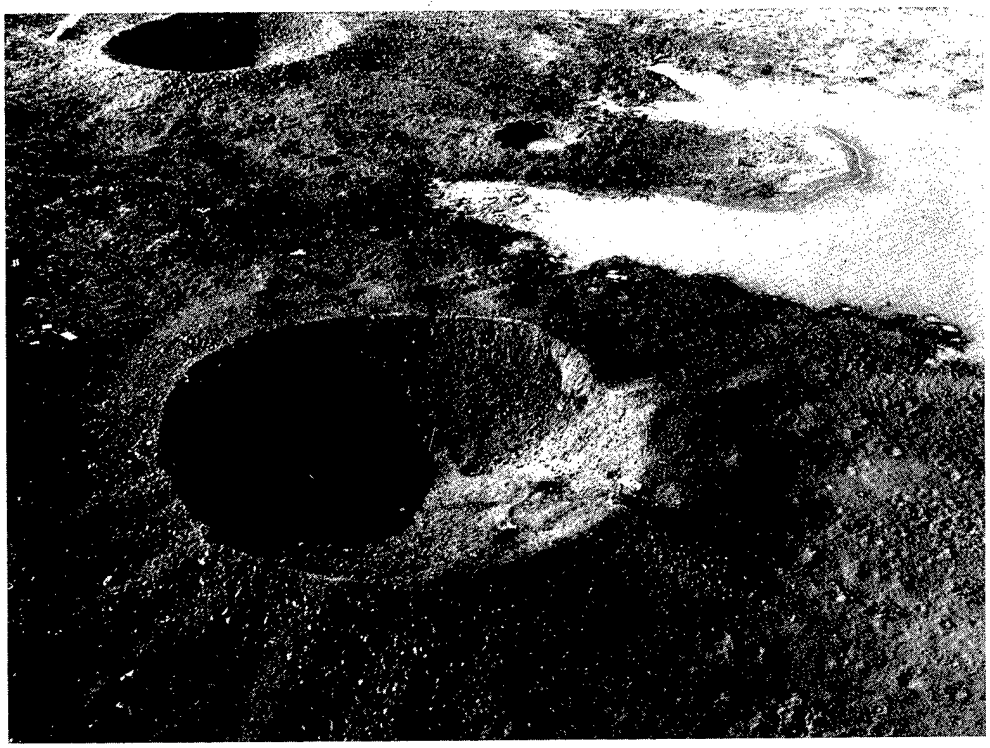

Fig. 52. Alfa crater, 1 November 1966.

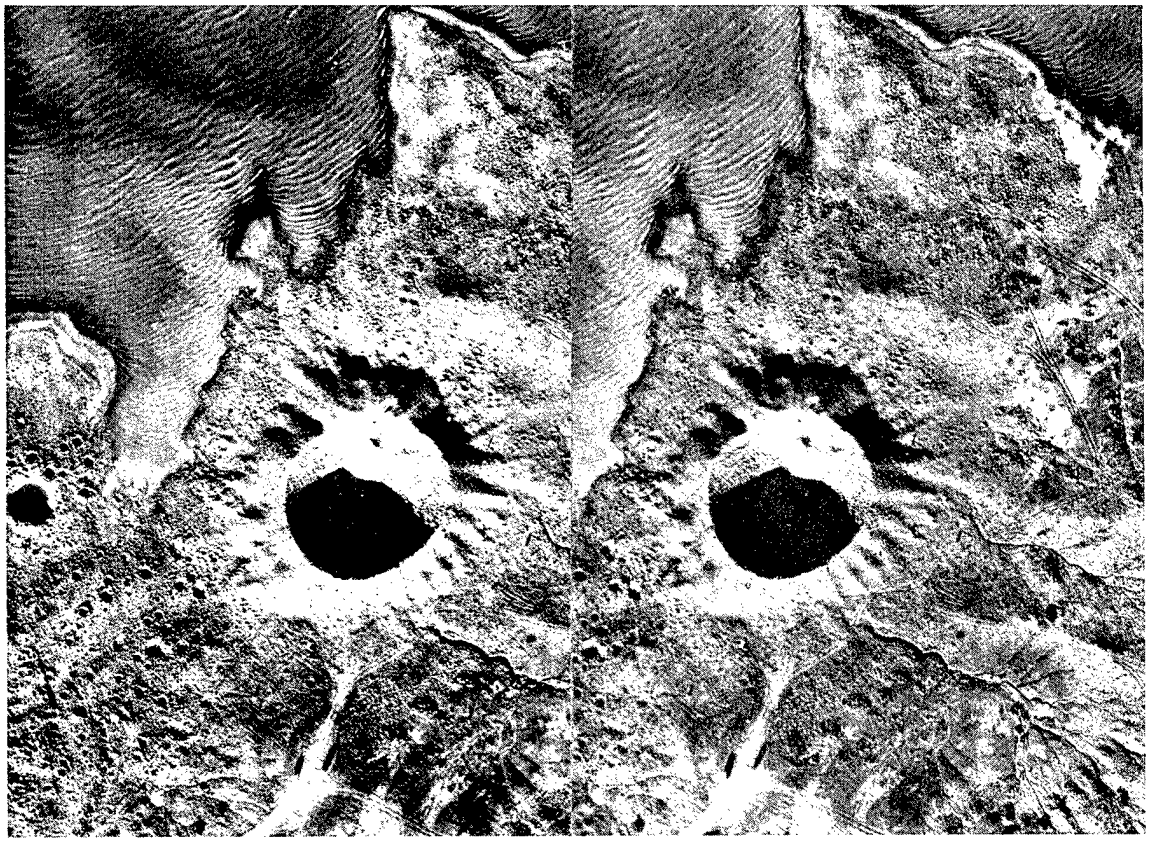

Fig. 53. Stereo-pair of Alfa crater.

Fig. 54. Fragmented ejecta block, Alfa Event.

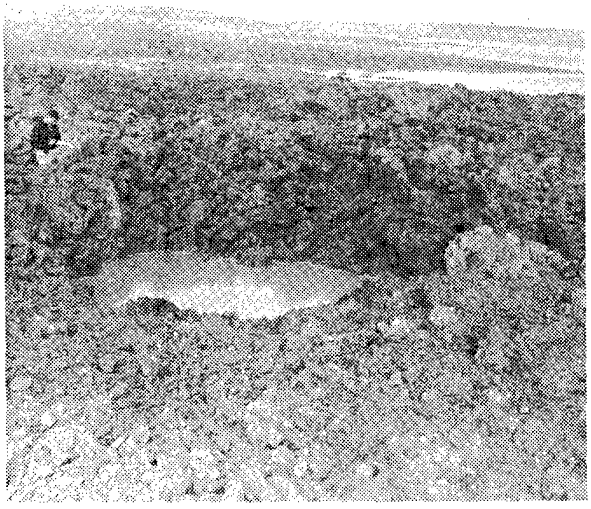

Fig. 55. Large impact crater from Alfa ejecta.

Fig. 56. Smaller impact craters from Alfa ejecta (note pencil).

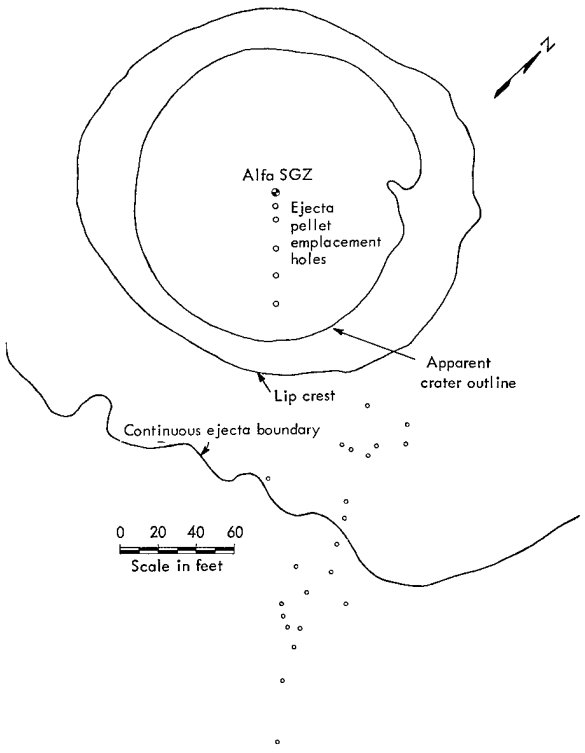

Fig. 58. Postshot locations of Alfa ejecta pellets.

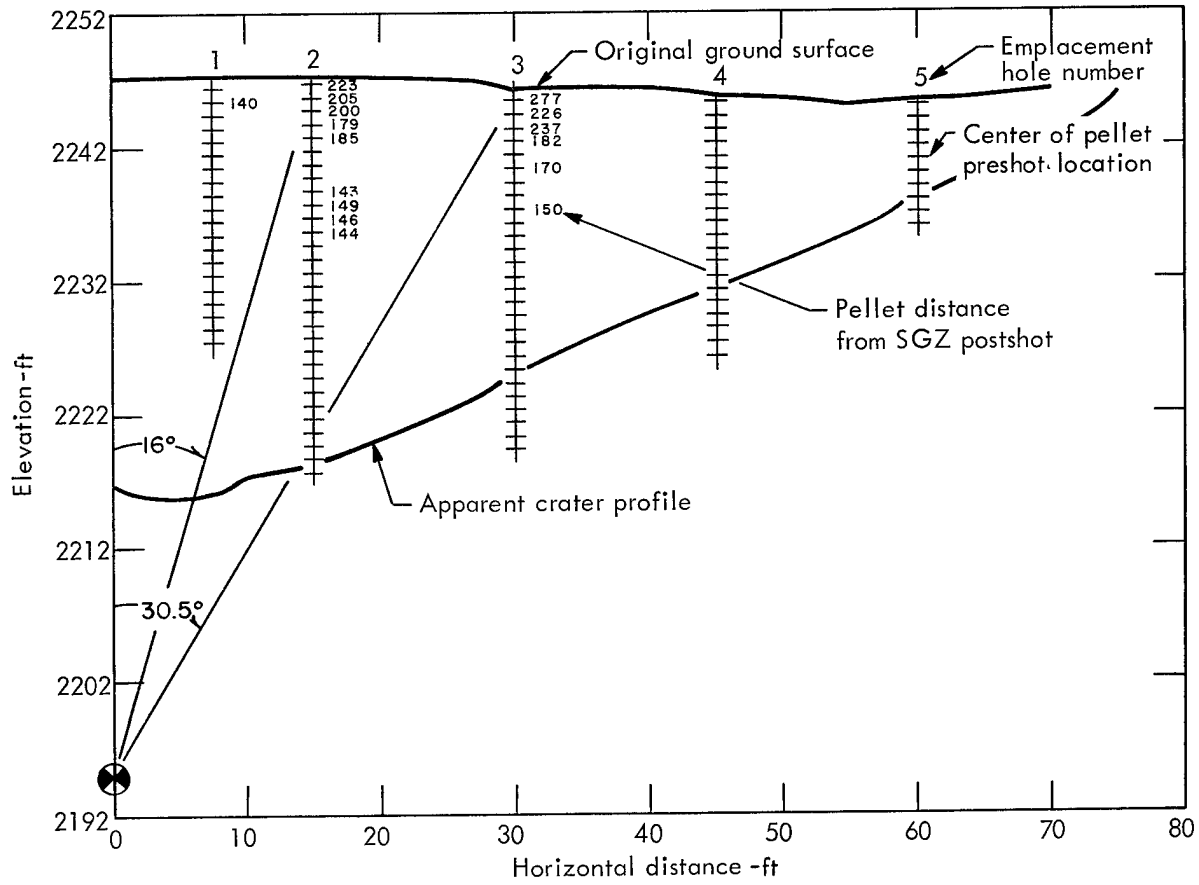

Fig. 57. Preshot and postshot locations of Alfa ejecta pellets.

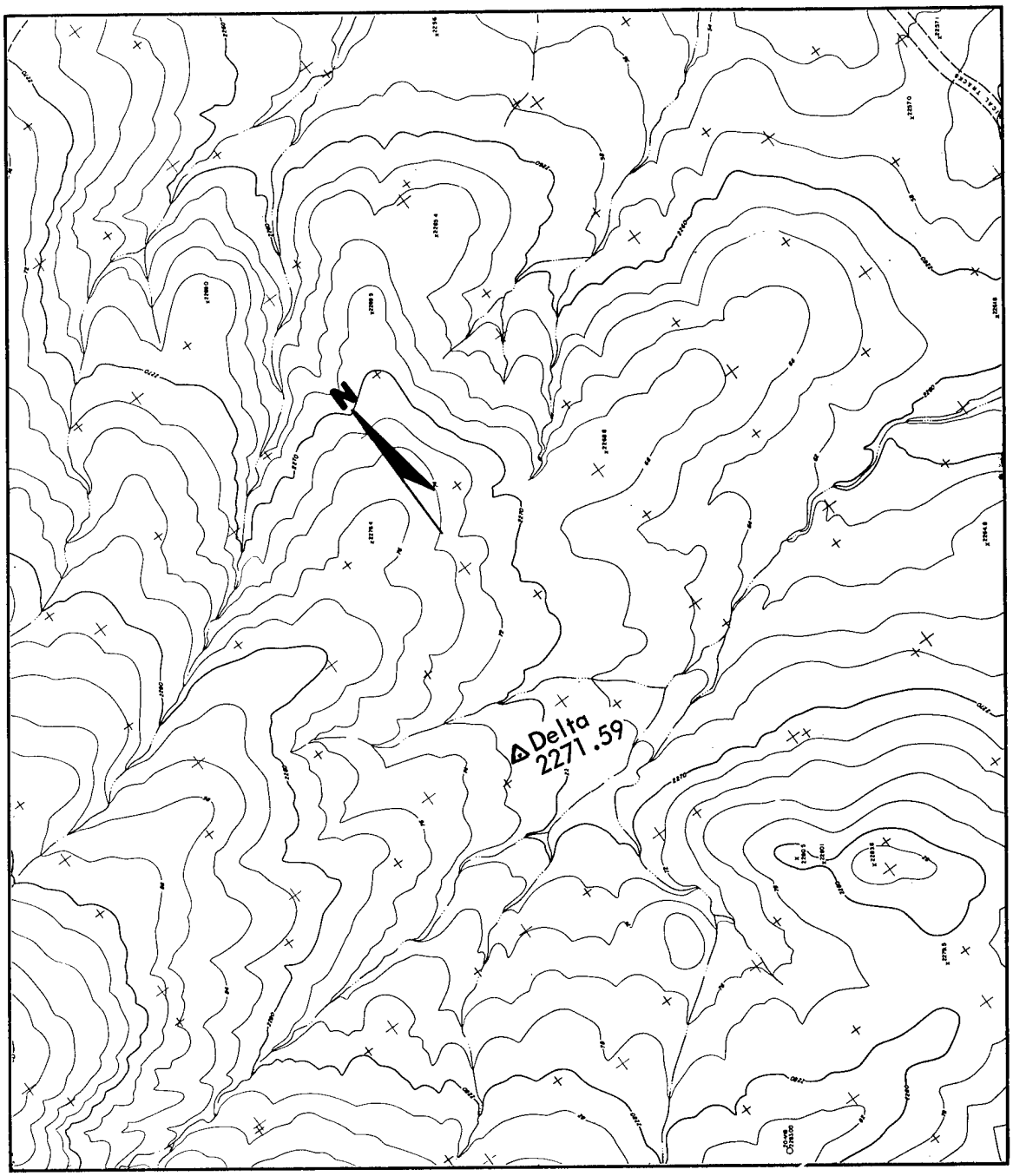

Fig. 59. Postshot topographic map for Pre-Gondola I Delta.

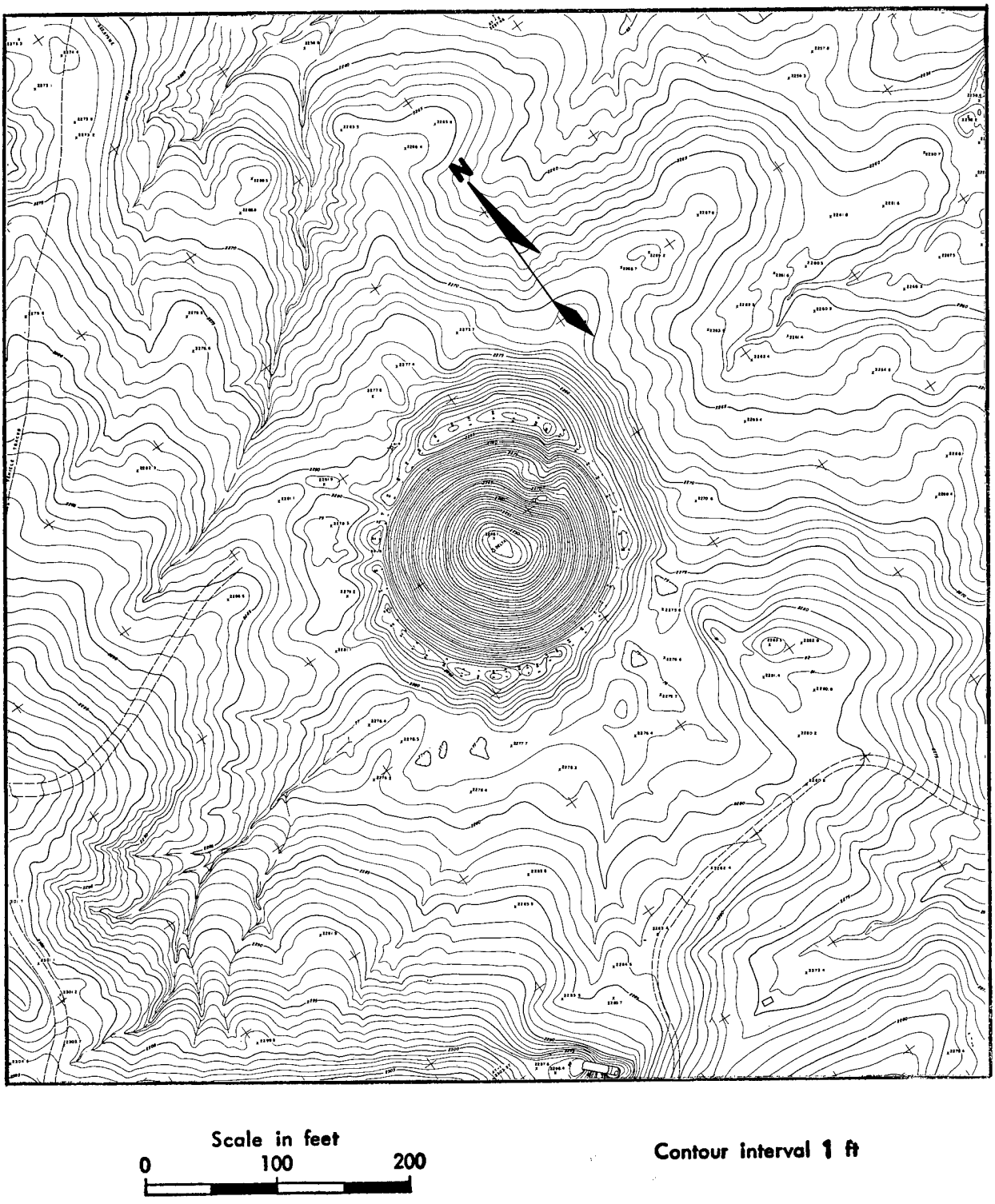

Fig. 60. Postshot topographic map for Pre-Gondola I Delta.

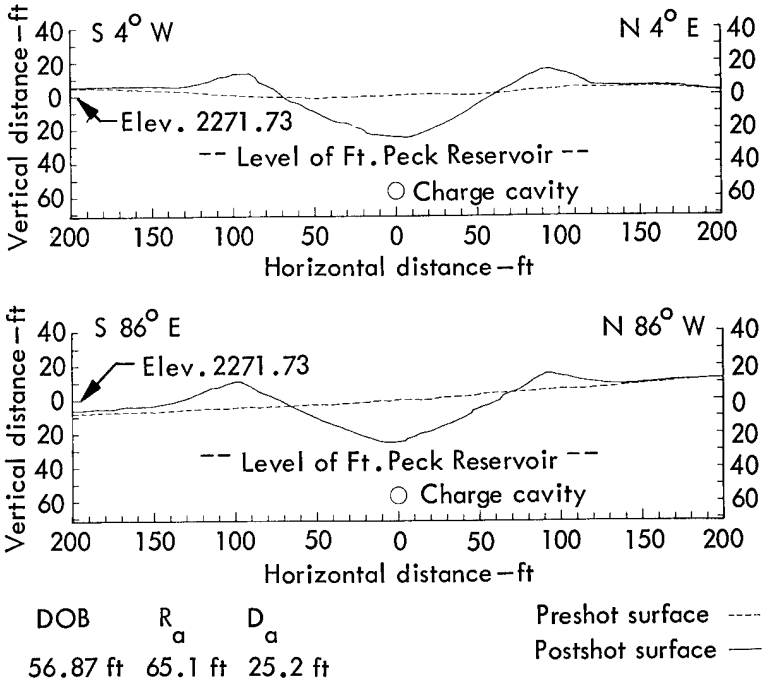

Fig. 61. Delta crater profiles.

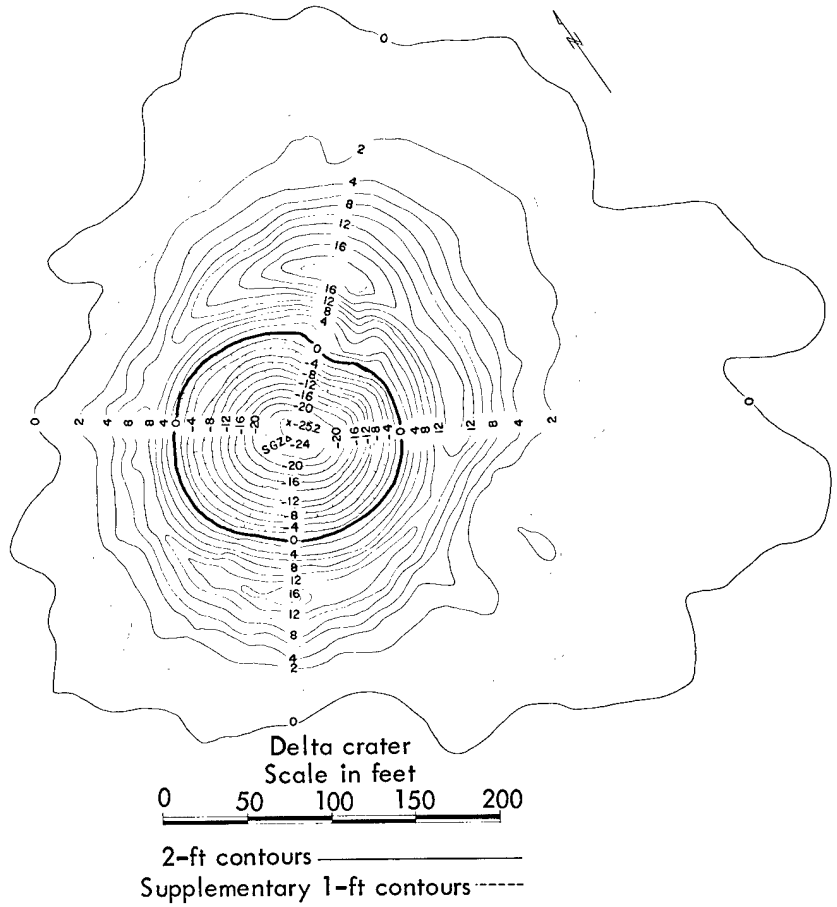

Fig. 62. Contour map of interval between preshot and postshot ground surface, Delta crater.

shows the elongated shape of the crater and the distribution of the ejected material.

The block-size of the Delta crater ejecta was not very different from that produced by the Alfa and Charlie Events, although the average block-size was probably somewhat greater. As seen in the aerial photograph of the Delta crater (Fig. 63), impact craters were practically nonexistent. Figure 64 shows that the ejecta lies much closer to the crater lip than for any of the other craters. Figure 65 shows one of the larger ejecta blocks that fragmented upon impact. The larger impact craters for Alfa and Charlie appeared to have been produced by similar missiles.

Figures 66 and 67 show the locations of the postshot positions of the recovered ejecta pellets. Thirty-one percent, the highest of the five ejecta arrays, of 106 ejecta pellets installed were recovered.

ANALYSIS AND INTERPRETATION

Apparent Crater Dimensions

The dimensions of the Pre-Gondola I cratering events provided the first reliable data that could be used to develop HE cratering curves for shale. However, because the physical properties of different shale media vary significantly, it is appropriate, at the present time, to limit use of the curves to craters in Bearpaw shale. Figures 68 and 69 show the Bearpaw shale cratering curves. The actual crater dimensions were scaled to 1 kt by the 3.4th root of the equivalent yield. The

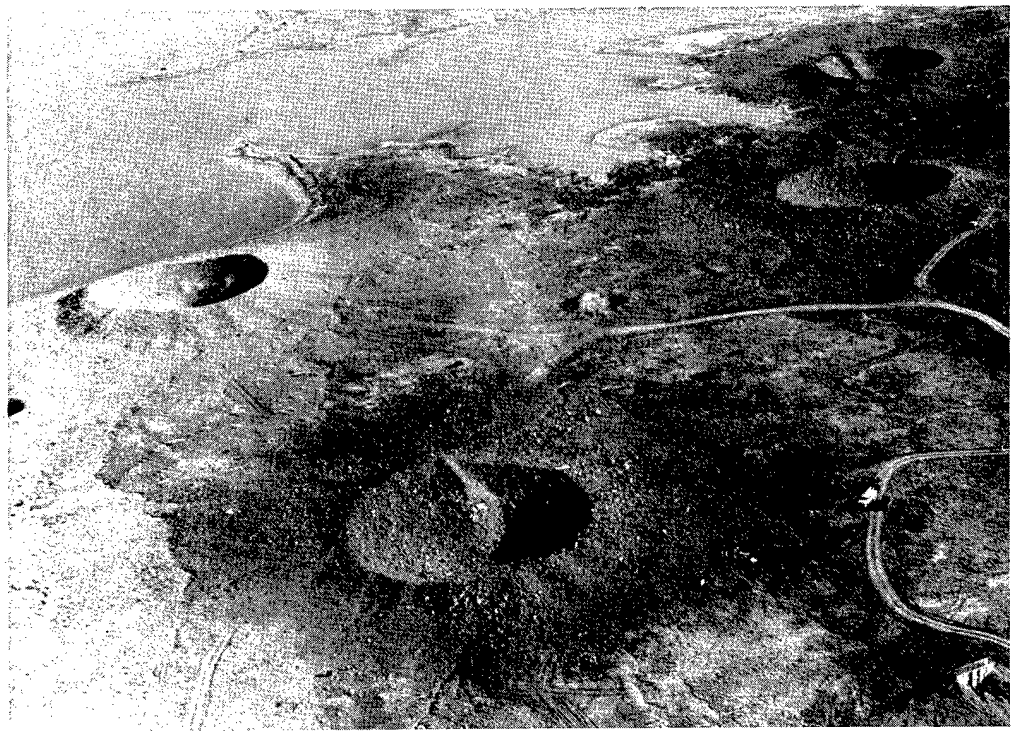

Fig. 63. Delta crater, 4 November 1966 (Charlie crater, left at shoreline; Bravo and Alfa, upper right).

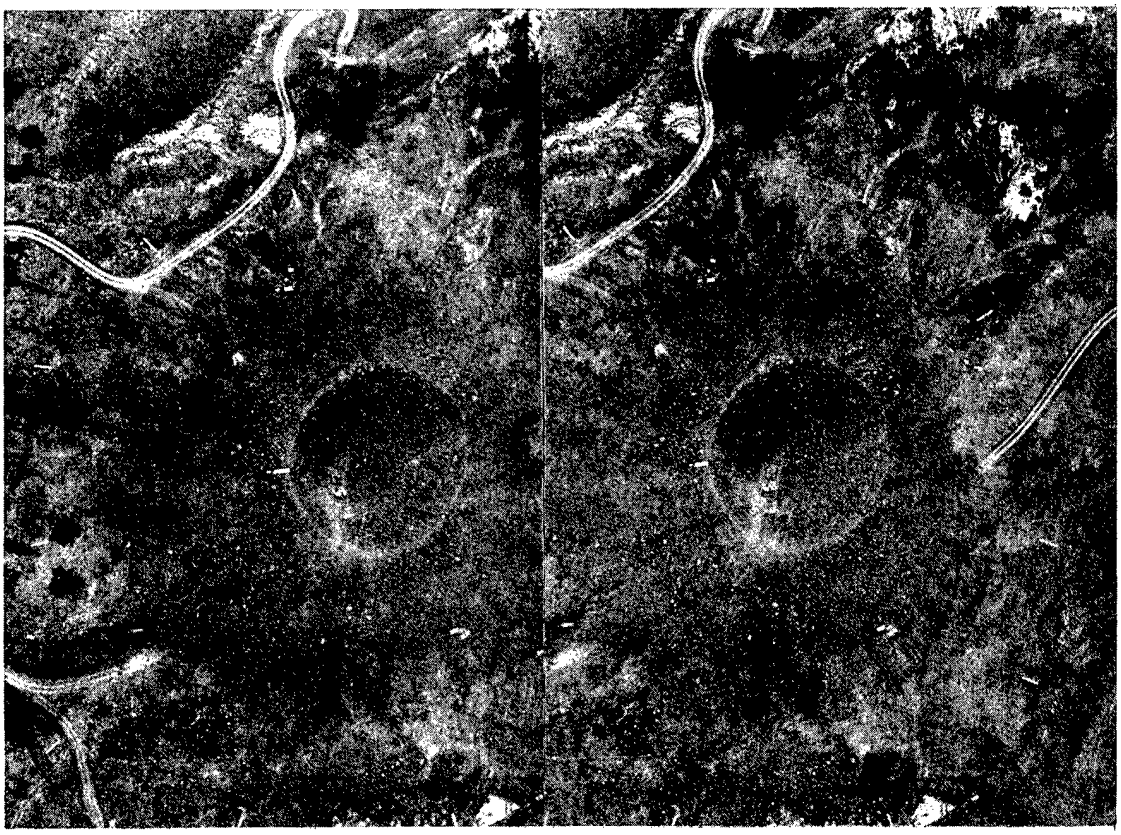

Fig. 64. Stereo-pair, Delta crater.

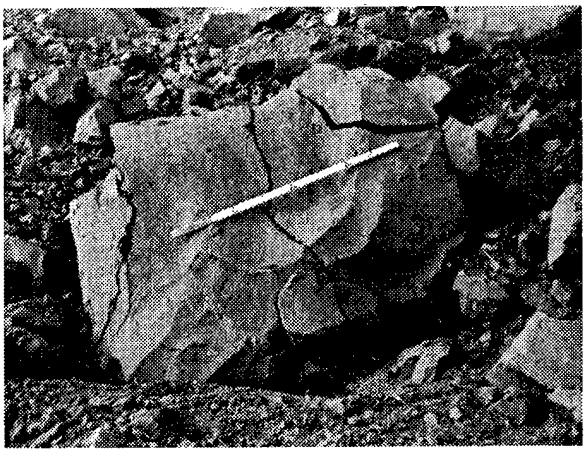

Fig. 65. Large ejecta block, Delta Event.

dashed portions of the curves are inferred from information available in Ref. 1. These cratering curves indicate that the optimum DOB for the apparent crater radius and depth is about 130 ft/kt$^{1/3.4}$.

The rapid decrease in the apparent crater dimensions with increasing charge depths deeper than the optimum depth is assumed to result principally from an increase in the volume of broken rock (bulking) and a decrease in ejecta velocities. An analysis of the preshot ground surface slopes and the deposition of material (such as the stemming) ejected at SGZ indicates that had events Alfa and Delta been on level ground they would have been shallower because the large ray of ejecta would have been deposited in the bottom of the crater. If this were true, the depths for Charlie and Bravo would be considered normal and those for Alfa and Delta anomalously high. On the other hand, the lower value of crater depth for

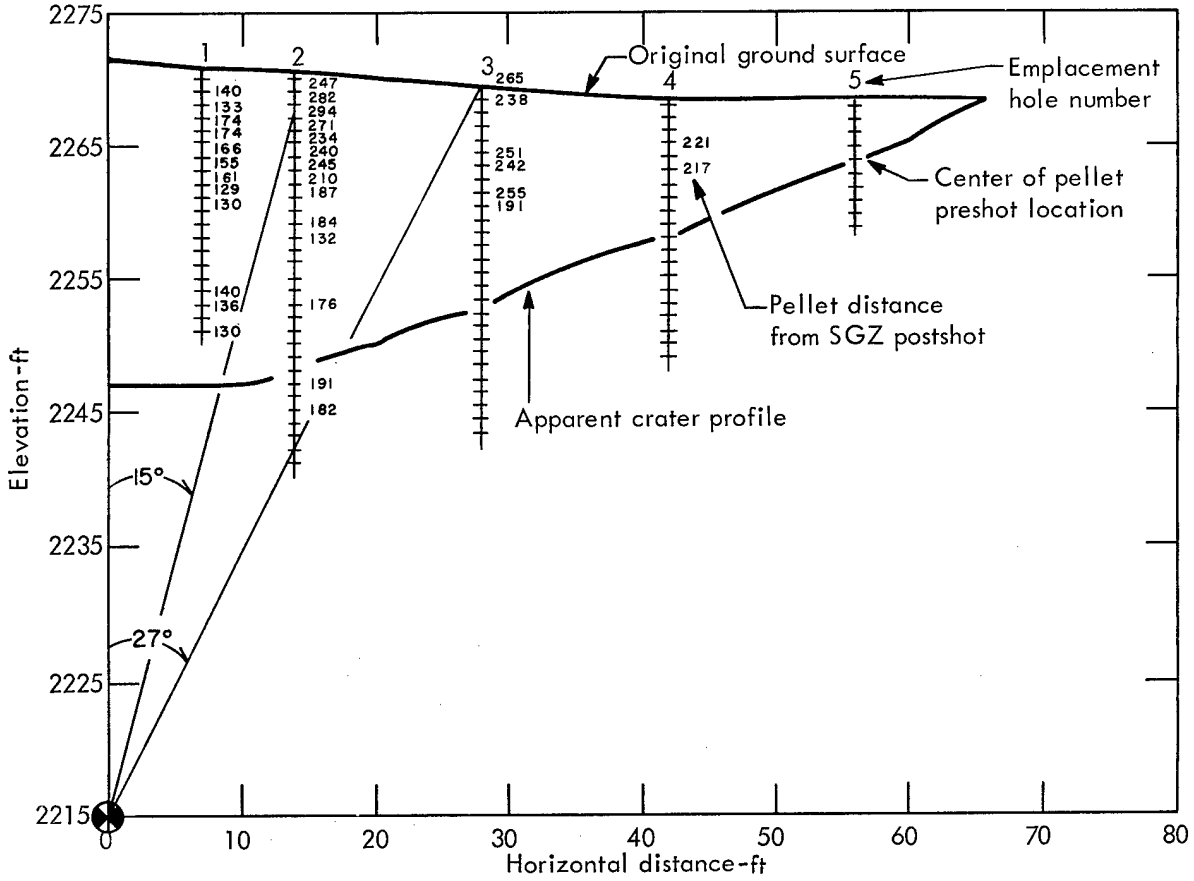

Fig. 66. Preshot and postshot locations of Delta ejecta pellets.

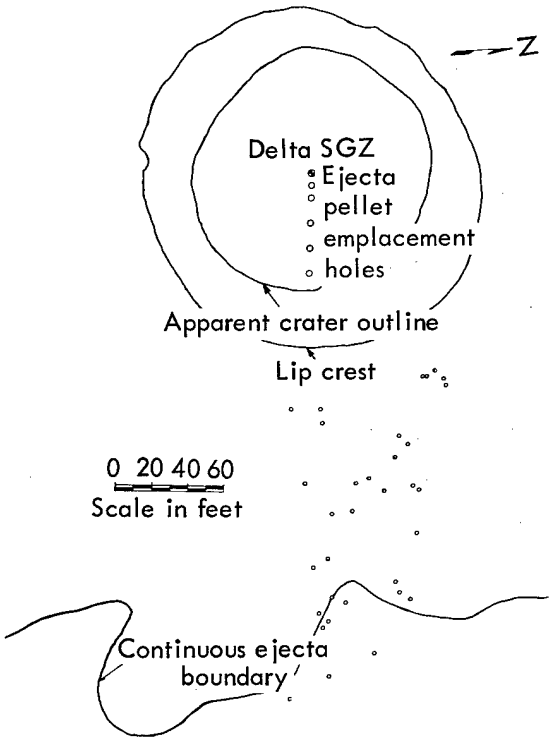

Fig. 67. Postshot location of Delta ejecta pellets.

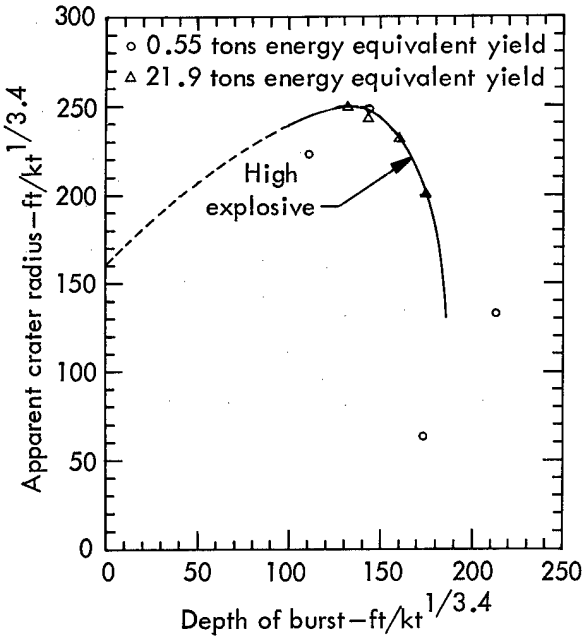

Fig. 68. Apparent crater radius vs depth of burst for Bearpaw shale.

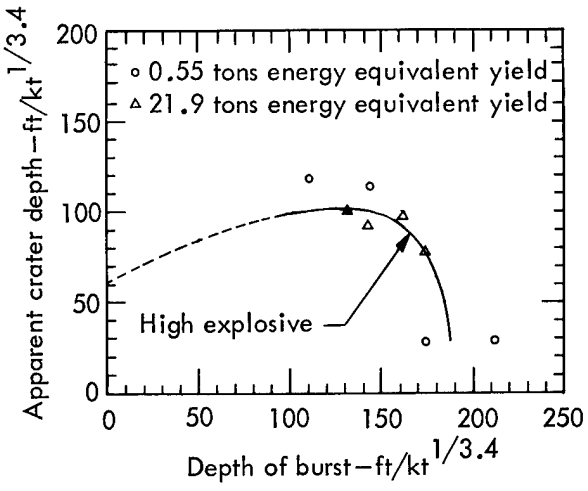

Fig. 69. Apparent crater depth vs depth of burst for Bearpaw shale.

the Bravo Event may be related to the block-size and the bulking factor of the fallback. In addition, a 2-m overburden at the site apparently affected surface motion phenomena.[13] It is concluded that until more is known about the effect of topography on crater dimensions, it is not possible to knowledgeably adjust the crater dimensions to compensate for the associated variations in ejecta distribution.

Comparison with Cratering Characteristics of Different Media

Harlan[6] compared the HE cratering curves and the average asymptotic slope of craters in Bearpaw shale, alluvium, and basalt.[14] The results of his findings are tabulated in Table VI. These data indicate that identical charges placed at optimum DOB will create significantly larger craters in Bearpaw shale than in alluvium or basalt. The slopes are also flatter for Bearpaw shale.

Apparent Crater Geometry[6]

Figure 70 shows the average crater profile of each of the Pre-Gondola I apparent craters. Each of the average crater profiles were adjusted vertically so that their deepest points coincided. An examination of the orthogonal and average profiles drawn for each of the craters shows that, while the average slope of the craters at the preshot ground surface (θ) is 29 deg, the average slope of the craters along most of the orthogonal

Table VI. Comparative cratering characteristics.

Parameter	Hard rock (basalt) ($ft/kt^{1/3.4}$)	Alluvium ($ft/kt^{1/3.4}$)	Bearpaw shale ($ft/kt^{1/3.4}$)
Limiting DOB for cratering	200	320	195
Optimum DOB (R_a)	140-150	160	130
Maximum R_a	153	187	250
Optimum DOB (D_a)	130-150	112	130
Maximum D_a	80	95	102
Ratio R_a/D_a	1.92	2.12	2.48
Average asymptotic slope (deg)	35.0	32.5	29.0

crater profiles is approximately 26 deg.[9] These slopes are significantly flatter than those observed in either alluvium or basalt.

Because only slight variations in the average crater profiles exist, the Charlie average crater profile was selected as representative and thus was used for comparison with the shape of a hyperbola (Fig. 71). From this figure, it is seen that the shape of the craters produced in Bearpaw shale by detonations at near optimum depths of burial can be closely approximated by a hyperbola.

Relative Apparent Lip Crest Dimensions

Table VII tabulates the average lip heights and lip crest radii and the H_{al}/R_a and R_{al}/R_a values of each crater.

Maximum Range of Missiles

Figure 72 and Table VIII present the maximum range of missiles. The $W^{1/3.8}$ energy equivalent scaling was found to provide the best correlation of all available data. The Bravo results were discounted

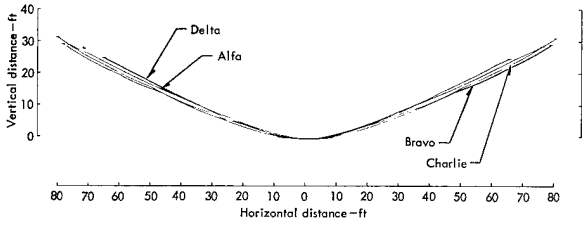

Fig. 70. Comparison of average crater cross sections.

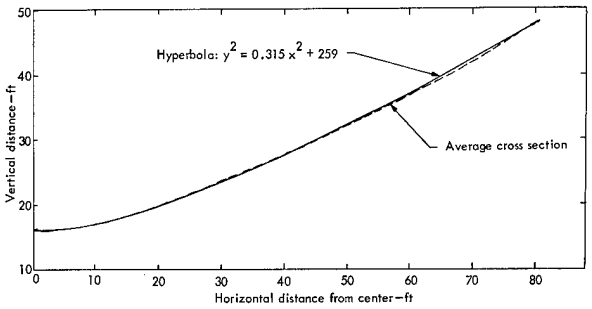

Fig. 71. Comparison of Charlie average crater cross section with hyperbola.

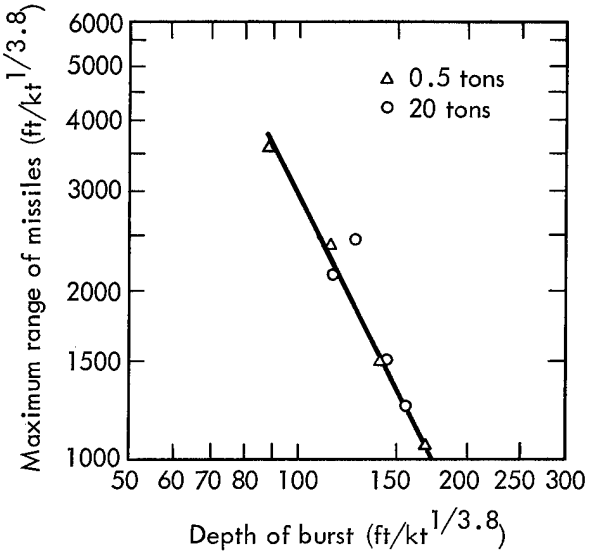

Fig. 72. Maximum range of missiles for Bearpaw shale (Ref. 6).

Table VII. Apparent lip crest data.[6]

	Charlie	Bravo	Alfa	Delta	Average
Average lip height, H_{al} (ft)	14.5	13.7	13.9	13.0	13.8
H_{al}/R_a	0.18	0.17	0.18	0.20	0.18
H_{al}/R_{al}	0.14	0.13	0.14	0.14	0.14
Average lip crest radius,					
R_{al} (ft)	101.8	102.1	100.4	94.5	99.7
R_{al}/R_a	1.27	1.32	1.30	1.45	1.34

Table VIII. Scaled maximum missile range, R_{me}.

	Units	Charlie	Bravo	Alfa	Delta
Energy equivalent yield	(kt)	0.02158	0.02130	0.02238	0.02226
Energy equivalent scaling factor	$(kt^{1/3.8})$	0.364	0.362	0.366	0.365
Actual R_{me}	(ft)	800	905	545	453
Scaled R_{me}	$(ft/kt^{1/3.8})$	2200	2500	1490	1240

because the Bravo site was overlain by 6 ft of overburden and the maximum missile range approaches that expected for alluvium. The equation of the line in Fig. 72 is:

$$\frac{R_{me}}{W^{1/3.8}} = 3 \times 10^{7} \left[\frac{DOB}{W^{1/3.8}}\right]^{-2}$$

where: R_{me} and DOB are in ft W is in kt.

In all cases the most distant missiles located and recorded consisted of 1/2- to 1-1/2-lb weathered clay-shale fragments rather than ejecta pellets placed in the material (Table VIII). The predicted maximum range of missiles would average 35% greater than actual if $W^{1/3.4}$ scaling from the 1000-lb SSC data were used.

Ejecta Studies

Table V summarizes the results of the ejecta studies. Figures 34, 35, 44-47, 57, 58, 66, and 67 show the source and final range of identified ejecta pellets. There are insufficient data to warrant drawing iso-distance contours on Figs. 34, 44, 46, 58, and 67. However, it is noted that ejecta pellets located near the surface in holes at 15 and 30 ft from SGZ achieved maximum range. The relationship between the scaled DOB and the preshot position of maximum range missiles can be qualitatively evaluated from ejecta pellet data and studies of ground surface motion,[9] but such an analysis is beyond the scope of this report.

CONCLUSIONS

As a result of the Pre-Gondola I detonation, the cratering characteristics of the Bearpaw shale at the Fort Peck site have been calibrated. The craters produced were both significantly deeper and particularly wider than craters produced in alluvium and basalt, and had flatter average crater slopes. The overall shape of the craters is hyperbolic.

APPLICATION OF RESULTS

Figure 73 shows the actual alignment used for the Pre-Gondola II row-charge cratering experiment on 25 June 1967. The charge spacings and DOB were based on Figs. 68 and 69. The alignment was chosen to expose the Pre-Gondola I craters to maximum dynamic loading. The fact that all design objectives were achieved by Pre-Gondola II attests to the success of the Pre-Gondola I Cratering Calibration Series.[15]

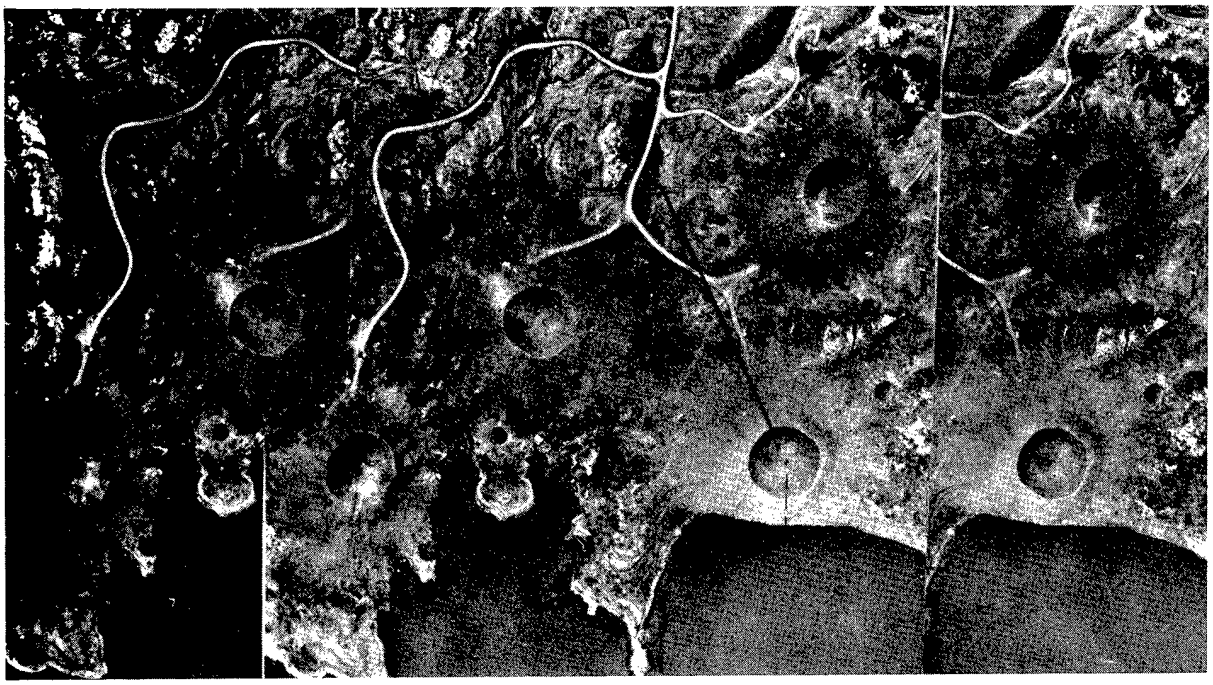

Fig. 73. Stereo-pairs, Pre-Gondola I craters, 5 November 1966 (showing alignment for Pre-Gondola II row-charge crater).

Surface Motion Studies

This chapter summarizes the surface motion studies subprogram which was reported separately[13] from the other crater studies programs described in the previous section. The motion of the ground surface resulting from subsurface detonations was studied to develop a better understanding of the cratering phenomena and to provide general diagnostic information concerning cratering physics. The Pre-Gondola I series offered a unique opportunity to obtain surface motion measurements for four detonations of equal yield at varying DOBs in a wet, clay-shale medium.

INTRODUCTION

Objectives

The following are the objectives of the study of the surface motion of this event:

1. To develop a method of predicting surface velocities for detonations in Bearpaw shale.
2. To utilize the surface motion as a primary tool in understanding the cratering mechanism for these detonations.

To accomplish these objectives, the scope of the program included consideration of the following aspects of surface motion:

1. Characteristic times to include initial target movement, peak spall, onset of gas acceleration, and peak velocity achieved.
2. Peak velocities over SGZ as well as velocities of targets out from SGZ, to determine the relationship of velocity with DOB.
3. The velocity decay with distance from SGZ.
4. The relative contribution of spall and gas acceleration to cratering in this medium.
5. The freefall target trajectories for correlation with ejecta studies.
6. The rising mound size and shape for correlation with crater measurement studies.

Background

Surface motion studies of single- and row-charge cratering events in both alluvium and basalt have led to a general understanding of the surface motion phenomena in these two media, although detailed information of single-charge detonations above the 20-ton level is meager, and detailed data exist for only one row event in each medium. The results of the 1000-lb Pre-Gondola Seismic Site Calibration Series indicated that the surface velocities of detonations in Bearpaw shale are somewhat higher than would be predicted from experience in basalt, and that gas acceleration is a more important mechanism in producing surface velocities in this medium than in basalt. There were also some indications from the Seismic Site Calibration Series that the distribution of ground surface velocities in Bearpaw shale was more like the distribution in alluvium than that in basalt.

Two phenomena are of interest in analyzing the surface motion produced by a subsurface detonation: spall and gas acceleration. Spall results from shock

wave interaction with the medium, and it should begin at or shortly after the arrival of the shock wave at the surface. Following the spall velocity peak, there is a much more gradual rise in velocity due to gas acceleration by the expanding gas cavity. The peak velocity achieved after the gas acceleration phase is the maximum velocity, after which the particles achieve a freefall trajectory, and little or no additional forces are generated by the explosive mechanism.

EXPERIMENTAL PROCEDURE

Surface motion data collection for Pre-Gondola I required the use of three techniques:

1. A falling mass release at zero time which fell in front of a graduated target recorded by high-speed photography. This provided a detailed velocity history of the SGZ area from the time of detonation until the peak spall velocity was achieved (~50 msec).

2. High speed photography of thirteen high contrast targets arranged on the surface at horizontal distances up to 100 ft on both sides of SGZ. These provided data from the time peak spall was achieved until the maximum velocity was attained (~250 msec).

3. Documentary photography at 64 frames/sec to provide a general picture of the mound as it rises to its maximum height and falls to the ground. This was supplemented by documentary photography from a helicopter.

Falling Mass Target

Data reduction was accomplished by means of microscopic examination of the film and data processing with a digital computer.[16,17] The falling mass target for each event (also referred to as a bowling ball target) is shown in Fig. 74. It consisted of a 16- by 4-ft plywood face mounted on a steel frame which was attached to a 6-in. pipe. The pipe was embedded in 5 ft of concrete. A bowling ball, painted white, and suspended at the top of the target, was released at the time of the detonation by means of a detonator inserted in the cord supporting the ball. The bowling ball served as a freefall reference point for measurement of the displacement of the plywood target which moved with the rising ground surface.

Surface Motion Targets

The visual surface targets consisted of 3-ft square black and white plywood panels mounted on 4-in. pipes which were emplaced in concrete to depths of not less than 3 ft. All targets were emplaced in a vertical position except the three targets to the right of the SGZ target for Bravo and Charlie and the three targets on both sides of SGZ for Alfa and Delta. These

Fig. 74. Bravo target array.

targets were each canted 20 deg from the vertical away from SGZ to determine whether canted targets would remain visible for a longer period of time than vertical targets. Previous experience on Pre-Schooner I[16] and Pre-Schooner II[18] has indicated that targets near SGZ which are placed vertically tend to rotate into the mound and disappear at an early time (~500 msec). A "pot" containing a 200,000-candle power baritol flare was bolted to the post cap of each target.

Figure 74 shows the Bravo array which was typical of Pre-Gondola I arrays.

Two reference targets of the same design as the surface motion array targets were placed 45 ft to either side of the camera line-of-sight and 200 ft in front of the target array. Figure 75 depicts the target array.

Figure 76 shows the preshot SGZ locations with respect to the two camera stations. The surface motion target arrays were perpendicular to lines-of-sight from

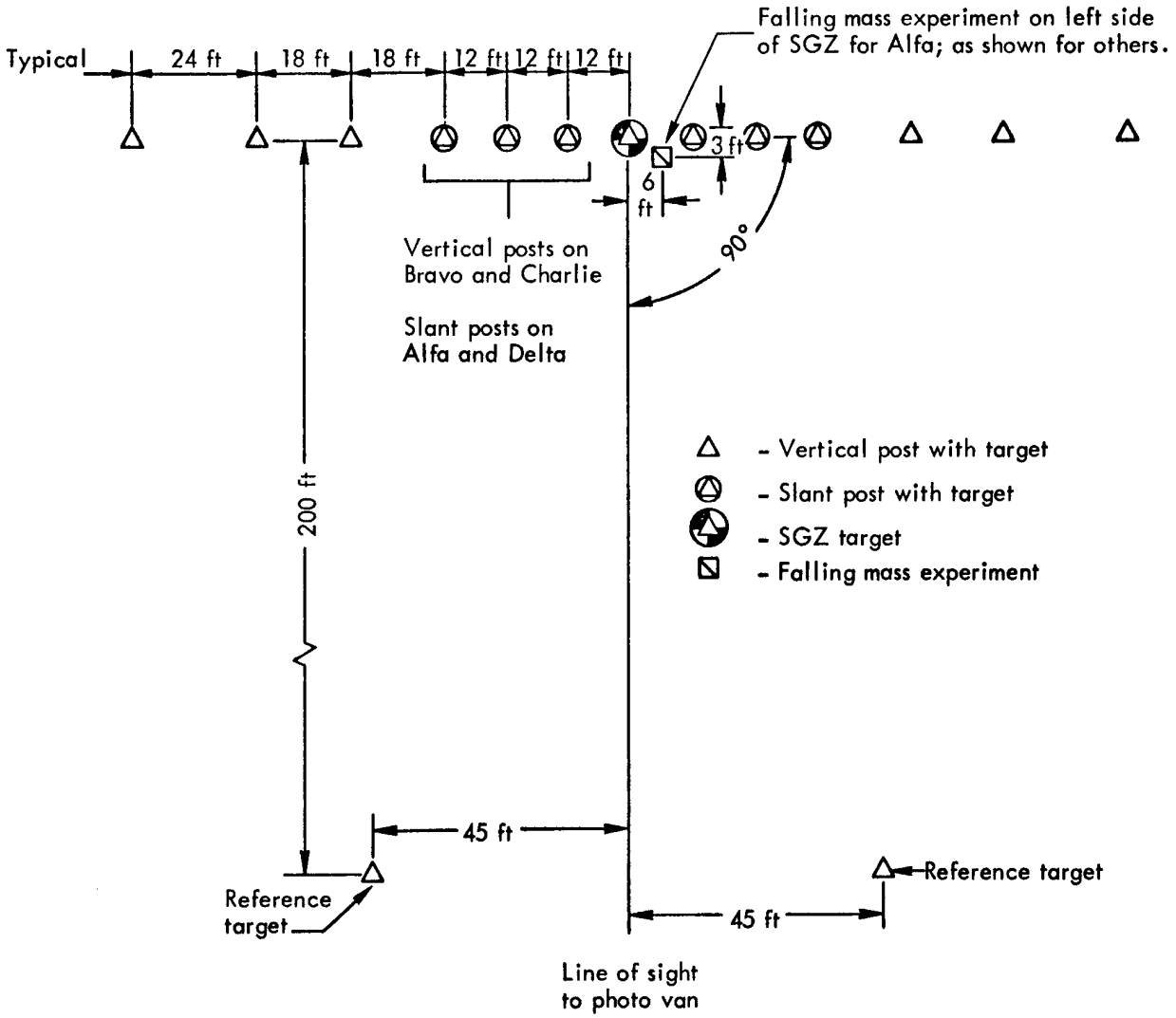

Fig. 75. Surface motion target array.

the photo van. The photo bunker housed the camera recording the motion of the bowling ball targets.

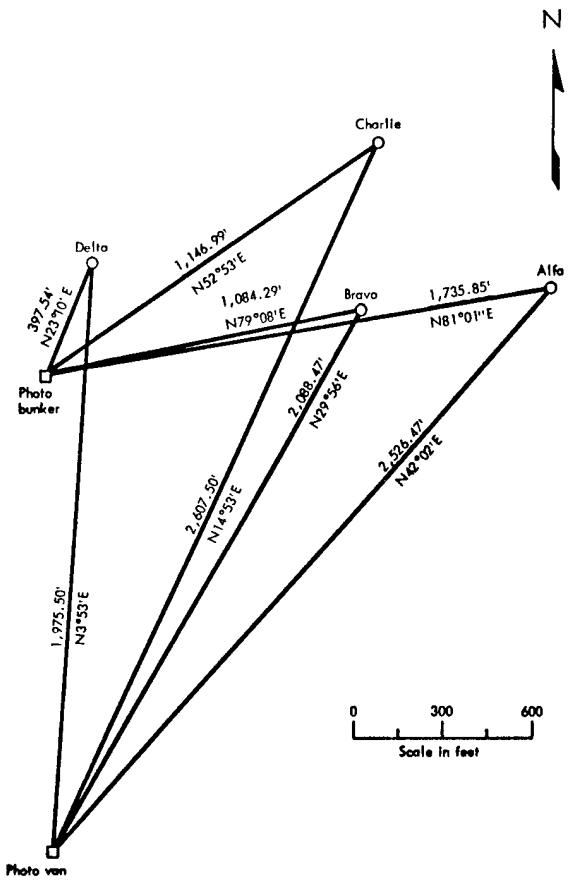

Fig. 76. Camera lines of sight.

Predicted Velocities[13]

A summary of the predicted velocities for the central nine targets is listed in Table IX. These predictions were based upon the results of the Seismic Site Calibration Series shots in the same medium and the following assumptions: (1) that surface velocities are related to scaled depth of burst ($DOB/W^{1/3}$), and (2) that the target velocities out from SGZ would vary in the same manner as did the velocities of 1000-lb shots.

RESULTS[13]

General

All cameras photographing the surface motion of each event operated satisfactorily, but problems including an early flash of burning material over SGZ caused a loss of data on the Bravo, Alfa, and Delta Events.

Peak velocities of all 13 surface motion targets were obtained for the Charlie and Delta Events, 12 of the 13 surface motion targets for Alfa, and 5 of the 13 for Bravo. Spall velocities were obtained from all

Table IX. Predicted peak target velocities.[13]

Target No.	Target position (ft)	Charlie[a] (fps)	Bravo (fps)	Alfa (fps)	Delta[a] (fps)
SGZ	0	231	200	162	142
1R	+12	224	188	153	140
2R	+24	175	152	132	127
3R	+36	128	118	109	108
4R	+54	82	77	73	75
1L	-12	211	188	153	132
2L	-24	163	152	132	112
3L	-36	124	118	109	90
4L	-54	74	77	73	64

[a]Values to right are greater because terrain sloped uphill to left and downhill to right.

targets on event Charlie, 10 targets on Bravo, and 9 targets on Alfa.

Complete velocity histories of the bowling ball targets on events Charlie and Bravo were obtained from zero time until the bowling ball hit the rising mound. Partial data were obtained from the Alfa and Delta bowling ball targets.

The peak velocity of the top of the rising mound was obtained for each event. Figure 77 shows a plot of peak SGZ velocity vs scaled depth of burst ($ft/kt^{1/3}$) for the four Pre-Gondola I shots and for the other high explosive and nuclear detonations. The Bearpaw shale line is slightly above the Buckboard basalt line for nitromethane detonations, and considerably above the Buckboard basalt line for nuclear detonations. The relationship for the peak SGZ velocities in Bearpaw shale can be written as:

$$V_{SGZ} \propto (dob)^{-2.1} \quad (1)$$

where V_{SGZ} = peak vertical velocity of SGZ target (ft/sec)

dob = scaled depth of burst ($ft/kt^{1/3}$).

The nuclear Buckboard basalt velocities have a similar relationship of:

$$V_{SGZ} \propto (dob)^{-1.6} \quad (2)$$

The exponent of the dob term in each equation represents the slope of the line in Fig. 77.

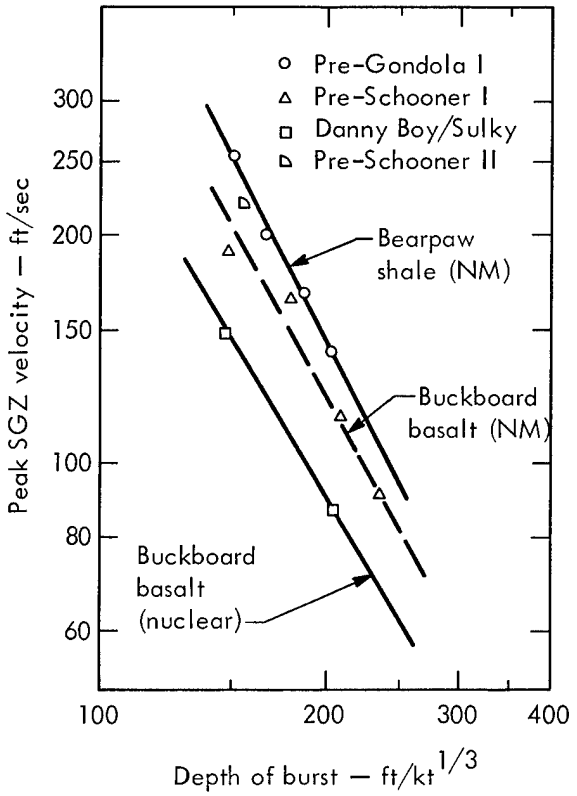

Fig. 77. Peak SGZ velocities vs depth of burst for selected events.

Charlie

The Charlie Event was the most successful detonation from a surface motion viewpoint because this was the only detonation of the four which was not accompanied by a bright flash of burning material shortly after zero time.

The mound reached a maximum height of 850 ft at 6 sec after detonation. At this time it was 500 ft wide at its base. No venting of gaseous material was visible at any time during the growth of the mound. It appeared that all of the gases produced by the explosion were contained beneath the rising mound of material, and when the mound collapsed, a volume of white vapor was expelled horizontally at the base of the mound in the base surge.

Figure 78 shows mound growth to 260 msec. Also shown on this figure are the target trajectories and the direction of movement of each target at 260 msec (the approximate time of freefall). The

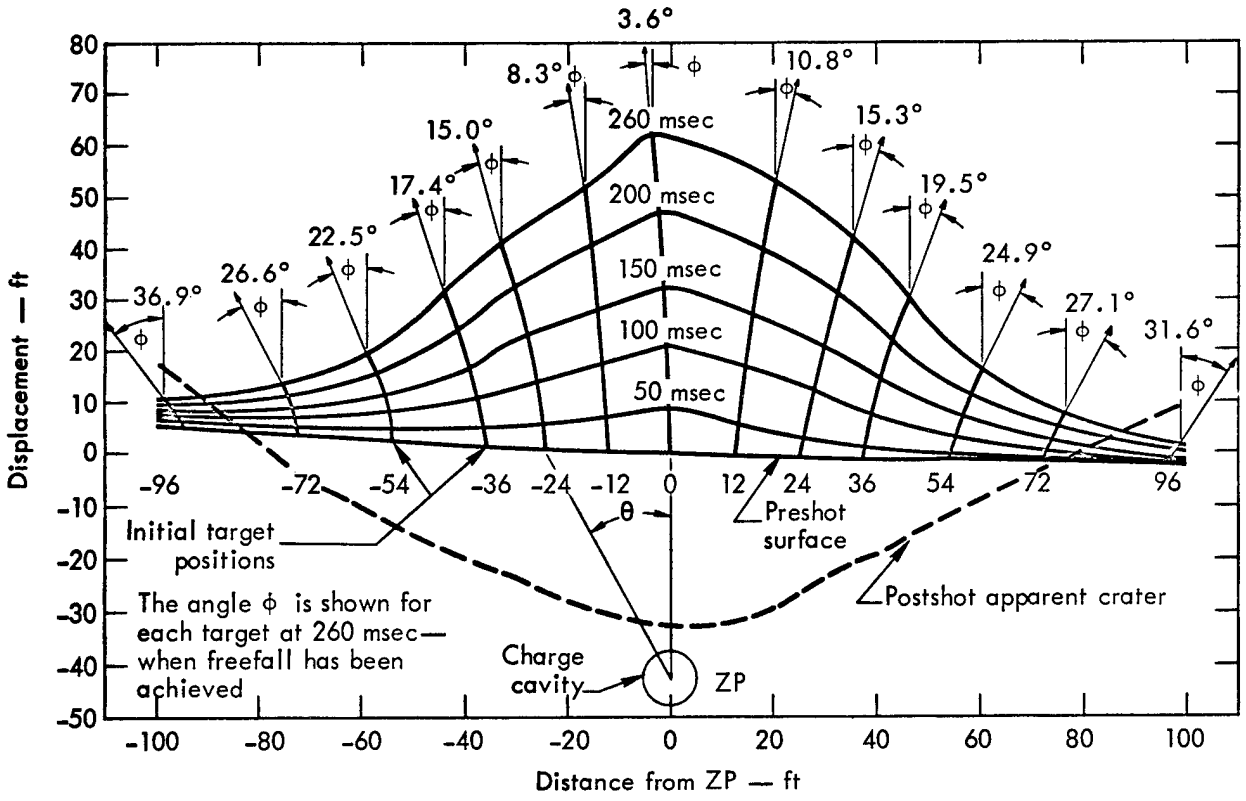

Fig. 78. Mound growth to 260 msec (Pre-Gondola I Charlie).

charge cavity and the postshot apparent crater profile are also superimposed on Fig. 78. Figure 79 shows the growth of the mound to 3 sec.

Figure 80 shows a plot of the total velocity and spall velocity vs preshot radial distance from ZP to each target base. Also shown is a plot of early phase peaks in the spall velocity plots. These were distinct peaks in spall velocity before a second rise to the maximum spall velocity exhibited by 6 of the 13 targets. The following is the relationship for the peak total velocities in Fig. 80:

$$V_{peak} \propto R^{-2.3} \qquad (3)$$

where V_{peak} = peak total velocity (ft/sec)

R = preshot radial distance from ZP to target base (ft).

The relationship for the spall velocities is:

$$V_{spall} \propto R^{-2.6} \qquad (4)$$

The slope of the early phase spall line is approximately the same as the peak spall line. On the average, the peak spall velocity is approximately 77% of the peak vertical velocity for the central nine targets.

Figure 81 shows the velocity vs time plot for the bowling ball target. The onset of spall at the surface occurs at 7 ± 2 msec. The peak velocity due to

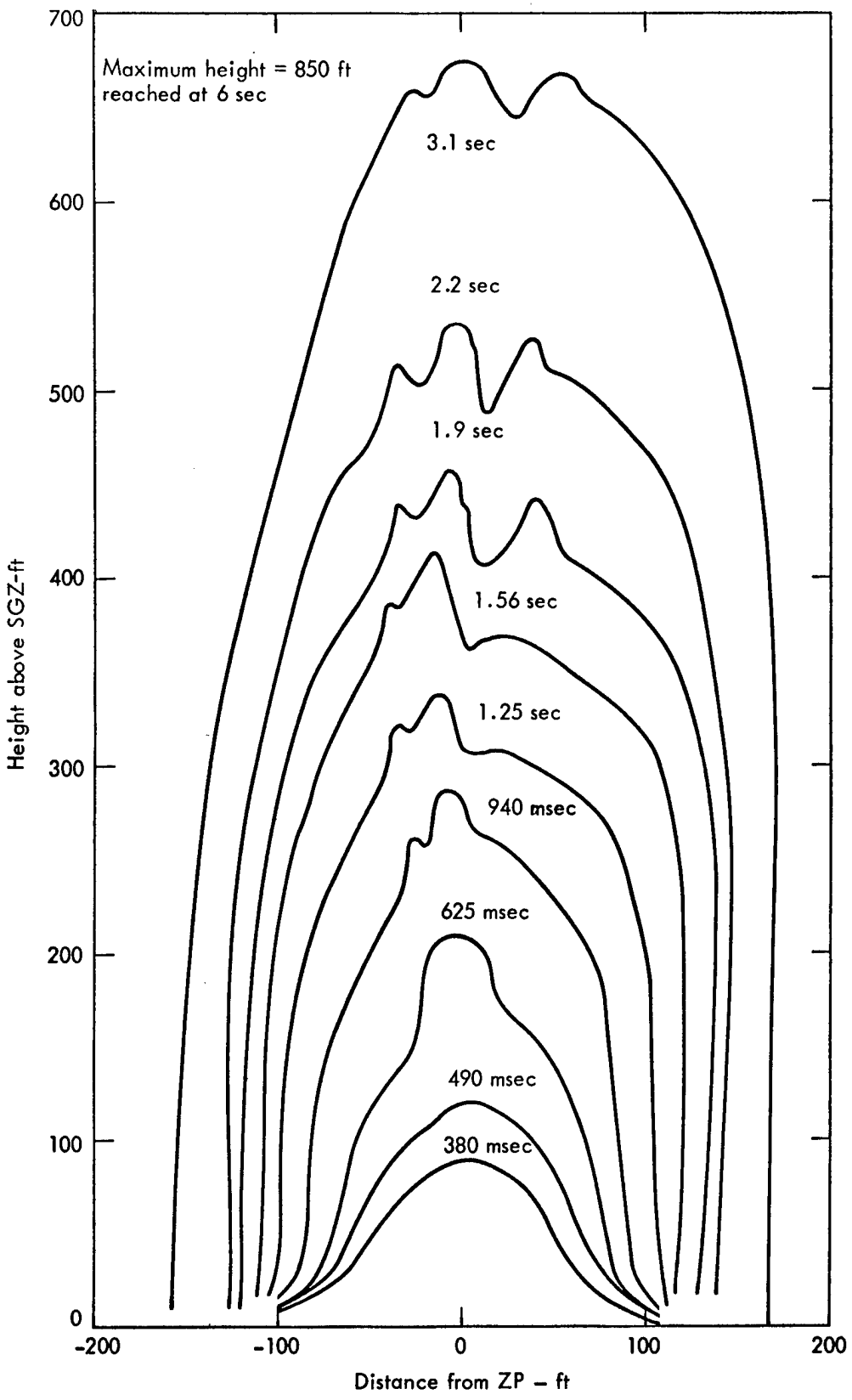

Fig. 79. Mound growth to 3.1 sec (Pre-Gondola I Charlie).

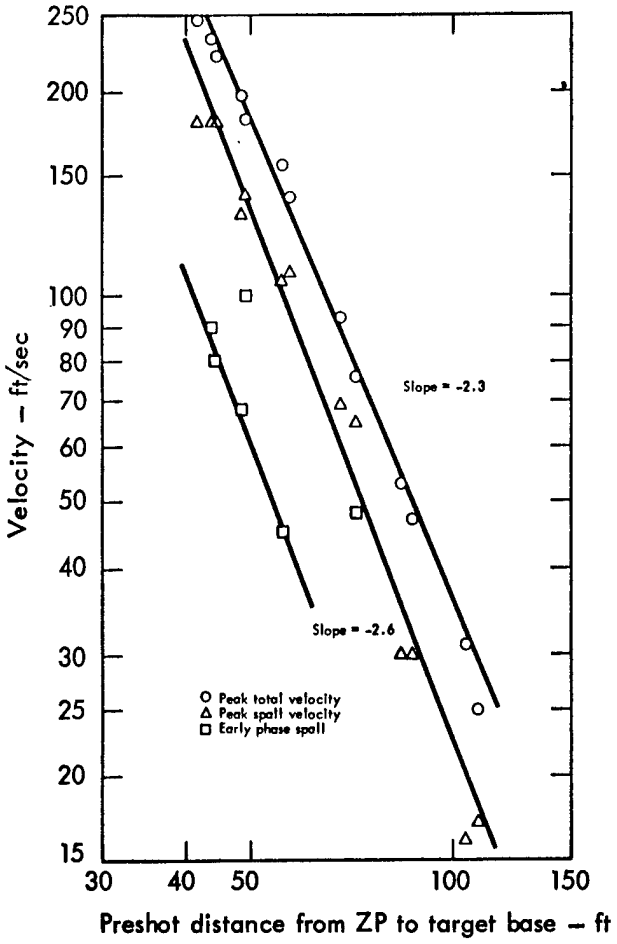

Fig. 80. Surface velocities vs radial distance from ZP to each target base (Pre-Gondola I Charlie).

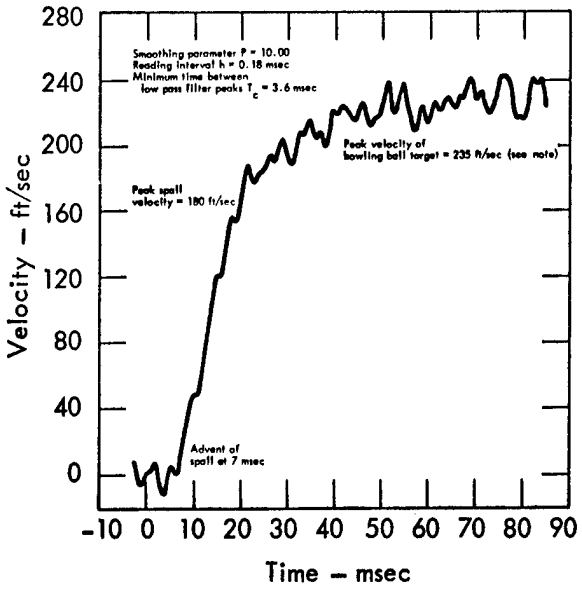

Fig. 81. Vertical velocity of bowling ball target (Charlie Event). Note: Since the bowling ball data extend only to 85 msec, the total influence of gas acceleration is not recorded, nor is the ultimate peak velocity from gas acceleration.

spall was 180 ± 4 ft/sec achieved at 21 msec. This peak was followed by a constant rise in velocity to 235 ± 6 ft/sec at 85 msec, at which time the bowling ball hit the rising mound.

Bravo

Figure 82 shows the growth of the mound from zero time to 260 msec. Also shown are the trajectories of five targets and their direction of movement (ϕ) at 260 msec. The postshot apparent crater and the preshot charge cavity are also shown. Figure 83 shows the mound growth to 4 sec. After approximately 1.5 sec large blocks of ejecta began to "pull away" from the main mound. In Fig. 83, the 2.7-sec, 3.2-sec, and 4-sec profiles are of this outer shell of large blocks. The Bravo Event was the only one for which this separation (from the main mound) of such large blocks was so pronounced.

Figure 84 shows plots of the peak total velocities and spall velocities vs the preshot distance from ZP to the target base. The peak total velocities can be represented by:

$$V_{peak} \propto R^{-2.2} \qquad (5)$$

It should be noted that the parameters are the same as for Eq. (3). The spall velocity line can be represented by:

$$V_{peak} \propto R^{-2.5} \qquad (6)$$

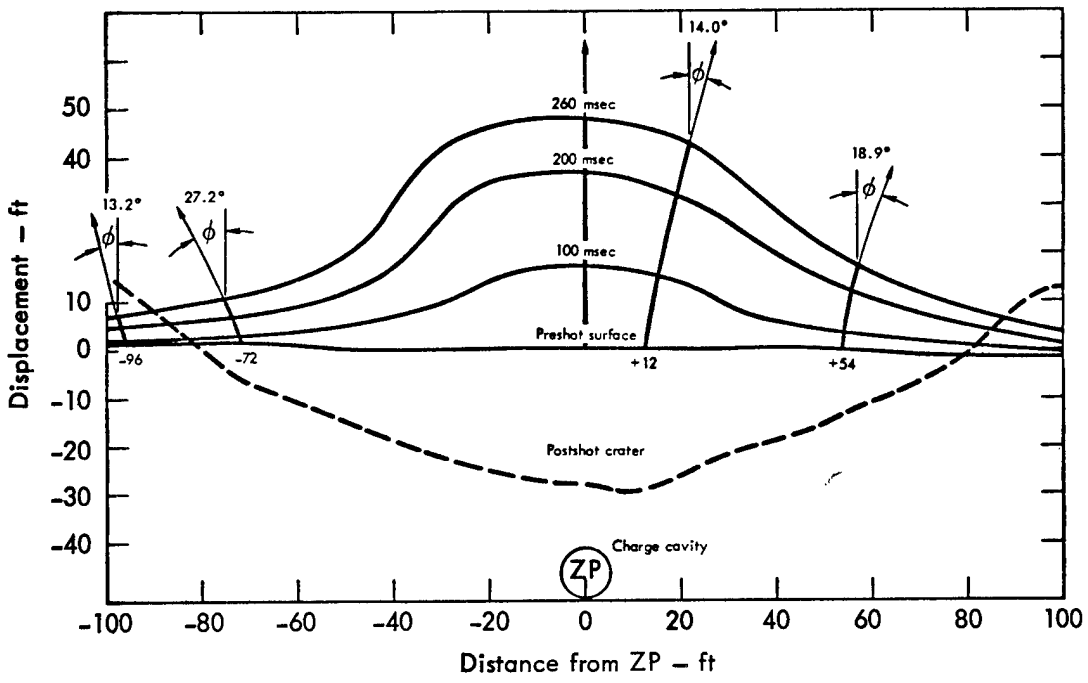

Fig. 82. Mound growth to 260 msec (Pre-Gondola I Bravo).

Figure 85 shows that the advent of spall was at 6 msec, after which time the velocity rose very gradually to a peak spall velocity of 155 ft/sec at 42 msec. It is interesting to compare the Bravo bowling ball results with the Charlie bowling ball results in Fig. 81. The velocity of the Charlie bowling ball target rose sharply to a peak spall velocity at 18 msec, while the Bravo velocity did not peak until 42 msec.

Contrasted with the sharp rise of the Charlie velocity, the Bravo velocity appears to be due more to gas acceleration than spall. However, the Bravo gas acceleration phase was not definitely evident in other surface motion target records and did not begin until about 60 msec after detonation. Christopher[13] believes this rise from 8 to 42 msec of the Bravo velocity is due to spall. He advances arguments which link both the slow spall velocity rise and unique ejecta blocks to geologic structure, primarily a six-ft thick soft cohesive overburden layer.[13]

Alfa

Figure 86 shows the mound growth and target trajectories to 280 msec after detonation. Figure 87 shows the mound growth to its maximum height of 350 ft at 3.8 sec after detonation.

Figure 88 shows a plot of the peak total velocity and spall velocity of each target vs the preshot distance from ZP to the target base. The peak total velocity line can be represented by:

$$V_{peak} \propto R^{-2.1} \qquad (7)$$

It should be noted that the parameters

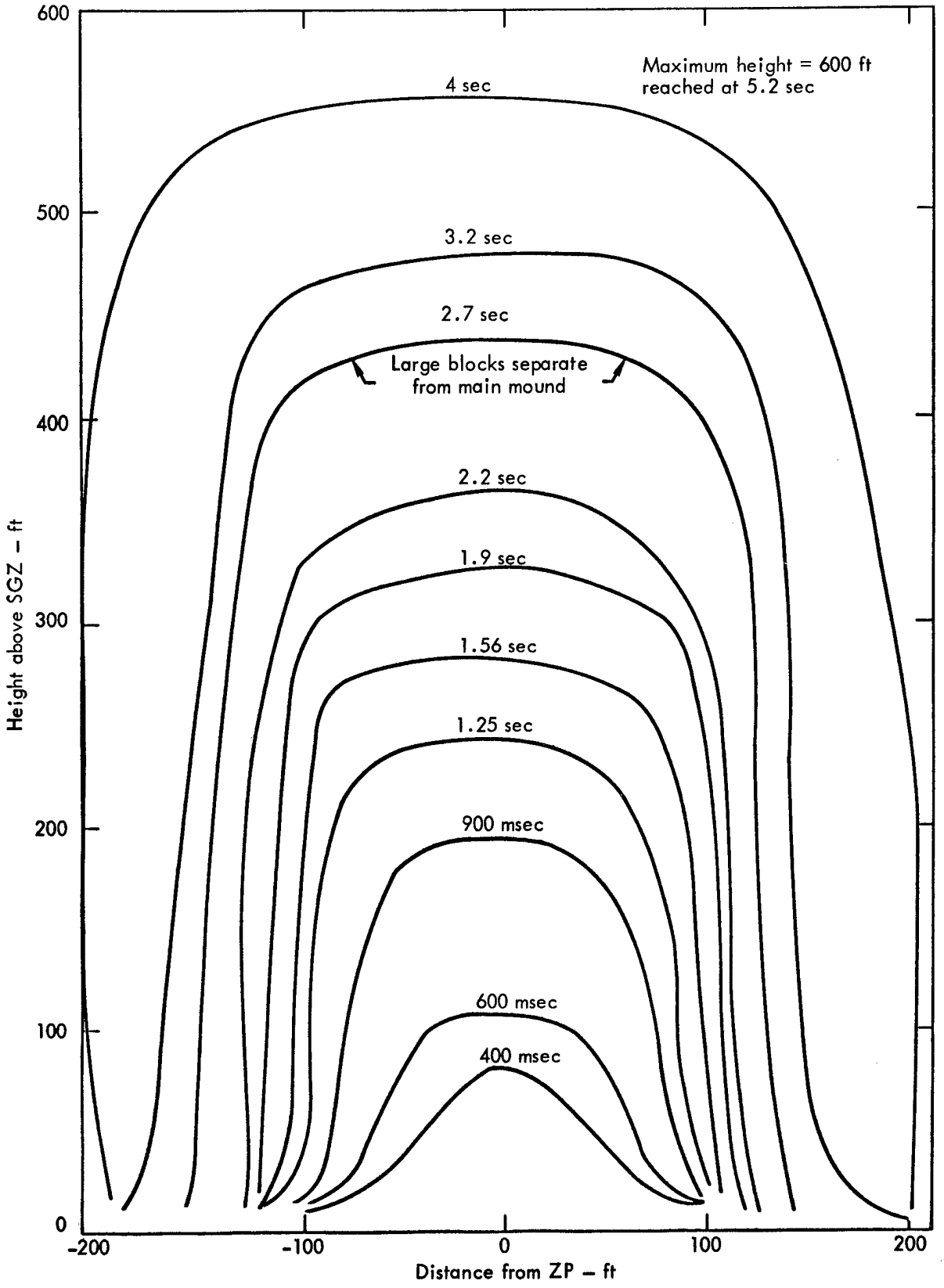

Fig. 83. Mound growth to 4 sec (Pre-Gondola I Bravo).

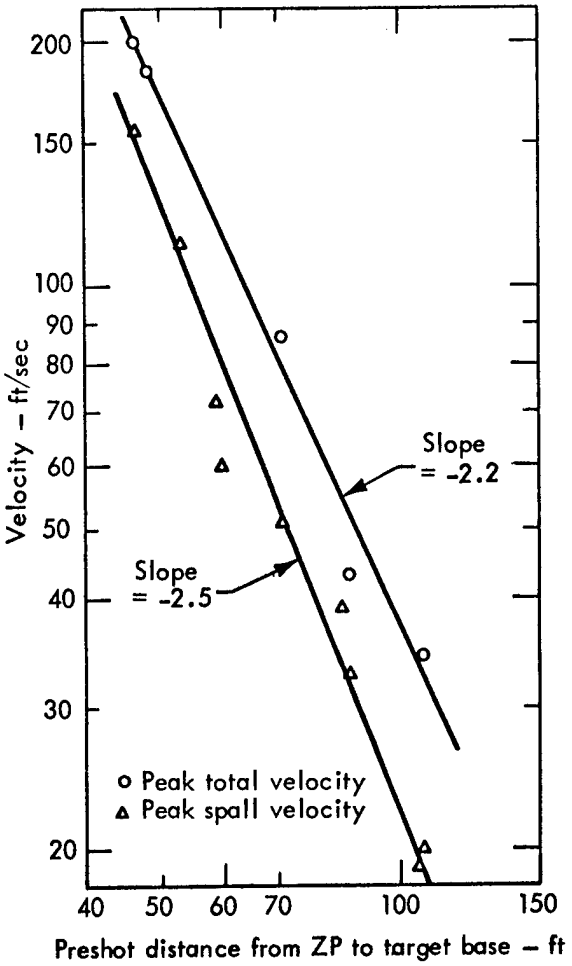

Fig. 84. Surface velocities vs preshot radial distance from ZP to target base (Pre-Gondola I Bravo).

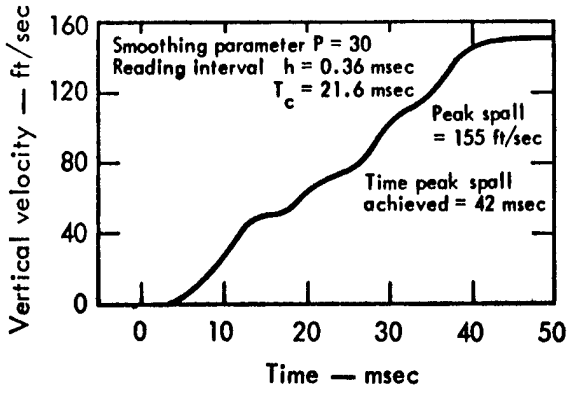

Fig. 85. Vertical velocity of bowling ball target (Bravo Event).

are the same as for Eq. (3). The spall velocities can be represented by:

$$V_{spall} \propto R^{-2.6} \qquad (8)$$

Figure 89 shows velocity vs time plot of the bowling ball target. The data were taken from the bowling ball film to 136 msec after zero time (when the bowling ball hit the mound) except for the interval from 7.3 to 52.8 msec when the brightness of the burning material obscured the images on the film. It is assumed that the advent of spall was concurrent with

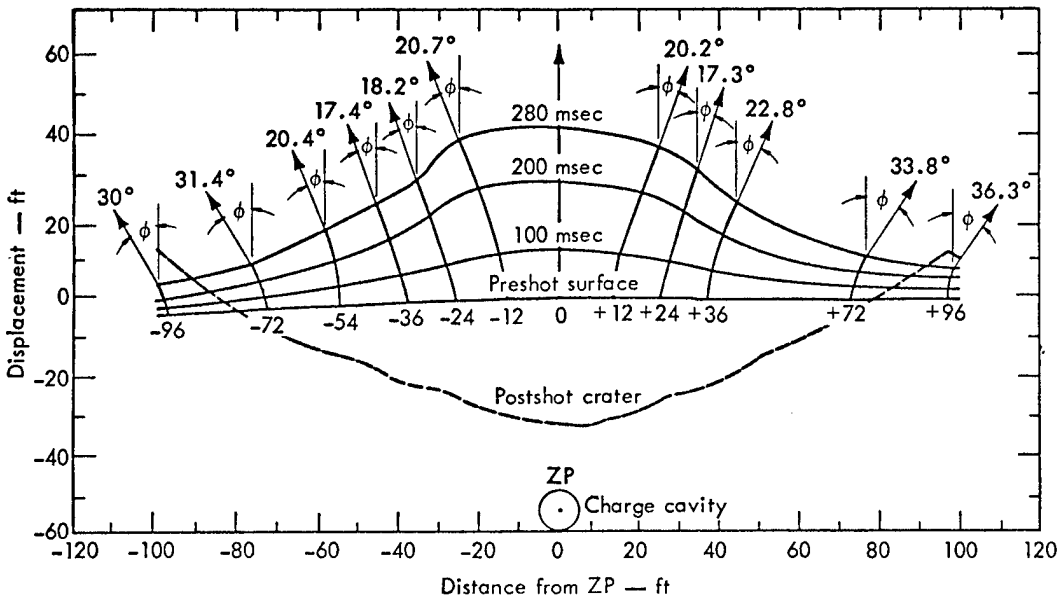

Fig. 86. Mound growth to 280 msec (Pre-Gondola I Alfa).

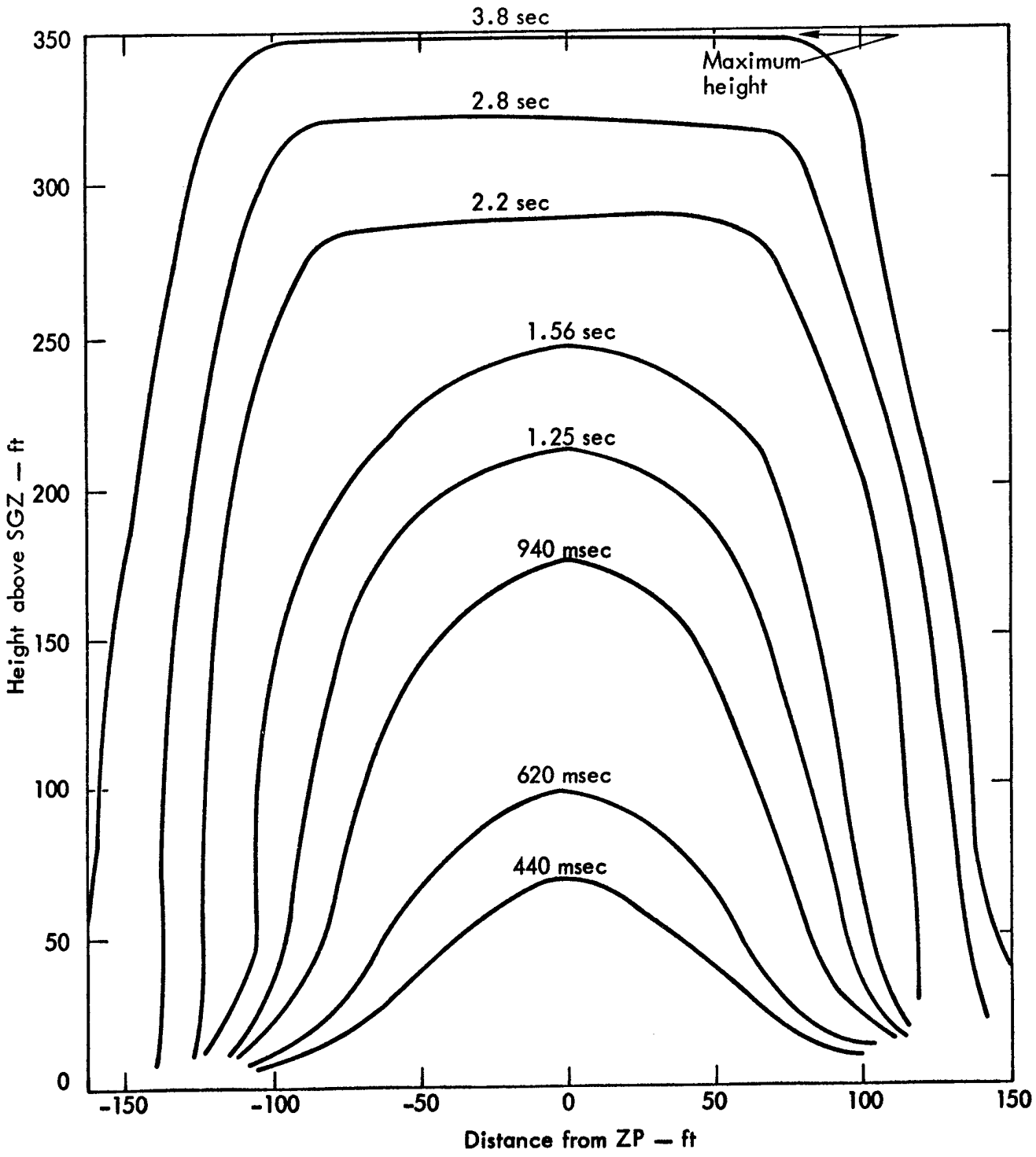

Fig. 87. Mound growth to 3.8 sec (Pre-Gondola I Alfa).

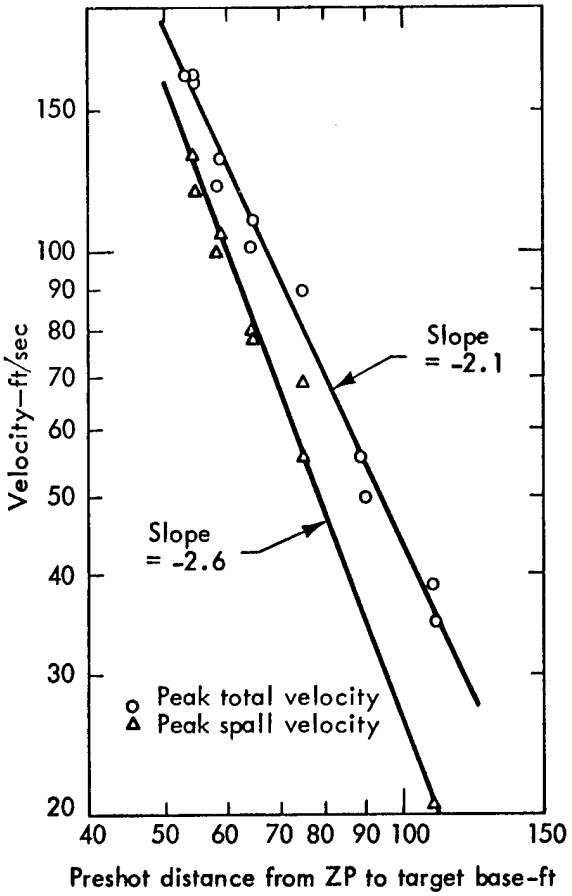

Fig. 88. Surface velocities vs preshot radial distance from ZP to target base (Pre-Gondola I Alfa).

the flash of burning material, and that peak spall velocity was reached before the target became visible.

Delta

Figure 90 shows the mound growth and target trajectories to 280 msec. Notice the slope of the preshot ground surface was about 5% or 4 deg over the entire

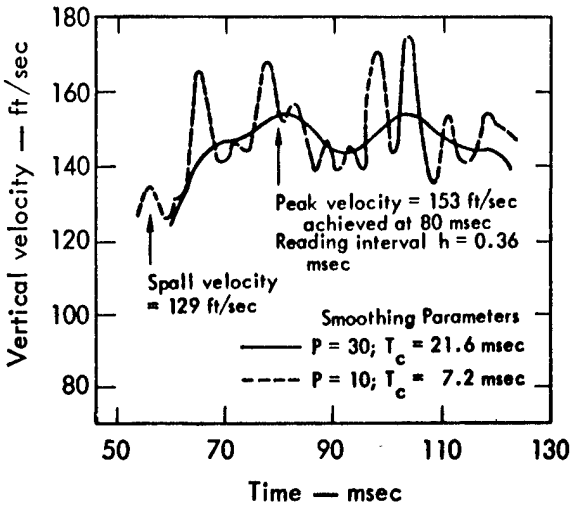

Fig. 89. Vertical velocity vs time for bowling ball target (Pre-Gondola I Alfa).

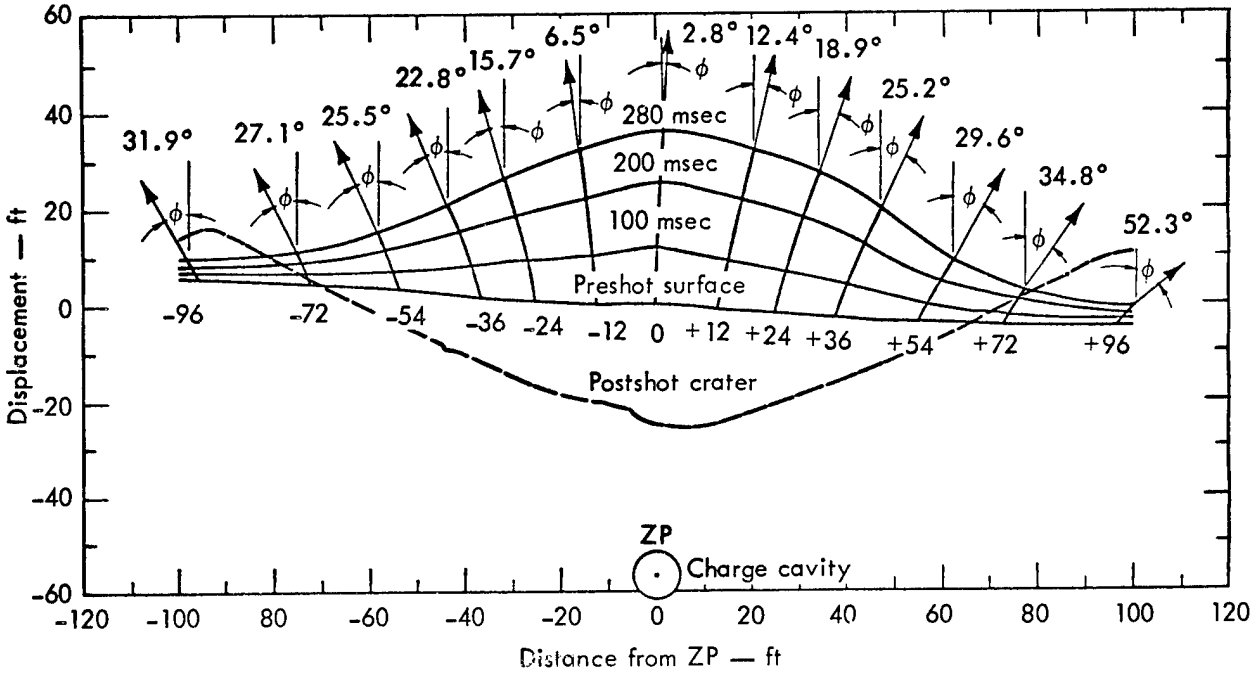

Fig. 90. Mound growth to 280 msec (Pre-Gondola I Delta).

target array (200 ft). The effect of the slope is clearly reflected in the angles ϕ in which the targets were moving at free-fall (280 msec).

Figure 91 shows the growth of the mound to its maximum height of 322 ft at 3.8 sec. A line is shown which is drawn from the ZP perpendicular to the preshot ground surface. Note how the mound grew with this line as its axis.

Figure 92 shows the shape of the mound as it fell between 4 and 7 sec after the detonation. Notice that the material in the downhill half of the mound fell well outside the crater lip crest.

Figure 93 shows a plot of the peak velocity vs the preshot distance from ZP to the target base for each target.

Figure 94 shows vertical velocity vs time for the bowling ball target which first became visible through a flash of burning material at 70 msec. The velocity appears to be rising at 70 msec to a peak at 83 msec of 135 ft/sec. It is probable that peak spall velocity had been achieved prior to 70 msec, and gas acceleration had already begun before the flash subsided. The spall velocity, therefore, was not measured.

DISCUSSION AND INTERPRETATION[13]

General

There are two basic limitations in a surface motion study of this nature: (1) the only points on the ground surface above the detonation which can be studied in detail are those at which targets are positioned, and (2) the analysis of one array of targets is, at best, a two-dimensional analysis. Experience from nuclear and HE detonations has indicated that the motion of points in between target positions can be validly inferred from the motion of the targets.[16,18,19] The four Pre-Gondola I detonations appeared (in the helicopter films) to be very symmetrical. It is concluded that the motion along one axis closely approximates the motion along any axis for all of the detonations with the possible exception of Delta. The Delta Event was under a surface with a 5% slope. However, the target array extended almost directly in line with the angle of the slope. Geologic conditions above the shot point could also have had an effect on the symmetry of the rising mound.[20]

Comparison of Surface Velocities of Pre-Gondola I with Those of Detonations in Other Media

In order to compare the observed surface motion velocities for the Pre-Gondola I events with those resulting from other detonations, explosive yield is scaled. Cube-root scaling of explosive energy yield (W) is generally considered valid based upon the reasonable assumption that the acceleration of gravity plays an insignificant role in influencing spall velocity.

It is desired to test an empirical power law rate of decay of velocity with distance from ZP by plotting the logarithm of velocity measured at SGZ against the logarithm of the DOB scaled by the cube root of the explosive energy yield (Figs. 95 and 96).

In Figs. 95 and 96 the SGZ peak spall and peak total velocities observed during the Pre-Gondola I events are compared with the same velocities for detonations in other media. Figure 95 shows the

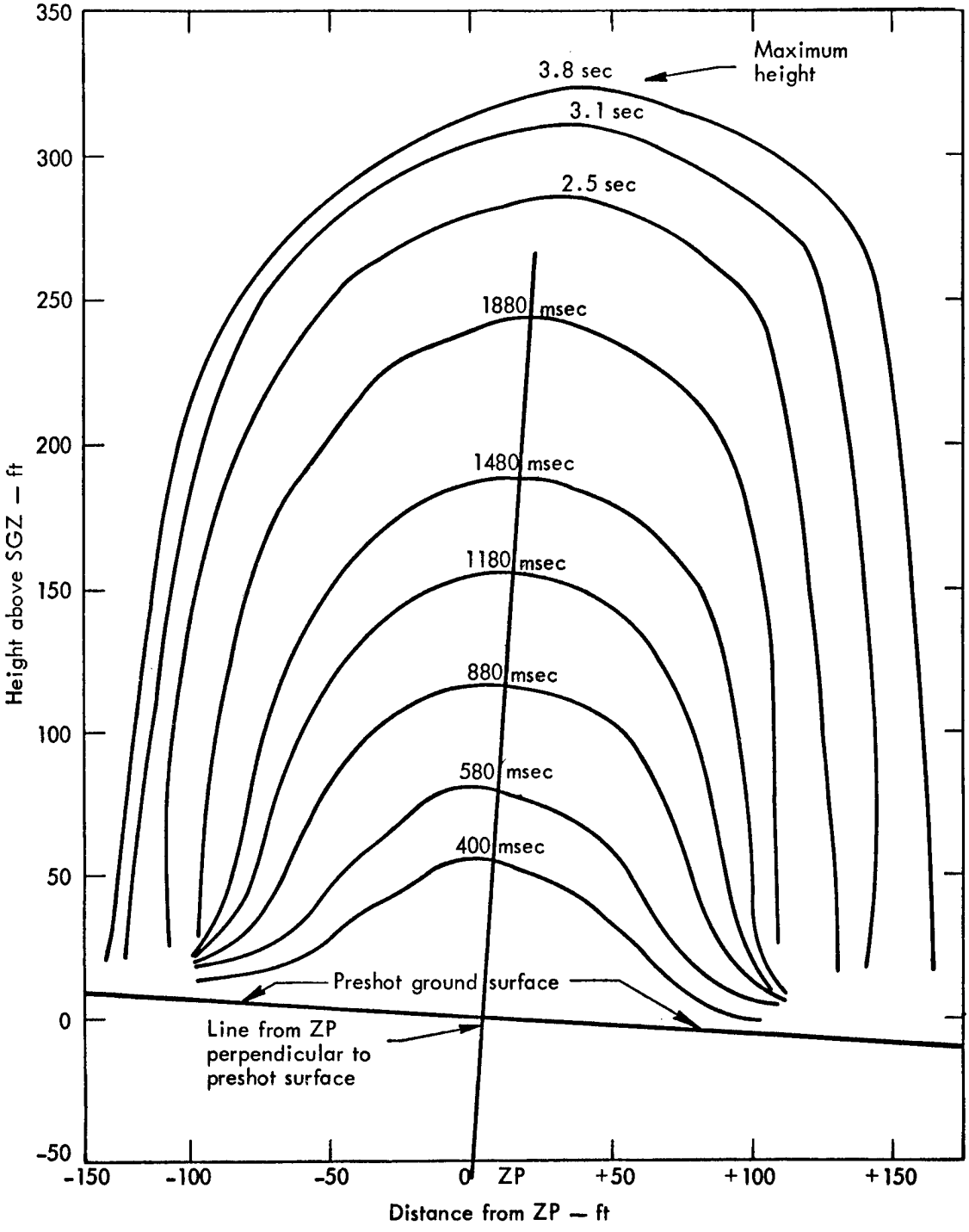

Fig. 91. Mound growth to 3.8 sec (Pre-Gondola I Delta).

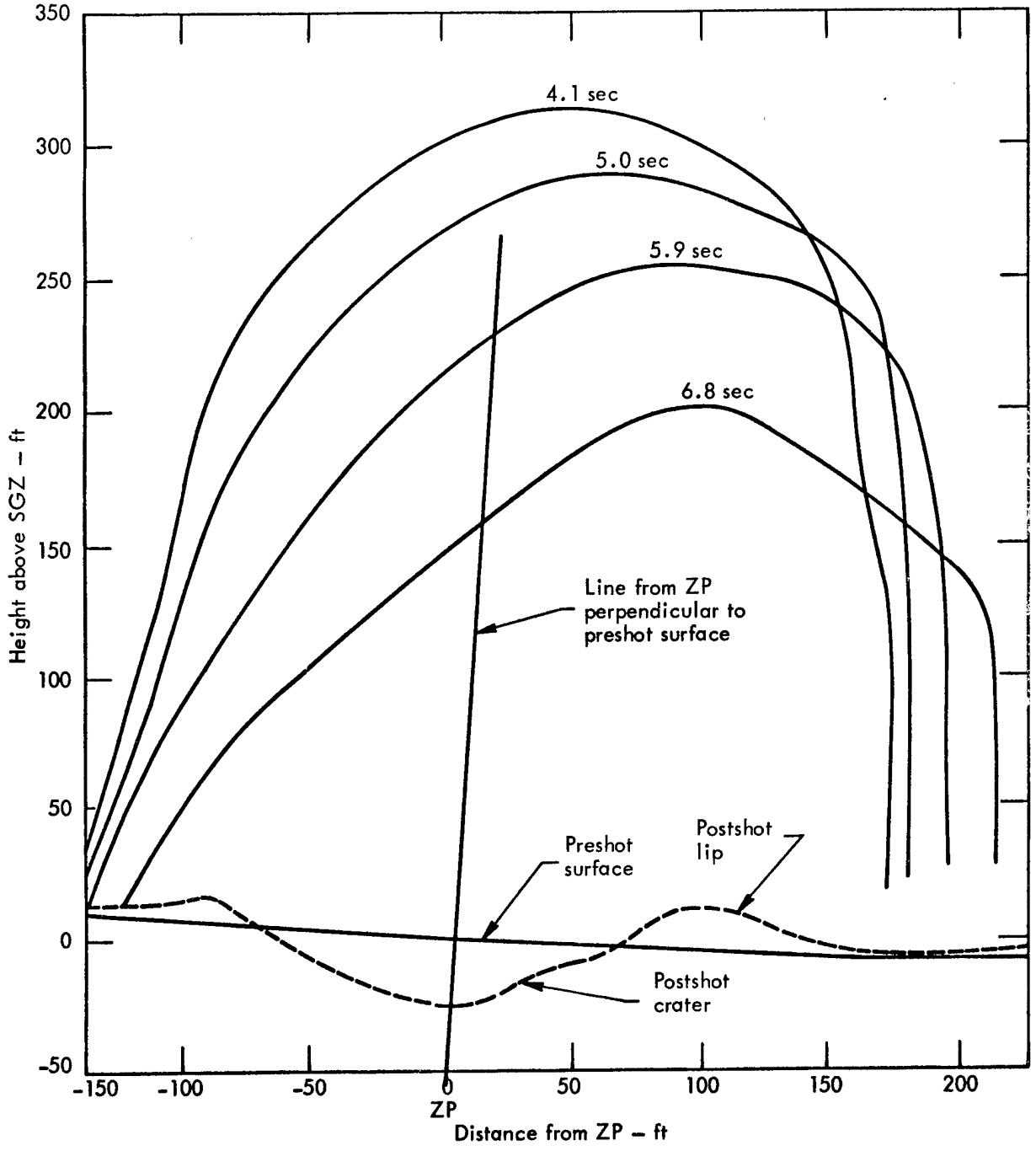

Fig. 92. Falling mound between 4 and 7 sec (Pre-Gondola I Delta).

peak spall velocity vs λ, the scaled depth of burst DOB/$W^{1/3}$, for nuclear detonations in basalt and HE detonations in basalt, alluvium, rhyolite, and shale. The Pre-Gondola I peak spall velocities appear consistent with the spall velocities from HE detonations in basalt, and are greater than the HE data in alluvium and rhyolite and nuclear data in basalt.

It should be noted that cube-root scaling may be inappropriate during the gas acceleration stage when the acceleration

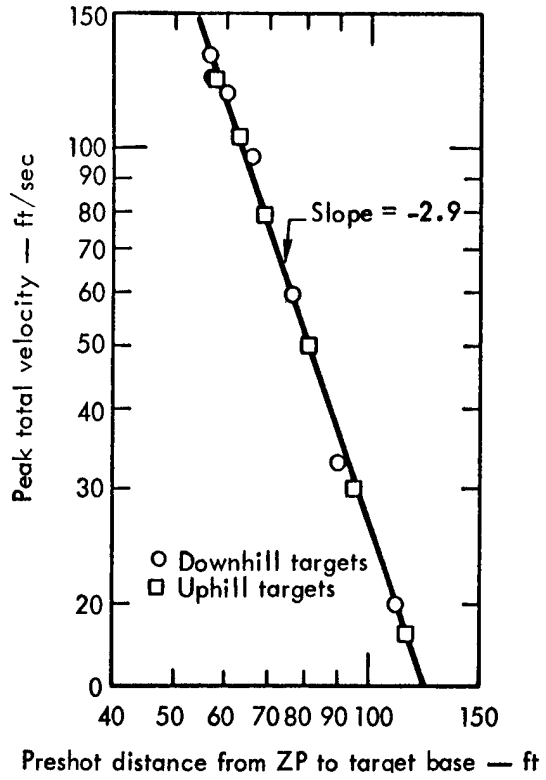

Fig. 93. Peak total surface velocities vs radial distance to ZP (Pre-Gondola I Delta).

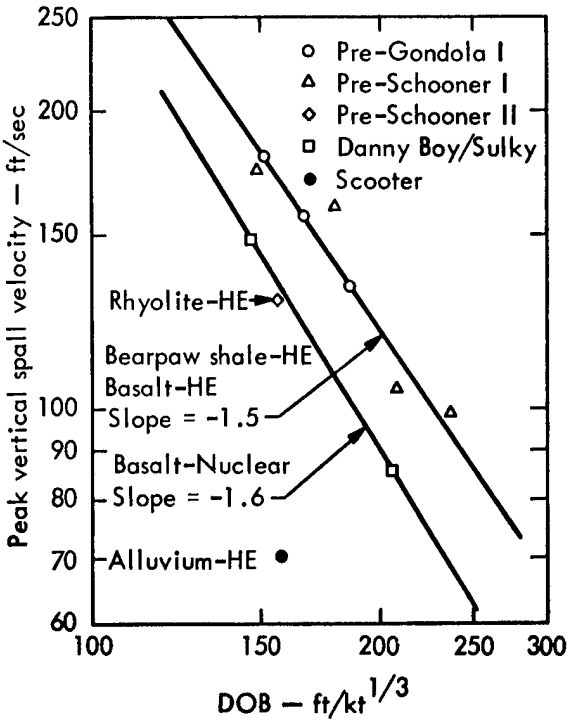

Fig. 95. Peak spall velocity vs scaled DOB for Pre-Gondola I and detonations in other media.

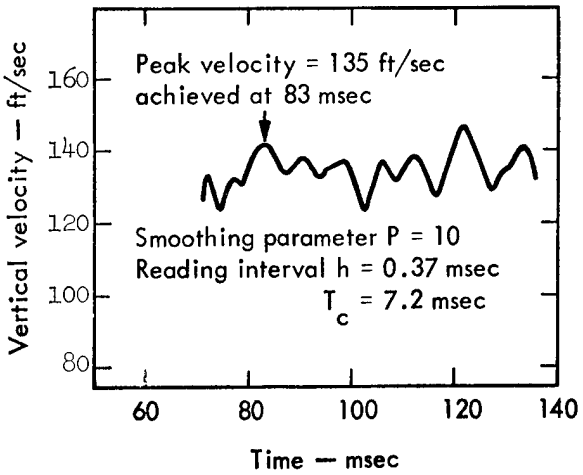

Fig. 94. Vertical velocity vs time for bowling ball target (Pre-Gondola I Delta).

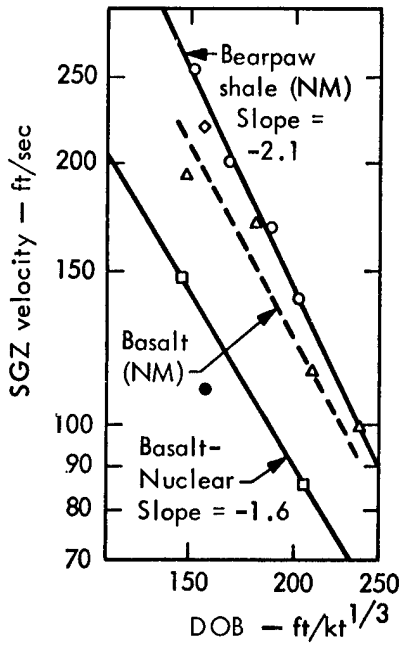

Fig. 96. Peak SGZ velocity vs scaled DOB for Pre-Gondola I and detonations in other media.

of gravity must be considered. The departure from cube-root scaling may not be severe, particularly for those detonations in which gas accelerations make a relatively small contribution to total peak velocity, such as detonations in basalt. The equation which best relates the data in Figs. 95 and 96 is:

$$V_0 = k_1 \lambda^{-n} \qquad (9)$$

where:

V_0 = characteristic SGZ velocity, such as peak spall or peak total velocity (ft/sec)

$\lambda = DOB/W^{1/3}$ = scaled depth of burst ($ft/kt^{1/3}$); DOB = depth of burst (ft);

W = explosive energy yield (kt)

k_1 = a constant primarily dependent upon the nature of the cratering medium, the particular velocity under study, and type of explosive.

n = a constant primarily dependent upon the nature of the medium.

The exponent n likely is a function of the explosive yield in the region of large energy dissipation (large amplitude motion). Local peculiarities in geology may also cause significant deviations from the power law exhibited in Eq. (9).

For peak spall velocities (shown in Fig. 95) the value of n in Eq. (9) which best describes HE data in shale and basalt is 1.5 ± 0.2.

For peak SGZ velocities, Fig. 96, the value of n for shale is 2.1 ± 0.2.

Surface Velocities Related to Preshot Radial Distance to ZP

One of the more meaningful approaches to the study of surface motion measurements is to seek empirical relationships between observed features of motion and time and spatial target positions. Consider a relationship between the peak vertical spall velocity and target position. To a first order of approximation, it is appropriate to use as a measure of target position the distance R between the preshot position of the target base and the center of the energy source (ZP). In this most simple formulation, the actual vector position, as measured by a direction as well as distance, is not considered. One seeks an empirical relationship of the form:

$$V = k_0 R^{-n_0} \qquad (10)$$

where

V = any typical velocity (such as peak vertical spall velocity or peak total velocity)

R = distance defined in the discussion above

k_0 = a constant determined by the particle velocity under study, the cratering medium, DOB, explosive yield, type of explosive, etc.

n_0 = an empirically determined constant dependent on much the same parameters as is k_0.

Empirical expressions of the form of Eq. (10) are readily demonstrated in logarithmic plots of V vs R. Data which satisfy Eq. (10) fit a straight line whose slope is the exponent of R. Plots of this

nature for each detonation were presented earlier in this section. Figures 97 and 98 are a summary of these previous plots.

Figure 97 shows the peak total velocity plots. Note that the slopes of the three shallowest detonations are very similar. There is no apparent reason why the Delta velocities should decay more rapidly than the velocities of the other events. The sloping ground surface may have produced this result. There have been some indications from laboratory-scale tests that the velocities of sloping surfaces decay more rapidly with distance from the shot point than do equivalent detonations under level surfaces, although results are not conclusive.[21] The Delta ground surface sloped at approximately 1/20, or 5% over the entire target array (200 ft). Another explanation might be that surface velocities decay more rapidly for deeper DOBs. This observation was made for HE data in basalt.[16]

Figure 98 presents plots of the vertical spall velocity vs preshot radial distance from ZP for the Charlie, Bravo, and Alfa Events. Spall velocities were not obtained for the Delta Event. The peak vertical velocities are plotted for this event in Fig. 98 for purposes of comparison because the slope of this line was similar to the slope of the spall velocity line for the other events.

In Fig. 98, the slopes of the lines for the three shallower detonations are very similar. By analyzing Delta's peak vertical velocities, it appears that the slope of the Delta peak spall velocity line would be steeper by about the same degree as that for the peak total velocity plots (Fig. 97).

For comparative purposes, the slope of the line for peak spall velocity vs scaled DOB for both HE and nuclear detonations in Buckboard basalt has been estimated as -6.0.[22,23] Therefore, the spall velocities decay much more gradually in Bearpaw shale than in basalt. The Scooter detonation in desert alluvium showed that radial stresses decayed with scaled distance to the -2.28 power.[24] Therefore, while velocities in Bearpaw shale are much higher than in desert alluvium, they appear to decay with distance in a similar manner.

Observed Versus Predicted Surface Velocities

The velocity decay out from SGZ used for this prediction is similar to Eq. (9):

$$V_{peak} = KR^{-n} \qquad (11)$$

where

V_{peak} = target peak total velocity (ft/sec)

K = constant

R = scaled distance from ZP to target base ($ft/kt^{1/3}$)

n = slope of line of log-log plot of V_{peak} vs R

The predicted value of n for all Pre-Gondola I detonations was 2.3.[13] The observed values for n are shown in Table X which lists the predicted and observed peak SGZ velocities.

The predicted and observed values of the peak SGZ velocities of the four detonations are extremely close. Only the value for the Charlie Event is significantly

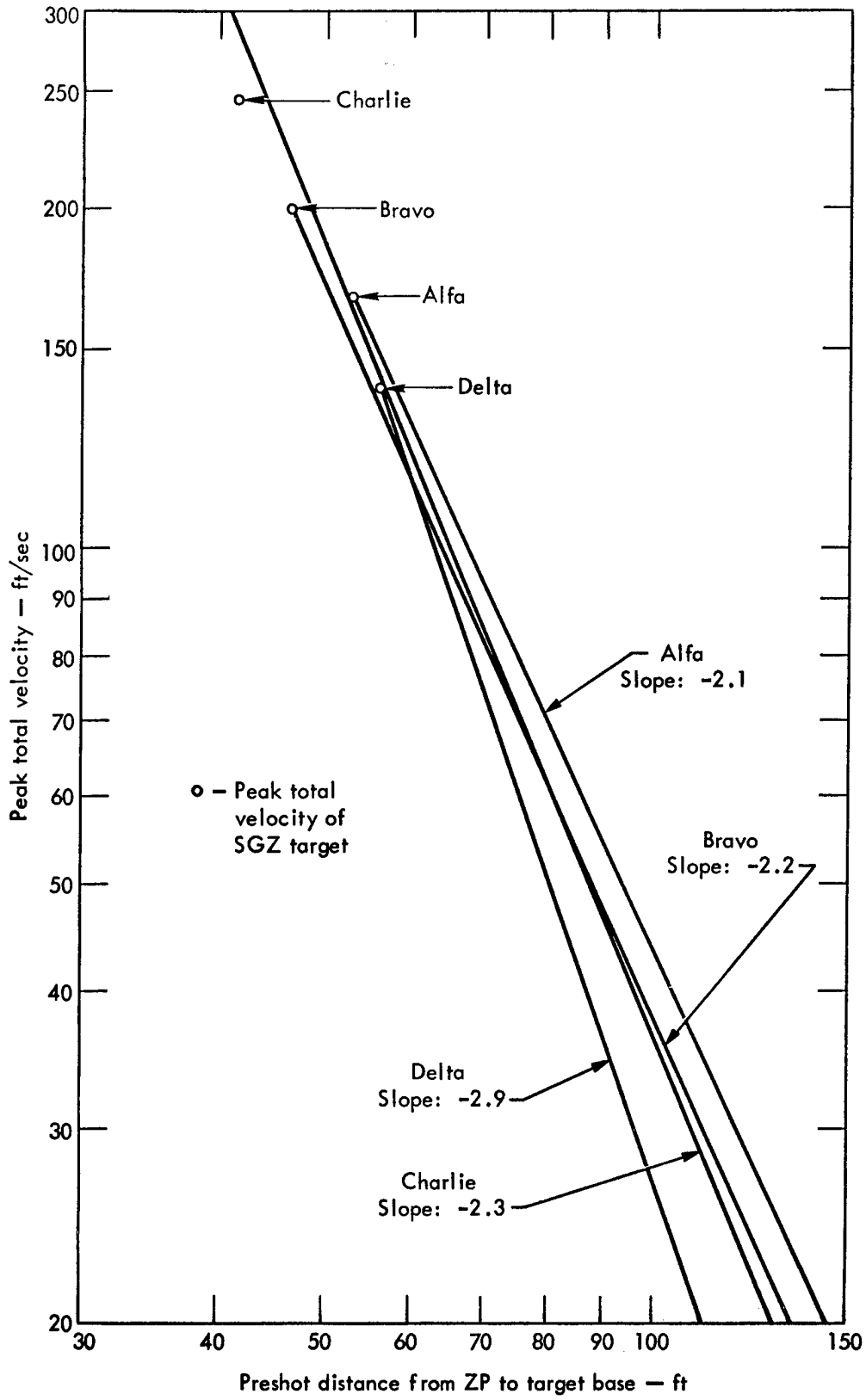

Fig. 97. Surface velocity decay out from SGZ.

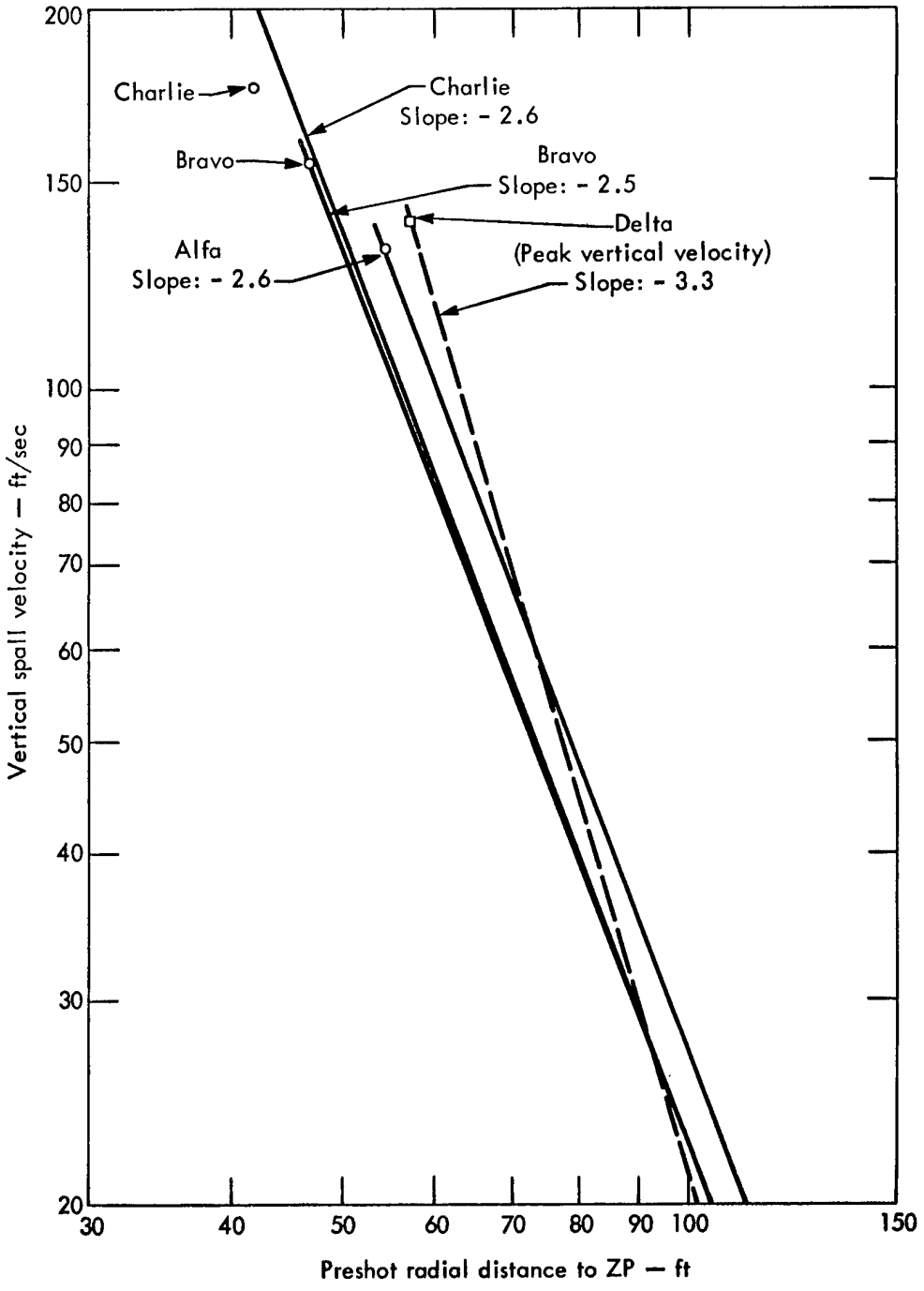

Fig. 98. Peak spall velocity vs preshot radial distance from ZP to target base.

Table X. Analysis of observed vs predicted surface velocities.

Event	Peak SGZ velocity		Slope of velocity plot (n) vs R	
	Predicted (fps)	Observed (fps)	Predicted	Observed
Charlie	231	255	2.3	2.3
Bravo	200	200	2.3	2.2
Alfa	162	167	2.3	2.1
Delta	142	139	2.3	2.9

different. The reason for this difference could be an inaccurate measurement of peak velocity for the SC-4 (1000-lb) shot, which may have been 10% higher than the velocity recorded.[13] Because SC-4 was the shallowest 1000-lb shot, it is probable that a higher velocity measurement on that detonation would have resulted in a significantly higher prediction for the Charlie Event (the shallowest of the 20-ton detonations).

Observed Relationship between Surface Motion and Crater Size

The scaled dimensions of the Pre-Gondola I craters were larger than for basalt, alluvium, or rhyolite, three media previously cratered. Approximately the same relationship exists for the surface velocities observed for detonations in these media. Crater size and observed peak SGZ velocity are directly related, although there does not appear to be simple relationship between velocities and exact crater dimensions. A general observation is that the higher the surface velocity imparted to the medium, the larger the crater for a given DOB.

An equally important parameter is the manner in which velocities decay out from SGZ. For events Charlie, Bravo, and Alfa, the velocities decayed with radial distance more gradually than had ever been exhibited on any previous cratering detonation. These three Pre-Gondola I detonations exhibited decay of peak total velocity out from SGZ with $R^{-2.2}$, compared to R^{-3} for rhyolite and R^{-6} for basalt (R = preshot radial distance to ZP).

More gradual decay of velocities out from SGZ seems to correlate directly with larger craters.

Another phenomenon observed for the Pre-Gondola I detonations which may have contributed to cratering efficiency was the total absence of massive venting at any time during the mound growth. Massive venting at early times (<250 msec) such as exhibited on Pre-Schooner Delta and on Pre-Schooner II, would appear to reduce the efficiency of the detonation in expelling the material from the crater. Massive venting at early times is accompanied by some drop in gas cavity pressure. It is the gas cavity pressure which expels much of the material from the crater area (after the material has been fractured and given an initial vertical velocity by the spall phenomena).

As discussed previously, the higher SGZ velocities, more gradual velocity decay out from SGZ, and absence of

massive venting all seem to be indicative of larger crater dimensions. Any analysis of cratering efficiency would have to include a thorough study of the preshot medium (the strength properties, fracture patterns, geologic structure, to name a few) as well as the properties, of the altered medium during the cratering phenomena. While the surface motion phenomenon provides insight for such an analysis, a complete study of the cratering phenomena is beyond the scope of this report.

A Method for Utilizing Results for Predicting Pre-Gondola II Surface Velocity

As previously discussed, one of the primary uses of the Pre-Gondola I surface velocity data is predicting surface velocities of future detonations in the Bearpaw shale, such as Pre-Gondola II (Table XI).

Pre-Gondola II was a row-charge cratering experiment on 28 June 1967. Three 20-ton and two 40-ton charges in a row were detonated simultaneously to produce a linear excavation connecting to the Charlie crater. Figure 73 shows the alignment which was centrally oriented with respect to the calibrated area. Reference 15 provides additional details.

The planned DOB for each Pre-Gondola II charge was 150 ft/kt$^{1/3.4}$.[15] This was an actual DOB of 48.8 ft for each 20-ton charge and 59.9 ft for each 40-ton charge. The peak SGZ velocity over each charge was predicted by using Fig. 96. The peak vertical spall velocity over each charge was predicted by using Fig. 95.

The velocities predicted in Table XI are actually velocities for 20- and 40-ton single charges. Pre-Gondola II was expected to exhibit higher velocities because of the boost given to the surface particles by adjacent charges. On Dugout, a row of five 20-ton charges in Buckboard basalt, the peak velocity along the top of the mound after gas acceleration was 40 m/sec[17] or 131 ft/sec. Pre-Schooner Alfa, a single-charge 20-ton detonation in Buckboard basalt at about the same DOB as Dugout, had a peak SGZ velocity after gas acceleration of about 115 ft/sec.[16] Therefore, an enhancement of about 14% in the peak SGZ velocities in Table XI was expected based on the Dugout results. Dugout had peak spall velocities of 105 ft/sec vs 120 ft/sec for Pre-Schooner Alfa. This provides no basis for altering the peak spall velocity predictions in Table XI.

The predicted Pre-Gondola II target velocity decay out from SGZ was based on Fig. 97. Because the Pre-Gondola II scaled DOBs were between Bravo and

Table XI. Surface velocity predictions for Pre-Gondola II.[13]

Charge size nitromethane (tons)	DOB (ft)	Energy equiv. (kt)	dob[a] ft/kt$^{1/3}$	Top of charge ft/kt$^{1/3}$	$V_{peak\ SGZ}$ (fps)	V_{spall} (fps)
20	48.8	0.022	174	156	190	145
40	59.9	0.044	170	151	200	152

[a]Scaled dimensions are indicated by lower case letters.

Alfa, the slope of the peak total velocity line for Pre-Gondola II should be about -2.2 ± 0.2.

One would expect the velocity decay off the side of the row to be more gradual than off the end of the row, because the row crater is larger to the side than it is off the end. Therefore, it was expected that the slope of the line (similar to Fig. 97 for the side target arrays on Pre-Gondola II) would be significantly less than the slope of the line for the south end target array.

Comparison of Predicted and Observed Velocities for Pre-Gondola II[25]

Table XII lists observed surface motions for Pre-Gondola II. Results show partial agreement with the predictions in the preceding paragraph. Assuming charge G to be representative of the three 20-ton charges, the observed spall velocity is considerably higher than the predicted value and the peak velocity is lower. If the 14% enhancement factor were disregarded, observed peak velocity would show closer agreement with the predicted value for a single 20-ton charge.

The 40-ton charge H showed rather high SGZ velocities and developed a partial vent at late times. The tabulated value of 250 fps for peak velocity over this charge is therefore an average value taken after gas acceleration, but before significant tertiary acceleration accompanying the partial vent. Spall and peak SGZ velocities over charge H were both higher than predicted, with the greatest discrepancy being spall velocity, as was the case for the 20-ton charges.

Decay of peak velocity as a function of distance was recorded off the south end of the Pre-Gondola row. Using the same power law representation as was used for velocity prediction, observed velocities decayed according to the -2.3 ± 0.1 power of slant distance from ZP. This result agrees well with the predicted decay exponent of -2.2 ± 0.2. Velocities off the side of the row were not obtained.

CONCLUSIONS

As a result of the Pre-Gondola I Cratering Calibration Series, the Bearpaw shale has been calibrated as to

Table XII. Observed vs predicted velocities, Pre-Gondola II.

Charge designation	Charge yield	Predicted velocity		Observed velocity		Observed /Predicted[b]	
		Spall (fps)	Peak[a] (fps)	Spall (fps)	Peak (fps)	Spall	Peak
E	40	N/A	N/A	145	190	—	—
F	20	145	217	165	195[c]	1.14	0.90
G	20	145	217	170	195	1.17	0.90
H	40	152	228	190	250	1.25	1.10
I	20	145	217	175	200	1.21	0.92

[a]Peak velocity includes 14% enhancement.

[b]Ratio of observed velocity to predicted velocity.

[c]Inferred from mound profile; SGZ target over charge F was lost before peak velocity could be recorded.

cratering characteristics. The peak surface velocities and the surface velocity distribution can be predicted for any yield and DOB with confidence (see preceding paragraph).

The surface motion data from the Pre-Gondola I series are available for use in the design of future experiments in this medium and for use in the prediction of surface velocities of future detonations in this medium. The data collected from these experiments can also be used in evaluating data collected from detonations in other media.

The spall velocities exhibited by the four Pre-Gondola I detonations were comparable to the spall velocities of HE detonations in Buckboard basalt (Pre-Schooner I) and were consistent with peak spall velocities of nuclear cratering detonations in Buckboard basalt.

The peak SGZ velocities exhibited were significantly higher than those for HE and nuclear detonations in Buckboard basalt and alluvium, and were slightly higher than the velocity of a HE detonation in rhyolite.

The peak spall and peak SGZ velocities are best related as follows:

$$V_0 \propto \lambda^{-n} \tag{12}$$

where $n = 1.5 \pm 0.2$ for peak spall velocities and 2.1 ± 0.2 for peak SGZ velocities and λ is the scaled DOB ($ft/kt^{1/3}$).

The decay of target velocities out from SGZ for the Pre-Gondola I detonations was much more gradual than for previous detonations in basalt or rhyolite and was similar to velocity decay in alluvium, although the alluvium velocities were much lower. The velocity decay exhibited by individual Pre-Gondola I detonations can be expressed by relating a characteristic velocity peak of surface particle, V (such as peak spall or peak total velocity), to that particle's preshot radial distance from the center of the energy source, R, as follows:

$$V \propto R^{-n_0} \tag{13}$$

where $n_0 = 2.5 \pm 0.3$ for peak spall velocities and 2.2 ± 0.3 for peak total velocities for the three shallower detonations. For Delta, the deepest detonation, no spall velocities were obtained, and the peak total velocity decay was characterized by $n_0 = 2.9 \pm 0.2$.

Engineering Properties Investigations

This section summarizes the Bravo shot time engineering properties technical program and relates it to the Bravo postshot investigations.[3] Detailed experimental procedures, results, and interpretations are contained in separate reports.[3,26,27]

INTRODUCTION

Four engineering properties technical programs were conducted during the Pre-Gondola I detonations. These programs and the agencies responsible for them are as follows:

1. Close-in ground motion, earth stress, and pore pressure measurements—WES.
2. Close-in displacement measurements—AFWL and NCG.
3. Stress and water level measurements at the Pre-Gondola sites—WES and NCG.
4. Slope displacement measurements—NCG.

The close-in measurements were made at the Bravo Event along two radial lines from SGZ. The layout for these measurements is shown in Fig. 99. Slope displacement measurements were made in each crater during the subsequent detonations and on an active landslide on the Fort Peck reservoir edge approximately 3 mi east of the Pre-Gondola site area. The location of this landslide is shown in Fig. 100.

CLOSE-IN GROUND MOTION, EARTH STRESS, AND PORE PRESSURE MEASUREMENTS

This technical program was performed by the Nuclear Weapons Effects Division, WES. Detailed discussions of the procedures and equipment used, data obtained, and analysis of data are included in Ref. 26. This section summarizes that information.

Shock Wave Velocity

Shock wave arrival times vs distance during the Bravo Event indicated a velocity of 6800 fps. A lower velocity of 5700 fps was observed during instrumentation of a 1000-lb seismic calibration cratering detonation (SC-2). The higher velocity observed during the Bravo detonation is attributed to the fact that the stress wave was traveling through a deeper layer with a higher compression wave velocity.

Peak Total Stresses

The peak total stress measurements vs distance obtained from Event Bravo ranged from 12,375 psi at a distance of 85 ft from SGZ to 171 psi at a distance of 930 ft from SGZ (Delta site). An attenuation rate of R^{-2} (R is radial distance from SGZ) has been derived from the total stress data.

Particle Velocities

Particle velocities vs distance obtained from the Bravo Event ranged from

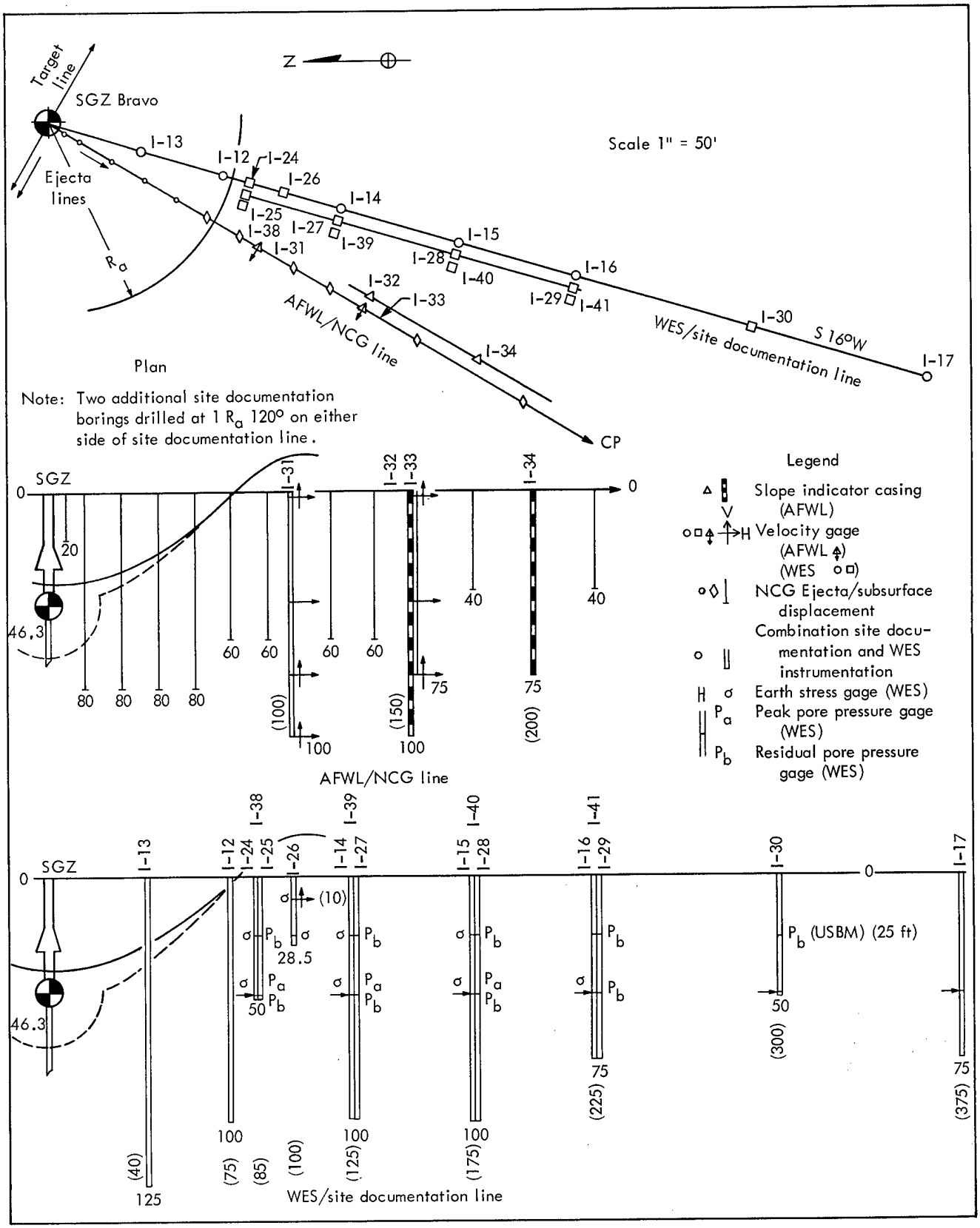

Fig. 99. Layout for close-in measurements for Pre-Gondola I Bravo.

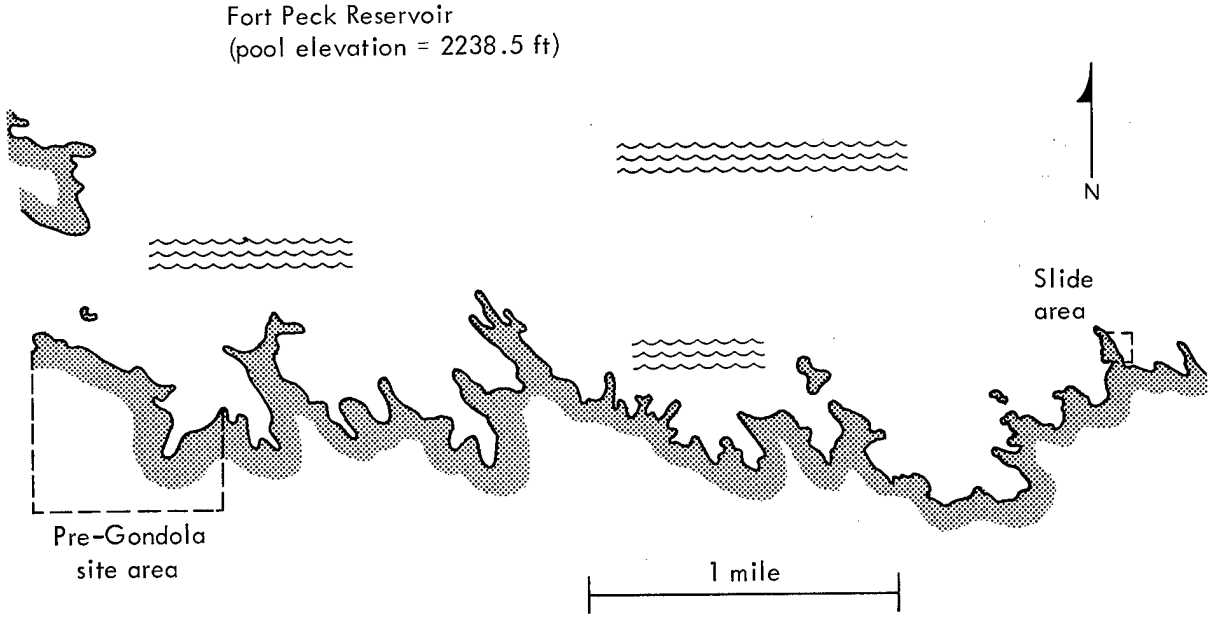

Fig. 100. Location of landslide.

at least 70 fps at a distance of 85 ft from SGZ to 5 fps at a distance of 375 ft from SGZ. The Bravo data show an irregular pattern of attenuation.

Pore Pressures

Only one peak pore pressure gage provided data at the time of the Bravo detonation. This gage located at a distance of 85 ft from SGZ indicated a peak pore pressure of 12,800 psi which is in good agreement with the measured peak total stress at that point. The residual pore pressure gages indicated a rapid initial falloff of detonation-induced pore pressures and then stabilized at higher than preshot pore pressures. Figure 101 shows contours of indicated excess pore pressures at the Bravo crater ten days after detonation.

CLOSE-IN DISPLACEMENT MEASUREMENTS

Two displacement measurement programs were conducted by AFWL and NCG during the Bravo Event. The measurements made by AFWL are reported in Ref. 27. The NCG measurements are reported in Ref. 3.

AFWL Measurements

No velocity gage data were obtained. Permanent displacements were obtained by means of a slope indicator to a depth of 17 ft in hole PG-I-32 (150-ft range) and to a depth of 38 ft in hole PG-I-34 (200-ft range). A record of vertical displacements to depths of just below 12 ft was obtained from scratch indicators in holes PG-I-32 and 34. Above 12 ft in each hole the initial motion was down; below 12 ft it was up.

NCG Measurements

Ejecta and subsurface displacements were measured by means of identifiable cylindrical pellets placed in vertical borings located as shown in Figs. 44 and 99. Pellets in each boring were

coded for identification and the elevation of each pellet was measured to the nearest 0.1 ft.

Postshot locations of the ejected pellets, or pellet fragments, were determined by normal field survey techniques. All locations were referenced to known stations along a radial from SGZ through the line of displacement measurement borings. The data obtained from determining the locations of the ejected pellets have been presented under Crater Measurements and Ejecta Studies.

The results of the subsurface displacement measurements of pellets not ejected are reported in Ref. 3. Preliminary displacements are shown in Fig. 102. The pellets were recovered during Bravo postshot investigations by trenching and hand excavation inside the crater (Fig. 103) and by augering an access hole near the expected location of pellets beyond the rim of the crater.

STRESS AND WATER LEVEL MEASUREMENTS AT THE ALFA, CHARLIE, AND DELTA SITES

The WES measured transient detonation-induced water pressures in undetonated explosive cavities and transient soil stresses at each remaining event site during the first three Pre-Gondola I detonations. NCG monitored water levels in open tube piezometers at each uncratered site during each event of the series (Fig. 104).

The maximum stresses experienced by an emplacement site were at the Alfa site during the Bravo Event. The soil stress outside the Alfa cavity was 308 psi and the water pressure inside the cavity was 126 psi. These values provide a stress (pressure) transmission factor of approximately 0.4.

Open tube piezometers were installed in two of three satellite exploratory

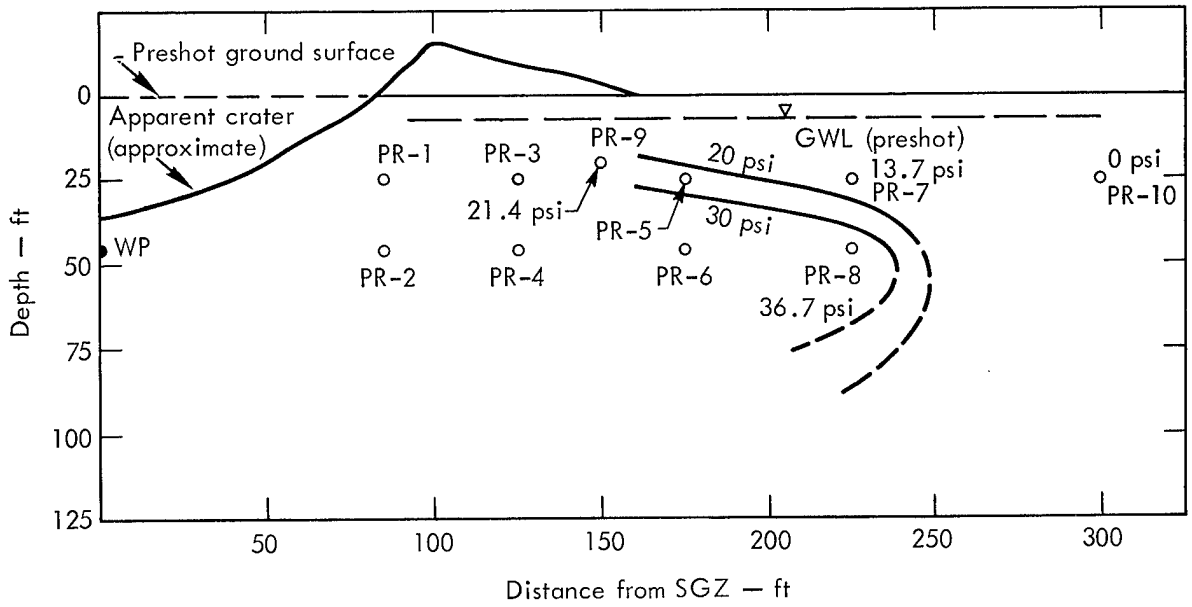

Fig. 101. Contours of indicated excess pore pressures (D + 10)—from Ref. 26.

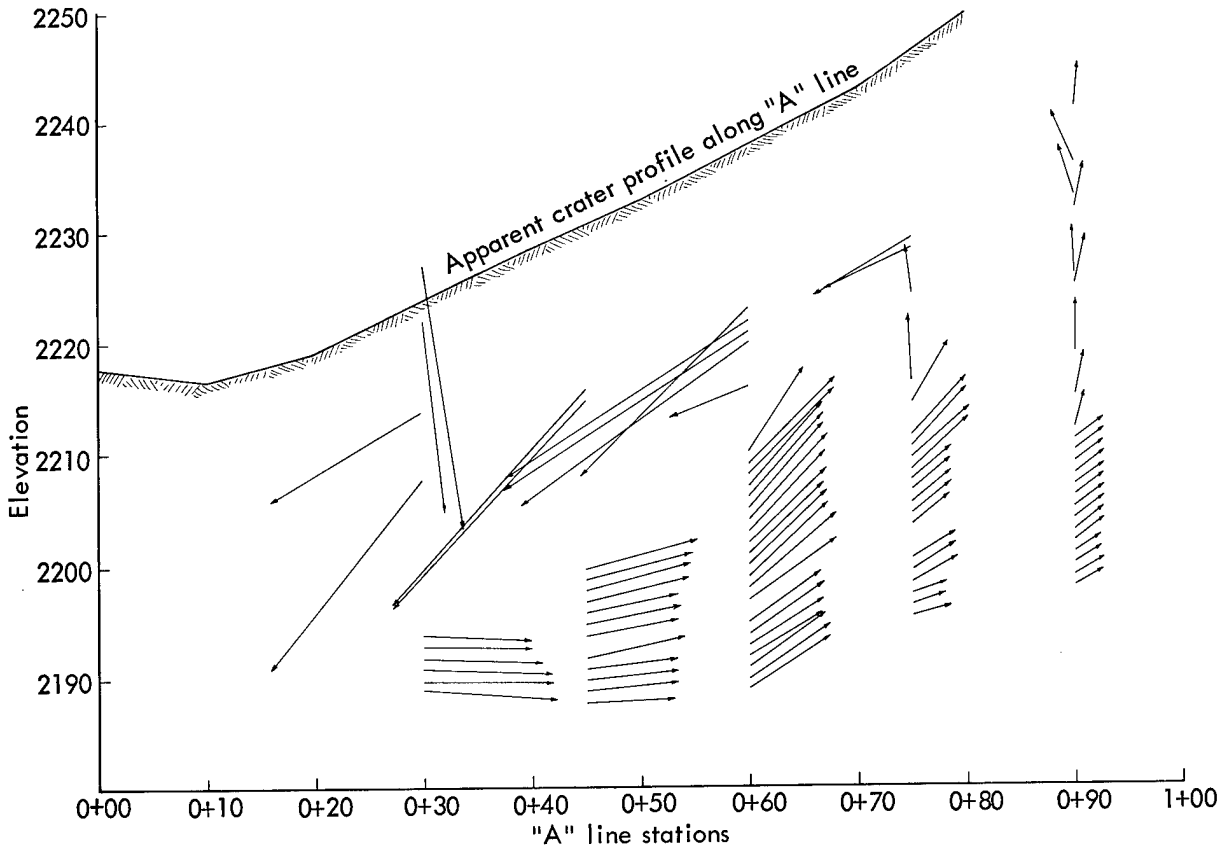

Fig. 102. Postshot subsurface displacements, Bravo crater.

Fig. 103. Recovery of subsurface displacement pellets inside Bravo crater during postshot investigations.

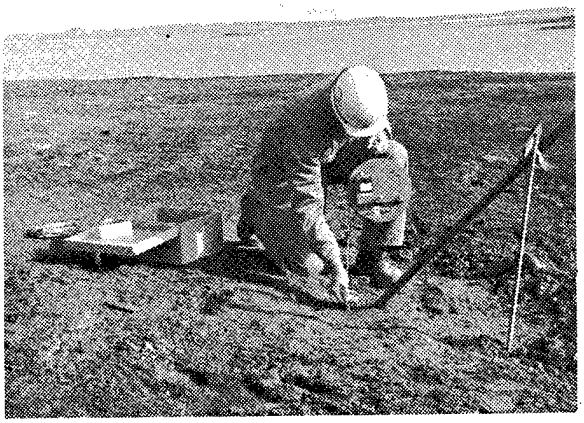

Fig. 104. Monitoring Charlie piezometer after Bravo detonation.

borings at each event site. Water level measurements in these piezometers and in the water-filled explosive cavities were taken at 2-hr intervals on shot days

and at one- or two-day intervals between shot days. All piezometers showed response to detonations.

SLOPE DISPLACEMENT MEASUREMENTS

This program consisted of making time displacement measurements on an active landslide and measuring relative displacements on the slope of the Pre-Gondola I craters.

Landslide Measurements

The location of the landslide mass where displacement measurements were made is shown in Fig. 100. The displacements were measured by surveying, in plan and elevation, the locations of pins set behind and in the slide mass. These survey measurements were made from 30 September to 4 November 1966. Figure 105 shows the configuration of the slide area and locations of reference stakes C, D, and E. The upper portion of the slide mass was moving downward and outward at a rate of 0.026 ft/day. The lower portion (toe) of the slide mass was moving in a similar manner at a rate of 0.035 ft/day. This indicates that the outer portion was slowly separating from the inner portion. The continuing displacement measurements indicate that the calculated ground motions of 0.03 g produced by each event had no effect on the rate of movement of the slide mass.

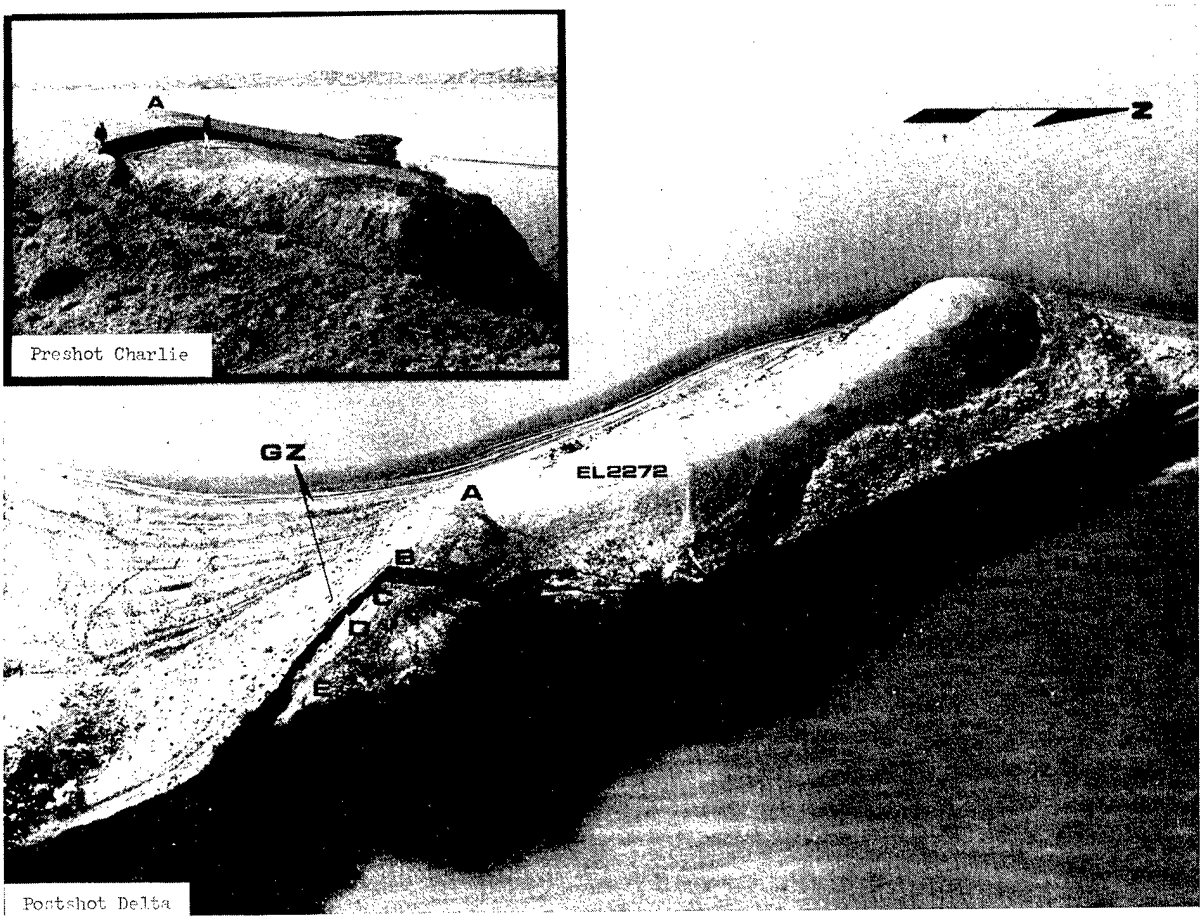

Fig. 105. Slope displacement measurements in landslide area.

Crater Slope Displacement Measurements

Crater slope displacement measurements were made at the Bravo and Charlie craters, each of which were subjected to ground motion from more than one succeeding event. Steel reference stakes 1/2 in. in diameter and 2 or 5 ft long were set along two orthogonal lines extending outward from SGZ to a distance of two crater radii. Similar sets of reference pins were set in the Alfa and Delta craters for future observation. Relative positions of the reference stakes were determined by transit and tape taking vertical angles and slope distances.

Very slight changes were noted on the Bravo crater slopes after the Alfa and Delta detonations. With the exception of one anomalous reading, these changes were in an inward and downward direction. These changes may be attributed to compaction and settlement of the ejecta fallback caused by ground motion induced by the Alfa and Delta detonations. Very slight changes in the Charlie crater slopes were noted after the Delta detonation.

The Alfa, Bravo, and Charlie craters and the pre-existing SC-2 crater were all observed daily during the Pre-Gondola I series. Only minor surficial adjustments in the crater slopes were noted.

The SC-2 crater was partially filled with water during the Pre-Gondola I series (Fig. 106). It was located 350 ft from the Bravo SGZ and, as a consequence, was subjected to severe ground motion and missile impacts from the Bravo Event. With the exception of modification of the crater lip by missile impact and possible slight bulging of the crater fallback surface in the south quadrant (which was the side near Bravo), the configuration of the crater was essentially unchanged during the Pre-Gondola I series (Fig. 43).

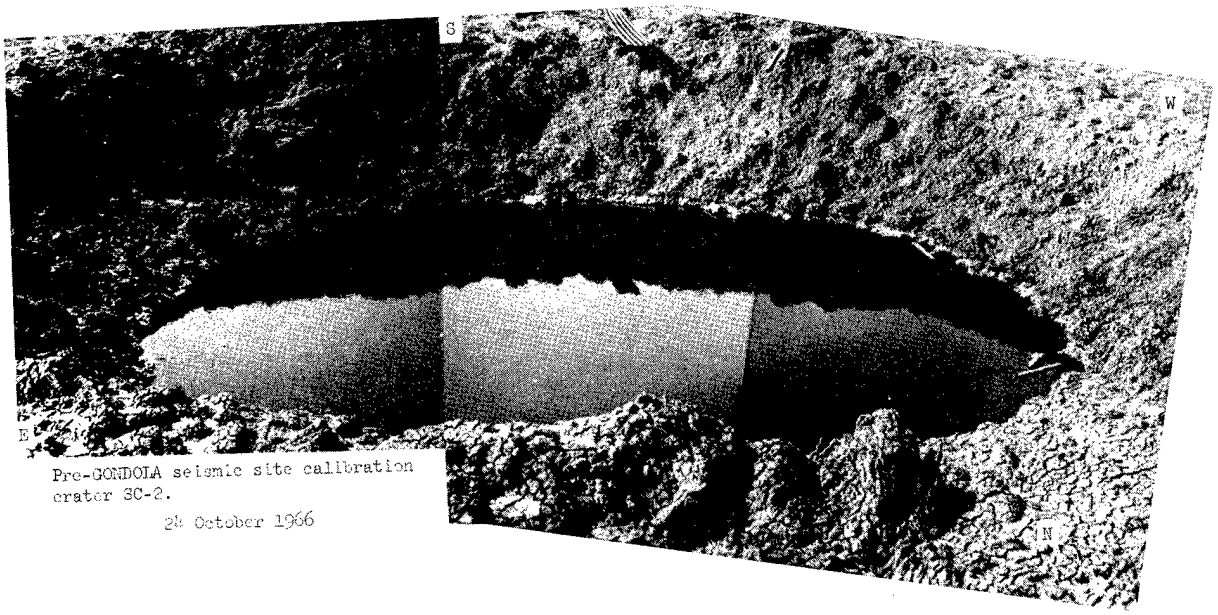

Fig. 106. SC-2 crater prior to Bravo detonation (note weathering; compare post-Bravo photograph, Fig. 43).

Seismic Studies

The seismic measurements made during Pre-Gondola I were part of a continuing data collection program which is primarily directed toward the seismic calibration of the site. A full discussion of the concept and scope of the Pre-Gondola seismic studies, together with a complete analysis, will be found in PNE 1100.[4] This section is limited to a presentation of the Pre-Gondola I data only. Seismic investigations are planned for all future experiments in the Pre-Gondola series of cratering experiments.

INTRODUCTION

The preliminary safety and technical aspects of seismic propagation in the region were evaluated on the basis of the earlier 1000-lb Seismic Site Calibration Series. The data collected during Pre-Gondola I were used to define further the propagation of seismic energy in the area in order to arrive at more reliable predictions for the 140-ton Pre-Gondola II row-charge experiment. Additional refinements were made to the prediction methods subsequent to the Pre-Gondola II detonation.

The following are the three seismic technical programs carried out during Pre-Gondola I:

Intermediate Range Measurements

This program to study seismic propagation involved the measurement of ground motion amplitudes at a number of locations along radial lines extending out to intermediate distances (~100 km) from SGZ. The program was conducted by LRL.[28]

Structures Instrumentation

This program consisted of the documentation of seismically induced motion at the Fort Peck Dam and other major structures associated with the dam. The recording stations for this study[29] of structural response were operated by WES.

Earth Dam Response

The measurement and analysis of the dynamic response of the embankment portion of the Fort Peck Dam were the responsibility of Montana State University under the sponsorship of the LRL. The purpose of this program is to develop an understanding of how earthfill embankments respond to seismic loading. Results of this program are not available at this time.

EXPERIMENTAL PROCEDURE

Procedures

The field operations of the different agencies were similar and differed only in detail. Ballard[29] and Power[28] give complete discussions of techniques and station operation. The operations of the various seismic technical programs were coordinated with Pre-Gondola Control by means of SSB and FM radio nets.

Station Locations

Intermediate Range Stations

The intermediate range stations (Fig. 107) were spaced at logarithmically increasing intervals away from SGZ.

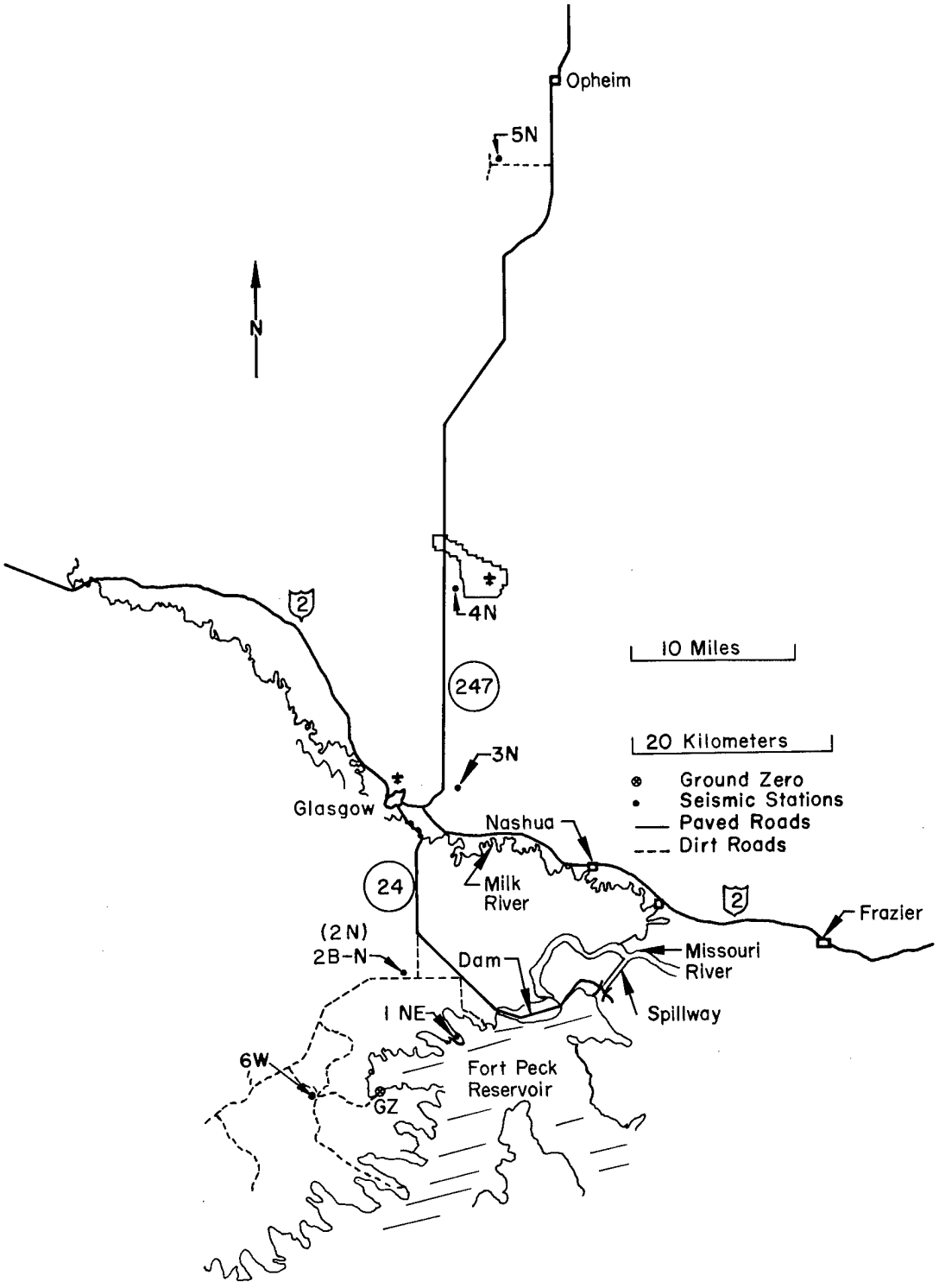

Fig. 107. Location map of LRL intermediate range stations.

Pertinent information describing station locations is tabulated in Table XIII.

The LRL instruments were located at the intermediate range stations for the Bravo Event only, except station 2N which was left in place during all four shots for the purpose of comparison. To provide data for Montana State University, the instruments were moved to the dam for the remaining three events in the series.

Structure Instrumentation Stations

The WES structures instrumentation stations are shown in Fig. 108 and pertinent details are tabulated in Table XIII. Figure 109 is an aerial view of the Fort Peck Dam and spillway showing the locations of WES Stations 1,2, and 3.

Instrumentation

Both the LRL and the WES instrumentation systems employed the same type of moving coil velocity transducers with a nominal natural frequency of 1 Hz. Detectors were arranged in triaxial arrays with the horizontal components oriented radially and transversely to SGZ.

All LRL velocity transducers were mounted in rigid triaxial frames which in turn were housed in protective fiberglas canisters. These geophone assemblies were buried 12 to 18 in. below the ground surface at each station. The canister was oriented, levelled, and firmly emplaced by tamping sand around it. The output from the geophones and a timing reference signal were recorded

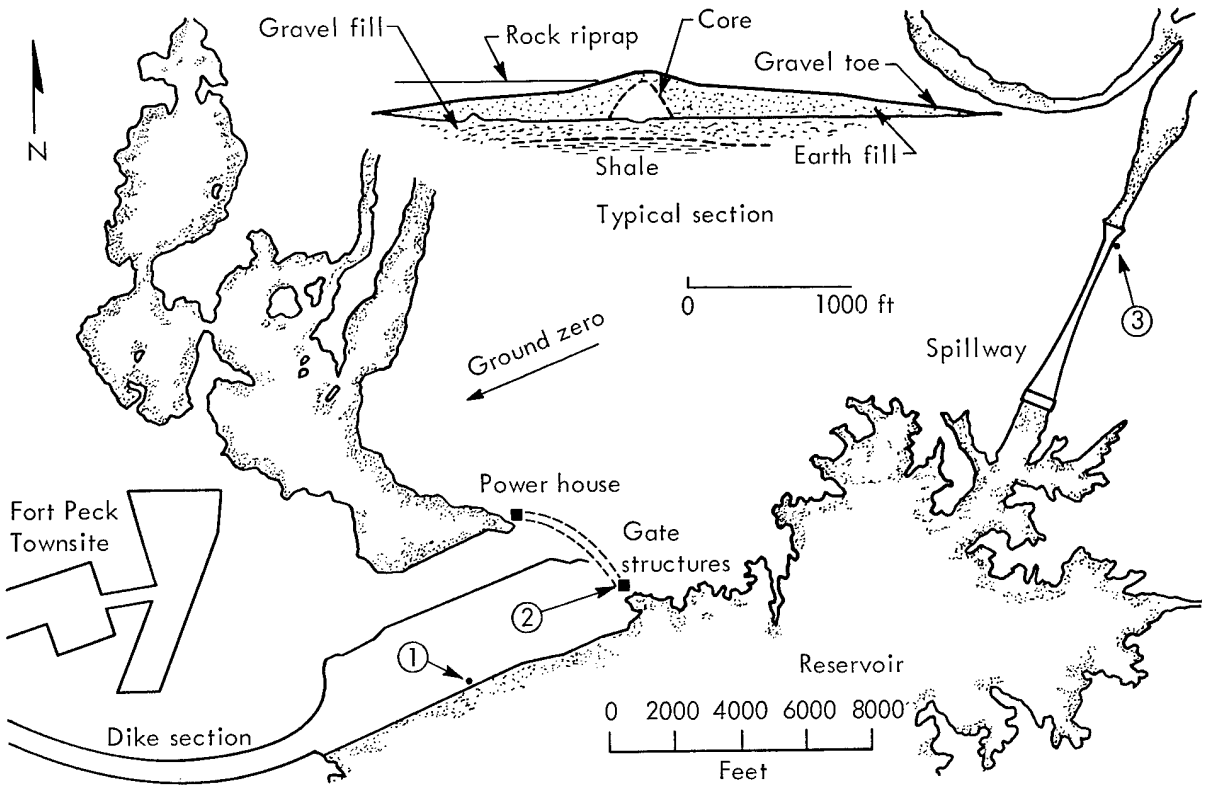

Fig. 108. Location map of WES structures instrumentation stations.

Table XIII. Locations of seismic recording stations

A. LRL intermediate range stations

Event	Station	Distance (km)	Location
Bravo	1NE	8.75	NE of GZ
All	2N	11.65	N of GZ
Bravo	3N	29.3	N of GZ
Bravo	4N	52.0	N of GZ
Bravo	5N	95.9	N of GZ
Bravo	6W	6.4	W of GZ

B. WES structures instrumentation stations

Event	Station	Distance (km)	Location
All	1	18.5	Top of dam at Station 58+00
All	2	20.1	Gate Control Structure No. 3
All	3	24.9	East wall of spillway

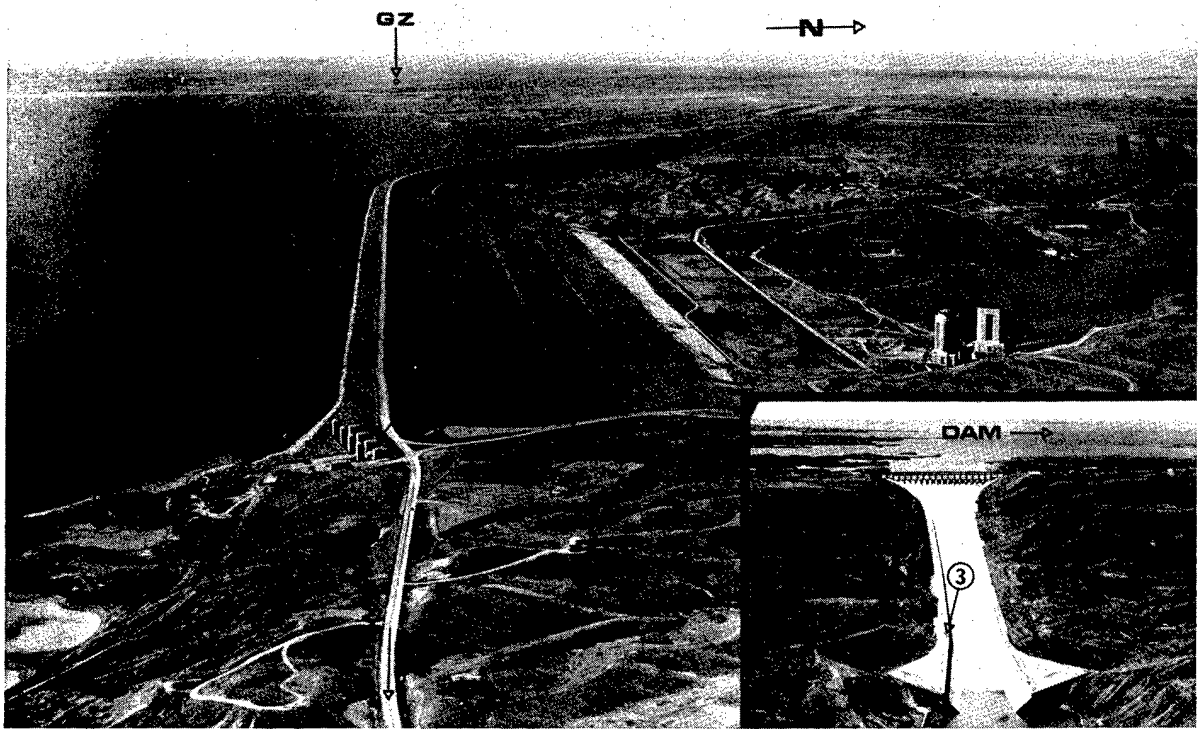

Fig. 109. Location of WES structures instrumentation stations.

on a four-channel FM type system developed by LRL.

At the WES installations the transducers were individually attached to the structure rather than mounted in a frame. The seismic signals were recorded on FM tape and on oscillographs at all of the WES locations.

RESULTS

Intermediate Range Measurements[28]

The results of the intermediate range measurements are presented in Fig. 110. Peak component particle velocities and the peak resultant velocity have been plotted for each station. No data were

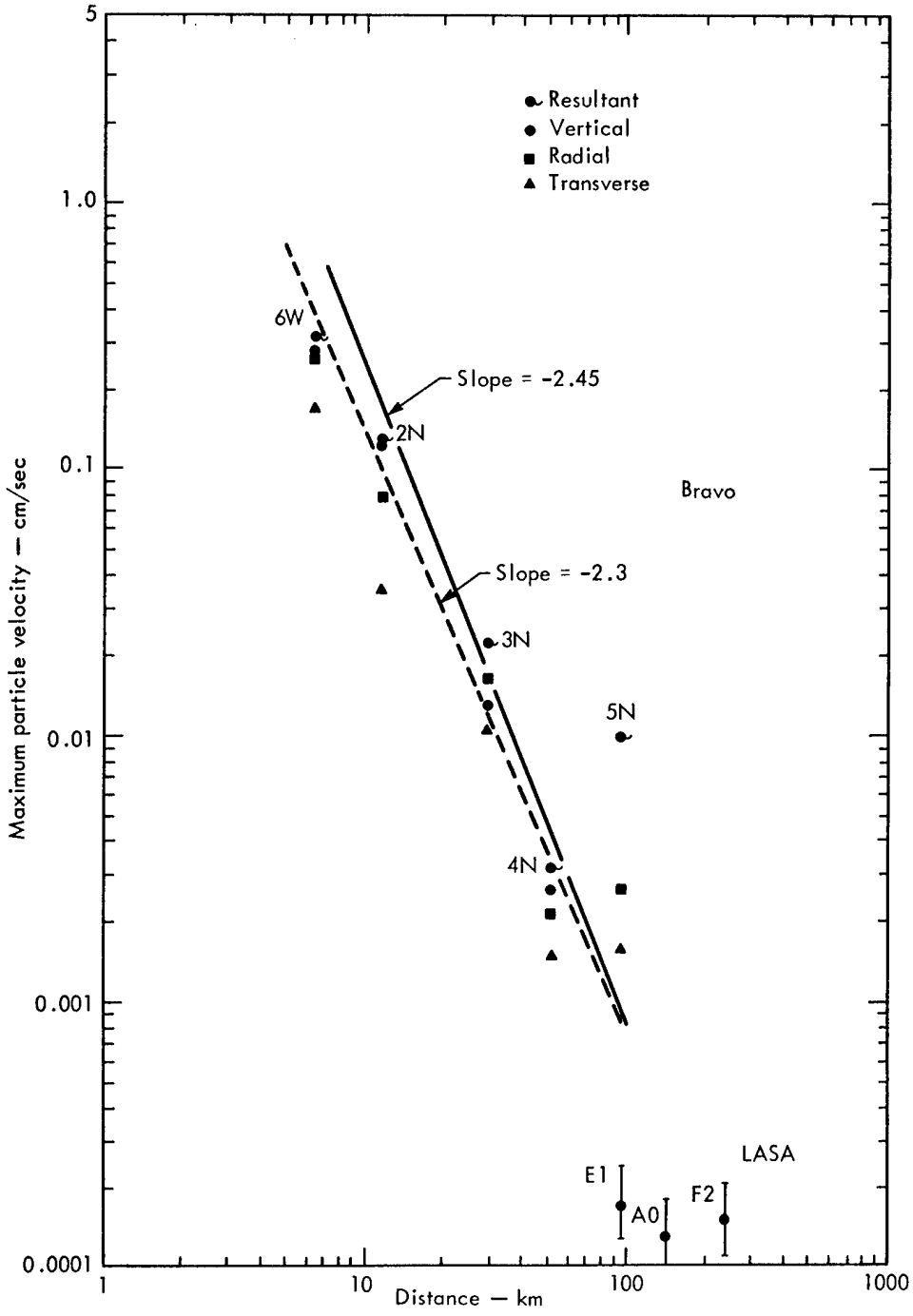

Fig. 110. Results of intermediate range measurements.

obtained at station 1NE because of instrument failure prior to shot time.

The values designated LASA were derived graphically from recordings of vertical particle displacement obtained from the Large Aperture Seismic Array, which is approximately centered about Miles City, Montana. Although these measurements were not part of the formal data collection program, they are included as a supplement to the intermediate range measurements. These derived particle velocities are probably accurate to not better than ±50%. It should also be noted that they were recorded along a line in the opposite direction of the LRL array to the north; however, the generally uniform geology of the region should permit their use as an extension of the LRL data.

Station 2N was in operation for all four shots, and the amplitudes are compared in Fig. 111. It is evident that the seismic amplitudes increase with DOB. A similar dependence was also noted for the 1000-lb Seismic Site Calibration Series.[4]

The intermediate range amplitudes recorded by the array of stations north of SGZ (i.e., neglecting station 6W) can be described by the inverse power law[28]

$$V_r = 85\ R^{-2.45}\ \text{cm/sec} \qquad (14)$$

where V_r is the particle velocity at a distance R km. The equation of a visual best fit to all of the data points* in Fig. 110, including station 6W, is[4]

$$V_r = 27\ R^{-2.3}\ \text{cm/sec} \qquad (15)$$

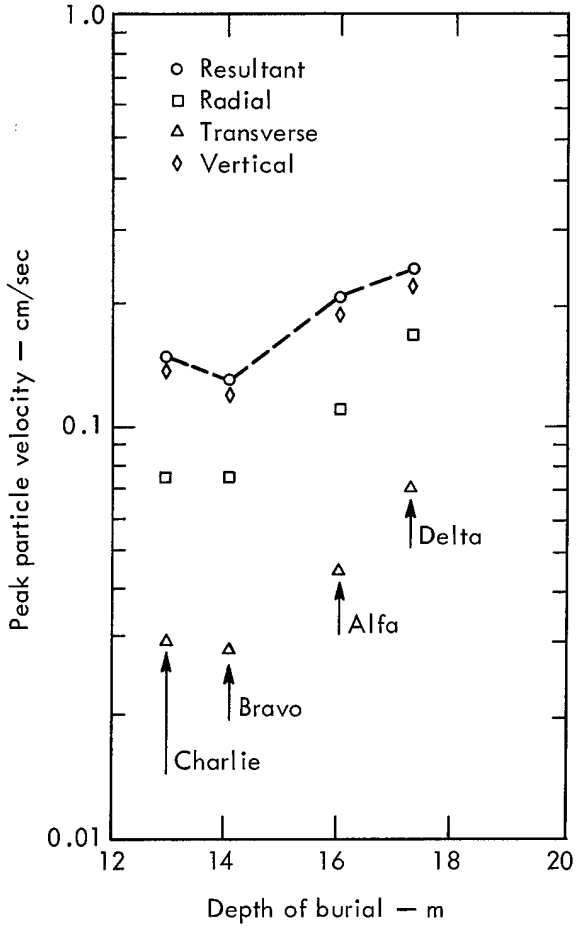

Fig. 111. Peak amplitudes at LRL Station 2N (2B-N) for Pre-Gondola I (Ref. 28).

Structures Instrumentation[29]

The results of the structures instrumentation program are shown in Table XIV. Peak component amplitudes are given for each of the WES stations. Figure 112 is a comparison of the peak component amplitudes at all WES stations for Delta, the event which generally

*The amplitudes recorded at station 5N were not taken into account in fitting a line to the data points in Fig. 110. The particle velocities reported for station 5N are anomalous because the resultant amplitude is an order of magnitude higher than the velocity intercept of the line through the remainder of the data points. It is possible that the high amplitudes may be the result of a calibration error.[4]

Table XIV. Peak motion data for Pre-Gondola I Events at WES structures instrumentation stations.[29]

Station	Component[a]	Peak velocity (cm/sec)	Frequency (Hz)
		Alfa	
1	V	2.6×10^{-2}	4.5
		2.6×10^{-2}	1.25
	R	1.9×10^{-2}	4.3
		2.6×10^{-2}	1.25
	T	3.3×10^{-2}	4.3
		4.2×10^{-2}	1.25
2	V	1.6×10^{-2}	4.3
	R	1.5×10^{-2}	4.3
	T	0.87×10^{-2}	4.3
3	V	1.5×10^{-2}	4.5
	R	0.75×10^{-2}	4.5
	T	0.62×10^{-2}	4.5
		Bravo	
1	V	2.5×10^{-2}	4.5
		2.5×10^{-2}	1.25
	R	2.0×10^{-2}	4.5
		2.3×10^{-2}	1.25
	T	2.9×10^{-2}	4.5
		3.6×10^{-2}	1.25
2	V	1.4×10^{-2}	3.5
	R	1.3×10^{-2}	3.5
	T	0.87×10^{-2}	3.5
3	V	—[b]	—
	R	—[b]	—
	T	—[b]	—
		Charlie	
1	V	2.8×10^{-2}	4.3
		2.9×10^{-2}	1.25
	R	1.9×10^{-2}	4.3
		2.7×10^{-2}	1.25
	T	2.5×10^{-2}	4.3
		4.2×10^{-2}	1.25
2	V	1.3×10^{-2}	4.3
	R	1.1×10^{-2}	4.3
	T	0.90×10^{-2}	4.3
3	V	1.1×10^{-2}	4.3
	R	—[c]	
	T	0.39×10^{-2}	4.3

Table XIV. (Continued)

Station	Component[a]	Peak velocity (cm/sec)	Frequency (Hz)
		Delta	
1	V	3.4×10^{-2}	4.3
		2.6×10^{-2}	1.25
	R	2.3×10^{-2}	4.3
		3.6×10^{-2}	1.25
	T	2.8×10^{-2}	4.1
		5.3×10^{-2}	1.25
2	V	1.5×10^{-2}	4.3
	R	1.5×10^{-2}	4.5
	T	0.93×10^{-2}	4.5
3	V	1.3×10^{-2}	4.3
	R	0.82×10^{-2}	4.0
	T	0.51×10^{-2}	4.0

[a]V - Vertical; R - Radial; T - Transverse.

[b]Recordings of Station 3 were lost due to amplifier power failure.

[c]Channel recording radial velocity at Station 3 was lost due to broken wire.

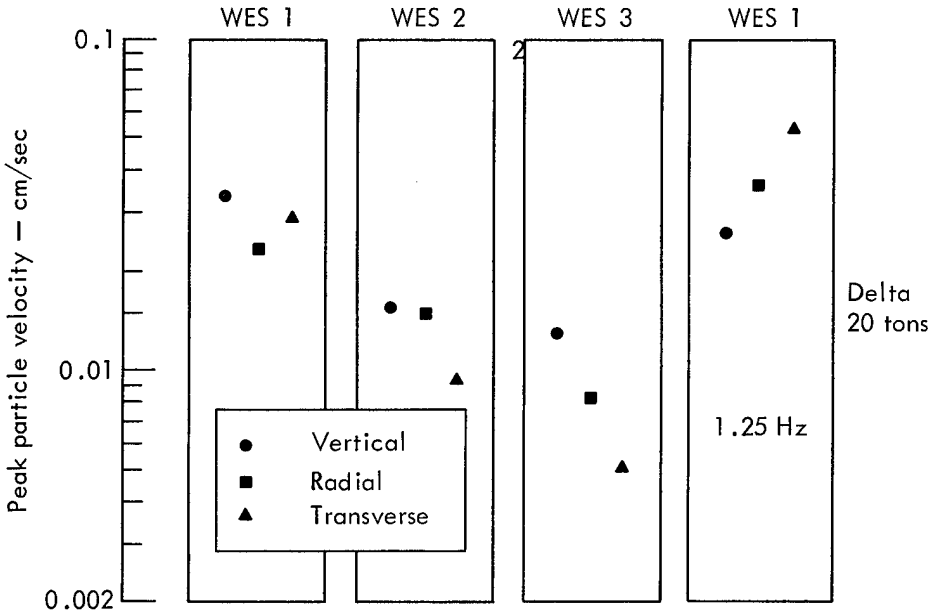

Fig. 112. Peak component velocities for Pre-Gondola I Delta.

produced the greatest amplitudes of the four shots.

The amplitudes of a low-frequency oscillation (approximately 1.25 Hz) are also plotted for WES Station 1. It is believed that this motion represents a fundamental mode of vibration of the dam. The 1.25-Hz oscillation was very pronounced on the recordings made on the dam; it is not evident on records taken elsewhere. The motion appears to be a resonance effect that builds up and decays a number of times over a span of about 30 sec, with the greatest amplitudes in the horizontal components.

The records from the WES stations for all 20-ton events are very similar with respect to waveforms and frequency content.

Cloud Development Studies

INTRODUCTION

Scope and Objectives

The Pre-Gondola I series of 20-ton cratering explosions presented the first opportunity to observe cloud development from cratering detonations in a water-saturated medium. Therefore, the objective of this technical program was to determine as completely as possible the time history of cloud development from initial formation to downwind dispersal for all events. To accomplish this objective, a three-part program was formulated: (1) photography of the developing cloud, (2) laser-radar (hereafter referred to as "lidar") tracking of the cloud, and (3) sampling of the particulates in the cloud. Meteorological data required in support of this program were provided by ESSA-ARFRO.

Background

Previous experience has shown that the clouds produced by high yield, chemical explosive cratering events are reasonably accurate models of the clouds produced by nuclear cratering events.[30-34] It has been assumed in nuclear cratering events that the early configuration of the visible cloud (at stabilization) contains the major portion of the radioactive material that eventually comprises the local fallout and the long-range airborne concentration at later times. Assumptions have also been made regarding the radioactivity concentration gradient through the cloud and the radioactivity-particle size distribution. Because no instrument or technique has shown the capability to probe a cloud with the necessary completeness, cloud concentration gradients have been assumed as either constant or gaussian in nature, even though cloud sampling has indicated that neither may be true. It follows, therefore, that data on cloud dimensions at stabilization (i.e., base surge radius, base surge height, main cloud radius, and main cloud height) and cloud volumes, cloud position in space, and internal cloud structure (particle concentration) as a function of time are important in quantitatively evaluating the radiological hazards from detonations associated with nuclear excavation projects. The predicted cloud configuration and dimensions at stabilization, and the cloud volume, position in space, and internal structure for a planned nuclear excavation detonation can be used to make fallout estimates and cloud diffusion calculations.

Theory

The model used in this study to describe the clouds generated by cratering explosions is that of Knox and Rohrer.[32] The cloud consists of two parts: a base surge cloud which expands primarily in a radial direction during early growth, and a main cloud which protrudes above it at about the center and grows primarily vertically. In the past, the presence or absence of a distinguishable main cloud and the relative maximum radius of the base surge for a nuclear event were assumed to be dependent on the amount of moisture contained in the media.

The base surge and main cloud dimensions from a cratering explosion are primarily functions of (1) the yield of the explosive, (2) the depth of burst, (3) the medium, and (4) the meteorological conditions prevailing.

The following scaling relationships have been adopted to permit comparison of data from cratering detonations of various yields:

Base Surge Dimensions

$$R_b \propto W^{0.3}$$
$$H_b \propto W^{0.2}$$

Main Cloud Dimensions

$$R_m \propto W^{0.45}$$
$$H_m \propto W^{0.2}$$

where:

W = yield of device
R_b = radius of base surge
H_b = height of base surge
R_m = radius of main cloud
H_m = height of main cloud

Cube root scaling ($W^{1/3}$) has been used for scaling the DOB to 1 kt.

Using these relationships, scaling curves have been prepared by various authors.[30,32,33,34] The scaling curves as revised in Ref. 34 were used to make cloud dimension predictions for the Pre-Gondola I events.

EXPERIMENTAL PROCEDURES

The field program to record the cloud development on Pre-Gondola I consisted of three parts: cloud photography, lidar pulsing of the cloud, and cloud sampling. Detailed information concerning these documentation techniques are presented in the following paragraphs:

Cloud Photography

The objective of the cloud photography program was to document the early growth of the cloud up to stabilization time. Any photography that extended beyond stabilization time was expected to be of assistance in the analysis of the lidar results. The elements required for this program included: (1) cloud camera stations, (2) a target array, and (3) meteorological data collection.

Camera Complement

There were four camera stations used in the four-event Pre-Gondola I series. Cloud photography cameras were used at three of these four stations. Figure 113 shows the positions of the ground cloud photography stations (Camera Station No. 1 and Camera Station No. 3) relative to the four SGZs. Camera Station No. 2 was used exclusively for the ground surface motion program. The fourth station consisted of a helicopter flying above and slightly to the east of the general SGZ area.

The cameras in Camera Station No. 1 were started by signal from the firing console at a preset time. The cameras in Camera Station No. 3 (Lidar Cloud Tracking Station) were started manually. Zero time was determined by observing the fiducial signal at SGZs on the 64-frame/sec film from Camera Station No. 1, and also on the 48-frame/sec film from the helicopter.

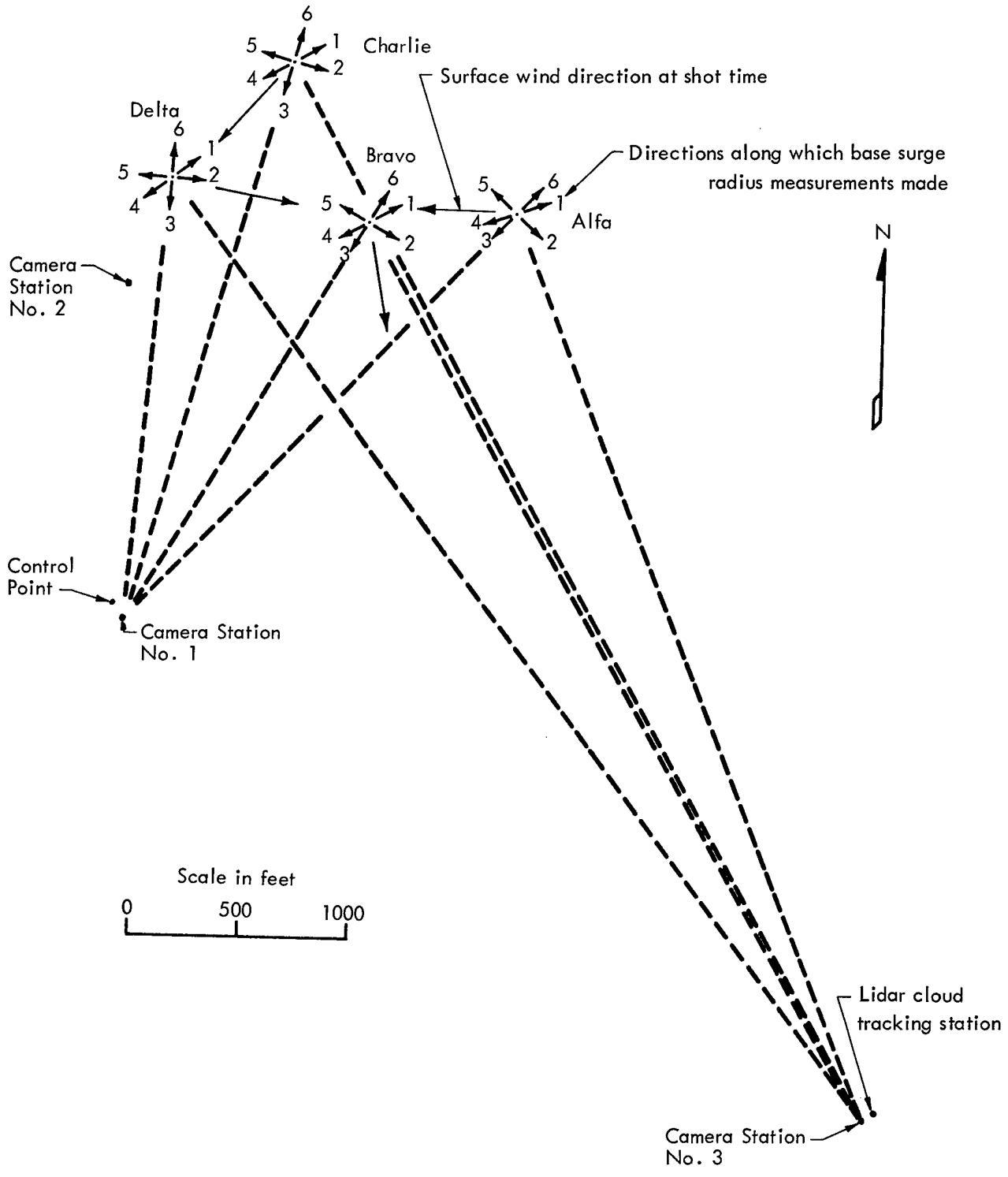

Fig. 113. Lidar and cloud camera station locations.

Target Array

To provide points of reference for the helicopter photography (because the camera had a variable field of view), an array of bright red plywood targets were placed on the surface in two orthogonal rows through SGZ for each event. Targets were floated on the water where necessary. The Control Point photo van (Camera Station No. 1) was in line with one of the target rows for each event. Each target consisted of a horizontal section on the ground and two orthogonal vertical sections, placing the target in view from any angle.

Meteorological Data

A radiosonde balloon was released from the vicinity of the Control Point at shot time for each event. Detailed temperature lapse rate data were needed up to the expected maximum height of the clouds. Other meteorological data recorded included wind speed and direction up to approximately 100,000 ft MSL.

The temperature lapse rate data were used to correct base surge cloud radius measurements to a neutral atmosphere condition and also to assist in understanding cloud rise phenomena. Wind data were needed for operational purposes and also to corroborate lidar cloud tracking data.

A meteorologist was on duty during the project to make weather predictions. Predictions were needed to establish approximate shot time and day for each event.

Lidar Cloud Tracking

To date, cloud measurements have been conducted for a number of cratering events. These measurements have utilized scientific photography to document the cloud development from initial formation to downwind dispersal. This type of photography has permitted the acquisition of data on the base surge radius, base surge height, main cloud radius, and main cloud height at the time of stabilization. However, later time cloud measurements cannot be obtained in this way. Most of the cameras used have a fixed field of view depending upon the lens being used, and, since they are often located in bunkers or in trailer vans, they cannot be easily rotated in order to follow the cloud. In those circumstances in which cameras can be used to follow the cloud, the dimensions of the field of view at the cloud position are unknown. Normally two cameras are positioned at right angles with respect to SGZ; consequently, only two sides of the cloud are visible, and it is difficult to obtain a reliable quantitative determination of the cloud volume.

The internal structure of a cloud cannot be determined by photographic methods. Also, the cloud photography yields no data when the cloud becomes subvisible. Therefore, it became desirable to find a technique that would give better and more detailed information on the position, motion, rate of growth, and internal structure of visible and subvisible clouds resulting from cratering explosions.

The SRI lidar system was operated on the Pre-Gondola I events to assess its capability: (1) to record the cloud position in space and to determine its volume as a function of time, and (2) to record the presence of the cloud after photographic

methods were no longer effective. Figure 114 is a photograph of the SRI lidar. Additional details are contained in Refs. 35 and 36.

In the SRI lidar a narrow, monochromatic pulsed beam of light is directed into the atmosphere and a portion of this light is scattered by particles or droplets in the beam path, producing a return signal which is received by a photomultiplier tube. The time at which the reflected light is received relative to the time the pulse of light left the transmitter permits a calculation of the distance of the reflecting particles from the lidar.

The position of the lidar is indicated in Fig. 113 immediately adjacent to Camera Station No. 3. A low platform was provided for the equipment on the Bravo Event. The cloud for this event drifted behind an equipment shelter, and consequently some late time data were lost. Therefore, before the second event a 15-ft tower was provided for the lidar which enabled a clear beaming path in all directions. This arrangement worked well for the remaining three events.

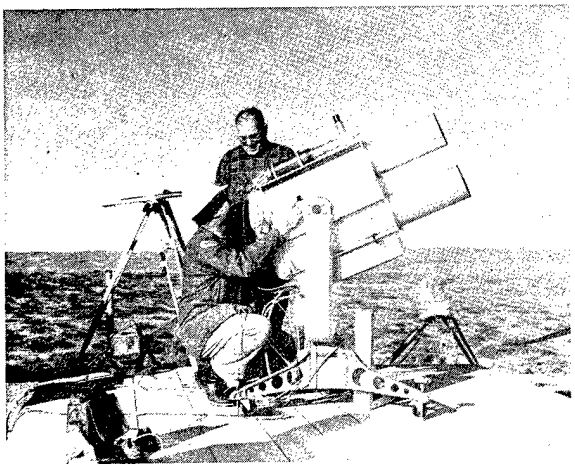

Fig. 114. SRI Mark V neodymium lidar.

Cloud Sampling

Cloud dust sampling was performed on the Pre-Gondola I series to permit an evaluation of a contemplated experiment for the Pre-Gondola II row-charge experiment. To investigate the escape fraction (ratio of the amount in the cloud to that originally at the shot point) for material originating at the shot point, several trace elements having high thermal neutron capture cross sections have been proposed as tracers. The cloud could be sampled for these trace elements following the event. Samples could be later exposed to high thermal neutron fluxes to activate the trace elements and to allow accurate content measurements to be made. The results could then be compared to the amounts originally placed within the explosive charge. In this series of experiments the purpose of the sampling program was to determine the background level for the various proposed trace elements in several typical samples, thereby making possible the selection of proper tracers and the estimation of the amount necessary for emplacement in the explosive charge.

Two sampling systems each including two Staplex type high-volume air samplers were used. One sampler was equipped with Hollingsworth and Vose No. 70 filter paper and the other with I. P. C. paper as a rough filter over the Hollingsworth and Vose No. 70 filter paper. Both sampling systems were set out just prior to each event in the predicted downwind direction for shot time. In all cases the systems were placed fairly close in

(between 600 and 1000 ft) to SGZ in anticipation of a diffuse cloud.

RESULTS

Cloud Photography

Good cloud photography was obtained for all four events. Measurements of cloud dimensions derived from cloud photography at the time of stabilization are summarized in Table XV. A brief description of each event follows in the order in which the events were detonated.

Event Bravo

The mound material from the Bravo Event rose to a maximum height of 700 ft. A small amount of stemming material stayed at this height for about 20 sec before a puff of steam developed and started to ascend. The puff of steam and fine stemming material (the stemming grout contained vermiculite) rose to approximately 1500 ft before going out of the field of view of the cameras. The base surge was very diffuse with a small amount of suspended dust particles in it.

Table XV. Pre-Gondola I cloud dimensions.[a]

		Charlie 28 Oct 66	Bravo 25 Oct 66	Alfa 1 Nov 66	Delta 4 Nov 66
Charge weight, tons NM		19.62	19.36	20.35	20.24
Depth of burst					
Actual (ft)		42.49	46.25	52.71	56.87
Scaled ($ft/kt^{1/3}$)[b]		154	169	186	201
Base surge dimensions					
Radius:	Predicted (ft)	1250	1085	860	730
	Observed (ft)	954	646	605	428
	Scaled ($ft/kt^{0.3}$)	3060	2055	1890	1340
	Time of observed value (sec)	44	32	30	17
	Temperature corrected (ft)	1110	859	526	346
	Temp. corr. scaled ($ft/kt^{0.3}$)	3550	2730	1640	1086
Height:	Predicted (ft)	720	610	480	420
	Observed (ft)	2200	1050	2700	1400
	Scaled ($ft/kt^{0.2}$)	4560	2320	5780	2990
	Time of observed value (min)	3	2	4	1.33
Main cloud dimensions					
Radius (ft)		—	not measured	—	—
Height:	Predicted (ft)	1900	1680	1330	1120
	Observed (ft)	—	1500	—	—
	Scaled ($ft/kt^{0.2}$)	—	3250	—	—
	Time of observed value (sec)	—	80	—	—

[a] From Ref. 36.

[b] Scaled dimensions determined using a nitromethane energy equivalent yield factor of 1.1 as follows: $\left(\frac{\text{tons NM} \times 1.1}{1000 \text{ tons}}\right)^{\text{exponent}}$ = scaling factor.

There was a very small indication of steam late in time (~35 sec) in the base surge development which quickly disappeared. Seven different measurements of base surge radius were averaged to give the value of 646 ft given in Table XV.

Event Charlie

The Charlie Event had the shallowest DOB of all four events, and, therefore, the largest cloud dimensions were expected. The first surprise was that there was no main cloud. The mound rose and fell, leaving no main cloud and injecting a large amount of visible vapor (presumed to be steam) into the already developing base surge. The base surge grew to an average radius of 954 ft (eight measurements). The injected vapor caused two portions of the base surge to rise rapidly to 1900 ft before it went out of view of the cameras.

The helicopter photography revealed that the base surge was in the form of a doughnut; i. e., hollow in the middle after the mound had collapsed. The ejection of the white visible vapor from the base of the falling mound could be seen very clearly. It is significant that no visible main cloud resulted from this detonation. There was as much, and maybe slightly more, dust in the base surge cloud in this event as in the Bravo Event.

Event Alfa

Again, in the Alfa Event, no main cloud was observed. The mound rose and fell and injected large amounts of visible vapor into the growing base surge. The base surge growth was the most symmetrical of any of the events as viewed from ground camera stations. After the vapor disappeared, it was evident that there were fewer suspended particles in this cloud than in the previous two.

Two sides of the surface near Alfa SGZ fell off in a slight grade from SGZ to the reservoir. The base surge grew faster in the downhill directions and developed to a larger final radius. Five measurements have been averaged to give a final base surge radius of 605 ft.

It is interesting to note that: (1) the cloud penetrated the inversion condition at 1500 ft and went on up through to the stable layer, and (2) although there were larger amounts of visible vapor (again presumed to be steam) available for injection into the base surge, there was no main cloud.

Event Delta

Because the Delta Event had the deepest DOB, the smallest cloud dimensions were expected. Again, the mound rose and fell and left no visible main cloud. The terrain was downhill in the direction the wind was blowing (13 knots), and the base surge grew faster in that direction and developed to a larger final dimension. Six measurements have been averaged to give a base surge radius of 428 ft.

Lidar Cloud Tracking

The overall objectives of this part of the program were exceeded in that the lidar demonstrated exceptional capability by: (1) making cloud volume measurements and tracking the position of the visible cloud for ~14 min on the first event (Bravo); (2) tracking first the visible cloud and then the subvisible cloud for a total tracking time of 30 min, and permitting volume estimates to be made

over this time span, on the second event (Charlie); (3) again tracking both the visible and subvisible cloud and permitting more definitive depth, width, and height measurements as a function of time, and permitting volume estimates to be made on the third event (Alfa); and (4) providing a detailed log backscatter cross section isocontour mapping as a function of time on the last event (Delta). The log backscatter cross section isocontours are proportional to particle density isocontours.

The lidar equipment operated in the field without any component failure during the entire period. A peak firing rate of 6 pulses/min was attained during the second and third events. On the last event (Delta), due to a simplification of the data recording format, a peak firing rate of 12 pulses/min was achieved.

Detailed data for the lidar cloud tracking experiment are contained in Ref. 36. Table XVI summarizes the performance of the lidar on Pre-Gondola I.

The ground tracks of the visible and subvisible clouds are shown in Fig. 115. High-resolution contours of relative density variations existing near the base of the cloud at various times are shown in Figs. 116, 117 and 118. The contours represent values of the return signal (corrected for the R^{-2} propagation law) expressed in decibels referenced to the return produced by the clear atmosphere.

These values do not correspond directly with reflectivity due to the effects of attenuation. Again, the relationship between optical reflectivity and particulate matter content of the cloud is not precisely known. As a first approximation, however, the contours of relative signal intensity provide a very good basis for inferring the variations with respect to density.

Cloud Sampling

Four cloud samples were taken on each event. The samplers were in a position to get good samples in all events (i.e., the cloud passed over the sample position). Due to the very diffuse nature of the clouds, the amount of dust collected in each case was small, and analysis of the samples gave a good test of the neutron activation method. In addition, small samples of ejecta were put in plastic bags immediately following each

Table XVI. Lidar data summary.[a]

Event	Number of lidar observations	Tracking time (min)	Maximum detection range	
			From GZ (m)	From lidar (m)
Bravo	50[b]	14[b]	2570	3630
Charlie	101	30	1900	3100
Alfa	87	22	2660	4010
Delta	117	15	5625	4125

[a]From Ref. 36.

[b]Run terminated early because cloud drifted behind equipment shelter.

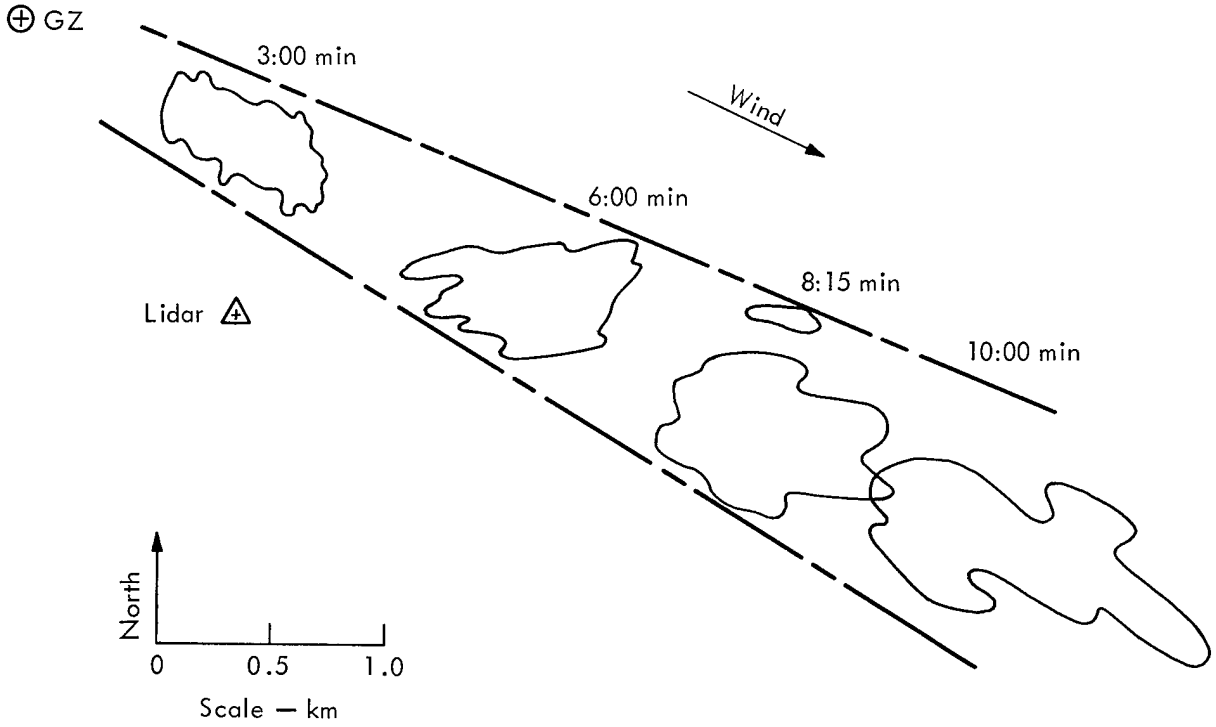

Fig. 115. Ground track of subvisible cloud, Delta Event (from Ref. 36).

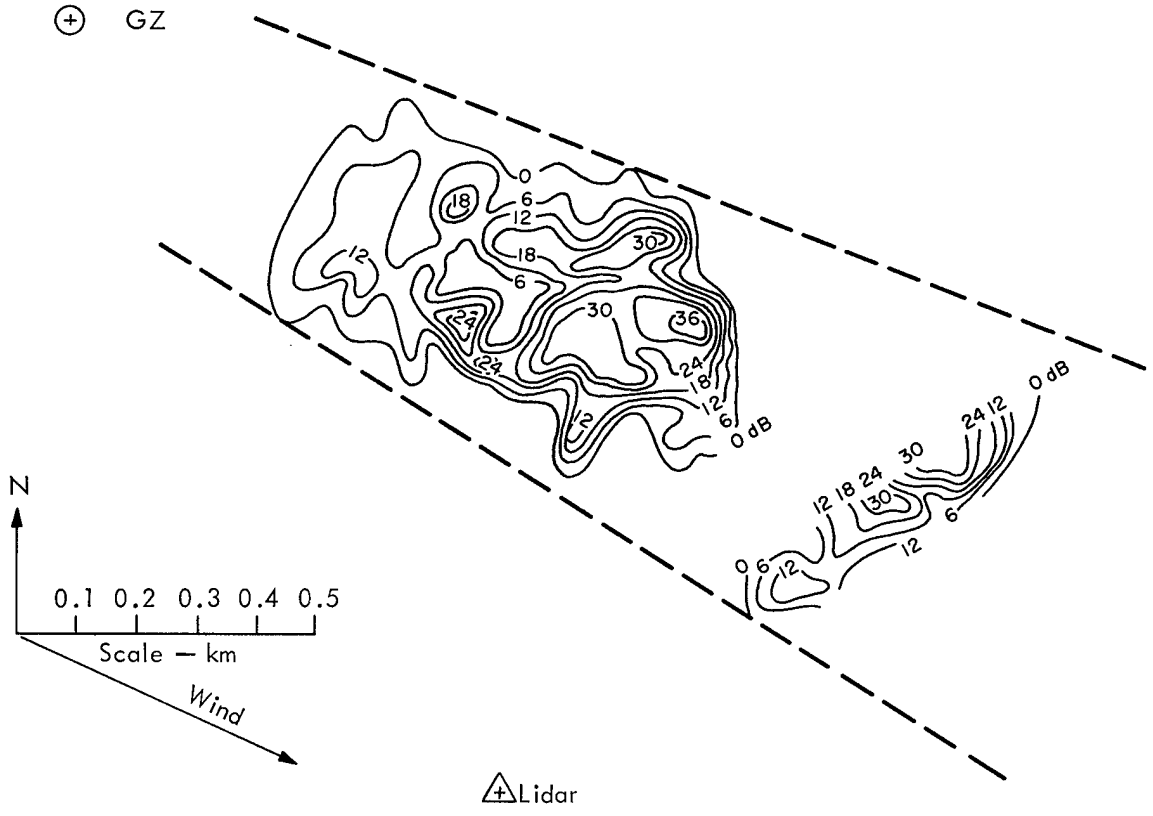

Fig. 116. Approximate density contours for subvisible cloud inferred from relative signal amplitude measurements (Delta: time, 3:00 min)—from Ref. 36.

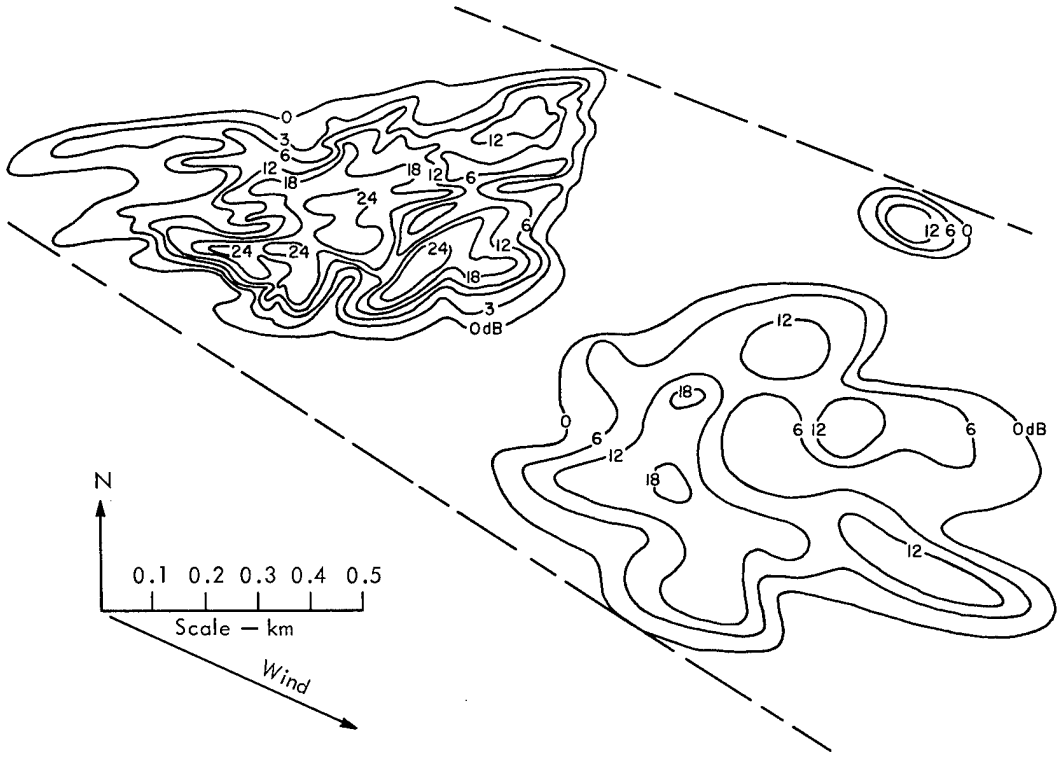

Fig. 117. Approximate density contours for subvisible cloud inferred from relative signal amplitude measurements (Delta: time, 6:00 and 8:15 min)—from Ref. 36.

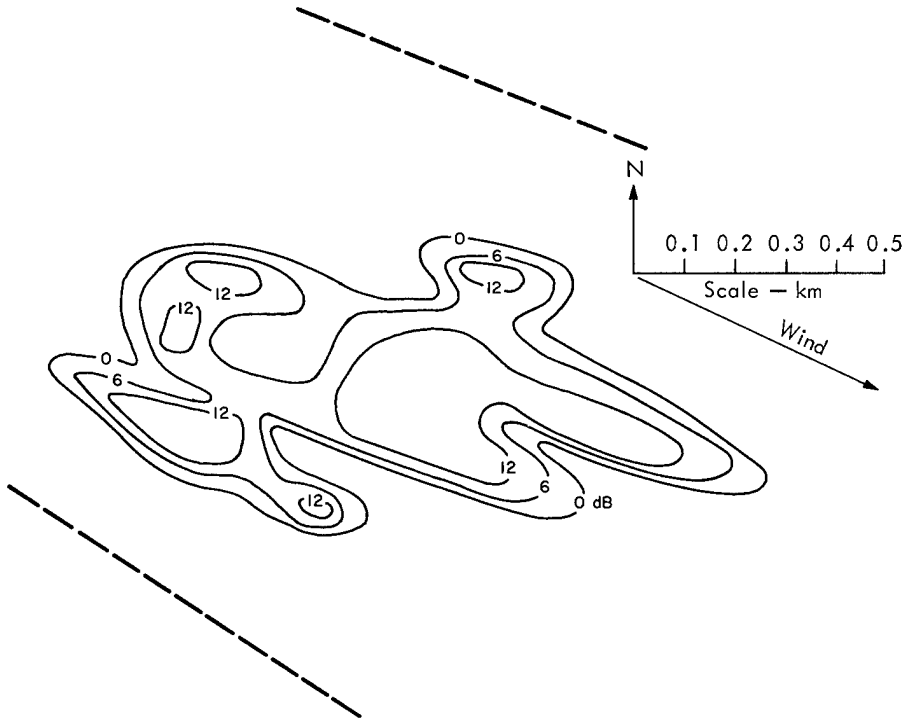

Fig. 118. Approximate density contours for subvisible cloud inferred from relative signal amplitude measurements (Delta: time, 10 min)—from Ref. 36.

event and brought back to the laboratory for activation analysis.

Activation analyses were performed by Cohen[37] and Brownlee.[38] The samples were subjected to neutron irradiation in the LPTR Reactor and subsequent gamma radiation analysis on a high-resolution germanium Ge(Li) detector counting system. The data so obtained were subsequently submitted to computer code data reduction techniques. Elements definitely found are listed in Table XVII. An indication of the relative abundance of each of the elements is also given in Table XVII. Brownlee[38] found that no significant amounts of the rare earths Pd, Cd, and In were found under the analysis conditions utilized. Sm and La are present naturally in sufficient amounts that they should be used as tracers only after careful consideration of other possibilities. Naturally occurring Eu is low enough that Eu could be considered for use as a tracer.

DISCUSSION AND INTERPRETATION

Unique Nature of Pre-Gondola I Clouds

The clouds observed on the four Pre-Gondola I events are unique when

Table XVII. Results of activation analysis of cloud and ejecta samples.[a]

Elements definitely found	Relative abundance
Sm(as 47.1-hr Sm-153)	Present in early spectra as prominent peak.
La(as 40.27-hr La-140)	Present in all spectra as a series of several prominent peaks.
Eu(as 12.5-yr Eu-152 from 9.3-hr Eu-152m)	Present in very small amounts.
Cr(as Cr-51)	Low
Au(as Au-198)	Low
Sb(as Sb-122 and -124)	Low
Ru(as Ru-103)	Low
Nd(as Nd-147)	Low
Cs(as Cs-134)	Low
Ag(as Ag-110m)	Very low; questionable presence.
Sc(as Sc-46)	Quite prominent; relatively high.
Fe(as Fe-59)	Quite prominent; relatively high.
Co(as Co-60 from Co-60m)	Low peaks in early spectra; prominent in later spectra.
Na(as Na-24)	Quite high; decays with 15-hr half-life; absent from later spectra.
Zn(as Zn-65)	Questionable
Ta(as Ta-182)	Low
Hf(as Hf-181)	Low
Pt	Low
Hg	Low

[a]Taken from Ref. 38.

compared to clouds observed on previous chemical explosive and nuclear explosive cratering events, all of which have been conducted in relatively dry media. The clouds had the following specific characteristics:

Small Amount of Suspended Particles

The amount of suspended particles present at an early time in the cloud was much less than had been observed on previous cratering events. The clouds themselves were very diffuse. Depending on the location of the observer, the clouds could no longer be easily seen from 3 to 5 min following zero time. The high water content of the medium is the most probable explanation. Many small (micron-size) particles are not available during cloud formation for suspension in the cloud due to the agglomerating action of the water present in the medium.

No Visible Main Clouds

There were no visible main clouds except for the Bravo Event. The fine vermiculite material in the stemming was the last material to fall during the mound collapse, but even this material had disappeared by approximately 40 sec in the Bravo and Charlie Events and even sooner in the deeper DOB events (Alfa and Delta). There was a small puff of steam which started at the peak of the mound rise in the Bravo Event. This puff of steam is not visible in the Camera Station No. 3 photography of the Bravo Event but is barely visible in the Camera Station No. 1 photography. The Bravo main cloud did not develop as a result of dynamic venting of explosive gases through the rising mound.

On previous chemical explosion events, the development of a main cloud follows a very definite breakthrough of the rising mound by cavity gases. In the Pre-Gondola I events the mound growth and collapse was similar to that observed in Danny Boy where there was no visible dynamic venting. Christopher[13] has noted the high spall and gas acceleration mound velocities observed on the Pre-Gondola I events. It is likely that this fast mound growth was able to stay ahead of (or absorb in void spaces) the late time cavity gas expansion thus resulting in no visible venting. More of the energy available in the expanding gas was used to move material as is evidenced by the larger craters observed.

It is likely that if any significant venting of cavity gases had occurred, it would have been easily visible. (Later, in the base surge development, steam was visible on all four events.) Because water is the primary detonation product[8,39] resulting from the detonation of confined charges of nitromethane, any significant venting certainly would have been visible in the cloud or documentary photography from Camera Station No. 1.

Steam Cloud Formation at Late Times

Among the most interesting aspects of these four events were the doughnut-shaped water vapor clouds observed during base surge development. Once the mound collapsed, the crater area was visible in the middle of the cloud. Day and Rohrer[35] concluded that in each event the water contributing to the observed water vapor clouds originated as a detonation product of the nitromethane.

Comparison of Dimensions with Past Cratering Event Clouds

The temperature-corrected scaled base surge radius dimensions from

Table XVI have been plotted as a function of scaled depth to permit a comparison with alluvium and basalt curves derived from previous cratering events (Fig. 119). The saturated clay shale curve lies between the basalt and alluvium curves and falls off more rapidly with scaled depth. This curve has been used to make predictions for the Pre-Gondola II row-charge event (28 June 1967).

Base surge height measurements reported in Table XVI are actually the

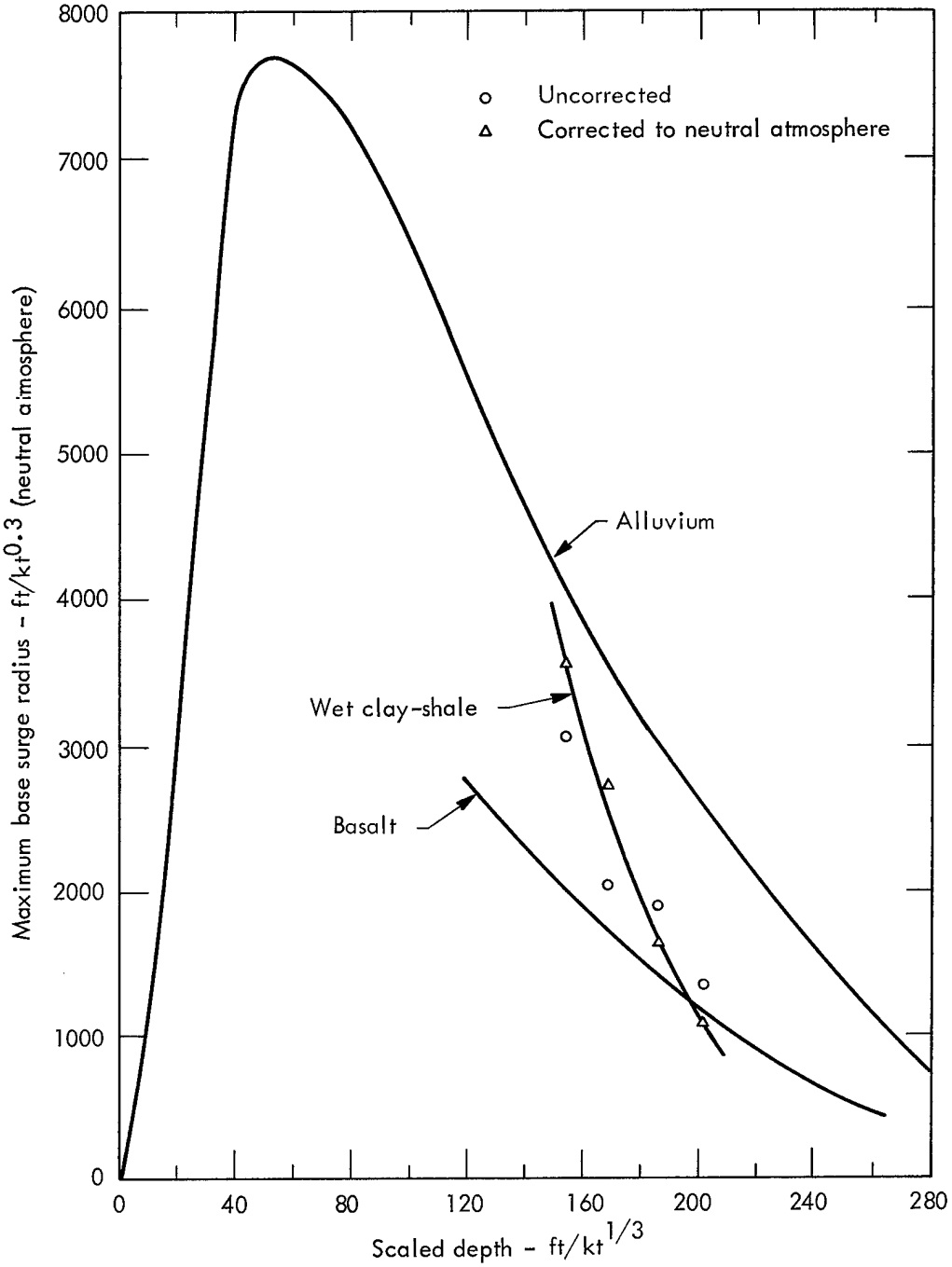

Fig. 119. Scaled base surge radius vs scaled DOB of wet clay shale.

heights to which the steam observed in the base surges rose before going out of view or becoming invisible. As such, it is not surprising that they differ so much from the predicted values, and, accordingly, it has not been deemed appropriate to plot them as a function of scaled depth. Because the same relative amounts of steam were probably available in other nitromethane cratering events, the difference in base surge heights is attributed to the lack of a high concentration of suspended dry particles which would effectively absorb the water vapor if present.

Significance of Lidar Results

Because of the diffuse nature of the clouds, the Pre-Gondola I series of events provided an excellent opportunity to test the capabilities of lidar for tracking explosion-produced clouds. The results of this program[36] indicate clearly that lidar tracking techniques can provide information on the position, motion, rate of growth, and internal structure of visible and subvisible cratering explosion clouds. The fact that no particulate matter was detectable by the lidar after 30 min illustrates the diffuse nature of the clouds when compared to cratering experiments in alluvium and basalt.

Use of the lidar was a new approach to the measurement of cloud dimensions, volume, and internal structure. The clouds produced by the four experiments in Pre-Gondola I were all rather tenuous in nature. The shot medium consisted of saturated shale, and considerable steam was observed in the clouds of all four cratering experiments. Several minutes after shot time, the clouds became quite diffuse with no recognizable geometry. Time-lapse photos taken from the same location as were the lidar data show that the clouds were essentially invisible to the camera between 3 and 5 min after detonation time. Despite the diffuse nature of the clouds, the lidar was able to detect them, and to determine with some accuracy the depth and position of the clouds up to 30 min after detonation time.

The lidar gave good representation of the internal structure of the Delta cloud, determining the relative density and the general distribution of matter within the cloud as well as the manner in which these factors changed with time due to diffusion and fallout.

In most cases, it was not possible to correlate cloud measurements from the photography with those obtained from the lidar because the lidar did not begin operation until several minutes had elapsed from detonation time. For the Alfa Event, however, some comparison is possible, and Fig. 120, showing measured cloud heights early in time, illustrates the good agreement between the cloud photography and the lidar.

The limit on time of tracking (time when no more return signals were received from the cloud) in these four events was as much due to the lack of suspended particles in the clouds as it was to the distance between the cloud position and the lidar site.

Development of a faster pulse rate unit and data display and recording method should give a much improved three-dimensional picture of the cloud. A lidar mounted in an aircraft (subsequently accomplished on Pre-Gondola II)

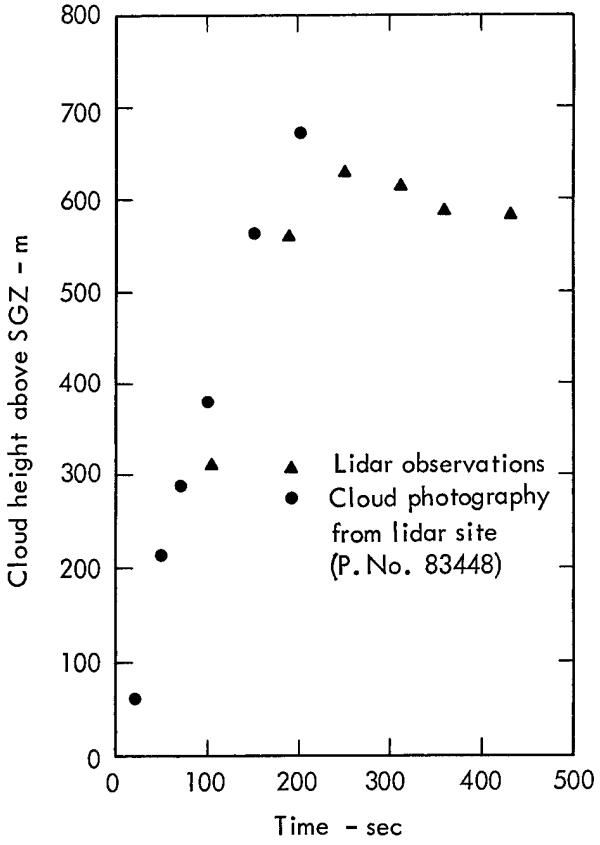

Fig. 120. Comparison of lidar and photography estimates of Alfa base surge height.

would greatly extend the range of the lidar in time.

The lidar should be used in future cratering experiments to provide valuable quantitative data when correlated with other measurement and sampling programs. In nuclear cratering events, the fallout and airborne radioactivity problem should be thus better defined than has been possible in the past.

Cloud Sampling

Activation analyses performed on cloud and ejecta samples taken during all four events indicate that there are several elements suitable for use as tracers which also exist naturally in the clay-shale at low concentrations. Among those elements which could be used as tracers are palladium, cadmium, indium, and europium.

Application of Results to Nuclear Detonations

Because no nuclear cratering events have been conducted in a medium similar to the wet clay-shale medium, it is interesting to make some interpretations as to the significance of the Pre-Gondola I results. The most significant result seems to be the lack of visible venting of cavity gases through the rising mound. If it is assumed that nuclear event in the same medium would also impart sufficient velocity to the overburden to prevent dynamic venting of cavity gases during mound rise, then the radioactivity finally making up the cloud should be injected into the base surge cloud in the same manner as the steam jets in the Pre-Gondola I series and should be greatly fractionated and consist primarily of volatile radionuclides. In other words, the radioactivity release, because it occurs at a later time (seconds), should be somewhat like that observed in the Danny Boy Event.

Detailed information on the internal structure of a cloud as a function of time from HE cratering events materially assists in understanding the fallout patterns and cloud diffusion phenomena to be expected from nuclear cratering events in similar media.

Biological Monitoring

INTRODUCTION

The Fort Peck Area Engineer, with participation by the Montana State Fish and Game Department provided game range control and conducted biological monitoring of the fish and wildlife in that part of the Charles M. Russell Game Range surrounding the Pre-Gondola site. Control included regulation of hunters and fishermen and roundup of pasturing livestock. Monitoring activities included surveying the movement of protected elk, deer, and similar game animals which frequented the site and experiments to determine the effects of the cratering explosions on captive native fish.

During the preparation for the experiments, the livestock were moved and the large game animals were frightened away. Consequently, the shot-time monitoring focused on experiments to determine the effects of the cratering explosions on captive native fish.

EXPERIMENTAL PROCEDURE

Preliminary Studies

The experimental plan for Pre-Gondola I was based on results of preliminary investigations during the 1000-lb Seismic Site Calibration Series. During Event SC-2 black crappie were placed in captive cages off-shore at distances of 300, 500, and 800 ft. There was no mortality of these or any other fish. During Pre-Gondola I the monitoring program was extended in scope for the first three events. Gill net catches in the vicinity of the test site prior to the Bravo Event identified gold eye, perch, sucker, northern pike, and sauger.

Soundings established the placement depth for "live boxes" or cages containing several species of fish representing those found in the area. The distances between the boxes and SGZ were arbitrary and subject to change for subsequent events.[40]

Cages used for holding the fish were approximately 8-in. × 8-in. × 24-in. size and were constructed of 3/8-in. × 1/2-in. mesh wire. The cages were suspended by a float and anchor system (one at each station) at depths of 1 to 10 ft below the water surface. No attempt was made to orient the cages in any particular direction with respect to the direction of the shock wave propagation.[40,41]

Prior to each event, several boxes of captive fish (representing those found in the area) were placed at surveyed locations at various depths and distances from SGZ. A control group of the same species of fish was observed prior to each detonation to determine normal mortality caused by captivity.

The captive fish were checked by a fisheries biologist for mortality rate and readily observable injuries, such as protruding eyes, external hemorrhage, ruptured air bladders, spleen, livers, and kidneys, and protruding viscera at the anus and buccal cavity. Traits such as loss of equilibrium and erratic flight were also recorded. Results of a previous NCG program to determine water shock effects on fish[42] were also studied by

the biologists in order to understand the differences in mortality when an explosive charge is detonated in water rather than on shore. No measurements were made to determine ground-blast or air-blast-induced water shock.

Bravo Event

Stations containing captive fish were set on a line from Bravo to an arbitrary point on the north shore of the South Fork of Duck Creek. Cages at 500, 600, and 2000 ft from SGZ contained one each of yellow perch, northern pike, gold eye, and sucker. Cages at distances of 900, 1200, and 1500 ft contained the same type of fish, except for northern pike.

A check of the captive fish approximately 30 min after detonation gave negative results. A gill net catch prior to the next (Charlie) event consisted only of gold eye.

Charlie Event

Stations containing captive fish were set on a line from Charlie SGZ to an arbitrary point on the north shore of the South Fork of Duck Creek at distances of 300, 500, 600, 700, and 1000 ft. The cage at a distance of 300 ft contained a northern pike, a perch, and a gold eye. The cage at 500 ft contained a northern pike, a crappie, a perch, a gold eye and a sucker. The cage at 600 ft contained a northern pike, two suckers, and a gold eye. The cage at 700 ft contained a northern pike, a perch, a sucker and a gold eye. The cage at 1000 ft contained a northern pike, a perch, a sucker and a gold eye. Each cage was checked 4 hr before and about 15 min after the detonation with negative results. A pair of gill nets retrieved prior to the next (Alfa) detonation resulted in a catch of several hundred gold eye and one pike.

Alfa Event

Because of the negative results of the two previous detonations and the shallowness of the adjacent waters, coverage during the Alfa Event was limited to one "live box" which contained the same fish used during the Bravo Event. This group of fish, consisting of two pike, four perch, and four suckers, was placed at a point located approximately 600 ft from the Alfa SGZ. The group was checked about 2-1/2 hr prior to detonation, and removed about 1 hr after the detonation. No dead or injured fish were noted. The two pike were set free in the reservoir. The perch and suckers were dissected to determine whether they had suffered any accumulative effects.

RESULTS

Bravo Event

Postshot examination of the captive fish revealed no immediate mortalities, no external damages and no change in behavior. No dead fish were noted in the waters adjacent to the test site (Fig. 121).

Charlie Event

A preshot check of all captive fish prior to detonation revealed only the gold eye stationed at 600 ft to be dead. Postshot examination revealed the gold eye at the 300-ft station to be near death. The gold eye stationed at distances of 500, 600, and 1000 ft were dead. No dead fish were noted in the waters adjacent to the test site. No external

Fig. 121. Recovering captive fish (post-Bravo).

damages were noted on any of the captive fish. A necropsy was performed on the collected gold eye, but no internal damage could be found. Death was attributed to excessive handling of these delicate fish.

Alfa Event

Postshot examination confirmed that there were no external or internal damage to the caged fish nor were fish noted in the waters adjacent to the Alfa detonation. Gold eye and pike remained in the area adjacent to the project site after completion of the detonations.

CONCLUSIONS

The accumulated effects of three detonations were not injurious or lethal to fish in adjacent waters. Gold eye and pike were not completely frightened away from the area by the detonations.

Appendix A

Pre-Gondola Technical Reports

Title of Report	Agency	Author and/or Technical Program Officer	Number
Pre-Gondola —			
Seismic Site Calibration	NCG	M. K. Kurtz B. B. Redpath	PNE 1100
Site-Selection Investigations	NCG/Omaha	H. A. Jack W. W. Dudley	PNE 1101
Pre-Gondola I —			
Technical Director's Summary Report	NCG	M. K. Kurtz et al.	PNE 1102
Geologic and Engineering Properties Investigations	NCG/Omaha	P. R. Fisher et al.	PNE 1103
Close-in Ground Motion, Earth Stress, and Pore Pressure Measurements	WES	J. D. Day et al.	PNE 1104
Intermediate Range Ground Motion	LRL	D. V. Power	PNE 1105
Structures Instrumentation	WES	R. F. Ballard	PNE 1106
Crater Studies: Crater Measurements Surface Motion Studies	 NCG NCG	 R. W. Harlan W. G. Christopher	 PNE 1107 Part I PNE 1107 Part II
Cloud Development Studies	NCG/LRL	W. C. Day R. F. Rohrer	PNE 1108
Close-in Displacement Studies	AFWL	C. J. Lemont	PNE 1109
Lidar Observations of Pre-Gondola I Clouds	SRI	J. W. Oblanas R. T. H. Collis	PNE 1110
Pre-Shot Geophysical Measurements	LRL-N	R. T. Stearns J. T. Rambo	PNE 1111

References

1. Isthmian Canal Studies: Crater Tests in Cucaracha and Culebra Formations, Panama Canal Company, Diablo Heights, Canal Zone, Memorandum 283-P, 30 April 1948.
2. Project Planning Concept, Wet Medium Cratering Experiments, Project Pre-Gondola, U. S. Army Engineer Nuclear Cratering Group, Livermore, 21 April 1966.
3. P. R. Fisher, Project Pre-Gondola I—Geology and Engineering Properties Investigations, U. S. Army Engineer Nuclear Cratering Group, Livermore, Rept. PNE-1103 (to be published).
4. Lt. Col. M. K. Kurtz and Lt. B. B. Redpath, Seismic Site Calibration, Project Pre-Gondola, U. S. Army Engineer Nuclear Cratering Group, Livermore, Rept. PNE-1100 (to be published).
5. Capt. W. W. Dudley and H. A. Jack, Project Pre-Gondola, Site Selection Investigations, U. S. Army Engineer Nuclear Cratering Group, Livermore, Rept. PNE-1101, November 1966.
6. Capt. R. W. Harlan, Crater Studies: Crater Measurements, Project Pre-Gondola I, U. S. Army Engineer Nuclear Cratering Group, Livermore, Rept. PNE-1107, Part II, December 1967.
7. R. T. Stearns and J. T. Rambo, Project Pre-Gondola I—Preshot Geophysical Measurements, U. S. Army Engineer Nuclear Cratering Group, Livermore, Rept. PNE-1111, July 1967.
8. D. L. Ornellas, Heat and Products of Detonation of Cyclotetramethylene Tetranitramine (HMX), 2, 4, 6-Trinitrotoluene (TNT, Nitromethane (NM), and Bis (2, 2-Dinitro-2-Fluoro-Ethyl)-Formal (FEFO), Lawrence Radiation Laboratory, Livermore, Rept. UCRL-70444 (Preprint), May 1967.
9. Lt. Col. M. K. Kurtz, A Report of the Scope and Preliminary Results of Project Pre-Gondola I, U. S. Army Engineer Nuclear Cratering Group, Livermore, NCG/TM 66-20, December 1966.
10. R. Terhune and J. T. Cherry, LRL, Private communication, 7 December 1966.
11. J. Toman, LRL, private communication, November 1966.
12. D. R. Stephens, LRL, private communication, 9 January 1966.
13. Capt. W. G. Christopher, Project Pre-Gondola I Crater Studies: Surface Motion, U. S. Army Engineer Nuclear Cratering Group, Livermore, Rept. PNE-1107, Part II (to be published).
14. Lt. Col. B. C. Hughes, Maj. R. H. Benfer, and F. H. Foster, Study of the Shape and Slope of Explosion-Produced Craters, U. S. Army Engineer Nuclear Cratering Group, Livermore, NCG/TM 65-8, November 1965.

15. Lt. Col. M. K. Kurtz, A Report of the Scope and Preliminary Results of Project Pre-Gondola II, U. S. Army Engineer Nuclear Cratering Group, Livermore, NCG/TM 67-9, 14 August 1967.
16. Capt. K. L. Larner, Project Pre-Schooner I Ground Surface Motion Study, U. S. Army Engineer Nuclear Cratering Group, Livermore, NCG/TM 65-2, 1965.
17. R. W. Terhune, Surface Motion Measurements—Project Dugout; Lawrence Radiation Laboratory, Livermore, Rept. PNE-603F, August 1966.
18. Capt. K. L. Larner and Capt. W. G. Christopher, Project Pre-Schooner II, Surface Motion Measurements, U. S. Army Engineer Nuclear Cratering Group, Livermore, Rept. PNE-513 (to be published).
19. A. T. Whatley, Project Sulky—Scientific Photography Final Report, Edgerton, Germeshausen & Grier, Inc., Las Vegas, Rept. PNE-710F, August 1965.
20. Capt. W. G. Christopher, A Model of the Formation of the Neptune Crater, U. S. Army Engineer Nuclear Cratering Group, Livermore, NCG/TM 66-13, revised 24 April 1967.
21. A. S. Vesic, Theoretical Studies of Cratering Mechanisms Affecting the Stability of Cratered Slopes, U. S. Army Engineer Waterways Experiment Station, Vicksburg, Mississippi (to be published).
22. R. W. Terhune, LRL, private communication, December 1966.
23. R. W. Terhune, LRL, private communication, September 1965.
24. W. R. Perret, et al., Project Scooter, Sandia Corporation, Albuquerque, Rept. SC-4602(RR), October 1963.
25. J. E. Lattery, NCG private communication, January 1968.
26. J. D. Day, D. W. Murrell, and W. C. Sherman, Project Pre-Gondola I—Close-in Ground Motion, Earth Stress and Pore Pressure Measurements, U. S. Army Engineer Waterways Experiment Station, Vicksburg, Mississippi, Rept. PNE-1104, September 1967.
27. J. G. Bratton and C. J. Lemont, Project Pre-Gondola I—Close-in Displacement Studies, Air Force Weapons Laboratory, Albuquerque, Rept. PNE-1109 (to be published).
28. D. V. Power, Intermediate Range Ground Motions, Project Pre-Gondola I, Lawrence Radiation Laboratory, Livermore, Rept. PNE-1105, July 1967.
29. R. F. Ballard, Jr., Structure Instrumentation, Project Pre-Gondola I, U. S. Army Engineer Waterways Experiment Station, Vicksburg, Mississippi, Rept. PNE-1106, August 1967.
30. M. D. Nordyke and others, Technical Director's Summary Report, Project Dugout, Lawrence Radiation Laboratory and U. S. Army Engineer Nuclear Cratering Group, Livermore, Rept. PNE-600F, December 1964.
31. R. F. Rohrer, Base Surge and Cloud Formation, Project Pre-Schooner, Lawrence Radiation Laboratory, Livermore, Rept. PNE-503F, April 1965.

32. J. B. Knox and R. F. Rohrer, Base Surge Analysis, Lawrence Radiation Laboratory, Livermore, Rept. PNE-304, September 1963.
33. W. C. Day and R. F. Rohrer, Cloud Development Studies, U.S. Army Engineer Nuclear Cratering Group and Lawrence Radiation Laboratory, Livermore, Rept. PNE-511, June 1966.
34. W. C. Day, Cloud Dimensions for Cratering Explosions, U.S. Army Engineer Nuclear Cratering Group, Livermore, NCG/TM 66-8, September 1966.
35. W. C. Day and R. F. Rohrer, Cloud Development Studies, U.S. Army Engineer Nuclear Cratering Group and Lawrence Radiation Laboratory, Livermore, Rept. PNE-1108, September 1967.
36. J. W. Oblanas and R. T. H. Collis, Lidar Observations of the Pre-Gondola I Clouds, Stanford Research Institute, Palo Alto, California, Rept. PNE-1100, July 1967.
37. J. J. Cohen, Lawrence Radiation Laboratory; private communication.
38. J. L. Brownlee, LRL, private communication.
39. J. P. Cress, Heat of Detonation, Energy Equivalent Yield, and Detonation Products of Nitromethane, U.S. Army Engineer Nuclear Cratering Group, Livermore (to be published).
40. J. C. Chandler (Biologist, Fort Peck Area Engineer Office), private communication, 4 November 1966.
41. C. K. Phenicie, Progress Report of the Fort Peck Reservoir Fishery Survey, Montana Fish and Game Commission, Bulletin No. 3, 1950.
42. Lt. Col. M. K. Kurtz, Jr., Consolidated Report, Operation Breakup, FY 66—Ice Cratering Experiments, Blair Lake, Alaska, U.S. Army Engineer Nuclear Cratering Group, Livermore, NCG/TM 66-7, 25 November 1966.

DISTRIBUTION

LRL Internal Distribution

Michael M. May

R. Batzel

J. Gofman

H. L. Reynolds

C. H. Haussmann

R. Rosengren

D. Sewell

C. Van Atta

P. Molthrop

F. Eby

E. Goldberg

G. Higgins

J. Carothers

S. Fernbach

J. Hadley

J. Kane

B. Rubin

J. Kury

P. Stevenson

J. Bell

E. Hulse

W. Decker

W. Harford

G. Werth

M. Nordyke

F. Holzer

D. Power

H. Tewes

J. Toman

2

LRL Internal Distribution (Continued)

J. Knox

E. Teller, Berkeley

D. M. Wilkes, Berkeley

L. Crooks, Mercury

TID Berkeley

TID File 30

External Distribution

D. J. Convey
Department of Mines and Technical Surveys
Ottawa, Ontario, Canada

G. W. Govier
Oil and Gas Conservation Board
Calgary, Alberta, Canada

R. Needham
LASA Data Center
Billings, Montana

U. S. Army Engineer Division
Lower Mississippi Valley
Vicksburg, Mississippi

U. S. Army Engineer District
Memphis, Tennessee

U. S. Army Engineer District
New Orleans, Louisiana

U. S. Army Engineer District
St. Louis, Missouri

U. S. Army Engineer District
Vicksburg, Mississippi

U. S. Army Engineer Division, Mediterranean
Leghorn, Italy

U. S. Army Liaison Detachment
New York, N. Y.

U. S. Army Engineer District, GULF
Teheran, Iran

U. S. Army Engineer Division, Missouri River 2
Omaha, Nebraska

U. S. Army Engineer District
Kansas City, Missouri

External Distribution (Continued)

U. S. Army Engineer District 2
Omaha, Nebraska

U. S. Army Engineer Division, New England
Waltham, Massachusetts

U. S. Army Engineer Division, North Atlantic
New York, N. Y.

U. S. Army Engineer District
Baltimore, Maryland

U. S. Army Engineer District
New York, N. Y.

U. S. Army Engineer District
Norfolk, Virginia

U. S. Army Engineer District
Philadelphia, Pennsylvania

U. S. Army Engineer Division, North Central
Chicago, Illinois

U. S. Army Engineer District
Buffalo, New York

U. S. Army Engineer District
Chicago, Illinois

U. S. Army Engineer District
Detroit, Michigan

U. S. Army Engineer District
Rock Island, Illinois

U. S. Army Engineer District
St. Paul, Minnesota

U. S. Army Engineer District, Lake Survey
Detroit, Michigan

U. S. Army Engineer Division, North Pacific
Portland, Oregon

U. S. Army Engineer District
Portland, Oregon

U. S. Army Engineer District, Alaska
Anchorage, Alaska

U. S. Army Engineer District
Seattle, Washington

U. S. Army Engineer District
Walla Walla, Washington

U. S. Army Engineer Division, Ohio River
Cincinnati, Ohio

External Distribution (Continued)

U. S. Army Engineer District
Huntington, West Virginia

U. S. Army Engineer District
Louisville, Kentucky

U. S. Army Engineer District
Nashville, Tennessee

U. S. Army Engineer District
Pittsburgh, Pennsylvania

U. S. Army Engineer Division, Pacific Ocean
Honolulu, Hawaii

U. S. Army Engineer District, Far East
San Francisco, California

U. S. Army Engineer District
Honolulu, Hawaii

U. S. Army Engineer District, Okinawa
San Francisco, California

U. S. Army Engineer District, South Atlantic
Atlanta, Georgia

U. S. Army Engineer Division, Canaveral
Meritt Island, Florida

U. S. Army Engineer District
Charleston, South Carolina

U. S. Army Engineer District
Jacksonville, Florida

U. S. Army Engineer District
Mobile, Alabama

U. S. Army Engineer District
Savannah, Georgia

U. S. Army Engineer District
Wilmington, North Carolina

U. S. Army Engineer Division, South Pacific
San Francisco, California

U. S. Army Engineer District
Los Angeles, California

U. S. Army Engineer District
Sacramento, California

U. S. Army Engineer District
San Francisco, California

U. S. Army Engineer Division, Southwestern
Dallas, Texas

External Distribution (Continued)

U. S. Army Engineer District
Albuquerque, New Mexico

U. S. Army Engineer District
Fort Worth, Texas

U. S. Army Engineer District
Galveston, Texas

U. S. Army Engineer District
Little Rock, Arkansas

U. S. Army Engineer District
Tulsa, Oklahoma

Mississippi River Commission
Vicksburg, Mississippi

Rivers and Harbors
Board of Engineers
Washington, D. C.

Corps of Engineer Ballistic Missile Construction Office
Norton Air Force Base, California

U. S. Army Engineer Center
Ft. Belvoir, Virginia

U. S. Army Engineering School
Ft. Belvoir, Virginia

U. S. Army Engineer Reactors Group
Ft. Belvoir, Virginia

U. S. Army Engineer Training Center
Ft. Leonard Wood, Missouri

U. S. Coastal Engineering Research Board
Washington, D. C.

U. S. Army Engineer Nuclear Cratering Group 100
Livermore, California

TID-4500, UC-35, Nuclear Explosions-Peaceful Applications 292

Printed in USA. Available from the Clearinghouse for Federal Scientific and Technical Information, National Bureau of Standards, U. S. Department of Commerce, Springfield, Virginia 22151
Price: Printed Copy $3.00; Microfiche $0.65.

WF/lh